UNIVERSITE DE LIMOGES

Ecole Doctorale SIMM
Science des Procédés Céramiques et de Traitements de Surface

UNIVERSITE DE SFAX

Ecole Doctorale Sciences et Technologies

Ecole Nationale d'Ingénieurs de Sfax-Tunisie

Thèse N°

THESE en cotutelle

Présentée pour obtenir le grade de :

Docteur de l'Université de Limoges & Docteur de l'Ecole Nationale d'Ingénieurs de Sfax

Discipline : Matériaux Céramiques et Traitements de Surface

Contrôle de l'attaque des sources aluminosilicates par la compréhension des solutions alcalines

Par

Ameni GHARZOUNI

Science des Procédés Céramiques et de Traitements de Surface (SPCTS)
Laboratoire de chimie industrielle-LR01ES26

Dirigée par Sylvie ROSSIGNOL
Co-encadrée par Samir BAKLOUTI et Emmanuel JOUSSEIN

Soutenue le 30 Septembre 2016, devant le jury composé de :

Guillaume RENAUDIN	Professeur des Universités, ENSCCF, Clermont-Ferrand	Rapporteur
Khaled BOUZOUITA	Professeur des Universités, IPEIM, Monastir-Tunisie	Rapporteur
Jocelyne BRENDLE	Professeur des Universités, IS2M, Mulhouse	Examinateur
Hassib TOUNSI	Maître de Conférences, FST, Sfax-Tunisie	Examinateur
Samir BAKLOUTI	Professeur des Universités, LCI, Sfax-Tunisie	Examinateur
Basma SAMET	Professeur des Universités, LCI, Sfax-Tunisie	Examinateur
Emmanuel JOUSSEIN	Maître de Conférences, GRESE, Limoges	Examinateur
Sylvie ROSSIGNOL	Professeur des Universités, SPCTS, Limoges	Examinateur

Remerciements

Ce travail a été mené au Laboratoire Science des Procédés Céramiques et Traitements de Surface (SPCTS) à Limoges et au laboratoire de Chimie Industrielle (LCI) à Sfax.
Je remercie Monsieur Thierry CHARTIER, directeur du SPCTS, de m'avoir accueillie au sein de ce laboratoire au cours de ma thèse.

Je tiens à exprimer ma profonde gratitude à Messieurs Guillaume RENAUDIN et Khaled BOUZOUITA, pour avoir jugé ce travail, ainsi que Madame Jocelyne BRENDLE pour avoir accepté la présidence de mon jury de thèse. De même, je voudrais exprimer toute ma gratitude à Madame Basma SAMET et Monsieur Hassib TOUNSI, pour avoir accepté de faire partie de mon jury de thèse.

Je voudrais également dire un très grand merci à ma Directrice de thèse, Madame Sylvie ROSSIGNOL, pour sa disponibilité, sa confiance et ses conseils avisés et constructifs tout au long de ce travail.

Mes remerciements s'adressent aussi à Messieurs Emmanuel JOUSSEIN et Samir BAKLOUTI, qui ont également encadré ce travail pour l'aide qu'ils m'ont apporté ainsi que le temps et l'énergie dépensés.

Je remercie Monsieur Jesus SANZ pour avoir accepté de m'accueillir à l'Institut de Science des Matériaux, ICMM, à Madrid. Un grand merci à Madame Isabel SOBRADOS pour sa disponibilité et sa gentillesse. Merci de m'avoir permis d'utiliser la Résonnance Magnétique Nucléaire et de m'initier à la déconvolution des spectres.

J'associe mes remerciements à tous les membres du laboratoire et de l'ENSCI, permanents, techniciens, secrétaires et à tous ceux qui, de près ou de loin, ont contribué à la réalisation et à l'aboutissement de ce travail.

Je souhaiterais également remercier mes amis et mes collègues (la liste est longue mais je nommerai tout de même William, Ahmed, Perrine, Marie, Aurélie, Julie, Najet, Laeticia, Sylvain, Rémi, Fabrice, Omar, Lamya...) pour leur soutien amical et chaleureux, pour toutes

les choses qu’ils m’ont apportées, pour les discussions et pour les soirées (généralement organisées par Perrine) au cours de ces trois années.

Ces remerciements seraient incomplets si je n'en adressais pas à mes parents et à mes deux adorables sœurs qui m’ont constamment soutenue. Un merci tout particulier à Helmi pour l’encouragement et la patience.

INTRODUCTION GENERALE

La recherche de nouveaux liants plus économiques, peu énergivores et moins polluants tels que les matériaux géopolymères a été privilégiée par les impératifs de la préservation de l'environnement et dans le cadre du développement durable. Ces liants résultent de l'activation d'une source aluminosilicate par une solution alcaline. Ils sont caractérisés par leur facilité de mise en œuvre, leurs propriétés d'usages satisfaisantes et la variété des domaines d'application tels que le génie civil, l'aéronautique, le traitement des déchets…

Le développement des matériaux géopolymères a permis un regain d'intérêt pour la chimie des silicates qui a été un peu marginalisée avec l'abondance des produits pétroliers. Avec la hausse du prix du pétrole, les silicates alcalins ont regagné le marché. Ils sont utilisés dans certaines colles, peintures, mastics, détergents, dans l'industrie du bâtiment, de la verrerie, de la céramique… En plus de leur intérêt industriel, les silicates forment la majeure partie de l'écorce terrestre et participent à l'écosystème. L'étude de la chimie et de la structure des silicates présente donc un intérêt afin d'appréhender la compréhension des mécanismes de géopolymérisation.

D'autre part, les minéraux argileux sont également utilisés comme précurseurs pour la synthèse des géopolymères. Parmi ces minéraux, les argiles kaolinitiques crues ou traitées thermiquement (métakaolins) ont été largement utilisées en raison de leur pureté et leur réactivité élevées. L'utilisation d'autres argiles semble être, d'une part, un enjeu économique profitable vu la réduction des coûts des matières premières et d'autre part, un enjeu environnemental qui permet la préservation des ressources naturelles. La Tunisie est dotée de nombreux gisements d'argiles qui ne sont pas entièrement exploités. Les argiles tunisiennes sont traditionnellement utilisées dans l'industrie de la céramique. Des applications plus innovantes consistent en leur utilisation comme ajout pouzzolanique ou pour la préparation des membranes de filtration. Par conséquent, il semblerait intéressant de les valoriser en tant que source aluminosilicate pour la synthèse des géopolymères. Il serait également utile d'évaluer la possibilité de recyclage des déchets géopolymères par leur réintégration dans de nouvelles formulations, afin d'aborder l'intégralité de cycle de vie de ces matériaux.

La littérature existante concernant ces matériaux est concentrée sur la versatilité des sources aluminosilicates qui peuvent être utilisées (métakaolin, cendre volante, laitier de haut fourneau…) et les propriétés d'usage des matériaux résultants. En revanche, peu d'études se sont intéressées à la possibilité de contrôler la réaction de géopolymérisation en maîtrisant la réactivité des matières premières. En effet, il est indispensable de contrôler la formation, la

structure et les propriétés d'usage afin de les adapter aux applications visées. Ceci permettra le développement et l'industrialisation des matériaux géopolymères.

Par conséquent, ce mémoire s'articule autour de quatre chapitres. Le premier est consacré à une étude bibliographique sur les matériaux consolidés à froid, plus précisément sur les matériaux géopolymères, leurs matières premières (source aluminosilicate et solution alcaline), leur mécanisme de formation, leur structure et leurs propriétés d'usage. Le deuxième chapitre évoque les matières premières utilisées, les protocoles expérimentaux et les techniques de caractérisations mis en œuvre lors de la présente étude. Le troisième chapitre est une synthèse des différents travaux qui ont été menés afin d'identifier les paramètres clés, qui régissent la réaction de géopolymérisation et permettent de prédire la structure et les propriétés d'usage des matériaux finaux. L'ensemble des différents travaux publiés (7 articles, 2 actes et 1 chapitre) est rassemblé dans le quatrième chapitre à savoir :

ACL1. The effect of an activation solution with siliceous species on the chemical reactivity and mechanical properties of geopolymers, A. Gharzouni, E. Joussein, S. Baklouti, S. Pronier, I. Sobrados, J. Sanz, S. Rossignol. J Sol-Gel Sci. Technol. 73 (2015) 250–259.

ACL2. Effect of the reactivity of alkaline solution and metakaolin on geopolymer formation, A. Gharzouni, E. Joussein, B. Samet, S. Baklouti, S. Rossignol, J. Non-Cryst. Solids. 410 (2015) 127-134.

ACL3. Addition of low reactive clay into metakaolin-based geopolymer formulation: Synthesis, existence domains and properties, A. Gharzouni, E. Joussein, B. Samet, S. Baklouti, S. Rossignol, Powder Technol. 288 (2016) 212-220.

ACL4. Recycling of aluminosilicate waste: Impact onto geopolymer formation, N. Essaidi, A. Gharzouni, L. Vidal, F. Gouny, E. Joussein, S. Rossignol, The European Physical Journal Special Topics, 224 (2015) 1707-1713.

ACL5. Recycling of geopolymer waste: Influence on geopolymer formation and mechanical properties A. Gharzouni, L.Vidal, N. Essaidi, E. Joussein, S . Rossignol, Materials and Design 94 (2016) 221-229.

ACL6. Control of polycondensation reaction generated from different metakaolins and alkaline solutions A. Gharzouni, I. Sobrados, E. Joussein, S. Baklouti, S. Rossignol, cement and concrete composite, submitted.

ACL7. Predictive tools to control the structure and the properties of metakaolin based geopolymer materials A. Gharzouni, I. Sobrados, E. Joussein, S. Baklouti, S. Rossignol, colloids and surface A, accepted.

ACTI1. Effect of the Reactivity of the Alkaline Solution and the Metakaolin on the Geopolymer Formation, A. Gharzouni, E. Joussein, S. Baklouti, S. Rossignol, Advances in Science and Technology, 92 (2014) 20-25.

ACTI2. Monitoring the structural evolution during geopolymer formation by ^{27}Al NMR, A. Gharzouni, E. Joussein, S. Baklouti, S. Pronier, I. Sobrados, J. Sanz, S. Rossignol. Ceramic Engineering and Science Proceedings, 36 (2016) 37-48.

Chapitre. Alkaline silicate solutions: An overview of their structure, reactivity and applications, L. Vidal, A. Gharzouni, S. Rossignol, 2nd edition of the Handbook of Sol-Gel Science and Technology, submitted.

CHAPITRE I

SYNTHESE BIBLIOGRAPHIQUE

I. INTRODUCTION

La recherche de nouveaux matériaux peu énergivores a permis le développement des matériaux consolidés à froid. La première partie de ce chapitre est dédiée à présenter quelques exemples de matériaux consolidés à froid. Par la suite, l'étude se focalise sur les matériaux géopolymères. Les matières premières utilisées pour l'élaboration de ces matériaux à savoir la solution alcaline et la source aluminosilicate et les paramètres qui régissent les interactions entre les deux précurseurs font l'objet de la deuxième partie. La dernière partie est une synthèse concernant le mécanisme de formation, la structure et les propriétés d'usage de ces matériaux.

II. LES MATERIAUX CONSOLIDES A FROID

Au cours des dernières décennies, il y a eu une prise de conscience de la nécessité de réduire la consommation d'énergie et l'impact environnemental des matériaux de construction traditionnels, par le développement de matériaux alternatifs peu polluants et moins énergivores, d'où le concept des matériaux consolidés à froid. Dans ce qui suit, il sera détaillé quelques exemples de matériaux consolidés à froid à savoir, les sols stabilisés, les liants hydrauliques, les matériaux de type sol-gel et les géopolymères.

1. Les sols stabilisés

Dans un contexte d'aménagement et de développement de l'infrastructure et au vu de la nécessité de réutiliser les sols (issus de la déconstruction) et chercher des voies alternatives peu énergivores et peu polluantes, la stabilisation des sols apparaît comme une solution prometteuse. Le sol est défini comme étant un matériau complexe composé d'une phase solide qui se présente sous la forme de particules minérales et / ou organiques, une phase liquide constituée d'eau interstitielle et une phase gazeuse [1]. Comme le sol ne répond pas aux exigences mécaniques demandées, il est nécessaire de le stabiliser, c'est-à-dire de modifier ses caractéristiques physicochimiques et mécaniques moyennant des agents chimiques tels que la chaux, les liants hydrauliques…[1, 2]. Par exemple, lors du traitement des argiles à la chaux, une floculation se produit immédiatement et des composés hydratés ayant des propriétés liantes se forment à long terme. Ce traitement entraîne l'amélioration du compactage, de la portance et de la résistance au gel des sols [3, 4]. Il a été également

démontré que le traitement de sol par un liant hydraulique diminue son indice de plasticité, réduit sa surface spécifique et la rend moins sensible au gonflement [5]. En revanche, ce type de traitement n'est pas exempt de problèmes et de limitations tels qu'une rigidité insuffisante ou des problèmes de gonflement [5]. Il faut aussi mentionner qu'il existe des normes [6] qui permettent d'identifier les sols justiciables au traitement selon la granulométrie, la plasticité, l'aptitude au tassement, la teneur en eau et la dureté.

2. Les liants hydrauliques

Les liants hydrauliques sont des matériaux qui durcissent au contact de l'eau et prennent leur résistance au cours du durcissement. Il s'agit d'un ensemble de réactions chimiques d'hydratation à savoir l'hydratation des silicates et des aluminates qui se déroulent simultanément mais pas indépendamment l'une de l'autre [7]. Dans le cas de ciment, les principaux composés à savoir le silicate tricalcique (C_3S), le silicate dicalcique (C_2S), l'aluminate tricalcique (C_3A) et le ferro-aluminate calcique (C_4AF) réagissent avec l'eau pour former de nouveaux composés insolubles qui entraînent la prise et le durcissement progressif du matériau. En effet, les C_3S et les C_2S se dissolvent sous forme d'ions qui interagissent entre eux et forment des silicates de calcium hydratés (C-S-H), à caractère liant et source de résistance, et de la portlandite ($Ca(OH)_2$). D'autre part, l'hydratation des aluminates est considérablement influencée par la présence du gypse. En effet, en absence du gypse, la réaction de C_3A avec de l'eau est très violente et très rapide. Par contre, en présence du gypse, les C_3A réagissent pour former l'ettringite qui cristallise en aiguilles à base hexagonale. La réaction d'hydratation de C_4AF est analogue à celle de C_3A mais elle est beaucoup plus lente et participe peu au développement de la résistance [8, 9, 10].

3. Les matériaux de type sol-gel

La gélification ou la synthèse sol-gel est un procédé de « chimie douce » qui a l'avantage de produire des matériaux homogènes et purs à température ambiante et à pression atmosphérique. Le gel est un réseau tridimensionnel poreux en équilibre avec le liquide contenu dans ses pores et obtenu à partir d'un sol [11]. Le procédé consiste à l'hydrolyse des précurseurs en présence d'un solvant selon l'équation 1 :

$$M - OR + H_2O \rightarrow M - OH + ROH \qquad \textbf{Eq 1}$$

avec M représente le cation métallique tel que le silicium et OR un groupement alcoolate. Puis, la formation de gel par des réactions de condensation selon les équations 2 et 3 :

$$=M - OR + HO - M= \rightarrow =M - O - M= + ROH \qquad \textbf{Eq 2}$$

$$=M - OH + HO - M= \rightarrow =M - O - M= + H_2O \qquad \textbf{Eq 3}$$

Les gels de silice sont généralement obtenus par gélification de suspensions de silice colloïdale [12], par acidification de solutions alcalines [13] ou à partir des sols résultant de la substitution de Na^+ par H^+ dans une solution de silicate de sodium [14].

4. Les géopolymères

Les géopolymères sont des gels d'aluminosilicates amorphes. Ils résultent de l'activation d'une source aluminosilicate par une solution alcaline à pression atmosphérique et à une température inférieure à 100° C [15]. Ils ont été tout d'abord synthétisés par Purdon [16] en 1940, puis par Glukhovsky [17] vers 1959 alors que le terme « géopolymère » n'a été introduit qu'en 1978 par le chimiste français Joseph Davidovits pour désigner à la fois leur caractère inorganique et leur structure analogue aux polymères. La formule chimique générale des géopolymères est : $M^+_n\{(SiO_2)_z, AlO_2\}_n, w\ H_2O$ avec n le degré de polymérisation, z le rapport molaire Si/Al et M^+ le cation monovalent. Les géopolymères sont formés d'un réseau tridimensionnel de tétraèdres SiO_4 et AlO_4, par des réactions de polycondensation et de géopolymérisation. En effet, le cation alcalin M^+ assure la neutralité en compensant le déficit de charge crée par la substitution d'un cation Si^{4+} par un cation Al^{3+}. Selon Davidovits [18], il est possible de distinguer trois familles de géopolymères en se basant sur la valeur du rapport Si/Al à savoir le poly(sialate), le poly(sialate-siloxo) et le poly(sialate-disiloxo).

Les matériaux consolidés à froid ont l'avantage d'avoir des propriétés comparables aux matériaux traditionnels mais avec une consommation d'énergie significativement réduite. Dans ce qui suit, les matériaux de type géopolymère seront étudiés plus profondément.

III. LES GEOPOLYMERES : MATIERES PREMIERES

1. Les solutions alcalines

Quoique considérées comme l'une des plus anciennes classes de produits chimiques, les solutions de silicate alcalin ont regagné de l'intérêt et sont actuellement utilisées dans diverses applications [19] comme liant, défloculant, émulsifiant et comme précurseur pour l'élaboration des matériaux géopolymères. Par conséquent, il apparaît indispensable de déterminer la structure et les caractéristiques de ces solutions.

a. Méthode de synthèse

Les solutions de silicate commerciales résultent de la fusion de carbonate ou de sulfate alcalin (M_2CO_3 ou M_2SO_4 avec M = Na ou K) et de sable (SiO_2) à haute température (1300-1500°C). Le verre de silicate alcalin obtenu est ensuite dissout dans l'eau [20, 21].

$M_2CO_3 + x\ SiO_2 \rightarrow M_2O, x\ SiO_2 + CO_2$ **Eq 4**

Les solutions de silicate peuvent également être obtenues par attaque à chaud de produits siliceux (verre ou silice amorphe) par des bases concentrées ou bien même par dissolution d'une source de silice réactive dans une solution d'hydroxyde alcalin [22, 23] (Équation 5) :

$2\ MOH + x\ SiO_2 \rightarrow M_2O\ x\ SiO_2 + H_2O$ **Eq 5**

Quelle que soit la méthode utilisée, les solutions de silicate alcalin sont caractérisées par le rapport SiO_2/M_2O ou Si/M. Ce dernier conditionne également la teneur en eau et par conséquent la densité de la solution.

b. Structure

La structure des solutions de silicate a été largement étudiée, cependant, elle demeure complexe à cause de la variété des formes d'anions (monomère, linéaire, cyclique, prismatiques ...) [24]. Les techniques spectroscopiques telles que la spectroscopie à Transformée de Fourier (IRTF) et la résonance magnétique nucléaire (RMN de ^{29}Si) ont apporté une contribution importante à la compréhension de la structure de ces solutions. La structure est classiquement décrite par la notation Q^n avec Q l'atome de silicium en coordinence tétraédrique et n représente le nombre d'atomes d'oxygène pontants et (4-n) le nombre d'atomes d'oxygène non pontants [25]. Les études par spectroscopie infrarouge ont prouvé l'existence de corrélation entre les nombres d'onde et les espèces Q^n [26]. Les différents nombres d'onde et les contributions attribuées relatives aux vibrations d'élongation

des liaisons Si-O-Si sont reportés dans le **Tableau 1**. En général, les bandes sont situées entre 800 et 1200 cm^{-1}.

***Tableau 1** : nombres d'onde et contributions attribuées relatives aux vibrations d'élongation des liaisons Si-O-Si [**11, 27**].*

Nombre d'onde (cm^{-1})	Contribution
1125 - 1200	ν_sSi-O-Si (Q^4)
1050 - 1099	ν_sSi-O-Si (Q^3)
1011 - 1014	ν_sSi-O-Si (Q^2)
850 - 920	ν_sSi-O-Si (Q^1)
800 - 875	ν_sSi-O^- (Q^0)

De même la RMN de ^{29}Si a mis en évidence la relation entre le déplacement chimique du noyau silicium et sa connectivité. Des exemples d'espèces siliceuses et leurs déplacements chimiques identifiés par RMN de ^{29}Si des solutions de silicate sont présentés dans le **Tableau 2** [28, 29, 30, 31].

***Tableau 2** : exemples d'espèces siliceuses et de leurs déplacements chimiques identifiés par RMN de ^{29}Si des solutions de silicate.*

Espèces siliceuses	Site Q^n	Représentation schématique	Déplacement chimique (ppm)
monomères	Q^0		-71,30
dimères	Q^1		-79,81
trimère linéaire	Q^1 Q^2		-79,34 -88,22
trimère cyclique	Q^2	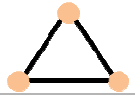	-81,43
tétramère cyclique	Q^2	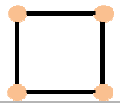	-87,29
hexamère prismatique	Q^3	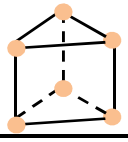	-88,83

c. Paramètres clés contrôlant l'état de polymérisation

L'état de polymérisation des solutions alcalines est conditionné par différent paramètres tel que le rapport Si/M, le taux d'eau et la nature du cation alcalin.

Dimas et al. [32] ont démontré qu'un faible rapport molaire SiO_2/Na_2O induit la formation des espèces de type Q^2, Q^1 et Q^0 et des espèces cycliques de types $Q^{2'}$ et $Q^{3'}$ **[33]**. Au contraire, une valeur de rapport SiO_2/Na_2O élevée favorise la formation des espèces plus polymérisées de type Q^3 et Q^4. Ceci est en relation avec le nombre d'atomes d'oxygène non pontants induit par la quantité de cations alcalins. Par la suite, il y a l'augmentation de la concentration des OH^- et la dépolymérisation des colloïdes donnant lieu à des monomères [34]. Dans le même contexte, Hunt et al. [35] ont démontré par spectroscopie Raman, que pour une concentration donnée en SiO_2, un rapport élevé de K_2O/SiO_2 favorisait la formation des monomères au détriment des oligomères (**Figure 1**) et par conséquent induisait une structure plus dépolymérisée.

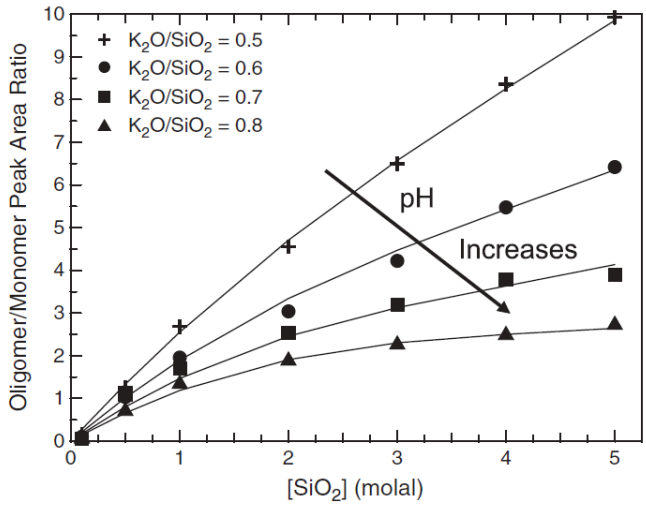

***Figure 1** : évolution de rapport des aires de contributions oligomères/monomères en fonction de la concentration [SiO_2] et du rapport K_2O/SiO_2 [35].*

Le nombre d'atomes d'oxygène non pontants par tétraèdre (NBO/T) peut être déterminé à partir de la composition chimique avec la formule (NBO/T = 2 [K_2O]/[SiO_2]) ou bien à partir des aires des différentes contributions fournies par RMN de ^{29}Si (NBO/T = 3*[Q^1]+2*[Q^2]+3*[Q^3]) [36]. La formation des atomes d'oxygène non pontants augmente avec l'augmentation de la proportion de M_2O (**Figure 2 (a)**). La **Figure 2 (b)** illustre l'évolution de la distribution des espèces siliceuses en fonction du NBO/T. L'augmentation du NBO/T se traduit par une prédominance des espèces dépolymérisées de type Q^2 et Q^1 et des espèces cycliques de type $Q^{2'}$, au profit d'une diminution des espèces de type Q^3 à partir d'un NBO/T égale 1 et une diminution significative jusqu'à la disparition des espèces de type Q^4.

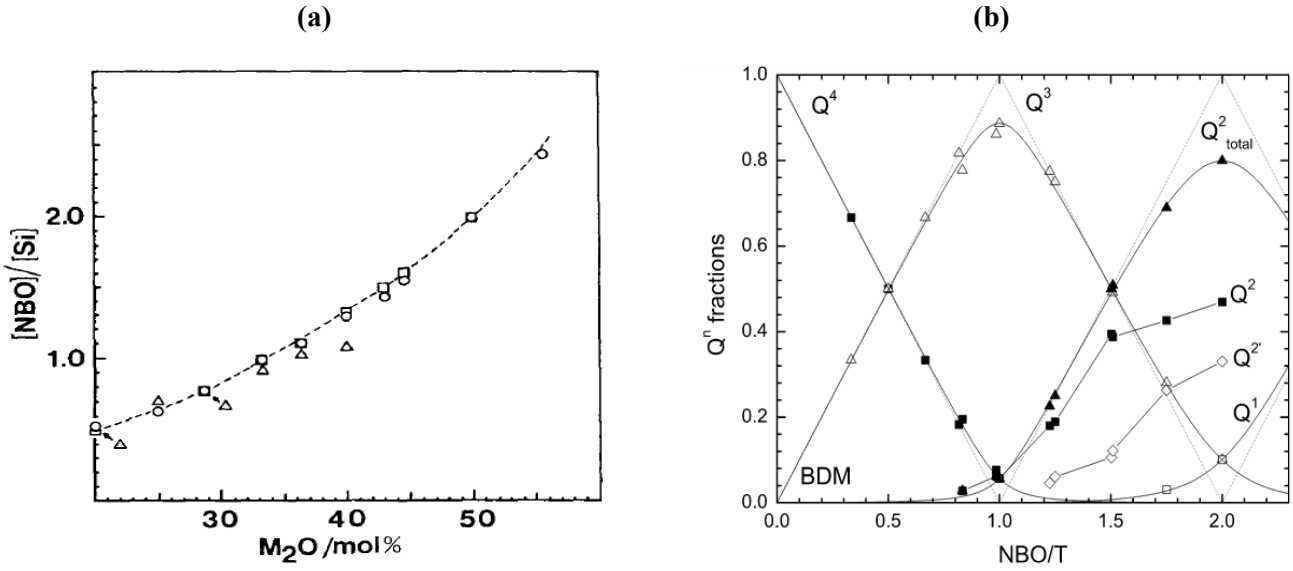

***Figure 2** : **(a)** évolution du rapport NBO/[Si] en fonction du pourcentage molaire de M_2O [33] et **(b)** spéciation des Q^n en fonction du NBO/T [36].*

En outre, le taux d'eau de la solution de silicate est aussi un paramètre important à souligner. Des études par spectroscopie RMN de ^1H ont prouvé que l'eau dans les solutions de silicate se présente sous la forme de groupement OH et de molécules de H_2O [37, 38]. Les groupements OH prédominent dans le cas d'un taux d'eau faible alors que les molécules de H_2O deviennent plus abondantes pour un taux d'eau élevé. De plus, il a été démontré que la quantité d'espèces OH est plus élevée pour les solutions les plus dépolymérisées, impliquant que leur formation est favorisée par les atomes d'oxygène non pontants [39].

Les différences de caractéristiques de cation (sodium ou potassium) influencent aussi la structure et la réactivité de la solution alcaline. En effet, les rayons ioniques des deux cations sont différents, respectivement de 99 et 138 pm pour le cation sodium et potassium. Ceci induit des sphères d'hydratation différentes [40]. La sphère d'hydratation de cation Na^+ est formée par six molécules d'eau alors que celle du potassium est de quatre. Ceci induit des différences au niveau des valeurs des enthalpies d'hydratation respectivement de 95 et 75 Kcal/mol pour les cations Na^+ et K^+ [41, 42].

L'influence du cation alcalin sur la taille des espèces silicatées a été mise en exergue par Diffusion des Rayons X aux Petits Angles (SAXS) [43]. La **Figure 3** montre les spectres SAXS obtenus pour des solutions d'activation à base de sodium et de potassium avec l'ajustement du modèle de sphère dure. Ces études ont démontré que la taille des espèces siliceuses est plus élevée dans le cas des solutions potassiques (r = 4,4 Å ± 0,1 Å) comparé aux solutions de sodium (r = 3,0 Å± 0,1 Å). Par ailleurs, l'excès de diffusion observé dans le

cas de spectre de la solution potassique comparé à celui de la solution sodique a été expliqué par des interactions prédominantes entre les espèces siliceuses dans le cas du potassium en raison du rayon moyen plus élevé.

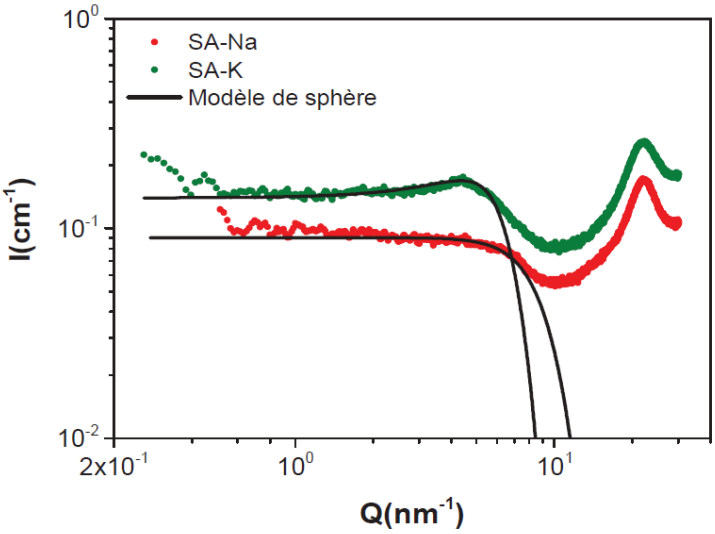

***Figure 3** : spectres de diffusion des solutions d'activation à base de sodium et de potassium avec l'ajustement du modèle de sphère dure [43].*

Le rapport Si/M, le taux d'eau et la nature de cation contrôlent la structure et l'état de polymérisation des solutions alcalines.

2. Les sources aluminosilicates

a. Utilisation des argiles comme source aluminosilicate

Les géopolymères peuvent être synthétisés à partir d'une grande variété de matériaux aluminosilicates tels que les argiles brutes ou calcinées. En se référant à la littérature [44, 45, 46, 47, 48, 49], la kaolinite et le métakaolin ont été fréquemment utilisés. Par exemple, les recherches menées par Xu et Van Deventer [50], sur la réactivité d'un mélange de kaolinite et de stilbite, ont révélé que l'ajout de la kaolinite à d'autres matériaux aluminosilicates est nécessaire pour la formation des gels. En plus, les impuretés présentes dans les argiles peuvent subir des réactions secondaires qui affectent la cinétique de la réaction de géopolymérisation, en jouant le rôle d'un catalyseur modifiant les propriétés mécaniques des matériaux géopolymères obtenus [51]. De même, différents travaux [52, 53, 54, 55, 56] ont évalué la réactivité d'autres minéraux argileux de différentes minéralogies en étudiant

l'influence de leur composition sur les performances des géopolymères obtenus. Récemment, deux argiles tunisiennes, une argile kaolinitique de la région de Tabarka et une argile illito-kaolinitique riche en hématite de la région de Médenine, ont été utilisés en tant que précurseurs d'aluminosilicate potentiels [53]. Il apparaît donc possible d'obtenir des matériaux consolidés à partir d'argiles brutes et calcinées, bien que les matériaux à base d'argiles calcinées présentent une meilleure résistance mécanique.

Afin de justifier le choix des argiles comme matière première pour élaborer les géopolymères, une présentation générale de ces matériaux ainsi que leur réactivité en présence d'un milieu alcalin doit être évaluée.

b. Généralités sur les argiles

Les argiles appartiennent à la famille des phyllosilicates. Ce sont des silicates hydratés organisés en feuillets et constitués de deux couches de base à savoir la couche tétraédrique (T), formée par deux plans d'atomes d'oxygène et un atome de silicium en coordinance IV, et la couche octaédrique (O) formée par deux plans d'atomes d'oxygène et de groupes hydroxyles et un atome de silicium en coordination VI. Les unités structurales de ces deux couches sont schématisées dans la **Figure 4**.

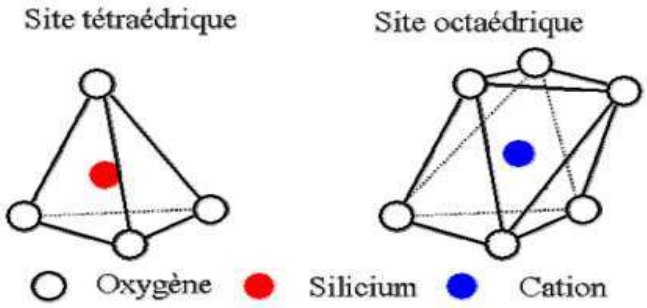

***Figure 4** : unités structurales des minéraux argileux [57].*

L'arrangement des différentes couche T et O induit trois types de structures :

- Le type 1:1 ou T-O formé d'une alternance de couche octaédrique et tétraédrique. La distance inter-réticulaire est d'environ 7,1 Å. Celui-ci est caractéristique de la famille des kaolins pour les alumineux à savoir kaolinite, dickite, nacrite et halloysite.
- Le type 2:1 ou T-O-T formé d'une couche octaédrique intercalée entre deux couches tétraédriques. L'épaisseur de feuillet varie de 10 à 15Å. L'illite, les vermiculites, les smectites, et les micas sont selon cette configuration.

- Le type 2:1:1 ou T-O-T+O formé d'un feuillet type T-O-T avec un espace interfoliaire comblé par une couche O. L'épaisseur de feuillet est d'environ 14Å. C'est le cas de la chlorite.

Ces feuillets sont séparés par un espace interfoliaire de taille variable selon la nature chimique du feuillet, le type de cation et la quantité d'eau.

c. Le métakaolin

Le métakaolin (Al_2O_3, $2SiO_2$) est un aluminosilicate anhydre et métastable qui résulte de la déhydroxylation de la kaolinite à partir de 550°C. Sa structure est amorphe mais peut contenir quelques traces de kaolinite résiduelle et d'impuretés comme l'illite, les micas et le quartz (dépendant de la source initiale). La structure désordonnée du métakaolin lui confère une réactivité chimique meilleure que la kaolinite. Murat et al [58] ont démontré que les caractéristiques cristallo-chimiques des kaolinites initiales pouvaient influencer le domaine de température permettant d'atteindre un degré maximal de désordre.

Les transformations structurales suite à la dehydroxylation de la kaolinite ont été étudiées par différentes techniques telles que l'analyse thermique, la diffraction des rayons X et la spectroscopie RMN [59, 60, 61, 62]. L'utilisation de la spectroscopie RMN de l'aluminium (^{27}Al) permet de déterminer pour la kaolinite et la metakaolinite respectivement, les bandes à 0 ppm relative à l'aluminium hexacoordiné et à 0, 28 et 57 ppm les trois contributions attribuées à l'aluminium hexacoordiné, pentacoordiné et tétracoordiné. La **Figure 5** montre l'évolution des différentes contributions en fonction de la température du traitement thermique de la kaolinite. Les courbes montrent une température optimale entre 750°C et 800°C à laquelle les contributions de l'aluminium, pentacoordiné et tétracoordiné atteignent leur valeur maximale et celle de l'aluminium hexacoordiné est à son minimum. Ceci permet d'estimer une réactivité maximale de métakaolin traité à une température 750°C et 800°C [63].

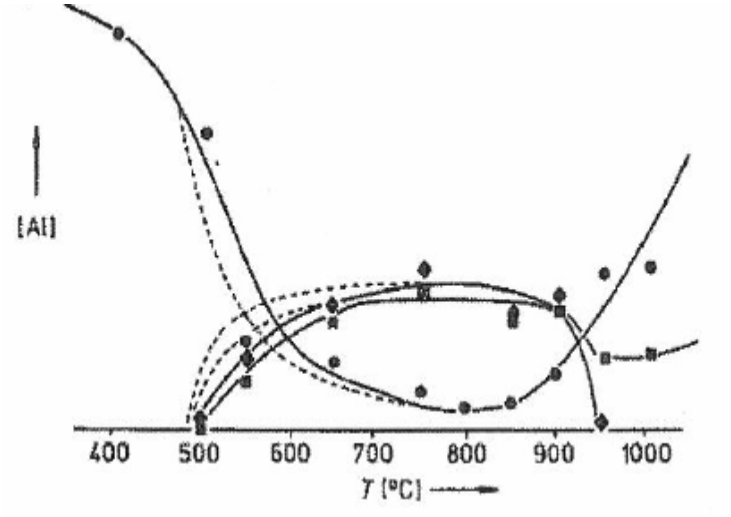

***Figure 5** : évolution des différentes contributions relatives à l'aluminium (■) tetracoordiné (♦) pentacoordiné et (●) hexacoordiné en fonction de la température du traitement thermique de la kaolinite [63].*

d. Utilisation des coproduits industriels comme source aluminosilicate

Divers coproduits industriels ont été utilisés pour l'élaboration des matériaux géopolymères tels que les cendres volantes [64, 65], les laitiers des hauts fourneaux [66, 67], les résidus miniers [68] et les déchets de béton et de construction [69, 70]. L'utilisation de ces coproduits qui prennent généralement le statut de déchet constitue un enjeu économique et environnemental profitable [71]. Selon leur réactivité, les coproduits incorporés peuvent participer aux réactions de formation du liant ou bien jouer le rôle de charges neutres ou bien modifier la réaction. De plus, il a été montré que leur faible réactivité comparé au métakaolin, peut engendrer des hétérogénéités de la structure des matériaux obtenues et par conséquent, une diminution de la résistance mécanique [72] à partir d'une certaine quantité limite. Gao et al. [73] ont montré qu' un taux de substitution de métakaolin par des cendres volantes allant jusqu'à 20% induit l'augmentation de la résistance à la compression. Onutai et al. [74] ont mis en évidence la possibilité d'introduire jusqu'à 40% de déchets d'hydroxyde d'aluminium dans un mélange géopolymérique afin d'obtenir une structure dense et une résistance en compression optimale. Par ailleurs, une étude [75] a été initiée pour évaluer l'influence de l'incorporation de différents types de granulats à savoir le schiste, le granite et le calcaire sur les propriétés des liants obtenus. Il a été démontré que la taille des granulats affecte la résistance à la traction.

Une autre étude [76] a montré la possibilité de formuler des matériaux géopolymères à partir de déchets de verre. Contrairement aux géopolymères à base de métakaolin, il n'est pas nécessaire de rajouter une solution de silicate alcalin étant donné que le déchet de verre contient déjà une proportion élevée d'alcalin. Une activation thermique à 40 ou 60 °C est nécessaire pour obtenir une résistance mécanique supérieure à 50 MPa en particulier pour le verre le plus fin (4000 cm^2/g). Il faut, néanmoins, préciser qu'une quantité d'atomes de calcium est présente dans ce type de matériau.

e. Paramètres contrôlant la dissolution de la source aluminosilicate en milieu basique

Au contact d'un milieu alcalin, le phénomène de dissolution des sources aluminosilicates est mis en évidence. La cinétique de cette dissolution dépend de plusieurs paramètres tels que la nature, la granulométrie et la cristallinité du matériau aluminosilicate, la valeur de pH du milieu et les conditions de saturation.

La nature du minéral argileux joue un rôle important dans son comportement dans un milieu alcalin. Une étude comparative de la dissolution de trois différents minéraux à savoir la kaolinite, l'illite et la montmorillonite en fonction de la valeur de pH à température ambiante a souligné une dissolution plus importante de la kaolinite en milieu basique (**Figure 6**). Ceci est dû à sa structure T–O qui permet une dissolution plus rapide de la couche octaédrique alumineuse entrainant la dissolution de la couche tétraédrique. Par contre, dans le cas de la structure T–O–T, la dissolution de la couche octaédrique est plus difficile puisqu'elle est située entre deux couches tétraédriques.

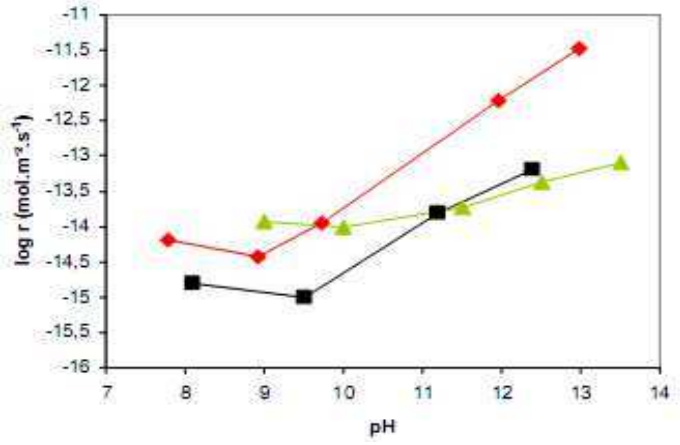

***Figure 6** : cinétiques de dissolution de (■) la kaolinite, de (♦) l'illite et de (▲) la montmorillonite en fonction de la valeur de pH [2].*

La granulométrie affecte aussi la dissolution vu qu'elle influence les interactions ioniques. Il a été démontré que plus la taille des particules est fine, plus la dissolution du silicium est favorisée [77]. L'impact de la cristallinité de la source aluminosilicatée sur sa dissolution a été mis en exergue. Il a été démontré que la cinétique de dissolution de la kaolinite en présence de KOH est liée à la stabilité de son arrangement structural, à la taille et la forme des particules et au nombre de défauts [78]. De plus, la teneur en aluminium réactif dans la source aluminosilicate joue un rôle crucial. En effet, l'aluminium se dissout plus rapidement que le silicium parce que les liaisons Al-O sont plus faibles que les liaisons Si-O et par conséquent plus facile à rompre [79].

La valeur de pH conditionne également la dissolution. En effet, l'augmentation de la valeur de pH induit une augmentation de la concentration des sites de surface déprotonés et favorise par conséquent la dissolution [80]. La **Figure 7** montre la variation des concentrations des espèces alumineuses et siliceuses obtenues à partir de la kaolinite en fonction de la valeur de pH [81]. En milieu basique, la concentration des espèces dissoutes augmente avec l'augmentation de la valeur de pH. La spéciation de l'aluminium est dominée par les espèces de type $Al(OH)_4^-$. Quant aux espèces siliceuses, une augmentation de la concentration des espèces dissoutes est observée à partir d'une valeur de pH égale à 10 avec la prédominance des espèces déprotonées $H_3SiO_4^-$.

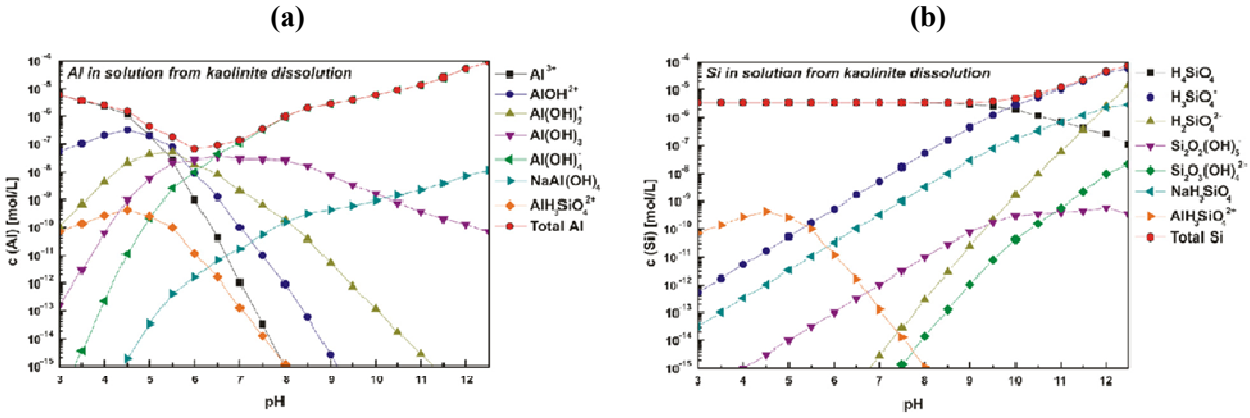

***Figure 7** : variation des concentrations des espèces **(a)** alumineuses et **(b)** siliceuses dissoutes à partir de la kaolinite en fonction de la valeur de pH [81].*

La dissolution des sources aluminosilicates dans un milieu alcalin dépend, d'une part, de leur caractéristique physicochimique, de leur structure et, d'autre part, de la valeur de pH du milieu.

IV. LES GEOPOLYMERES : MECANISME DE FORMATION, STRUCTURE ET PROPRIETES D'USAGE

1. Mécanisme de formation

De nombreux auteurs ont tenté d'appréhender le mécanisme de formation des géopolymères en utilisant différentes techniques de caractérisation. Provis et al. [82] considèrent qu'il est difficile de différencier les étapes de la réaction vu qu'elles se produisent simultanément et rapidement. Néanmoins, ils ont réussi à modéliser la cinétique de la réaction en utilisant l'énergie dispersive de diffraction de rayons X in situ. D'autres auteurs ont eu recours à des techniques d'analyse structurales plus précises, telle que la spectroscopie RMN. Rahier et al. [83] ont suivi les changements moléculaires au cours de la synthèse des matériaux moyennant la spectroscopie RMN de ^{27}Al et de ^{29}Si. Ils ont constaté que les géopolymères résultaient de réactions combinées et complexes. En effet, la diminution de la concentration des ions OH^- au début de la réaction est à l'origine de la formation d'un composé aluminosilicate intermédiaire qui conduit ensuite à un matériau géopolymère. Récemment, Favier et al. [84] ont mené une étude par spectroscopie RMN statique, pour suivre l'évolution de la concentration totale d'Al tétraédrique dans le liquide interstitiel et de la corréler à l'évolution du module d'élasticité de la pâte géopolymère. Une étude RMN de ^{1}H a permis de définir le processus de géopolymérisation comme une succession de quatre étapes à savoir (i) une première période d'initiation (de 0 à 15 min), (ii) suivie d'une période de formation d'oligomères (de 15 à 150 min), (iii) ensuite une période de réorganisation (de 150 à 350 min) pendant laquelle la dissolution est ralentie à cause de la formation du gel et (iv) enfin une période de polycondensation (de 360 à 1200 min) où la formation de réseau tridimensionnel domine [85]. Les analyses thermiques différentielle (ATD) et thermogravimétrique (ATG) lors de la formation ont été également utilisées dans la détermination du taux de géopolymérisation [86]. Les mélanges réactifs ont été maintenus à 70°C pendant deux heures. En fonction de la courbe de flux thermique obtenue et les pertes de masse associées, quatre zones ont été définies dénotant les différentes réactions à savoir la réorganisation des espèces, la dissolution du métakaolin, la formation d'oligomères et enfin, la réaction de polycondensation. En résumé, il y'a un consensus sur le mécanisme de géopolymérisation (**Figure 8)** qui consiste dans un premier temps à la dissolution de la source aluminosilicate sous l'effet de la solution alcaline donnant lieu à des oligomères de type $Si[OH]_4$ et $Al[OH]_4$. Ensuite, ces oligomères se réorganisent. Enfin, une réaction de

polycondensation permet la polymérisation et la condensation d'un réseau tridimensionnel. [87, 88].

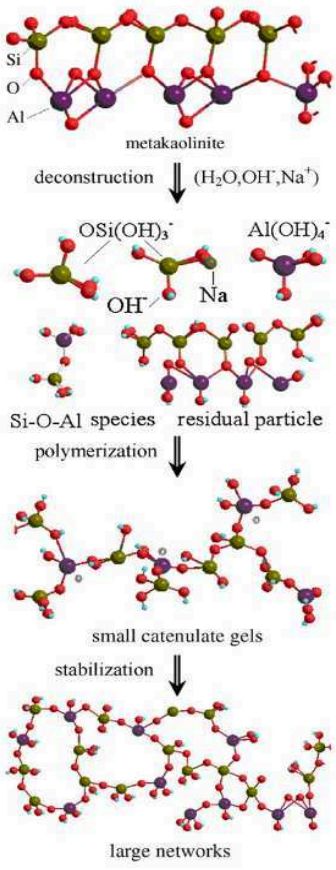

***Figure 8** : mécanisme de géopolymérisation [88].*

Malgré les modèles existants décrivant la réaction de géopolymérisation, le mécanisme n'est pas encore entièrement élucidé comme il est fortement dépendant des matières premières utilisées. Ainsi, il est intéressant d'évaluer l'influence de la réactivité des précurseurs sur l'évolution structurale des matériaux géopolymères.

2. Structure et microstructure

Les matériaux géopolymères sont caractérisés par une structure amorphe. Les diffractogrammes des rayons X montrent généralement un dôme centré au alentour de 30° (2θ) [89, 90, 91] mais également la persistance des phases non ou faiblement dissoutes tel que le quartz et la mullite (**Figure 9**) [92, 93]. Il est également notable que l'augmentation de la concentration de la solution activatrice favorise l'amorphisation des matériaux obtenus [93].

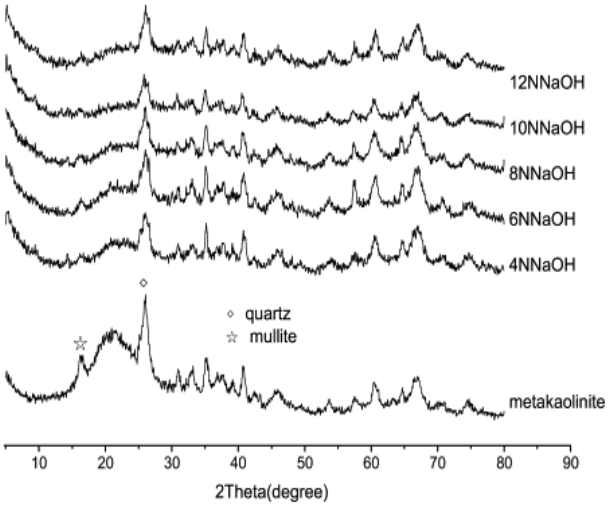

***Figure 9** : diffractogrammes de la métakaolinite et des matériaux géopolymères à base de solutions de NaOH à différentes concentrations [93].*

La structure des géopolymères a été également investiguée par spectroscopie RMN de ^{27}Al et de ^{29}Si [94]. La **Figure 10 A(a)** montre un exemple typique de spectre RMN de ^{27}Al d'un géopolymère à base de métakaolin et d'une solution alcaline sodique [95]. Le spectre met en évidence que l'aluminium est majoritairement en coordinence IV (~ 60 ppm) en plus de l'existence de traces d'aluminium en coordinence VI (~ 0 ppm) indiquant qu'une quantité de métakaolin n'a pas réagi ou la présence d'impuretés micacées [96]. La large bande (de -85 à 95 ppm) relative au spectre RMN de ^{29}Si (**Figure 10 A(b))** peut être décomposée en cinq contributions relatives aux espèces de type Q^4 (m Al) (**Figure 10 B**) avec $0 \leq m \leq 4$ est le nombre de Al deuxième voisin [97].

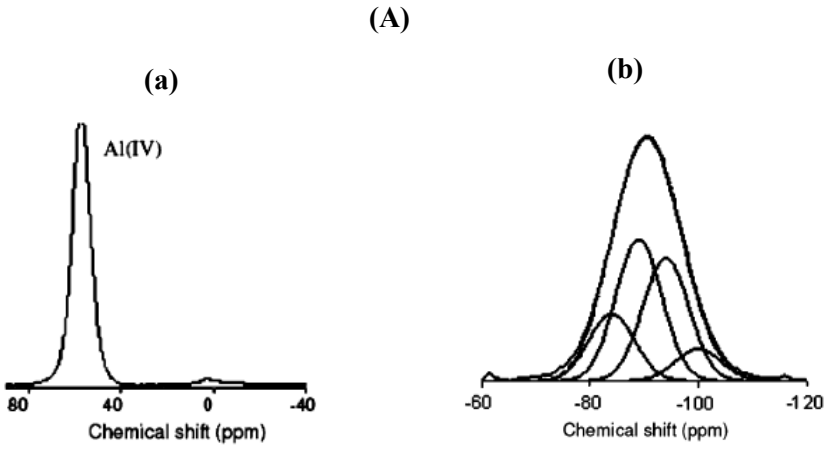

(B)

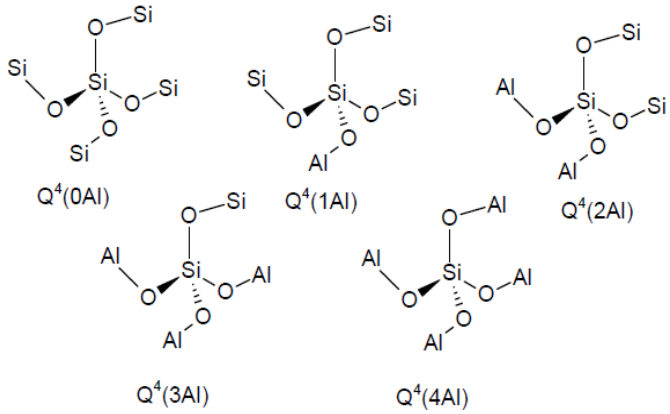

Figure 10 *: **(A)** exemples typiques de spectres RMN de **(a)** ^{27}Al et de **(b)** ^{29}Si d'un géopolymère à base de métakaolin et d'une solution alcaline sodique (20 h, 85 °C) [95] et **(B)** coordination de silicium décrite par la notation Q^4 (m Al) [97].*

De plus, il a été prouvé que l'ordre chimique du silicium et d'aluminium dans les géopolymères est significativement influencé par la nature des matières premières utilisées, le type du cation alcalin et les conditions opératoires de synthèse [96, 98]. A titre d'exemple, la **Figure 11** montre la variation des différentes contributions de silicium Q^4 (m Al) en fonction du rapport Si/Al et du cation alcalin.

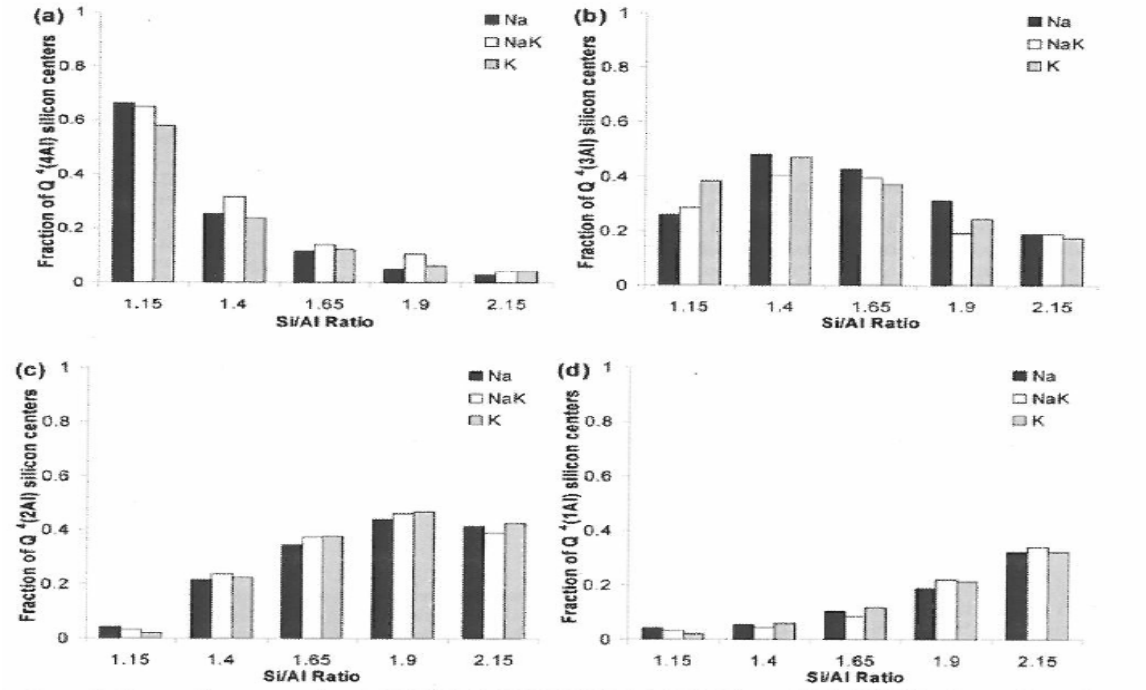

Figure 11 *: variation des différentes contributions **(a)** Q^4 (4 Al), **(b)** Q^4 (3 Al), **(c)** Q^4 (2 Al) et **(d)** Q^4 (1 Al) en fonction du rapport Si/Al en présence de différents cations alcalins [96].*

Les différences de distribution des espèces sont plus significatives pour un rapport Si/Al < 1,65. Par conséquent, le cation alcalin n'affecte pas la structure moléculaire des matériaux géopolymères ayant des valeurs de rapports Si/Al élevés. Il est aussi notable que les géopolymères à base de potassium ont une fraction Q^4 (4 Al) plus faible et une fraction Q^4 (3 Al) plus élevé que les géopolymères à base de sodium ou mixte, indiquant un degré de désordre plus élevé dans le cas de potassium [96].

La microstructure des matériaux géopolymères a été observée par microscopie électronique à balayage (MEB) et à transmisssion (MET) [49, 99]. Une photo MEB typique des matériaux géopolymères à base de métakaolin est présentée dans la **Figure 12 (a).** L'influence des rapports molaires Si/Al et Na/Al sur la microstructure a été mise en exergue [96, 100, 101]. Une microstructure homogène a été obtenue pour des rapports Si/Al et Na/Al de 2,5 et 1,25, respectivement. Les structures hétérogènes résultent généralement des caractéristiques des matières premières (efficacité du traitement thermique et granulométrie) ou bien de la difficulté de dissoudre la source aluminosilicate suite à la faible disponibilité des ions M^+ et OH^- de la solution d'activation. De plus, il a été montré que l'augmentation du rapport Si/Al entraîne une meilleure dissolution du métakaolin et par conséquent une structure plus homogène des matériaux finis.

Des informations à l'échelle nanométrique ont été fournies par microscopie électronique à transmission (MET). La micrographie MET d'un géopolymère à base de métakaolin (**Figure 12 (b)**) montre que la structure est formée de petites entités avec des pores dispersés dans les interstices. La taille et la distribution de ces entités sont directement liées aux matières premières et aux conditions de mise en œuvre. En effet, ces facteurs régissent la réorganisation des espèces et la densification de la structure. Autef et al. [49] ont prouvé que la réactivité du métakaolin peut engendrer des variations nanostructurales. Selon le métakaolin utilisé, la structure peut être formée d'une ou plusieurs phases telles que la phase géopolymère, des plaquettes de kaolinite, une phase riche en silicium et une phase riche en aluminium.

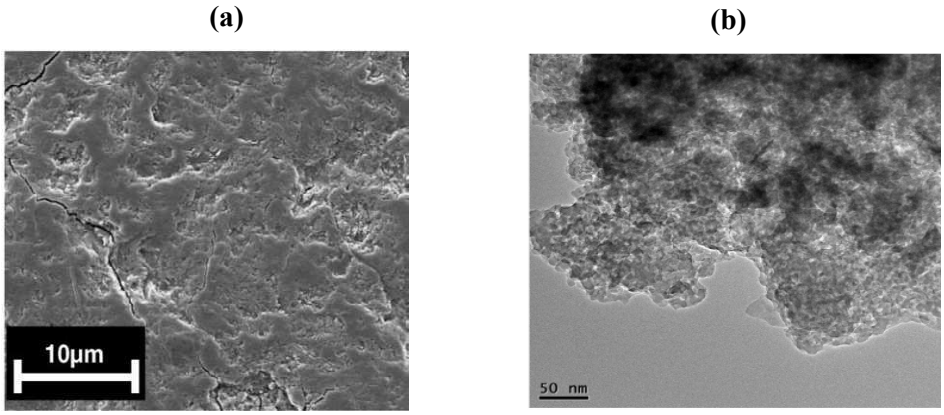

***Figure 12** : micrographies (a) MEB d'un géopolymère avec Si/Al =1,6 [102] et (b) MET d'un géopolymère à base du métakaolin [49].*

3. Propriétés d'usage

Les matériaux géopolymères possèdent des propriétés d'usages (mécaniques, thermiques…) satisfaisantes. Plusieurs auteurs se sont focalisés sur les propriétés mécaniques et les paramètres qui les régissent. Duxson et al. [102] ont mis en évidence l'impact du rapport Si/Al sur les propriétés mécaniques. Ils ont montré que les échantillons avec un rapport molaire Si/Al > 1,65 présentent une meilleure résistance à la compression et un module d'Young plus élevé. Par contre, au dessus d'un rapport Si/Al = 1,9, il y'a eu dégradation des propriétés mécaniques due aux espèces n'ayant pas réagi. Steveson et al. [103] ont montré que les propriétés mécaniques sont intimement liées à la microstructure. Plus la microstructure est fine et dense, meilleures sont les résistances à la compression. Le cation alcalin peut aussi influencer les propriétés mécaniques, puisque les géopolymères à base de potassium montrent des résistances à la compression plus élevées que celles à base de sodium. Il a été montré aussi que les résistances à la compression augmentent avec l'augmentation de la concentration de la solution de NaOH de 4 à 12 mol. L^{-1}. D'autres auteurs [104,105] se sont intéressés à l'effet du rapport solide/liquide (S/L) sur les contraintes à la compression. Un rapport optimal de 0,8 conduit aux meilleures résistances mécaniques. En effet, un rapport S/L très faible c'est-à-dire un excès de la quantité d'activateur liquide favorise la dissolution de la source aluminosilicate mais perturbe par la suite la réaction de polycondensation vu que la diffusion des espèces dissoutes devient plus difficile. Ceci fragilise la structure et diminue les résistances mécaniques. En revanche, un rapport S/L très élevé entraîne l'hétérogénéité de la structure à cause des particules solides non-dissoutes ce

qui dégrade les propriétés mécaniques. L'effet des phases cristallines provenant de la source aluminosilicate et qui persistent dans les matériaux géopolymères a été étudié. Deux comportements sont distingués, à savoir les phases cristallines qui jouent le rôle de renfort et améliorent les propriétés mécaniques telles que le quartz et d'autres phases, qui diminuent les résistances mécaniques telles que la mullite et le corindon [106, 107]. De plus, il a été mis en évidence, que l'incorporation de fibres comme renforts améliore la ductilité et la résistance mécanique des matériaux géopolymère [108, 109, 110].

Ces données soulignent l'importance de certains paramètres sur la formation et sur les propriétés d'usage résultantes des matériaux géopolymères. Cependant, peu de données sont relatives à l'influence conjointe d'une source aluminosilicate et d'une solution alcaline.

V. OBJECTIF DE L'ETUDE

L'objectif de cette étude est d'identifier les paramètres clés responsables de la genèse des matériaux géopolymères afin de contrôler leur formation et leurs propriétés d'usage. Ceci est basé sur la maîtrise de la structure des matières premières et de leurs interactions.

Afin d'atteindre cet objectif, plusieurs moyens ont été mis en œuvre à savoir :

(i) l'identification des paramètres qui régissent la réactivité des matières premières (différentes solutions alcalines et sources aluminosilicates) et l'impact de leur réactivité sur la faisabilité des matériaux géopolymères. Ceci sera corroboré aux cinétiques de formation et à l'identification des réseaux formés.

(ii) la détermination de l'impact de la réactivité des matières premières sur la structure et leur corrélation avec les propriétés mécaniques et la porosité.

(iii) l'établissement d'un modèle de réactivité permettant de définir des lois prédictives pour contrôler la réaction de géopolymérisation et les propriétés d'usage des matériaux finis. Tout ceci afin d'évaluer la possibilité de recyclage de déchet géopolymère et d'autre part de l'adapter à une argile tunisienne de faible réactivité.

VI. BIBLIOGRAPHIE

[1] N. Cabane, Sols traités à la chaux et aux liants hydrauliques : Contribution à l'identification et à l'analyse des éléments perturbateurs de la stabilisation, thèse de doctorat, Ecole des Mines d'Alès, 2005, p. 11.
[2] N. Maubec, Approche multi-échelle du traitement des sols à la chaux étude des interactions avec les argiles, thèse de doctorat, Université de Nantes, 2010, p. 21-29.
[3] M. Boutonnet et J. Livet, Sols traités en assises de chaussée. Influences du traitement des limons sur leur comportement au gel. Bulletin de liaison des laboratoires des Ponts et Chaussées n° 133 (1984) p 83-90.
[4] P. Sherwood, Soil stabilisation with cement and lime. HMSO (1995) p 153.
[5] R. Croisé, Traitement des sols aux liants hydrauliques, revue forestière française p 428-429.
[6] AFNOR NF P 11-300, Exécution des terrassements. Classification des matériaux utilisables dans la construction des remblais et des couches de forme d'infrastructures routières (1992) p. 21.
[7] A. Messi. Propriétés des ciments pouzzolaniques élaborées à partir de latérites actives. Thèse de doctorat, INSA de Lyon, 1988, p. 256.
[8] S. Brunauer, and S.A. Greenberg. The Hydration of Tricalcium Silicate and β -Dicalcium Silicate at Room Temperature". Proc. of the IV Int. Syrup. On the Chemistry of Cement, Washington 1960. Washington, I (1962) 135-165.
[9] D. Knbfel and J.F. Wang, Early Hydration of Quick Cements in the System $C_{ll}A_7.CaF_2$-C_2S-$C_2(A,F)$, Advanced Cement Based Materials, 1 (1993) 77-82.
[10] J. Stark, Recent advances in thefield of cement hydration and microstructure analysis, Cem. Concr. Res. 41 (2011) 666-678.
[11] M. T. Tognonvi, Physico-chimie de la gélification du silicate de sodium en milieu basique, Thèse de Doctorat, université de Limoges, 2009.
[12] C. Song-Yuan, Network formation in polymerising and aggregating silica sol-gel systems. Thèse de Doctorat, Ecole Polytechnique Fédérale de Lausanne, 1992.
[13] M.J. Munoz-Aguado, M. Gregorkiewitz, Sol-gel synthesis of microporous amorphoussilica from purely inorganic precursors. J. colloid and Interface Sci. 185 (1997) 459-465.
[14] T. Gerber, B. Himmel, C. Hübert, WAXS and SAXS investigation of structure formation of gels from sodium water glass. J. Non-Cryst. Solids.175 (1994) 160-168.
[15] J. Davidovits, Geopolymer Chemistry and Applications, 2nd ed. Saint-Quentin, France: Institut Geopolymer, 2008.
[16] A. O. Purdon, The action of alkalis on blast furnace slag. Journal of the Society of Chemical Industry, 59 (1940) 191-202.
[17] D. Glukhovsky, G.S. Rostovskaja, et G.V. Rumyna, High strength slag-alkaline cements, Communications of the 7th International Congress on the Chemistry of Cement, 3 (1980) 164-168.
[18] J. Davidovits, Geopolymers - inorganic polymeric new materials, Journal of Thermal Analysis, 37 (1991) 1633-1656.
[19] H.H Weldes, K.R Lange, Properties of soluble silicates, Ind. Eng. Chem 61 (1969) 29-44.
[20] R.K. Iler, The chemistry of silica: solubility, polymerization, colloid and surface properties, and biochemistry. New York: Wiley-Interscience, 1979.
[21] Soluble silicate, SIDS Initial Assessment Report, OECD SIDS, UNEP publication.

[22] S.S. Kouassi, Étude de la dissolution d'un réseau silicaté en présence d'une solution alcaline, thèse de doctorat, Université de Limoges, 2011.
[23] A. Paul, Chemistry of Glasses, Edition Chapman and Hall, New York, 1982.
[24] T.W. Swaddle, Silicate complexes of aluminum (III) in aqueous systems. Coord Ch Re. 219 (2001) 665-686.
[25] G. Engelhard, D. Zeigan, H. Jancke, D. Hoebbel , Z. Weiker, High resolution ^{29}Si NMR of silicates and Zeolites. Anorg. Allg. Chem. 418(1975) 17-28.
[26] S.A. MacDonald, C.R Schardt, D.J Masiello Dispersion analysis of FTIR reflection measurements in silicate glasses. J. Non-Crystal Solids. 275 (2000) 72-82.
[27] J. Tan, S. Zhao, W. Wang, G. Davies, X. Mo, The effect of cooling rate on the structure of sodium silicate glass. Mater. Sci. Eng. B, 106 (2004) 295-299.
[28] S. Sjöberg, Silica in aqueous environments, J. Non-Cryst. Solids. 196 (1996) 51-57.
[29] R.K. Harris, M.J. O'Connor, E.H Curzon, O.W. Howarth, Two-Dimensional Silicon-29 NMR Studies of Aqueous Silicate Solutions, J. Magn. Reson. 57 (1984) 115-122.
[30] C.T. G. Knight, A two-dimensional silicon-29 nuclear magnetic resonance spectroscopic study of the structure of the silicate anions present in an aqueous potassium silicate solution. J. Chem. Soc. Dalton Trans**.** (1988) 1457-1460.
[31] H. Cho, A.R. Felmy, R. Craciun , J.P Keenum , N. Shah and D.A. Dixon, Solution State Structure Determination of Silicate Oligomers by ^{29}Si NMR Spectroscopy and Molecular Modeling. J. Am. Chem. Soc. 128 (2006) 2324-2335.
[32] D. Dimas, I. Giannopoulou, D. Panias Polymerization in sodium silicate solutions: a fundamental process in geopolymerization technology, J. Mater. Sci. 44 (2009) 3719-3730.
[33] H. Maekawa, T. Maekawa, K. Kawamura and T.Yokokawa The structural groups of alkali silicate glasses determined from ^{29}Si MAS-NMR. J. Non Cryst. Solids. 127 (1991) 53-64.
[34] A.S. Brykov, V.V. Danilov, E. Yu. Aleshunina, State of silicon in silicate and silica-containing solutions and their binding properties, Russian Journal of Applied Chemistry. 81 (2008) 1717-1721.
[35] J.D. Hunt, A. Kavner, E.A.Schauble, D. Snyder, C.E. Manning. Polymerization of aqueous silica in H_2O-K_2O solutions at 25-200 °C and 1 bar to 20 kbar. Chem. Geol. 283 (2011) 161-170.
[36] W.J. Malfait, W.E. Halter, Y. Morizet, B.H. Meier, R. Verel, Structural control on bulk melt properties: Single and Double quantum ^{29}Si NMR spectroscopy on alkali-silicate glasses, Geochimi. Cosmochim. Acta.71 (2007) 6002-6018.
[37] R.F. Bartholomew, B.L Butler, H.L Hoover, C.K.Wu, Infrared spectra of a water-containing glass. J. Am. Ceram. Soc. 63 (1980) 481-485.
[38] B.C. shmidt, H. Behrens, T. Riemer, R. Kappes, R. Dupree, Quantitative determination of water speciation in aluminosilicate glasses: a comparative NMR and IR spectroscopic study. Chem. Geol. 174 (2001) 195-208.
[39] S. Yamashita, H. Behrens, B.C. Schmidt, R. Dupree, Water speciation in sodium silicate glasses based on NIR and NMR spectroscopy, Chemical Geology, 256 (2008) 231-241.
[40] J.P. Jolivet, Condensation des cations en solution aqueuse-Chimie de surface des oxydes, dans De la solution à l'oxyde, Savoirs actuels, InterEditions / CNRS Editions, 17, Paris, 1994.
[41] L. Degrève, S.M. Vechi, C.Q. Junior, The hydration structure of the Na^+ and K^+ ions and the selectivity of their ionic channels, Biochimica et Biophysica Acta (BBA) - Bioenergetics 1274 (1996) 149-156.
[42] J. Mähler and I. Persson, A Study of the Hydration of the Alkali Metal Ions in Aqueous Solution, Inorg. Chem. 51 (2012) 425-438.

[43] P. Steins, Influence des paramètres de formulation sur la texturation et la structuration des géopolymères, thèse de doctorat, université de Limoges, 2014.
[44] Z. Zuha, X. Xiao, Z. Huajun et C. Yue, Role of water in the in the synthesis of kaolin-based geopolymer, Appl. Clay Sci. 43 (2009) 218-223.
[45] P. Duxson, The structure and thermal evolution of metakaolin geopolymers, Thèse de Doctotat, Université de Melbourne, 2006, p.355.
[46] X. Yao, Z. Zhang, H. Zhu et Y. Chen, Geopolymerization Process of Alkali-Metakaolinite Characterized by Isothermal Calrimetry, Thermochimica Acta, 493 (2009) 49-54.
[47] A. Elimbi, K.H. Tchakoute and D. Njopwouo, Effects of calcination temperature of kaolinite clays on the properties of geopolymer cements, Constr. Build. Mater. 25 (2011) 2805-2812.
[48] A. Autef, E. Joussein, A. Poulesquen, G. Gasgnier, S. Pronier, I Sobrados, J. Sanz, S. Rossignol, Role of metakaolin dehydroxylation in geopolymer synthesis, Powder Technol. 250 (2013) 33-39.
[49] A. Autef, E. Joussein, A. Poulesquen, G. Gasgnier, S. Pronier, I Sobrados, J. Sanz, S. Rossignol, Influence of metakaolin purities on potassium geopolymer formulation: The existence of several networks, J. Colloids and Interface Sci. 408 (2013) 43-53.
[50] H. Xu and J.S.J. Van Deventer, The geopolymerisation of alumino-silicate minerals. International Journal of Mineral Processing, 59 (2000) 247-266.
[51] K. Komnitsas and D. Zaharaki, Geopolymerisation: A review and prospects for the minerals industry, Minerals Engineering. 20 (2007) 1261-1277.
[52] A. Buchwald, M. Hohman, K. Posern, E. Brendler, The suitability of thermally activated illite/smectite clay as raw material for geopolymer binders. Appl. Clay Sci. 46 (2009) 300-304.
[53] N. Essaidi, B. Samet, S. Baklouti, S. Rossignol, Feasibility of producing geopolymers from two different Tunisian clays before and after calcination at various temperatures, Appl. Clay Sci. 88–89 (2014) 221-227.
[54] K.J.D. Mackenzie, S. Komphanchai, R. Vagane, Formation of inorganic polymers (geopolymer) from 2:1 layer lattice, J. Eur. Ceram. Soc. 28 (2008) 177-181.
[55] C. Ruiz-Santaquiteria, A. Fernández-Jiménez, J. Skibsted, A. Palomo. Clay reactivity: Production of alkali activated cements. Appl. Clay Sci.73 (2013) 11-16.
[56] S. Selmani, N. Essaidi, F. Gouny, S. Bouaziz, E. Joussein, A. Driss, A. Sdiri, S. Rossignol, Physical–chemical characterization of Tunisian clays for the synthesis of geopolymers materials, J. Afr. Earth. Sci. 103 (2015) 113-120.
[57] M. Perronet, Réactivité des matériaux argileux dans un contexte de corrosion métallique, Thèse de doctorat, Institut National Polytechnique de Lorraine, 2005, p. 282
[58] M. Murat, M.E.M. Chbihi, D. Mathurin. Heat of solution of different kaolinites and metakaolinites in hydrofluoric acid. Effect of crystal-chemical characteristics. Ind. Ceram. (Paris) 822 (1976) 799-801.
[59] G. W. Brindley and M. Nakahira, The kaolinite mullite reaction series, J. Amer. Ceram. Soc. 42 (1959) 311-324.
[60] G.B. Mitra, S. Bhattacherjee, X-ray diffraction studies on the transformation of kaolinite into metakaolin: I Variability of interlayer spacings. The Am. Mineral. 54 (1969) 1409-18.
[61] T. Watanabe, H. Shimizu, K. Nagasawt, A. Masuda and H. Saito, ^{29}Si- and ^{27}Al-MAS/NMR Study of the thermal transformations of kaolinite, Clay Minerals. 22 (1987) 37-48.
[62] V. Balek, M. Murat, The emanation thermal analysis of kaolinite clay minerals. Thermoch. Acta. 282 (1996) 385-97.

[63] J. Rocha, J. Klinowski, Solid-State NMR studies of the structure and reactivity of Metakaolinite, Angew. Chem. Int. Ed. Engl. 29 (1990) 553-554.
[64] W.D.A. Rickard, R. Williams, J. Temuujin, A.van Riessen, Assessing the suitability of the three Australian fly ashes as an aluminosilicate source for geopolymers in high temperature applications. Mater. Sci. Eng. A. 528 (2011) 3390-3397.
[65] F. Messina, C. Ferone, F. Colangelo, R. Cioffi, Low temperature alkaline activation of weathered fly ash: Influence of mineral admixtures on early age performance, Constr. Build. Mater. 86 (2015) 169-177.
[66] I. Ismail, S.A. Bernal, J.L. Provis, R. San Nicolas, S. Hamdan, J.S.J. van Deventer, Modification of phase evolution in alkali-activated blast furnace slag by the incorporation of fly ash. Cem. Concr. Compos. 45 (2014) 125-135.
[67] H. Xu, W. Gong, L. Syltebo, K. Izzo, W. Lutze, I.L. Pegg, Effect of blast furnace slag grades on fly ash based geopolymer waste forms, Fuel 133 (2014) 332-340.
[68] F. Pacheco-Torgal, J. Castro-Gomes, S. Jalali, Investigations about the effect of aggregates on strength and microstructure of geopolymeric mine waste mud binders, Cem. Concr. Res. 37 (2007) 933-941.
[69] L. Evangelista, J. de Brito. Mechanical behaviour of concrete made with fine recycled concrete aggregates, Cem. Concr. Compos. 29 (2007) 397-401.
[70] K. Komnitsas, D. Zaharaki, A. Vlachou, G. Bartzas, M. Galetakis, Effect of synthesis parameters on the quality of construction and demolition wastes (CDW) geopolymers, Adv. Powder Technol. 26 (2015) 368-376.
[71] G. Habert, C. Ouellet-Plamondon, Recent update on the environmental impact of geopolymers, RILEM Technical Letters 1 (2016) 17-23.
[72] J. He, J. Zhang, Y.Yu, G. Zhang, The strength and microstructure of two geopolymers derived from metakaolin and red mud-fly ash admixture: a comparative study, Constr. Build. Mater. 30 (2012) 80-91.
[73] X. Gao, Q.L. Yu, H.J.H. Brouwers, Reaction kinetics, gel character and strength of ambient temperature cured alkali activated slag-fly ash blends, Constr. Build. Mater. 80 (2015) 105-115.
[74] S. Onutai, S. Jiemsirilers, P. Thavorniti, T. Kobayashi, Aluminium hydroxide waste based geopolymer composed of fly ash for sustainable cement materials. Constr. Build. Mater. 101 (2015) 298-308.
[75] F. Pacheco-Torgal, J. Castro-Gomes, S. Jalali, Investigations about the effect of aggregates on strength and microstructure of geopolymeric mine waste mud binders, Cement and Concrete Research, 37(6) (2007) 933-941. Cem. Concr. Res. 37(6) (2007) 933-941.
[76] M. Cyr, R. Idir, T. Poinot, Properties of inorganic polymer (geopolymer) mortars made of glass cullet, J Mater Sci 47 (2012) 2782-2797.
[77] C. Isabella, G C. Lukey, H. Xu, J S.J. van Deventer, The Effect of Aggregate Particle Size on Formation of Geopolymeric Gel, Proceedings Advanced Materials for Construction of Bridges, Buildings, and Other Structures III, 2003.
[78] M. Pentrak, J. Madejova, P. Komadel, Acid and alkali treatment of kaolins .Clay Minerals, 44 (2009) 511523.
[79] N. Granizo, A. Palomo, A. Fernandez-Jiménez, Effect of temperature and alkaline concentration on metakaolin leaching kinetic. Ceramics International, 40 (2014) 8975-8985.
[80] W. Stumm, Reactivity at the mineral-water interface: dissolution and inhibition. Colloids and Surfaces - Physicochemical and Engineering Aspects, 120 (1997) 143-166.
[81] N. Huittinen, Th. Rabung, A. Schnurr, M. Hakanen, J. Lehto, H. Geckeisb, New insight into Cm (III) interaction with kaolinite – Influence of mineral dissolution Geochimica et Cosmochimica Acta. 99 (2012) 100-109.

[82] J.L. Provis, J.S.J. van Deventer, Geopolymerisation kinetics. 2. Reaction kinetic modelling, Chem. Eng. Sci. 62 (2007) 2309-2317.
[83] H. Rahier, J. Wastiels, M. Biesemans, R. Willlem, G. Van Assche, B. Van Mele, Reaction mechanism, kinetics and high temperature transformations of geopolymers, Mater. Sci. 42 (2007) 2982-2996.
[84] A. Favier, G. Habert, N. Roussel, J. d'Espinose de Lacaillerie, A multinuclear static NMR study of geopolymerisation, Cem. Concr. Res. 75 (2015) 104-109.
[85] M. Xia, H. Shi, X. Guo, Probing the structural evolution during the geopolymerization process at an early age using proton NMR spin-lattice relaxation, Mater. Lett. 136 (2014) 222-224.
[86] A. Autef, E. Joussein, G. Gasgnier, S. Rossignol, Role of the silica source on the geopolymerization rate: A thermal analysis study, J. Non-Cryst. Solids. 366, 2013, 13-21.
[87] H. Xu, Geopolymerisation of Aluminosilicate Minerals, PhD Thesis, Department of Chemical Engineering, University of Melbourne, Australia, 2001.
[88] X. Yao, Z. Zhang, H. Zhu et Y. Chen**,** Geopolymerization Process of Alkali-Metakaolinite Characterized by Isothermal Calrimetry, Thermochimica Acta, 493 (2009) 49-54.
[89] S. Alonso, A. Palomo, Calorimetric study of alkaline activation of calcium hydroxide-metakaolin solid mixtures, Cem. Concr. Res. 31 (2001) 25-30.
[90] M.L Granizo, S. Alonso, M.T. Blanco-Varela, A Palomo, Alkaline activation of metakaolin: Effect of calcium hydroxide in the products of reaction, Journal of the American Ceramic Society, 85 (2002) 225-231.
[91] Barbosa V.F.F, MacKenzie K.J.D, Thaumaturgo C, Synthesis and characterisation of materials based on inorganic polymers of alumina and silica: sodium polysialate polymers », International Journal of Inorganic Materials, 2 (2000) 309-317.
[92] J. Davidovits, Geopolymers - Inorganic polymeric new materials, Journal of Thermal Analysis, 37 (1991) 1633-1656.
[93] H. Wang, H. Li, F. Yan, Synthesis and mechanical properties of metakaolinite-based geopolymer, Colloids and Surfaces A: Physicochemical and Engineering Aspects. 268 (2005) 1-6.
[94] J. Davidovits, In: Davidovits J, Orlinski J (eds) Proceedings of geopolymer '88—first European conference on soft mineralurgy. Universite De Technologie De Compeigne, Compeigne, France, (1988) 149-166.
[95] P. Duxson, A. Fernandez-Jimenez, J. L. Provis, G. C. Lukey, A. Palomo, J. S. J. van Deventer Geopolymer technology: the current state of the art, J. Mater. Sci. 42 (2007) 2917-2933.
[96] Duxson, J.L. Provis, G.C. Lukey, F .Separovic, J.S.J Van Deventer. ^{29}Si NMR Study of Structural Ordering in Aluminosilicate Geopolymer Gels, Langmuir. 21 (2005) 3028.
[97] G. Engelhardt, D. Hoebbel, M. Tarmak, A. Samoson, E. Lippmaa. ^{29}Si-NMR-Untersuchungen Zur Anionenstruktur von Kristallinen Tetramethylammonium-alumosilicaten Und -alumosilicatlösungen. Zeitschrift Für Anorganische Und Allgemeine Chemie 484 (1982) 22-32.
[98] Fernandez Jimenez A, Palomo A, Sobrados I, Sanz J The role played by the reactive alumina content in the alkaline activation of fly ashes, Micropor Mesopor Mater. 91 (2006) 111.
[99] W.M. Kriven, J.L. Bell, M. Gordon, Microstructure and microchemistry of fully-reacted geopolymers and geopolymer matrix composites. Ceram Trans. 153 (2003) 227-250.

[100] M. Rowles, R. Matthew, B. H. O'Connor, Chemical and Structural Microanalysis of Aluminosilicate Geopolymers Synthesized by Sodium Silicate Activation of Metakaolinite, J. Am. Ceram. Soc. 92 (2009) 2354-2361.
[101] M. Rowles, et B. O'Connor. Chemical optimisation of the compressive strength of aluminosilicate geopolymers synthesised by sodium silicate activation of metakaolinite. J. Mater. Chem. 13 (2003)1161-1165.
[102] P. Duxson, J.L. Provis, G.C. Lukey, S.W. Mallicoat, W.M. Kriven, Understanding *the* relationship between geopolymer composition, microstructure and mechanical properties, Colloids Surf. A. 269 (2005) 47-58.
[103] M. Steveson, K. Sagoe-Crentsil. Relationships between composition, structure and strength of inorganic polymers. J. Mater. Sci. 40 (2005) 2023-2036.
[104] M. Lizcano, A. Gonzalez, S. Basu, K. Lozano, M. Radovic, Effects of Water Content and Chemical Composition on Structural Properties of Alkaline Activated Metakaolin-Based Geopolymers, J. Am. Ceram. Soc. 95 (7) (2012) 2169-2177.
[105] Y.M. Liew, H. Kamarudin, A.M. Mustafa Al Bakri, M. Bnhussain, M. Luqman, I. Khairul Nizar, C.M. Ruzaidi, C.Y. Heah, Optimization of solids-to-liquid and alkali activator ratios of calcined kaolin geopolymeric powder, Constr. Build. Mater. 37 (2012) 440-451.
[106] L. Atmaja, H. Fansuri, A. Maharani, Crystalline phase reactivity in the synthesis of fly ash–based geopolymer, Indo. J. Chem. 11 (2011) 90-95.
[107] A. Autef, E. Joussein, G. Gasgnier, S. Rossignol, Role of the silica source on the geopolymerization rate: A thermal analysis study, J. Non-Cryst. Solids. 366 (2013) 13-21.
[108] Z. Li, Y. Zhang, X. Zhou, Short Fiber Reinforced Geopolymer Composites Manufactured by Extrusion, Journal of Materials in Civil Engineering. 17 (2005) 624-631.
[109] W. Li, J. Xu, Mechanical properties of basalt fiber reinforced geopolymeric concrete under impact loading, Materials Science and Engineering: A. 505 (2009) 178-186.
[110] A. Natali, S. Manzi, M.C. Bignozzi, Novel fiber-reinforced composite materials based on sustainable geopolymer matrix, International Conference on Green Buildings and Sustainable Cities, Procedia Engineering. 21 (2011) 1124-1131.

CHAPITRE II

Matières premières, protocoles expérimentaux et techniques de caractérisation

I. INTRODUCTION

Ce chapitre présente les différentes matières premières utilisées lors de ces travaux et les protocoles expérimentaux pour la synthèse des matériaux de type géopolymères. Il présente également les différentes techniques de caractérisation physico-chimiques, structurales, microstructurales et mécaniques mises en œuvre.

II. LES DIFFERENTES MATIERES PREMIERES UTILISEES

1. Les précurseurs liquides

Six solutions commerciales de silicate (cinq solutions de silicate de potassium et une solution de silicate de sodium) ont été utilisées. Les données concernant les solutions sont répertoriées dans le **Tableau 1**.

Tableau 1 *: données relatives aux différentes solutions de silicate commerciales.*

	Nom	**Fournisseur**	**Si/M (M = Na ou K)**	**H_2O (% massique)**	**ρ (g/cm^3)**
Silicate de potassium	S_K0	Chemical labs[1]	1,69	76,0	1,18
	S_K1	Woellner[2]	1,70	76,0	1,18
	S_K2		1,52	68,7	1,31
	S_K3		0,67	59,4	1,51
	S_K4		0,45	52,7	1,65
Silicate de sodium	S_{Na}		1,70	64,2	1,36

2. Les précurseurs solides

Différents types de précurseurs solides ont été utilisés au cours de ces travaux. Les caractéristiques des différents précurseurs solides sont répertoriées dans le **Tableau 2**.

La préparation des solutions alcalines a été réalisée à l'aide d'hydroxyde de sodium ou de potassium ainsi que de silice amorphe. La synthèse des différents mélanges réactifs a été effectuée à l'aide de six métakaolins de pureté et de réactivité différente. En plus, une argile provenant de la carrière de Medenine située au sud de la Tunisie, caractérisée par une couleur rouge, a été utilisée. L'argile a été initialement concassée, broyée puis calcinée à 700°C pendant 5 heures et enfin tamisée jusqu'au passage au travers d'un tamis de 80 µm de granulométrie.

[1] Chemical Labs, 605 Springs Road, Bedford, MA 01730 (USA).
[2] Woellner GmbH, Wöllnerstraße 26, D-67065 Ludwigshafen, Germany.

***Tableau 2** : caractéristiques des différents précurseurs solides.*

	Nom	Fournisseur	Composition / pureté (%)	D_{50} (µm)	Si/Al	Méthode de calcination
Hydroxyde de sodium	NaOH	Sigma-Aldrich[3]	/ 97,0			
Hydroxyde de potassium	KOH		/ 85,2			
Silice amorphe	SiO_2		SiO_2 : 99,9	0,2		
Métakaolin	M1	Imerys[4]	SiO_2 : 55,0 Al_2O_3 : 40,0	10,0	1,17	Four rotatif
	M2		SiO_2 : 55,0 Al_2O_3 : 39,0	8,0	1,19	Four flash
	M3		SiO_2 : 54,0 Al_2O_3 : 46,0	6,0	1,00	Four statique
	M4		SiO_2 : 52,4 Al_2O_3 : 45,3	6,0	0,98	Four flash
	M5	Argeco[5]	SiO_2 : 59,9 Al_2O_3 : 35,3	20,0	1,44	
	M6		SiO_2 : 58,4 Al_2O_3 : 37,4	25,0	1,33	
Argile calcinée	Argile de medenine (Me)	Carrière de Medenine	SiO_2 : 59,8 Al_2O_3 : 21,8	8,0	2,33	Four statique

III. PROTOCOLES EXPERIMENTAUX

1. Synthèse des matériaux consolidés

Différentes formulations ont été synthétisées à partir de différentes solutions alcalines et sources d'aluminosilicates afin de vérifier la faisabilité des matériaux consolidés. Le protocole de synthèse est présenté sur la **Figure 1**.

Concernant les solutions alcalines, **le taux et la nature des espèces siliceuses en fonction du rapport Si/M et de la nature de cation** ont été étudiés. Les données relatives à ces solutions sont reportées en **Annexe II-A**.

Afin d'étudier les interactions entre les solutions et les métakaolins, **des mélanges à base de différentes solutions de silicate et métakaolins (My)** ont été formulés. Des pastilles de MOH (M= K ou Na) ont été dissoutes dans les solutions commerciales de silicate alcalins, afin de fixer le rapport Si/M à 0,5 et 0,7, respectivement pour les solutions à base de potassium (S_K1 et S_K3) et sodium (S_{Na}). La quantité de métakaolin ajoutée varie de 12 à 24 g.

[3] CABOT GmbH, Rheinfelden, Kronenstr.2, D-79618 Rheinfelden (Allemagne)
[4] AGS,F-17270 Clérac (France)
[5] Argeco Développement, Rue Fournie Gorre 47500 FUMEL (France)

La possibilité de **recyclage des déchets géopolymères** a été évaluée par broyage et tamisage à 80 µm des déchets puis réintégration comme source d'aluminosilicate par addition ou substitution du **20 % de la masse de métakaolin M1** en présence des solutions alcalines S_K1 et S_K3.

Des liants géopolymériques ont également été préparés à partir de métakaolin et d'argile Tunisienne calcinée. **Des mélanges de métakaolin (M3) et d'argile (Me)** avec des taux de substitution de 0 à 100% **en présence de la solution S_K1 avec différents rapports Si/K** (variant de 0,4 à 0,7) ont été analysés.

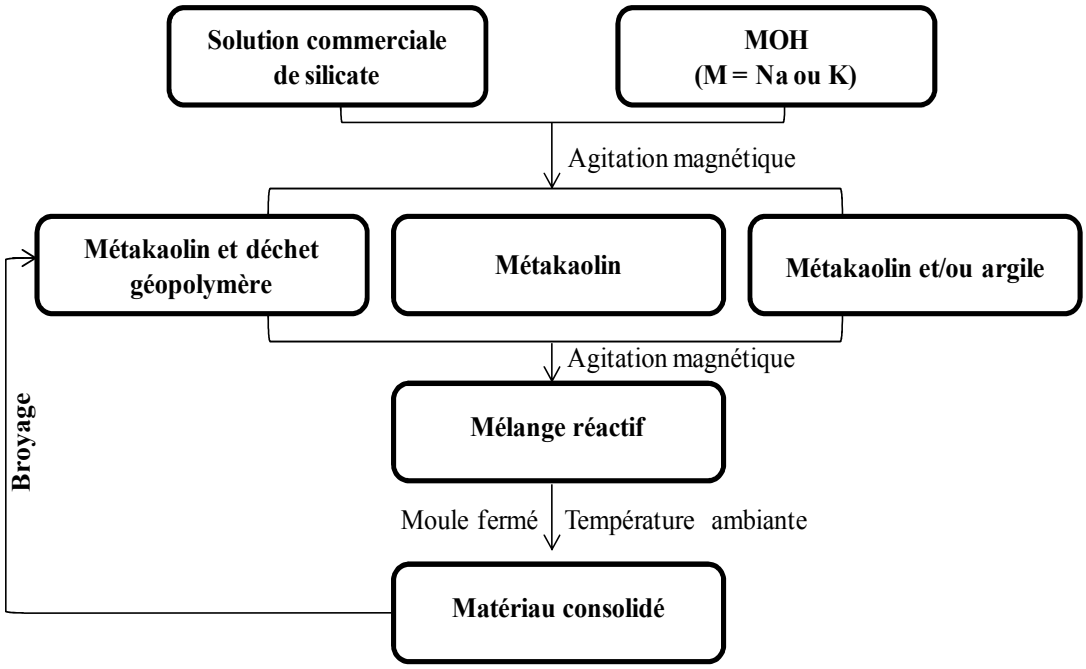

***Figure 1** : protocole de synthèse des matériaux géopolymères.*

2. Nomenclature

Les nomenclatures générales des différents types d'échantillons (**Figure 1**) sont répertoriées dans le **Tableau 3**. Les nomenclatures détaillées qui ont été utilisées pour désigner les différents échantillons tels que les solutions silicatées et les matériaux consolidés sont répertoriées en **Annexe II-A** et **Annexe II-B**.

Tableau 3 *: nomenclatures utilisées pour les différents types d'échantillons.*

Echantillonnage	Nomenclature
Solutions commerciales	$\mathbf{S_M}$
Solutions après ajout de l'hydroxyde alcalin	$\mathbf{S_M'}$
Matériaux géopolymères à base de métakaolin	$\mathbf{S_M My}$
Matériaux géopolymères à base de métakaolin et de géopolymère recyclé	$\mathbf{S_K x M1_{1\pm z} G_z}$
Matériaux géopolymères à base de métakaolin et d'argile de Medenine	$\mathbf{S_K 1^n M3_{1-w} Me_w}$

Les différents paramètres sont :

- « **S_M** » le type de la solution utilisé ($S_M = S_K x$ avec x varie de 0 à 4 ou S_{Na}),
- « **My** » le type de métakaolin (y allant de 1 à 6),
- « **G** » le géopolymère recyclé,
- « **z** » le taux de substitution ou d'addition de géopolymère broyé au métakaolin M1,
- « **n** » le rapport molaire Si/K de la solution alcaline (n variant de 0,4 à 0,7),
- « **Me**» l'argile de Medenine calcinée,
- « **w**» le taux de substitution du métakaolin M3 par l'argile Me (w= 0; 0,5; 0,75 et 1).

Par exemple, l'échantillon $S_K1^{0,7}M3_{0,5}Me_{0,5}$ est composé d'un mélange 50-50 de métakaolin M3 - argile Me et le rapport molaire Si/K de la solution alcaline après ajout de KOH à la solution de silicate S_K1 est égale à 0,7.

IV. TECHNIQUES DE CARACTERISATION

1. Caractérisations physico-chimiques

a. Mesure de la valeur de pH

Les mesures des valeurs de pH ont été réalisées à l'aide d'un appareil Schott Instrument Lab860 équipé d'une électrode pour pH basique à 25 °C. Afin de suivre la variation de la valeur de pH au cours de la réaction de géopolymérisation, les échantillons ont été placés dans des tubes (Ø : 35 mm et H : 70 mm) et recouverts d'eau en conservant les rapports masse de géopolymère sur masse d'eau ($m_{géopolymère}/m_{eau}$ = 0,08 [1]) pour chaque mesure. L'électrode a ensuite été placée dans le mélange et la valeur de pH a été relevée toutes les trois minutes.

b. Demande en eau (mouillabilité)

La demande en eau d'une poudre, exprimée en µL/g, correspond au volume d'eau qui peut être adsorbé par 1 gramme de poudre jusqu'à saturation. À cet équilibre, l'ensemble peut être représenté comme une association de particules dont les porosités intrinsèques et inter-particulaires sont comblées par le liquide. Cette grandeur dépend directement de la granulométrie, de la surface spécifique et de la morphologie de la poudre. Elle permet ainsi de caractériser la réactivité de la poudre vis-à-vis du liquide utilisé. L'évaluation de cette demande en eau a été effectuée de la façon suivante : un gramme de poudre est pesé puis déposé sur une lame de verre. A l'aide d'une micropipette, l'eau est ajoutée à la poudre (microlitre par microlitre) jusqu'à saturation visuelle de l'ensemble granulaire.

c. Mesure de la surface spécifique (BET)

La méthode BET (Brunauer, Emmett et Teller) est une technique permettant d'obtenir la surface spécifique d'une poudre mais aussi d'un milieu poreux. La surface spécifique ou aire massique d'une poudre est l'aire correspondant à la totalité des interfaces solide/gaz exprimée par unité de masse solide. Sa détermination expérimentale repose sur le principe d'adsorption d'azote à basse température. La méthode consiste à déterminer le volume d'une monocouche de molécules gazeuses adsorbées sur la surface de l'échantillon. La surface de la monocouche étant égale à celle du solide, connaissant le volume de gaz adsorbé, la surface spécifique de l'échantillon peut être déduite selon l'équation 1 **:**

$$S = (V_m * N_a * s) / (V_M * m) \qquad \textbf{Eq 1}$$

où S est la surface spécifique (m^2/g), Vm le volume de gaz adsorbé correspondant à une monocouche (cm^3/mol), N_a : nombre d'Avogadro (mol^{-1}), s la surface occupée par une molécule de gaz soit $16{,}2.10^{-20}$ m^2 pour l'azote, V_M le volume molaire de l'azote (cm^3) et m la masse de l'échantillon (g).

Les mesures ont été effectuées sur un appareil Micrometrics Tristar II 3020. L'échantillon est au préalable dégazé pendant quatre heures à 200 °C.

d. Porosimétrie par intrusion de mercure (PIM)

La porosimétrie par intrusion de mercure (PIM) permet d'évaluer la distribution en taille des pores ouverts et interconnectés et de déterminer de manière quantitative la structure poreuse des solides. La porosimétrie à mercure est basée sur la loi capillaire qui régit la

pénétration du liquide dans les pores de petite taille. Cette loi, dans le cas d'un liquide non mouillant tel que le mercure, est exprimée par l'équation de Washburn (**Équation 2**):

$$D = (1/P)*4\gamma\cos\varphi \qquad \textbf{Eq 2}$$

où D est le diamètre du pore, P est la pression appliquée, γ la tension de surface du mercure et φ l'angle de contact entre le mercure et l'échantillon.

Les tests de porosimétrie par intrusion de mercure sont réalisés à l'aide d'un porosimètre Micrometrics Autopore IV 9510 capable de détecter des pores dont le diamètre est compris entre 360 µm et 3 nm et un volume d'intrusion et d'extrusion de mercure de 0,1 µL. La pression de mercure augmente progressivement de 0,0007 à 413,6854 MPa. L'échantillon a été préalablement placé à l'étuve à 50 °C pendant 12 heures. L'étape de séchage permet l'élimination de l'eau pour ne pas empêcher par la suite l'insertion du mercure dans le réseau poreux [2]. Ensuite, l'échantillon est introduit dans un pénétromètre hermétique. Le pénétromètre est introduit dans une chambre basse pression pour les pores de taille élevée, puis dans une chambre haute pression pour déterminer les pores de plus faibles dimensions. La **Figure 2** présente l'évolution de la dérivée de volume d'intrusion de mercure en fonction de la taille des pores pour les échantillons $S_{Na}M2$ et $S_{Na}M5$. Les tailles médianes des pores sont de l'ordre de 0,026 µm et 0,056 µm pour les échantillons $S_{Na}M2$ et $S_{Na}M5$ respectivement.

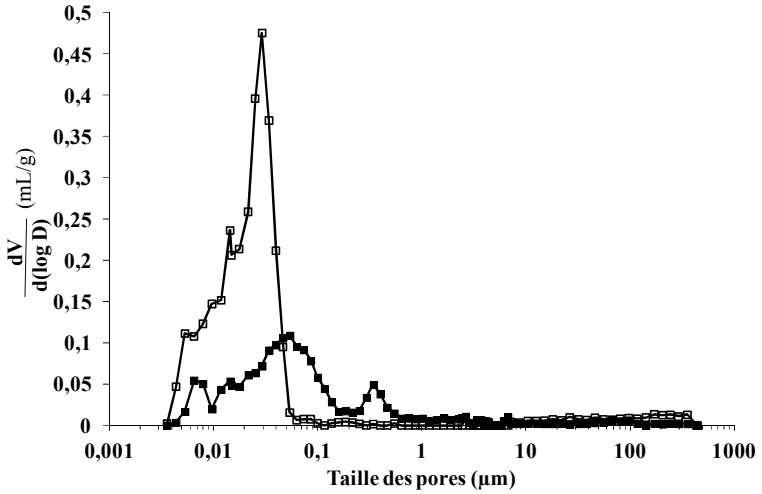

***Figure 2** : évolution de la dérivée de volume d'intrusion de mercure en fonction de la taille des pores pour les échantillons (□) $S_{Na}M2$ et (■) $S_{Na}M5$.*

2. Comportement en température : analyses thermiques

Ce type d'analyse permet de déterminer l'évolution thermique d'un échantillon en fonction du temps ou de la température. L'analyse thermique différentielle (ATD), couplée à l'analyse thermogravimétrique (ATG), met en évidence les changements d'états physico-chimiques des composés soumis à des variations de température. L'analyse thermique différentielle mesure la différence de température entre l'échantillon et un creuset vide servant de référence. Il est ainsi possible de suivre les transformations qui ont lieu aux différentes températures au sein de l'échantillon. L'analyse thermogravimétrique permet quant à elle de suivre l'évolution de la masse de l'échantillon lors d'un cycle thermique, révélant la perte d'eau ou d'espèces gazeuses.

Protocole expérimental

Les analyses ont été réalisées avec un appareil SDT Q600 TA Instruments, dans des creusets en platine sous un flux d'air de 100 cm^3/min. Les données sont ensuite traitées grâce au logiciel TA Universal Analysis.

Les solutions de silicate sans ou avec ajout d'hydroxyde alcalin ont été étudiées par analyse thermique. Le cycle utilisé est une rampe de 5 °C/min jusqu'à une température de 350 °C. Plusieurs pics endothermiques ont été observés à différentes températures inférieures à 200°C (**Figure 3 (a)**). Généralement, les deux pics détectés vers 40°C (I) et 95°C (II) et accompagnés par les pertes de masses les plus élevées sont attribués au départ de l'eau libre et physisorbée [3]. Le troisième pic au alentour de 114°C (III), accompagné d'une perte de masse moins importante, correspond au départ de l'eau liée. Enfin, un quatrième pic, observé vers 175°C (IV) et associé à une perte de masse très faible, est probablement du aux interactions ioniques entre les oligomères [4].

Afin d'étudier la formation des liants ainsi que leur comportement en température après consolidation, les analyses ont été réalisées selon le cycle suivant : un palier à 50 °C durant deux heures suivi d'une montée à 800 °C à une vitesse de 10 °C/min. À l'aide de la dérivée première du flux de chaleur en fonction du temps, il est possible de définir plusieurs phénomènes endothermiques intervenant lors de la formation du matériau [5] (**Figure 3 (b) et (c)**). Quatre zones peuvent êtres distinguées : la zone 1 correspond à la réorganisation des espèces, la zone 2 est attribuée à la dissolution de métakaolin, la zone 3 est relative à la formation des oligomères et la zone 4 est associée à la réaction de polycondensation. Il est également possible d'évaluer l'énergie nécessaire pour la formation des oligomères à partir de l'aire de pic endothermique de la zone 3.

Le comportement thermique des matériaux consolidés est analysé sur des matériaux préalablement broyés. Le cycle thermique utilisé est une rampe de 20 °C/min jusqu'à une température de 1350 °C. Les courbes ATD-ATG **(Figure 3 (d)**) obtenues permettent de déterminer le pourcentage d'eau contenu au sein du matériau consolidé.

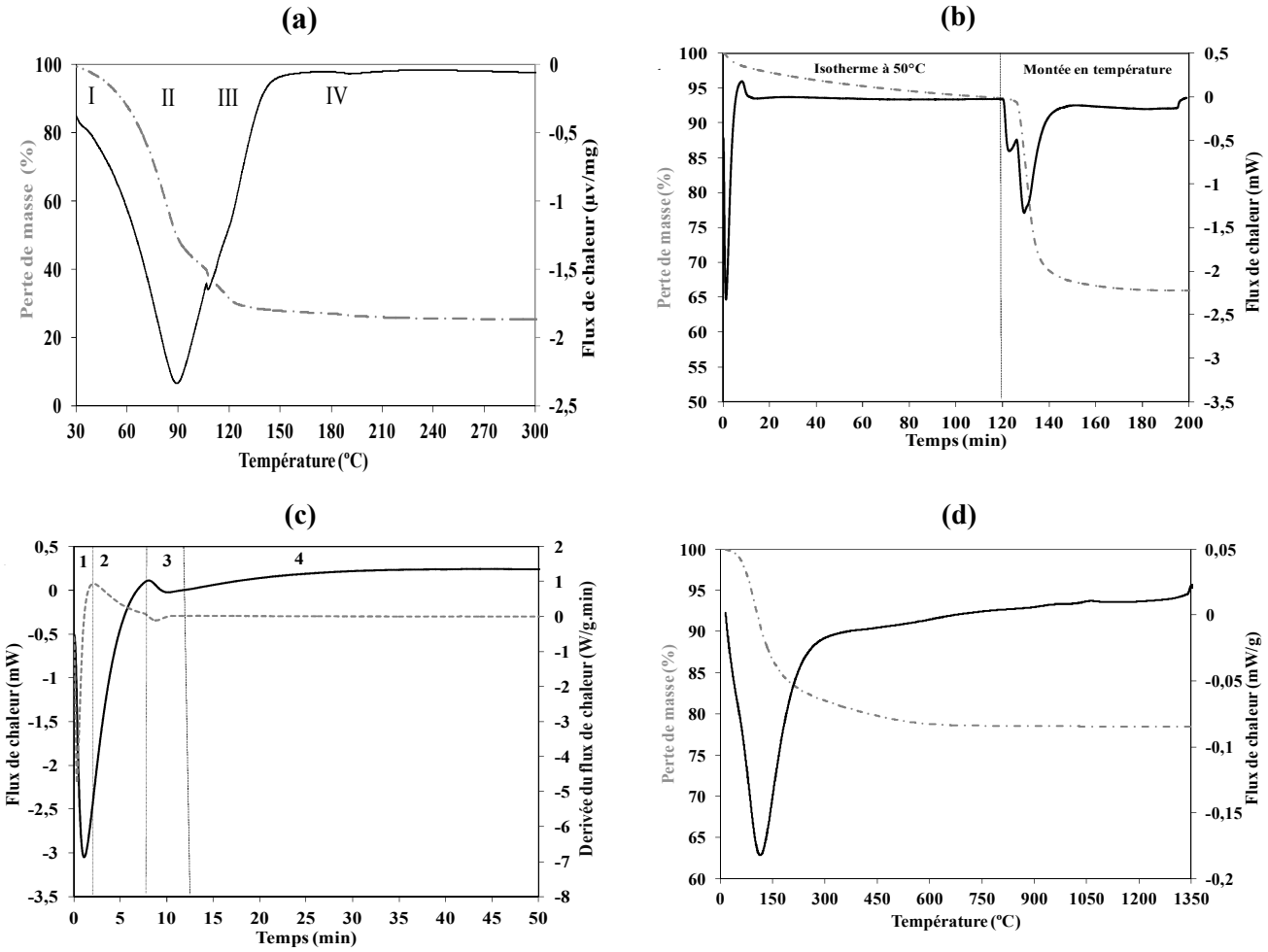

***Figure 3** : courbes d'ATD-ATG de (a) la solution S_K1, (b, c) la formation d'un liant $S_{Na}M1$ et (d) d'un géopolymère consolidé S_K3M1.*

3. Caractérisations structurales et microstructurales

a. Spectroscopie infrarouge à transformée de Fourier (IRTF)

La spectroscopie infrarouge permet de caractériser le matériau (liquide ou solide) à partir de son interaction avec le rayonnement infrarouge. Lorsqu'un échantillon est irradié, les liaisons chimiques qui sont excitées à leur énergie de vibration propre absorbent sélectivement le signal. Ainsi, le spectre obtenu permet d'identifier les différents groupements moléculaires présents dans l'échantillon. Les solutions de silicate ainsi que les matériaux

géopolymères sont composés d'un cation alcalin (noté M), de silicium et d'aluminium. La présence de ces trois éléments va induire un grand nombre de liaisons possibles (Si-O-Si, Si-O-Al, Si-O, Si-O-M, O-Si-O), possédant chacune différents modes vibrationnels.

Les mesures par spectroscopie infrarouge ont été réalisées sur un appareil ThermoFicher Scientific Nicolet 380 en mode ATR (Attenuated Total Reflectance). La poudre, la solution ou le mélange à étudier sont simplement déposés sur le diamant de l'appareil avant les acquisitions. Les acquisitions sont réalisées entre 500 et 4000 cm^{-1}, le nombre de scans est de 64 et la résolution de 4 cm^{-1}. Les données sont ensuite traitées grâce au logiciel OMNIC (Nicolet instrument). Le dioxyde de carbone de l'air produisant des perturbations du signal entre 2400 et 2280 cm^{-1}, une ligne droite est substituée à cette portion du spectre afin d'éliminer ce bruit de fond. Une correction automatique de la ligne de base et une normalisation des spectres sont également effectuées afin de permettre la comparaison des différents résultats.

Les solutions ont été étudiées par des mesures ponctuelles en déposant quelques gouttes de solution sur le diamant (**Figure 4 (a)**). Des analyses au cours de la formation d'un liant ont été réalisées en déposant quelques gouttes de milieu réactif sur le diamant. Les acquisitions se font alors toutes les 10 minutes pendant 13 heures. L'évolution des liaisons au sein du matériau est ainsi décrite par la superposition des 72 spectres obtenus (**Figure 4 (b)**). Suite au traitement des spectres, il est possible de tracer l'évolution de la position de bande Si-O-M (M = Si ou Al), traduisant la substitution des liaisons Si-O-Si par les liaisons Si-O-Al. La pente de la courbe durant les premières minutes de réaction permet d'évaluer la cinétique de substitution [6].

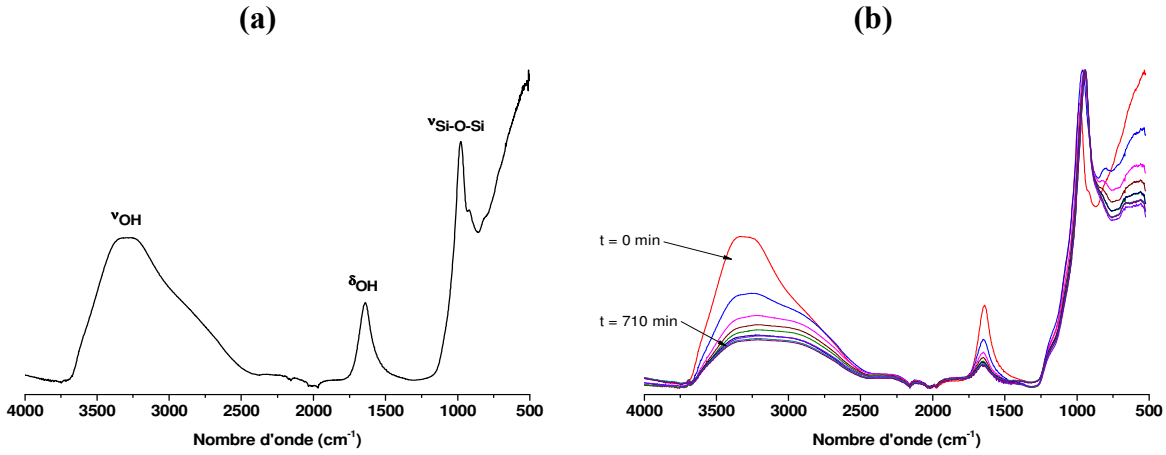

***Figure 4** : **(a)** Spectre IRTF de la solution S_K3 et **(b)** suivi de la formation de l'échantillon S_K1M1.*

b. Résonance magnétique nucléaire (RMN)

La spectroscopie par résonance magnétique nucléaire permet de caractériser les molécules ou les espèces chimiques, possédant un ou plusieurs noyaux magnétiques de spin nucléaire non nul (rapport gyromagnétique non nul). L'analyse des spectres de RMN renseigne sur l'environnement électronique du noyau (sphère de coordinence). Dans le cas des différentes formulations, les environnements du silicium (^{29}Si) et de l'aluminium (^{27}Al) ont été étudiés. Leurs caractéristiques intrinsèques en solution sont regroupées dans le **Tableau 4**. Les mesures de RMN sont réalisées à température ambiante à l'aide d'un spectromètre Bruker AVANCE-400 de l'ICMM à Madrid.

***Tableau 4** : principales caractéristiques des noyaux ^{27}Al et ^{29}Si [7].*

Noyau	Spin	Moment quadripolaire Q (10^{-28}m^2)	Abondance naturelle N (%)	Sensibilité (comparée au ^{1}H)	Rapport gyromagnétique	Fréquence de résonance (MHz) sous 9,7 T
^{27}Al	5/2	0,15	100,0	21.10^{-2}	6,976	104,26
^{29}Si	1/2	0,00	4,7	369.10^{-2}	-5,314	79,49

Protocole expérimental

RMN des liquides

Les solutions de silicates ont été analysées par RMN du silicium (^{29}Si). Les spectres ont été enregistrés avec une fréquence de résonance de 79,49 MHz. Les spectres en RMN du ^{29}Si (I = 1/2) ont été obtenus en mode statique avec une impulsion $\pi/2$ (4 µs) utilisant un filtre à 500 kHz pour améliorer le rapport signal sur bruit. Le nombre de scans collecté est de 400 et le temps entre chaque acquisition est de 10 secondes afin de minimiser les effets de saturation. Les déplacements chimiques du ^{29}Si ont été mesurés en utilisant un standard externe de tetraméthylsilane (TMS). L'erreur pour le déplacement chimique a été estimé inférieure à 0,5 ppm. L'erreur concernant la détermination des intensités relatives des différentes contributions a été évaluée inférieure à 5 %. Pour les mélanges réactifs géopolymères, la RMN de ^{27}Al en mode statique a été utilisée à différents temps de la formation à savoir 0, 2, 6 et 24 heures. Le ^{27}Al est un noyau quadripolaire (spin I> 1/2), ce qui signifie qu'il y a une distribution de charge asymétrique dans le noyau en raison de la non-symétrie des protons et des neutrons. La difficulté des noyaux quadripolaires implique une relaxation rapide à l'état liquide et un élargissement du premier et du second ordre dans un état solide [8]. Les niveaux d'énergie sont déplacés par l'interaction quadripolaire, ce qui peut limiter la détermination

quantitative des différentes contributions [9]. Cependant, à l'état liquide, l'interaction quadripolaire peut être négligée et la fréquence de nutation est assimilable à celle d'un spin 1/2 [10]. Une solution d'$AlCl_3$ a été utilisée comme référence. Les spectres RMN ont été enregistrés après une impulsion π/8 (1,5 ms) en utilisant un filtre de 1 MHz.

RMN des solides

Les métakaolins et les géopolymères consolidés ont été analysés par RMN-MAS haute résolution à température ambiante avec une sonde MAS tournant à 10 kHz. La fréquence de résonance utilisée est de 104,26 MHz pour le signal ^{27}Al et 79,49 MHz pour le signal ^{29}Si. Les spectres en RMN-MAS du ^{29}Si (I = 1/2) ont été obtenus avec une impulsion π/2 (4 µs) utilisant un filtre à 500 kHz. Afin d'enregistrer les transitions centrales de l'aluminium (^{27}Al) (I = 5/2), une impulsion de π/8 (1,5 µs) lui a été appliquée et un filtre à 1 MHz.

Pour l'ensemble des échantillons, les spectres obtenus en RMN du silicium ou de l'aluminium ont été traités et décomposés à l'aide du logiciel Winfit (Bruker). La **Figure 5** présente deux exemples de décomposition du spectre RMN ^{29}Si de la solution S_K1 (**Figure 5 (a)**), du géopolymère $S_{Na}M2$ (**Figure 5 (b)**), et deux autres exemples de décomposition de spectre RMN ^{27}Al du métakaolin M5 (**Figure 5 (c)**) et de mélange réactif S_K1M4 à t=2h (**Figure 5 (d)**). Les données relatives aux différentes contributions sont reportées en **Annexe II-C**.

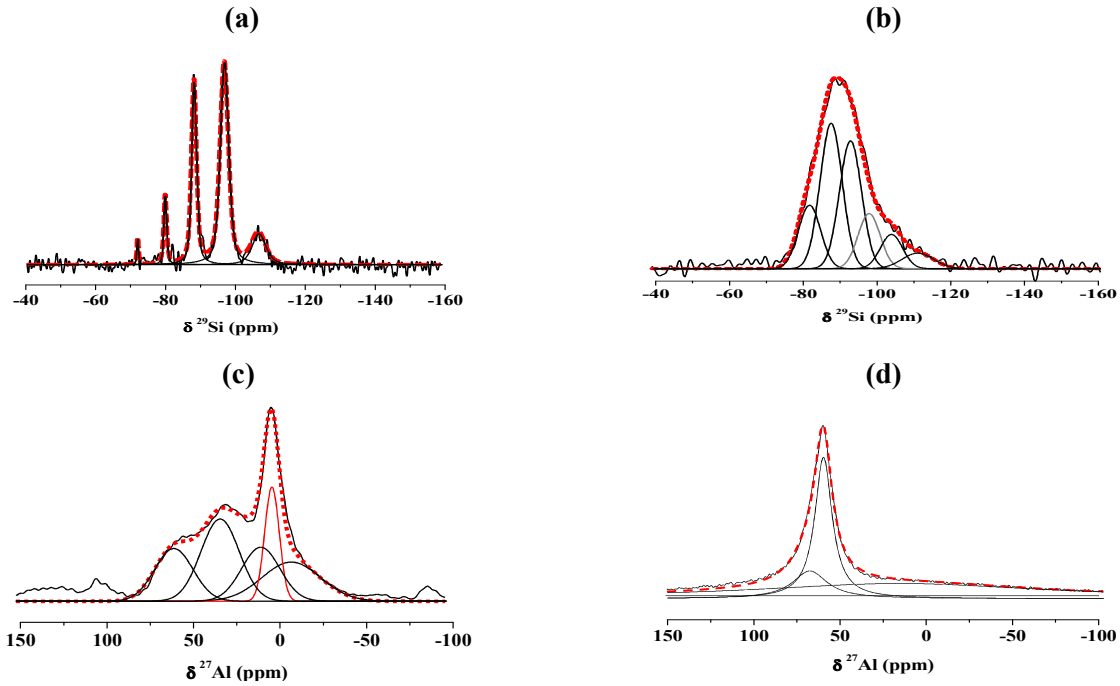

***Figure 5** : Exemples de décomposition des spectres RMN ^{29}Si de **(a)** la solution S_K1 et de **(b)** géopolymère $S_{Na}M3$ et des spectres RMN ^{27}Al du **(c)** métakaolin M5 et de **(d)** mélange réactif S_K1M4 à t=2h.*

c. Diffraction des rayons X (DRX)

La diffraction des rayons X est une technique d'analyse structurale fondée sur l'interaction entre les rayons X et la matière, consistant à envoyer un faisceau de rayons X de longueur d'onde λ sur un échantillon solide. Brièvement, lorsque cette longueur d'onde est du même ordre de grandeur que les distances inter-réticulaires (d), le faisceau est diffracté par les plans cristallins selon la loi de Bragg (**Équation** 3**)**. Les rayons diffusés interfèrent et conduisent au phénomène de diffraction.

$$2d_{hkl}\sin\theta=\lambda \qquad \textbf{Eq 3}$$

Les différents diffractogrammes ont été obtenus sur un appareil Brucker D8 équipé d'une anode en cuivre (CuKα =1,5418 Å) et d'un monochromateur arrière en graphite. Les échantillons sont préalablement broyés mécaniquement puis tamisés à 63 µm. La gamme d'analyse est comprise entre 5° et 120° (2θ). Le temps d'acquisition est de 0,5 s avec un pas de 0,014° (2θ). Les phases cristallines ont été identifiées par comparaison avec les fiches de références PDF (Power Diffraction File) du ICDD (International Center for Diffraction Data) à l'aide du logiciel EVA (Brucker-AXS). La **Figure 6** présente les diffractogrammes obtenus sur le métakaolin M1 et le géopolymère S_K1M1.

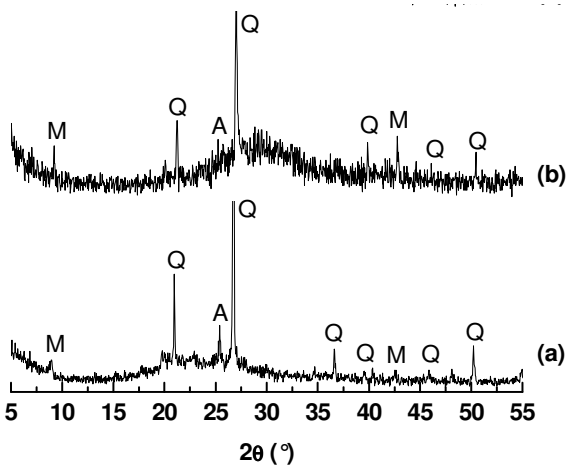

***Figure 6** : diffractogramme de (a) métakaolin M1 et de (b) géopolymère S_K1M1 (PDF files ; Q : quartz (01-078-1252), M : micas (00-002-0058), A : anatase (04-014-8515).*

d. Microscopie électronique

Microscopie électronique à balayage (MEB)

La microscopie électronique à balayage est une technique de caractérisation de surface permettant des observations jusqu'à l'échelle nanométrique. Son principe est basé sur l'interaction électron-matière. La détection des électrons secondaires et rétrodiffusés émis par

l'échantillon soumis à un faisceau électronique permet de reconstituer l'image de l'objet en contraste morphologique ou chimique respectivement.

Les observations ont été réalisées à l'aide d'un microscope électronique à balayage Cambridge Stereoscan S260 Instruments. Les échantillons sont préalablement métallisés au platine (Pt) et fixés sur un porte-échantillon à l'aide de pâte ou de pastille carbone.

Microscopie électronique en transmission (MET)

La microscopie électronique en transmission est la seule technique susceptible de donner des informations structurales et chimiques à l'échelle nanométrique. Brièvement, les électrons produits par la source sont accélérés puis focalisés sur l'échantillon par des lentilles condenseurs. Après l'interaction électron-matière, il apparaît à la sortie de l'échantillon un faisceau transmis et un ou plusieurs faisceaux diffractés. Il est ainsi possible de visualiser pour un même objet l'image correspondante, l'image du plan focal de la lentille objectif (diagramme de diffraction) et des analyses ponctuelles.

Les analyses ont été réalisées à l'aide d'un microscope électronique en transmission (MET) de type JEOL 2100F HR 200 kV. Cet appareil possède une imagerie conventionnelle à haute résolution (0,19 nm) et un détecteur pour la spectrométrie X (EDX). Les échantillons ont été préparés soit par dépôt goutte sur grille, soit en coupe par ultramicrotomie après inclusion dans une résine.

4. Essais mécaniques (compression)

Les essais de compression réalisés imposent la rupture de l'échantillon par un chargement dans une seule direction. Il permet de déterminer dans la direction de sollicitation, le module d'élasticité E et la contrainte maximale σ_{max} à la rupture nommée parfois résistance mécanique. Les mélanges réactifs sont placés dans des pots cylindriques (Φ = 15 mm et H = 49 mm. Les cylindres obtenus servent d'éprouvettes pour les essais de compression et sont démoulés juste avant l'essai. Ils sont rectifiés à l'aide d'une meule diamantée afin d'obtenir un élancement (hauteur/diamètre) au minimum égal à 2 [11] et des faces parfaitement parallèles et planes (**Figure 7 (a)**). Après rectification, l'éprouvette est centrée sur la presse d'essai. Pour pallier aux défauts de planéité des plateaux de la presse, du papier multi-plis est appliqué entre l'éprouvette et les deux plateaux. La répétition des essais permet de vérifier la répétabilité des résultats et d'éliminer les valeurs aberrantes liées à la présence de défauts au sein des éprouvettes.

Pour chaque composition de géopolymères, dix éprouvettes sont démoulées, rectifiées et testées après 7 jours. Les tests de compression sont réalisés à l'aide d'un appareil LLOYD EZ20 Instrument (AMETEK, UK) équipé d'une cellule de charge de 20 kN. Les éprouvettes sont soumises à une charge croissante jusqu'à la rupture à la vitesse de 0,1 $mm.min^{-1}$. La **Figure 7 (b)** présente les profils de contrainte en fonction de temps obtenus lors des essais sur l'échantillon S_K1M1 âgé de 7 jours. À partir de ces données, il est possible de calculer une valeur moyenne de contrainte à la rupture avec une erreur de plus ou moins 4 MPa.

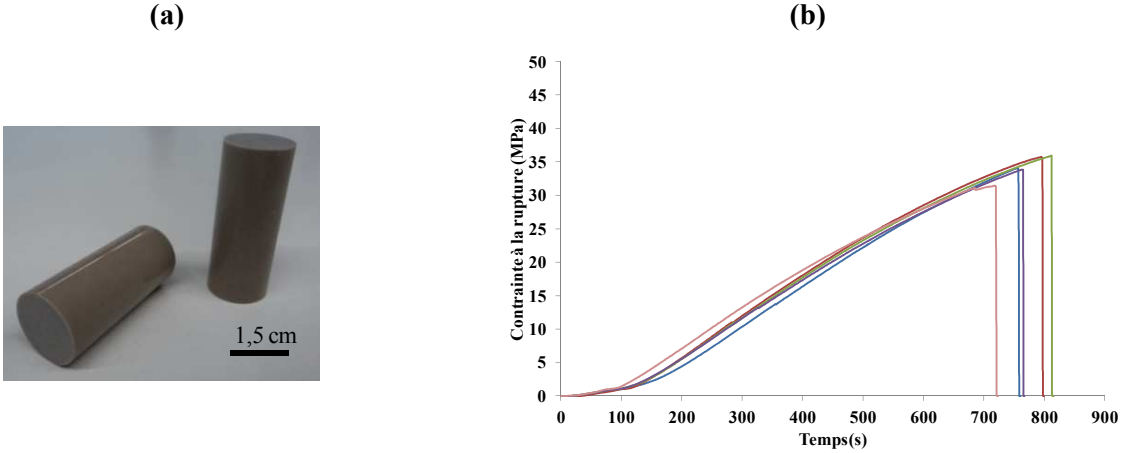

***Figure 7** : (a) éprouvettes de compression rectifiées et âgées de sept jours de l'échantillon S_K1M1 et (b) profils des courbes de contrainte à la rupture en fonction de temps.*

V. BIBLIOGRAPHIE

[1] E. Prud'homme, P. Michaud, E. Joussein, J.M. Clacens, S. Rossignol, Durability of inorganic foam in solution: The role of alkali elements in the geopolymer network, Corrosion Sci. 59 (2012) 213-221

[2] C. Galle, Effect of drying on cement-based materials pore structure as identified by mercury intrusion porosimetry - A comparative study between oven-, vacuum-, and freeze-drying, Cem. Concr. Res. 31 (2001) 1467-1477.

[3] K. B. Langille, D. Nguyen, J.O. Bernet, D.E. Veinot, Mechanism of dehydration and intumescence of soluble silicates. I, Effect of silica to metal oxide molar ratio. J. Mater. Sci. 26 (1991) 695-703.

[4] E. Prud'homme, P. Michaud, E. Joussein, A. Smith, C. Peyratout, I. Sobrados, J. Sanz, S. Rossignol, Geomaterial foams : role assignment of raw materials in the network formation. J Sol-Gel Sci. Technol. 61(2) (2012) 436-448.

[5] A. Autef, E. Joussein, G. Gasgnier, S. Rossignol, Role of the silica source on the geopolymerization rate: A thermal analysis study, J. Non-Cryst. Solids. 366 (2013) 13–21.

[6] E. Prud'homme, P. Michaud, E. Joussein, J.M. Clacens, S. Rossignol, Role of alkaline cations and water content on geomaterial foams: Monitoring during formation, J. Non-Cryst. Solids 357 (2011) 1270-1278.

[7] R.K. Harris, B.E. Mann. Introduction in NMR and the periodic table. Editions Academic Press of London, New York, San Francisco, 1978.
[8] D. Iuga, C. Morai, Z. Gan, D.R. Neuville, L. Cormier, D. Massiot, NMR Heteronuclear Correlation between Quadrupolar Nuclei in Solids, J. Am. Chem. Soc. 127 (2005) 11540-11541.
[9] P.P. Man and J. Klinowski, Quantitative Determination of Aluminium in Zeolites by Solid-state ^{27}AI N.M.R.Spectroscopy, J. Chem. Soc. Chem. Comm. 19 (1988) 1291-1294.
[10] A. Favier, Mécanisme de prise et rhéologie de liants géopolymères modèles, thèse Université de Paris-Est, 2013.
[11] ASTM D1633 – 00. Standard Test Methods for Compressive Strength of Molded Soil Cement Cylinders. 2007.

CHAPITRE III

Synthèse des résultats expérimentaux issus des publications

I. INTRODUCTION

Lors de cette étude, diverses solutions alcalines et sources aluminosilicates ont été utilisées afin d'exacerber leur effet sur la formation et la structure des matériaux géopolymères. Dans la première partie de l'étude, les paramètres qui régissent la réactivité des matières premières ont été identifiés à partir de trois solutions alcalines et six métakaolins. Ensuite, la faisabilité des matériaux géopolymères a été évaluée à partir des précurseurs précédemment caractérisés, afin de déterminer les domaines d'existence de ces matériaux dans le diagramme ternaire Si-Al-M/O. Une composition a été sélectionnée et caractérisée au sein de chaque ternaire afin d'évaluer l'effet des précurseurs sur les mécanismes de formation, la structure et les propriétés d'usage. Toutes ces données ont été exploitées pour étudier des liants à base de déchet géopolymère et lors de la valorisation d'une argile tunisienne de faible réactivité. Ainsi, un modèle de réactivité a été établi permettant de contrôler la réaction de géopolymérisation et les propriétés qui en découlent.

II. PARAMETRES INFLUENÇANT LA REACTIVITE DES MATIERES PREMIERES

Les données physicochimiques et structurales des matières premières, à savoir la solution alcaline et la source d'aluminosilicate, étant les paramètres cruciaux influençant la formation des matériaux géopolymères ont été déterminées. Cette partie est basée sur les résultats présentés au sein des publications ACL1, ACL2, ACL6 et ACL7.

1. Réactivité d'attaque de la solution alcaline

L'influence du taux et de la nature des espèces siliceuses sur la réactivité des solutions alcalines a été évaluée à partir de cinq solutions commerciales de silicate de taux d'eau et rapports molaires Si/M différents. Afin de faciliter l'exploitation des résultats et la comparaison entre les solutions, seules les données concernant les solutions S_K1, S_K3 et S_{Na} sont présentées.

Les solutions de silicate commerciales sans ou avec ajout d'hydroxyde alcalin (MOH avec M = K ou Na) ont été étudiées par analyse thermique (ATD-ATG) (**Figure 1. (a, b)**). Quelle que soit la solution, la différence entre les intensités des pics endothermiques et les pertes de masse associées suggèrent des différences d'interactions au sein des espèces silicatées entre

les trois solutions. Les attributions des différents pics ont été énoncées au chapitre II. Les deux solutions à base de potassium sont caractérisées par des différences de perte de masse (74 % et 54 % pour S_K1 et S_K3 respectivement) et d'intensité de pic endothermique dues au rapport Si/M et au taux d'eau différent. En effet, au sein de la solution S_K1, l'eau est facilement piégée dans la structure à cause de la taille plus élevée des anions [1] alors que la solution S_K3, contenant des espèces de plus petite taille, l'effet est moindre. Le changement de cation dans le cas de la solution S_{Na}, de taux d'eau similaire à S_K3, induit une perte de masse plus élevée (67 %). Ceci peut être expliqué par la différence de sphère d'hydratation de Na^+ comparé à K^+ entrainant un taux d'eau structurale supérieur qui sera éliminé en température [2]. Après ajout de MOH, la diminution des intensités des pics et des pertes de masse associées (**Figure 1. (c, d)**) révèle que l'addition de MOH entraîne la formation de colloïdes de plus petite taille.

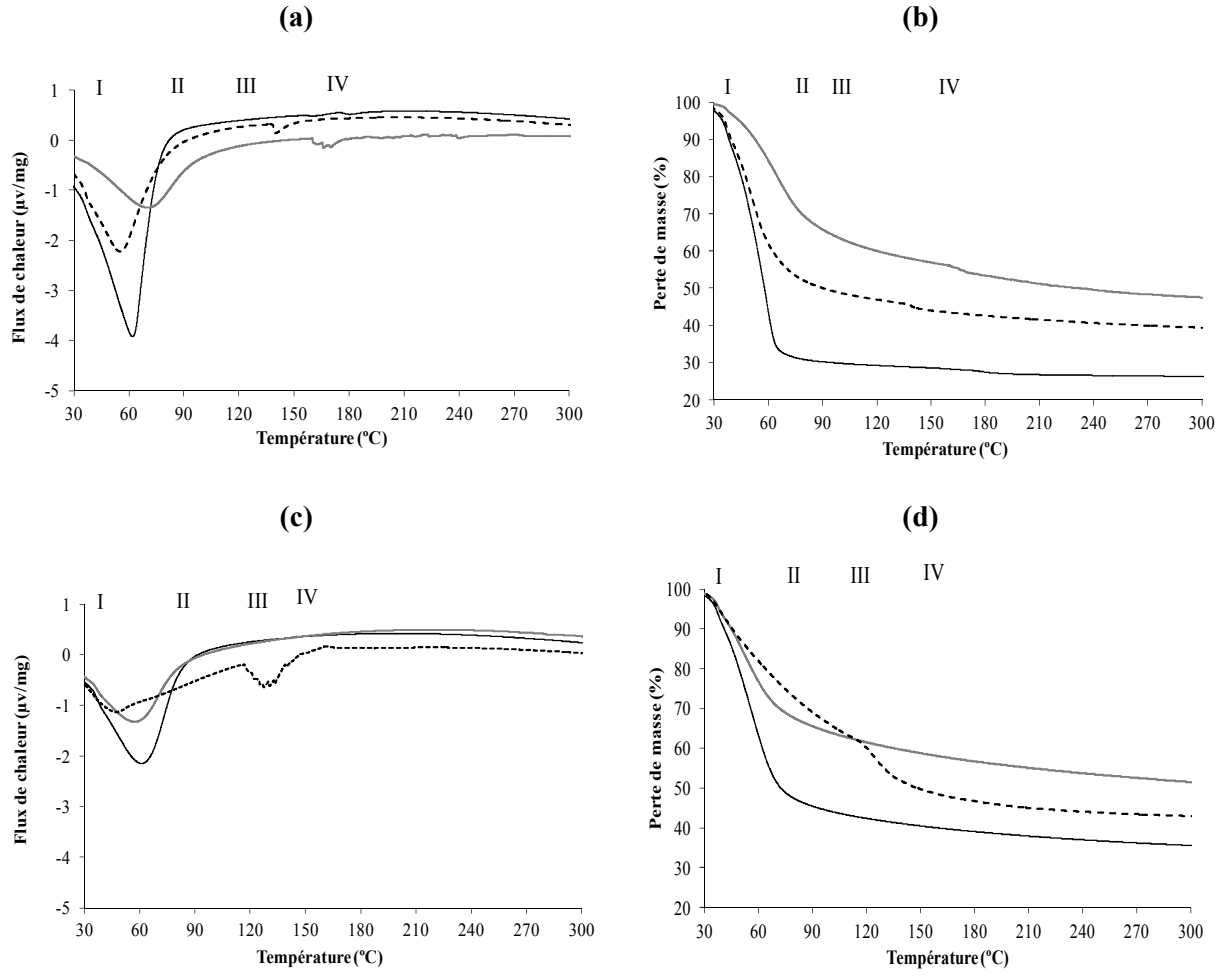

***Figure 1** : courbes ATD-ATG des solutions (A. a, b) avant et (B. c, d) après ajout de l'hydroxyde alcalin aux solutions (—) S_K1, (—) S_K3 et (---) S_{Na}.*

Afin de mieux comprendre les différences structurales, la **Figure 2** présente les spectres RMN de ^{29}Si obtenus pour les trois solutions précédentes. Les aires des différentes contributions et leurs attributions sont reportées en **Annexe III.A**. Les solutions S_K1 et S_{Na} (Si/M =1,7) sont majoritairement formées d'espèces siliceuses condensées de type Q^4, Q^3 et Q^2 [**3**]. Alors que dans le cas de la solution S_K3 (Si/K = 0,7), les espèces dépolymérisées (Q^0 et Q^1) prédominent ainsi que les espèces cycliques (Q^{2c} et Q^{3c}) [**4**]. L'ajout de l'hydroxyde alcalin entraîne à chaque fois une prédominance des espèces dépolymérisées (Q^0 et Q^1) et cycliques (Q^{2c} et Q^{3c}) soulignant à nouveau la dépolymérisation des solutions de silicate.

Compte tenu de la similitude des spectres, il est difficile d'exacerber les différences entre les solutions surtout après ajout de l'hydroxyde alcalin. Pour cela, le nombre d'atomes d'oxygène non pontants par tétraèdre (NBO/T) a été calculé selon la formule (NBO/T = ($3*Q^1 + 2*Q^2 + Q^3$)/100) [5] et tracé en fonction de la concentration en cation alcalin [M] pour toutes les solutions (**Figure 3**).

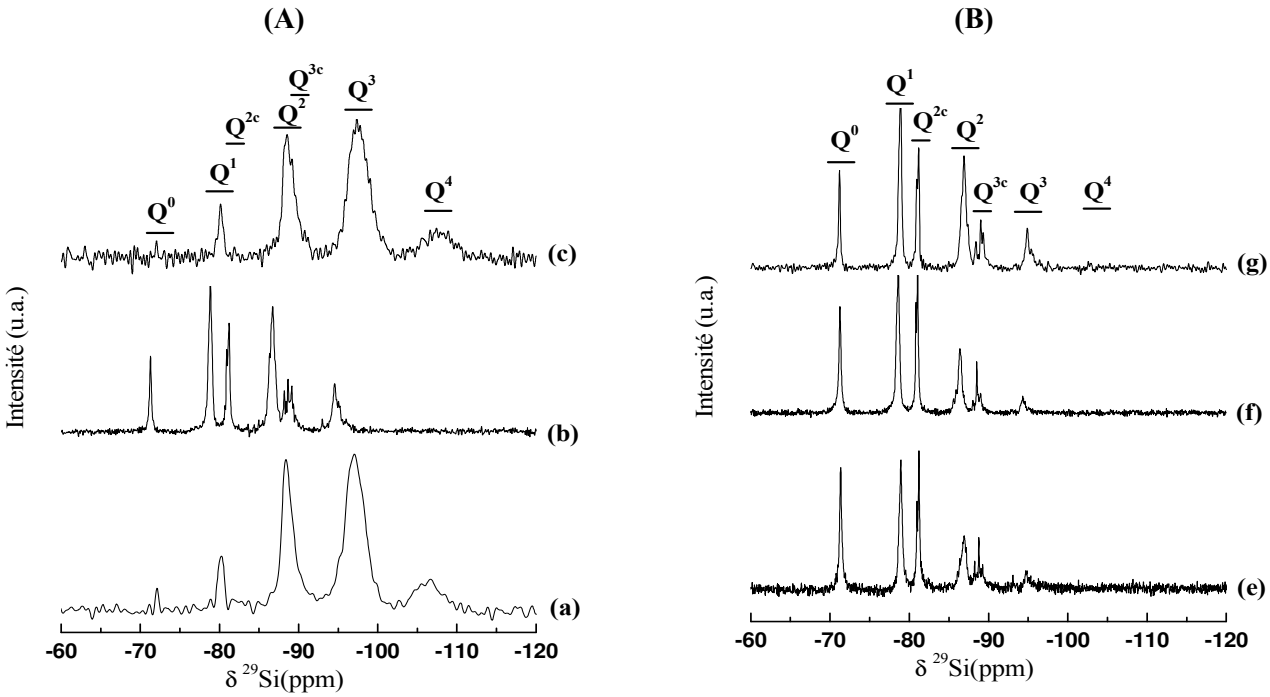

***Figure 2** : spectres RMN de ^{29}Si des (A) solutions mères (a) S_K1 (b) S_K3 et (c) S_{Na} et (B) des solutions après ajout d'hydroxyde alcalin (e) S_K1' (f) S_K3' et (g) S_{Na}'.*

La valeur de NBO/T augmente avec l'augmentation de la concentration en cation alcalin. Cela est en accord avec le degré de dépolymérisation lié au rapport Si/M. La concentration en cation alcalin et la valeur de NBO/T plus élevées dans le cas de S_K3 comparé à S_K1 et S_{Na} sont dues au rapport Si/M élevé et à l'abondance des espèces condensées dans S_K1 et S_{Na} (Q^4,

Q^3 et Q^2). Après ajout de l'hydroxyde alcalin, la concentration en cation alcalin de S_K3' (Si/M = 0,5) est plus élevée que celle de la solution S_K1'(8,88 et 5,04 mol.l^{-1} pour S_K3'et S_K1' respectivement) à cause des différents taux d'eau initiaux entrainant une valeur de NBO/T plus élevée. En effet, le cation alcalin agit comme un modificateur de réseau en rompant les liaisons entre les espèces siliceuses condensées dans la solution de silicate générant plus d'atomes d'oxygène non-pontants. Le changement de cation induit les mêmes phénomènes mais pour des rapports Si/M plus élevés (le NBO/T est égale à 1,87 pour un rapport Si/M de 0,7 et une concentration [M] de 8,3 mol.l^{-1}). La différence entre les cations alcalins de diffusion et de taille différente influence la nature et la quantité des espèces cycliques. En effet, des études de spectroscopie Raman [6] ont démontré l'existence des chaînes, des cycles et des monomères différents en fonction du cation alcalin et de rapport Si/M (**Annexe III. B**).

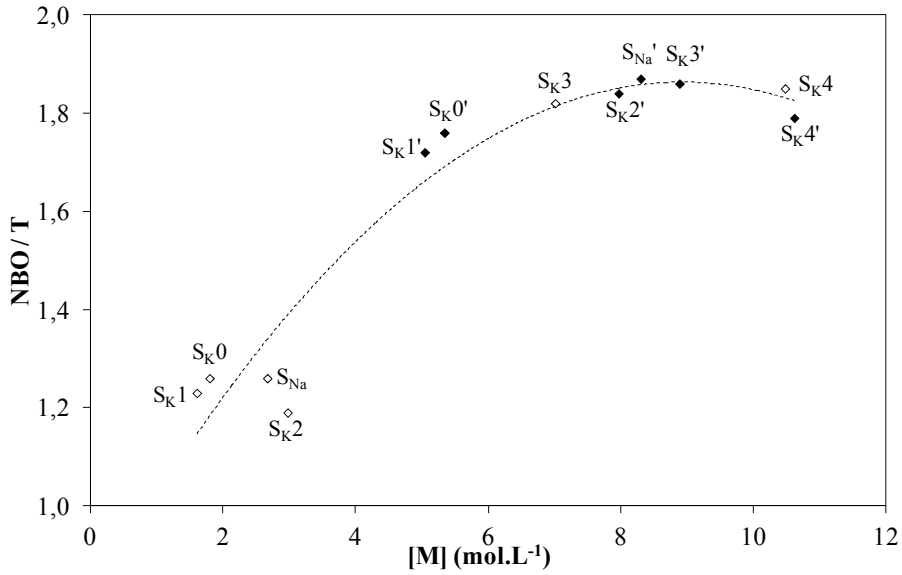

Figure 3 *: évolution du nombre d'atomes d'oxygène non-pontants (NBO/T) en fonction de la concentration en cation alcalin [M] pour les différentes solutions (◊) avant et (♦) après ajout de MOH.*

La réactivité d'attaque des solutions alcalines est contrôlée par le rapport molaire Si/M, le taux d'eau et la nature du cation alcalin. Il a été également mis en exergue un domaine de réactivité en fonction du rapport Si/M pour des solutions alcalines, compris entre 0,5 et 0,7.

2. Réactivité de surface de la source aluminosilicate

Après avoir déterminé les paramètres d'influence qui contrôlent la réactivité des solutions alcalines, l'étude s'est focalisée sur l'effet des propriétés physico-chimiques et structurales de six sources d'aluminosilicates ayant subi des modes de préparation différents (ACL2, ACL6 et ACL7). Les compositions minéralogiques ont été déterminées par diffraction des rayons X (**Figure 4. (A)**). Tous les métakaolins présentent un dôme amorphe et différentes phases cristallines indiquant différents degrés de pureté. Les métakaolins M3 et M4 sont les métakaolins les plus purs, alors que les metakaolins M1 et M2 contiennent des phases cristallines telles que le quartz, la kaolinite, la muscovite et l'anatase. Le taux d'impuretés augmente pour les métakaolins M5 et M6 puisqu'ils contiennent respectivement, de l'hématite, de la calcite et de la mullite.

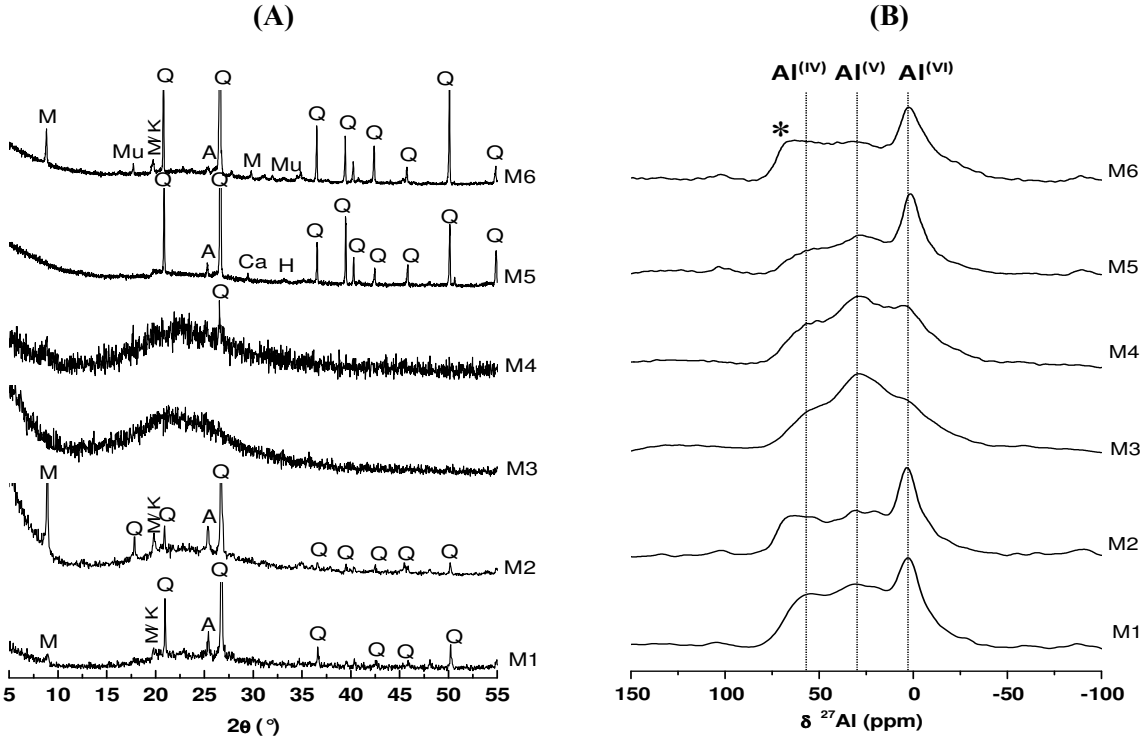

***Figure 4** : **(A)** diffractogrammes et **(B)** spectres RMN ^{27}Al des différents métakaolins (* $Al^{(IV)}$ de la mullite) des différents métakaolins. PDF files (Q: Quartz (01-083-2465), K: Kaolinite (00-012-0447), M: Muscovite (00-003-0849), A: Anatase (01-071-1166), H: Hematite (01-079-1741), Ca: Calcite (00-005-0586), Mu: Mullite (01-089-2814)).*

L'étude structurale par RMN ^{27}Al (**Figure 4. (B)**) corrobore les résultats de diffraction des rayons X, mettant en exergue les différentes proportions des contributions $Al^{(IV)}$, $Al^{(V)}$ et $Al^{(VI)}$ pour chaque métakaolin (**Annexe III. C**). Il est à noter que la distinction de la proportion d'aluminium tétraédrique ($Al^{(IV)}$) provenant des phases cristallines (muscovite et mullite) et

celle relative à l'aluminium tétraédrique propre à la phase amorphe de métakaolin plus réactif a été possible. Ceci permet de calculer la quantité d'aluminium réactif au sein de la source aluminosilicate.

De même, les données physicochimiques telles que la mouillabilité et le taux d'amorphe ont permis de distinguer la réactivité d'attaque vis-à-vis d'une solution [7]. Toutes ces caractéristiques ont donc permis d'estimer le taux de réactivité des métakaolins (**Figure 5**). Les évolutions quasi identiques de ces deux critères ont donc permis d'établir un ordre de réactivité de la source aluminosilicate qui est M4 ≥ M3 ≥ M2 > M1> M5 ≥ M6. Les métakaolins les plus réactifs sont caractérisés par des rapports molaires Si/Al faibles (Si/Al ≤ 1,2) et des valeurs élevées de mouillabilité (≥ 760 µl/g), de phase amorphe (≥ 63%) et de la proportion d'aluminium tétraédrique réactif (≥ 19%). La réactivité des métakaolins sera vérifiée par l'étude de leur comportement en présence de solutions alcalines.

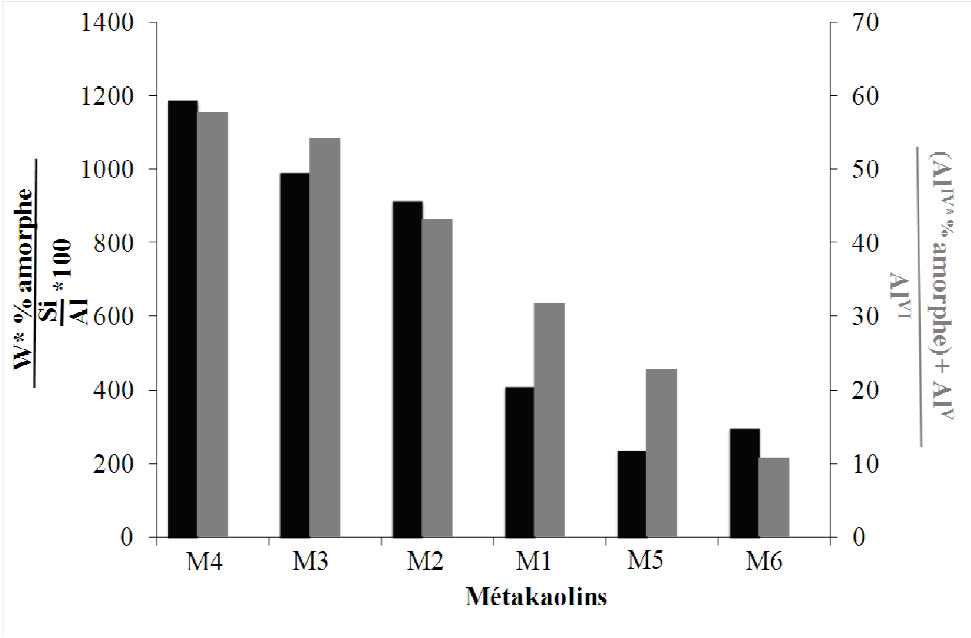

Figure 5 *: évaluation des taux de réactivité des différents métakaolins à partir de leurs caractéristiques (■) physico-chimiques et (■) structurales.*

La réactivité de surface de métakaolin est contrôlée par la valeur de la mouillabilité, du taux d'amorphe et de la proportion d'aluminium tétraédrique réactif.

III. FAISABILITE DES MATERIAUX GEOPOLYMERES A PARTIR DE DIFFERENTS METAKAOLINS ET SOLUTIONS ALCALINES

Après avoir identifié les paramètres responsables de la réactivité des matières premières, la faisabilité des matériaux géopolymères a été évaluée, à partir des solutions alcalines et des métakaolins précédemment caractérisés (ACL7).

1. Domaines d'existence des géopolymères dans le diagramme ternaire Si-Al-M/O

L'étude de faisabilité a été menée afin de déterminer les domaines d'existence des matériaux géopolymères dans le diagramme ternaire Si-Al-M/O [8]. Trente-six compositions pour chaque solution alcaline et métakaolin ont été évaluées. Ensuite, les matériaux géopolymères ont été identifiés en raison de leur homogénéité, leur aspect lisse et brillant et leur consolidation rapide (≤ 24 h). Des tests de suivi par spectroscopie infrarouge ont permis d'affiner la zone d'existence des matériaux géopolymères selon la composition molaire des mélanges réactifs (%Si, %Al et %K). La **Figure 6** présente les domaines pour les métakaolins M1, M2 et M5 en présence des trois solutions S_K1, S_K3 et S_{Na}. Les données relatives aux autres métakaolins sont reportées en **Annexe III. D**. En général, les domaines d'existence des matériaux géopolymères sont assez limités et dépendent des deux précurseurs utilisés. Pour la solution S_K1 (**Figure 6 (A)**), les zones des géopolymères sont similaires pour les métakaolins les plus réactifs (M1 et M2) alors qu'elle est très limitée dans le cas du métakaolin le moins réactif (M5) du à la faible quantité de phase aluminosilicate réactive disponible dans ce métakaolin.

Néanmoins, pour la solution S_K3 (**Figure 6 (B)**), les zones d'existence des géopolymères sont assez similaires quel que soit le métakaolin. Dans ce cas, la faible réactivité du métakaolin est compensée par la réactivité élevée de la solution alcaline.

Pour la solution S_{Na} **(Figure 6 (C))**, la zone est plus petite en présence du métakaolin M2 malgré sa réactivité élevée. Dans ce cas, la viscosité élevée de la solution S_{Na} [9] et la diffusion plus faible de l'ion sodium [10], en présence d'un métakaolin de valeur élevée de mouillabilité, ne permet pas des échanges facilités entre les espèces réduisant ainsi la faisabilité des mélanges.

Il existe donc une relation entre la faisabilité des matériaux géopolymères et la réactivité des matières premières.

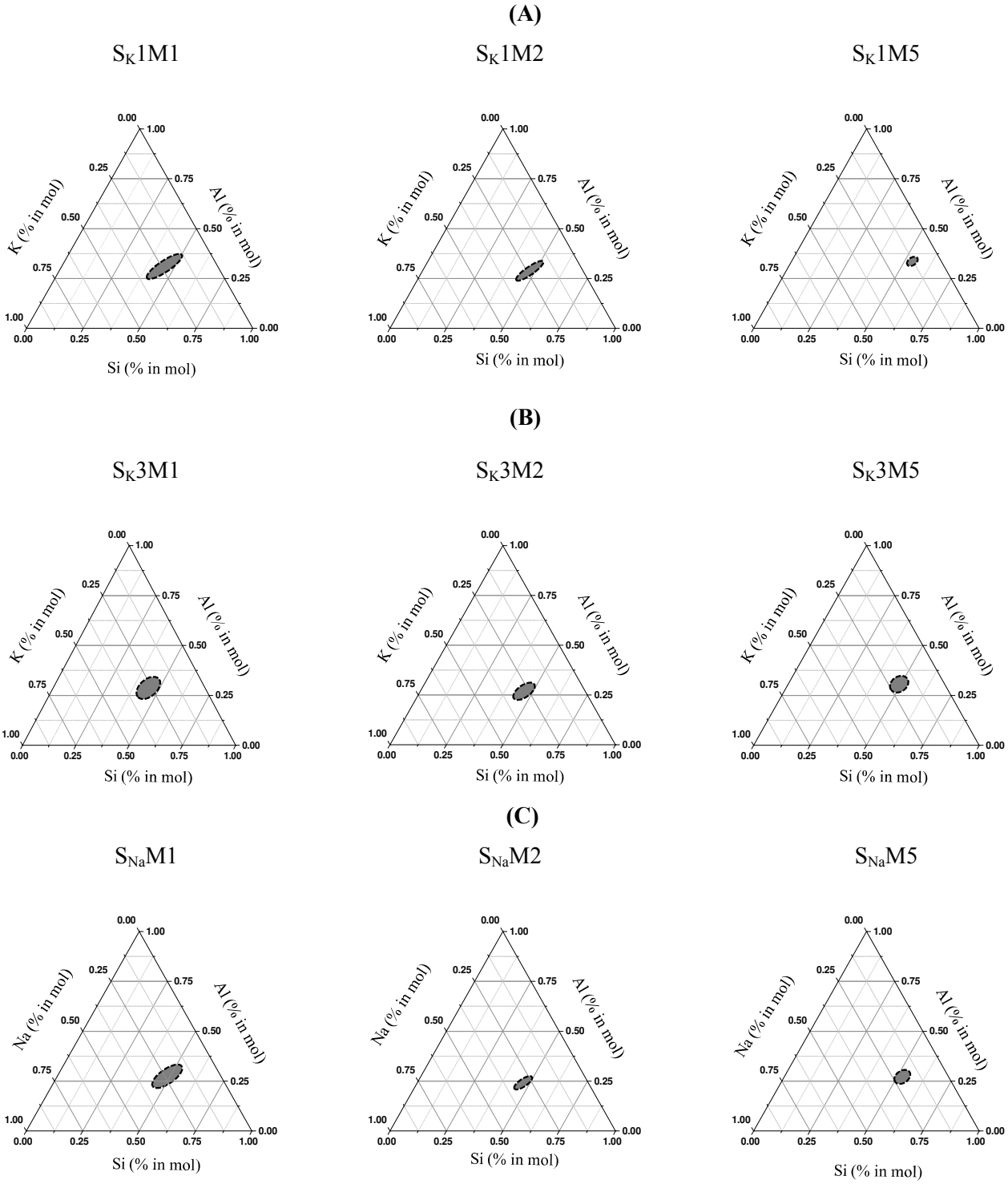

***Figure 6** : définition des domaines d'existence des matériaux géopolymères à partir des métakaolins M1, M2 et M5 en présence des solutions (A) S_K1 (B) S_K3 et (C) S_{Na}.*

2. Corrélation entre les domaines d'existence et les propriétés des matières premières

Pour faciliter l'exploitation des différents ternaires obtenus et corréler les zones d'existence à la réactivité des matières premières, les domaines de variation des rapports des concentrations en aluminium et en alcalin liés à la sphère de déplacement du cation M au sein du mélange réactif ([Al]*d_{M-O}) / [M]) ont été délimités pour tous les mélanges à base des différents métakaolins (**Figure 7**).

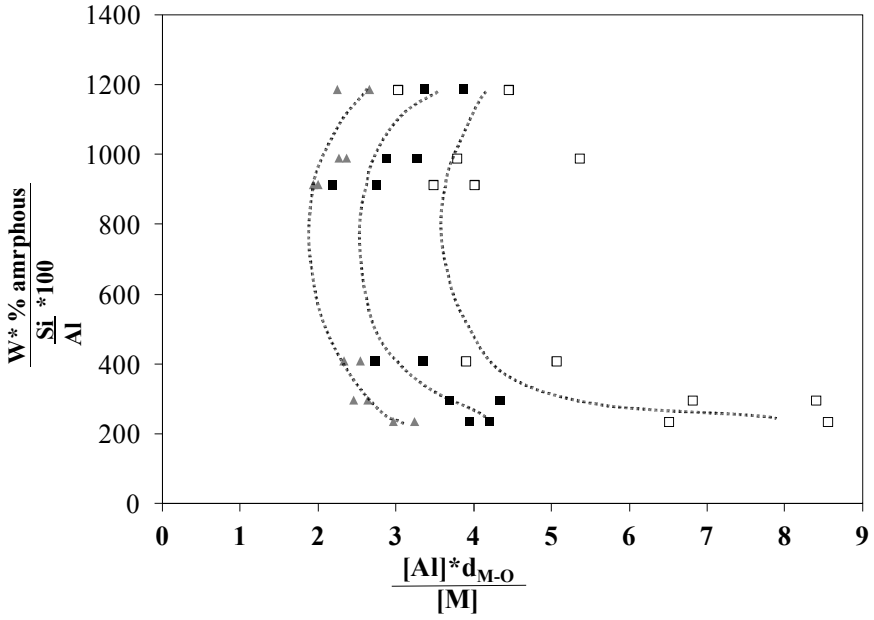

***Figure 7** : domaines de variation des concentrations au sein du mélange réactif ([Al]* d_{M-O})/ [M] permettant l'obtention des matériaux géopolymères pour les différents métakaolins en présences des solutions (□) S_K1, (■) S_K3 et (▲) S_{Na}.*

Trois mêmes comportements sont notables délimitant des fuseaux de rapport de concentrations qui dépendent des caractéristiques initiales des solutions d'activation. C'est pour des valeurs proches de concentrations en Al et en M que sont retrouvées les solutions S_{Na} et S_K3, alors que dans le cas de S_K1, les domaines de variation des concentrations sont plus étendus et décalés vers des valeurs de concentration en Al plus élevées. Ceci démontre qu'il sera possible de déterminer des zones de géopolymérisation pour des solutions très réactives et donc une cinétique de géopolymérisation plus favorisée. En revanche pour S_K1, il y aura un retard de réaction et il faudra un apport en aluminium plus important surtout dans le cas des métakaolins moins réactifs (M5 et M6). La légère différence entre S_{Na} et S_K3 est due à la différence de viscosité et d'espèces cycliques présentes. Ces courbes semblent être délimitées par un « nez de courbe ». Les courbes très rapides peuvent être reliées à des zones très

réactives de saturation pour les métakaolins de ((W*% amorphe)/((Si/Al)*100) > 700). A l'inverse, les courbes très lentes pour des faibles rapports sont en relation avec des zones de précipitation hétérogènes.

La concentration en alcalin et en aluminium ainsi que les caractéristiques des métakaolins conditionnent la faisabilité des matériaux géopolymères.

IV. EFFET DES PRECURSEURS SUR LE MECANISME DE FORMATION DES GEOPOLYMERES

Après avoir étudié l'effet des précurseurs sur les domaines d'existence des matériaux géopolymères dans le diagramme ternaire Si-Al-M/O et identifier les paramètres clés influençant la faisabilité, une composition a été sélectionnée et caractérisée au sein de chaque ternaire (**Annexe II-B)**, afin de comprendre l'effet des précurseurs sur les mécanismes de formation.

1. Cinétique de la réaction : analyse thermique in-situ

Cette analyse (ATD-ATG) in-situ renseigne sur la cinétique de la réaction à partir des différents phénomènes endothermiques et les pertes de masses associées aux différents mécanismes réactionnels de formation [11]. Cette partie se focalise sur l'effet de la réactivité des précurseurs sur la cinétique de formation des oligomères (**Chapitre II et ACL 6**). La **Figure 8 (a)** présente la variation de l'énergie nécessaire à la formation des oligomères, en fonction de la quantité d'aluminium responsable de cette formation (nAl) et le temps de début de formation de cette phase (t). Quel que soit l'échantillon, la valeur de l'énergie diminue pour un faible rapport nAl/t. La formation des oligomères intervient pour des temps courts pour les métakaolins les moins réactifs M5, M6, M1 et M3 comparé à M2 et M4. Ceci révèle une dissolution incomplète de ces métakaolins, en raison de leur plus faible capacité de libérer les espèces alumineuses et de la stabilité des impuretés dans un milieu alcalin. La faible disponibilité des espèces alumineuses réactives limite la formation des oligomères induisant une énergie supérieure (de 1,8 à 3,1 KJ / mol pour S_K1M2 et S_K1M5 respectivement). Ce résultat met l'accent sur l'importance de la spéciation en aluminium et la distribution des ions $[Al(OH)_4]^-$ dans la formation des matériaux géopolymères [12]. L'effet de la réactivité du métakaolin est donc plus prononcé en présence de la solution S_K1.

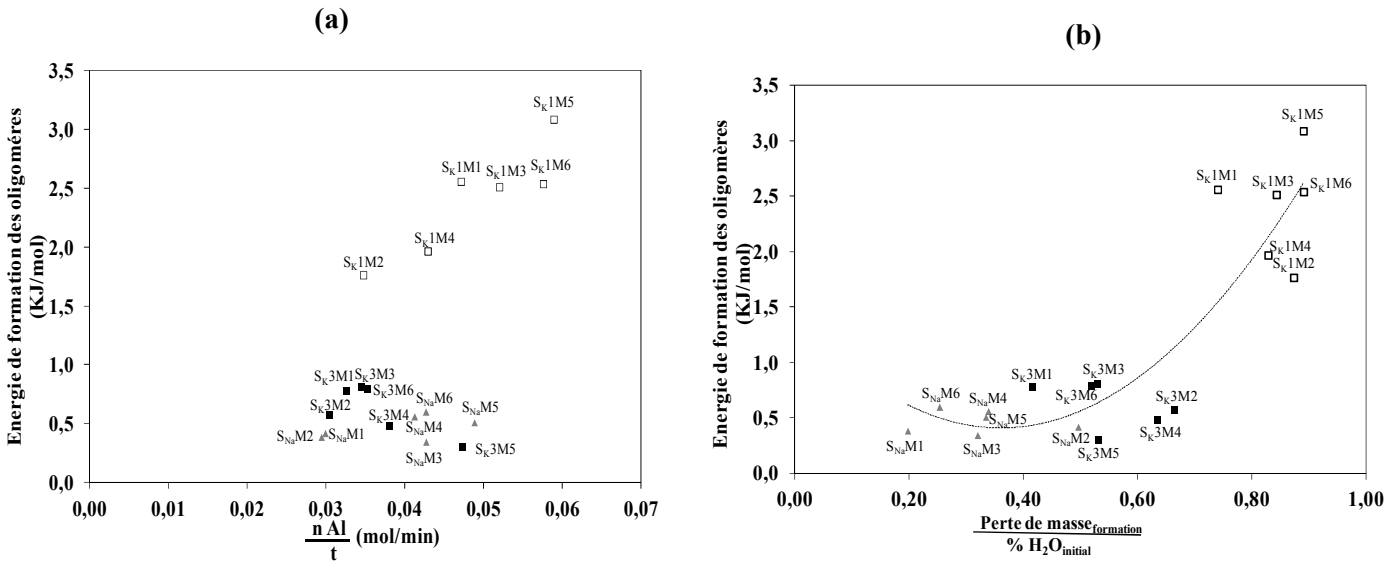

Figure 8 *: variation de l'énergie de formation des oligomères en fonction de* ***(a)*** *(nAl /t) et de* ***(b)*** *la perte de masse au cours de la formation pour les différents échantillons.*

Dans le cas des solutions S_{Na} et S_K3, l'effet de la réactivité plus élevée des solutions est notable et masque les différences induites par le métakaolin utilisé. La quantité plus importante d'espèces siliceuses dépolymérisées et d'atomes d'oxygène non pontants libérés permettent une meilleure dissolution des métakaolins même les moins réactifs (temps plus élevé) et une formation plus facile des oligomères (énergie plus faible).

Par conséquent, il apparaît que les différentes étapes de la réaction, en particulier la formation des oligomères, soient directement liées à la réactivité des précurseurs. Les solutions les plus réactives sont capables de contrebalancer la faible réactivité de métakaolin.

Afin de corréler la cinétique de formation à la perte d'eau durant la formation, la variation de l'énergie a été tracée en fonction de la perte de masse par rapport à la quantité d'eau dans le mélange initial pour les différents échantillons étudiés (**Figure 8 (b)**). Il est notable que les échantillons à base de la solution S_K1 libèrent plus d'eau durant la formation (0,74 à 0,89 pour S_K1M1 et S_K1M6) et nécessitent plus d'énergie pour former les oligomères. Alors que les échantillons à base des solutions S_{Na} et S_K3 présentent des valeurs d'énergie et des pertes d'eau plus faibles (de 0,41 à 0,66 pour S_K3 et de 0,20 à 0,34 pour S_{Na}). Ce résultat peut être expliqué par la teneur initiale plus élevée d'eau et la réactivité plus faible de la solution S_K1 par rapport aux solutions S_K3 et S_{Na}. En effet, une importante quantité d'eau à éliminer est un facteur inhibant pour la formation d'oligomères et les réactions de polycondensation [13], justifiant ainsi une énergie plus élevée nécessaire pour la formation des oligomères. Pour la solution S_K3, la plus faible connectivité entre les espèces siliceuses favorise la disponibilité

des ions OH^- [14] et accélère donc la formation d'oligomères. De plus, le comportement des mélanges à base de la solution S_{Na} est dû à la différence de taille et de la sphère d'hydratation des deux cations alcalins. En effet, l'énergie libre d'hydratation des ions Na^+ qui est supérieure à K^+ rend l'élimination de l'eau plus difficile dans le cas du sodium [15].

Ainsi, la disponibilité des espèces alumineuses et siliceuses et la nature de cation contrôlent la cinétique et l'énergie nécessaire pour la formation des oligomères.

2. Type de réseau formé : spectroscopie IRTF in-situ

L'analyse thermique in-situ fournit des informations sur la cinétique de formation mais ne permet pas d'appréhender l'effet des précurseurs sur l'évolution des liaisons et les réseaux formés à l'ordre local. C'est pourquoi les mélanges ont été étudiés par spectroscopie infrarouge in-situ. La **Figure 9** présente les valeurs de déplacement de la position de la bande Si-O-M en fonction des valeurs de pente obtenues pour les différents échantillons.

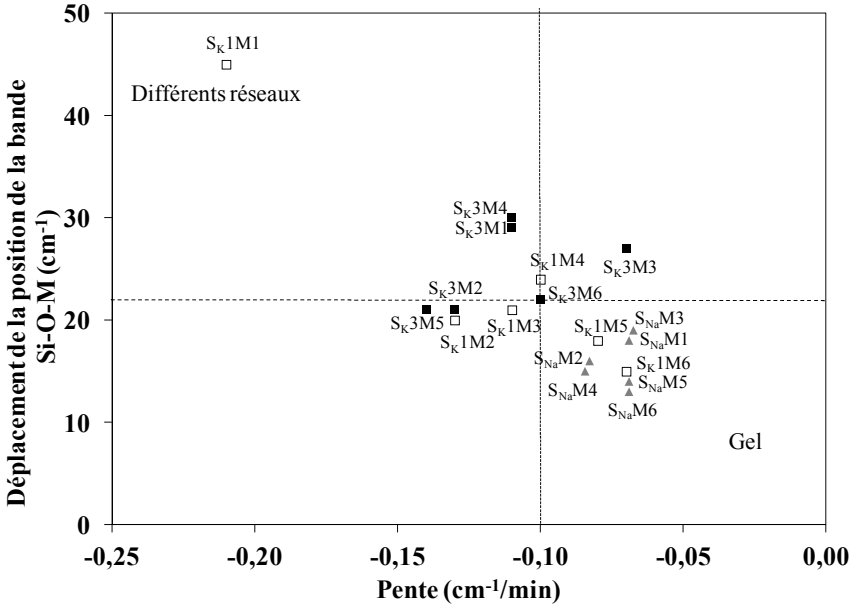

Figure 9 *: variation de la valeur de déplacement de la position de la bande Si-O-M en fonction de la pente pour les différents échantillons.*

En se basant sur des travaux antérieurs [16], il est possible de délimiter des zones indiquant le(s) réseau(x) formé(s) selon la valeur de déplacement et de la pente. Des valeurs très élevées de déplacement et de pente (> 35 cm^{-1} et > -0,15 cm^{-1}/min) renseignent sur la formation de différents types de liaisons chimiques et par conséquent la coexistence de différents réseaux. Tandis que des valeurs faibles de déplacement et de pente (< 15 cm^{-1} et < -

0,05 cm^{-1}/min) indiquent la formation d'un réseau de type gel. L'intersection de ces deux zones est associée à la formation d'un réseau géopolymère majoritaire.

En présence de la solution S_K1, et selon la réactivité de métakaolin, il y a formation d'un ou plusieurs réseaux. Plus le métakaolin est réactif, c'est à dire capable de libérer rapidement les espèces alumineuses et siliceuses, plus la formation de réseau géopolymère est favorisée. Avec la solution S_K3, quel que soit le métakaolin, la réactivité de la solution favorise la formation de réseau géopolymère au détriment des autres réseaux. Les espèces siliceuses très réactives, provenant de cette solution, favorisent la dissolution des métakaolins, même les moins réactifs, et facilitent la formation des oligomères et les réactions de polycondensation.

Les échantillons à base de S_{Na} sont situés à la limite entre la zone géopolymère et la zone des gels. Ce résultat ne contredit pas les résultats précédents concernant la réactivité élevée de la solution S_{Na}. Les valeurs de pente plus faibles peuvent être dûes à la plus faible diffusion du cation Na comparé à K ce qui peut ralentir la cinétique de la réaction.

La réactivité des précurseurs est responsable de la formation d'un ou plusieurs réseaux.

3. Taux de la réaction : RMN de ^{27}Al in-situ

Afin d'avoir des informations structurales détaillées sur la formation des géopolymères en fonction de la réactivité des précurseurs, douze mélanges réactifs à base des solutions S_K1 et S_K3 et les différents métakaolins ont été étudiées par RMN ^{27}Al à différents temps de la réaction (0, 2, 6 et 24 heures). Un exemple des spectres obtenus pour l'échantillon S_K1M2 est présenté sur la **Figure 10 (A).** L'allure des spectres obtenus dépend de la nature du métakaolin (**Figure 4**) et de l'interaction avec la solution alcaline. En effet, cette dernière se traduit d'une part par la consommation de l'aluminium pentacoordiné et hexacoordiné ($Al^{(V)}$ et $Al^{(VI)}$) indiquant la dissolution de métakaolin et d'autre part par l'augmentation de la contribution de l'aluminium tétracoordiné ($Al^{(IV)}$) indiquant la formation de réseau géopolymère [17, 18, 19]. Afin de comparer les différents échantillons, le taux de formation d'$Al^{(IV)}$ a été tracé en fonction du temps dans la **Figure 10 (B)** pour deux métakaolins (M1 et M4) et deux solutions (S_K1 et S_K3) de différentes réactivités.

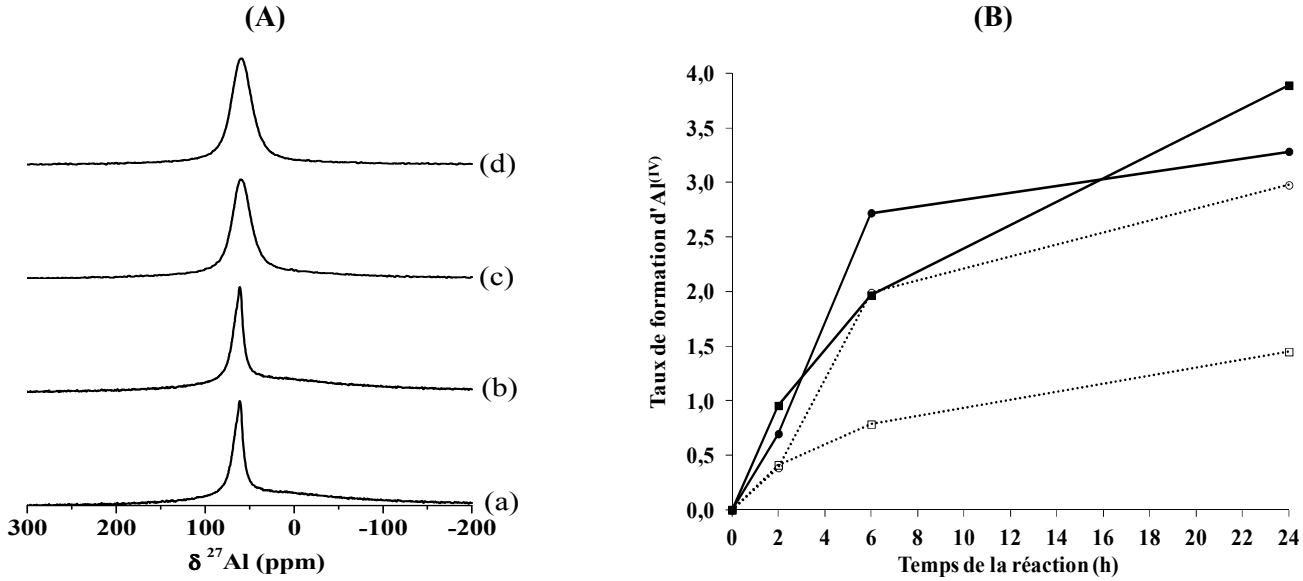

Figure 10 : (A) *exemple de spectres RMN ^{27}Al obtenus à* ***(a)*** *0,* ***(b)*** *2,* ***(c)*** *6 et* ***(d)*** *24 heures pour l'échantillon S_K1M4* et ***(B)*** *d'évolution du taux de formation d'$Al^{(IV)}$ ($Al^{(IV)}_{ti}$- $Al^{(IV)}_{t0}$) / $Al^{(IV)}_{t0}$) en fonction du temps pour les échantillons (□) S_K1M1, (○) S_K1M4, (■) S_K3M1 et (●) S_K3M4.*

Des différences sont mises en exergue en fonction de la réactivité des précurseurs. Par exemple, l'utilisation d'un métakaolin plus réactif (M4 comparé à M1) permet une augmentation importante de la formation des espèces $Al^{(IV)}$ surtout à partir de deux heures de réaction. De même, en présence d'une solution plus réactive (S_K3 comparé à S_K1), la formation des $Al^{(IV)}$ semble être plus facile, plus rapide et plus favorisée. Ces résultats sont en accord avec les données d'analyse thermique et de spectroscopie IRTF confirmant que la cinétique et le taux de la réaction dépendent de la réactivité des précurseurs. Le rôle de la source d'aluminosilicate est lié à la disponibilité des espèces d'aluminates réactives (en particulier $Al^{(IV)}$ et $Al^{(V)}$) jouant un rôle thermodynamique, tandis que l'influence de la réactivité de la solution alcaline est d'ordre cinétique. En effet, les espèces réactives de la solution alcaline sont capables d'induire des réactions de polycondensation, même à partir d'espèces aluminosilicates les moins réactives pour former le réseau géopolymère.

L'évolution structurale du mélange réactif est fortement liée à la réactivité des précurseurs.

V. EFFET DES PRECURSEURS SUR LES RESEAUX STRUCTURAUX ET LES PROPRIETES FINALES

Les spécificités observées au niveau du mécanisme de formation selon la réactivité des précurseurs utilisés, laissent présager des différences de structure et de propriétés d'usage des matériaux finaux.

1. Statuts de l'eau et structure poreuse

L'eau, étant un facteur important influençant la structure des matériaux géopolymères, a été évaluée par analyse thermique. L'évolution de la perte de masse à 800°C par rapport à la quantité d'eau présente au sein d'une mole de mélange initial a été tracée en fonction de l'énergie d'oligomèrisation dans la **Figure 11**. La perte de masse, diminuant quand l'énergie augmente, révèle que plus la cinétique de formation est rapide, plus l'eau reste piégée dans les pores ou liée dans le réseau géopolymère. De plus, il est noté une quantité d'eau plus importante piégée dans les échantillons à base de solution S_{Na} par rapport à celles à base de S_K3 et S_K1. Ce résultat peut être expliqué par la différence de sphère d'hydratation entre les deux cations alcalins, en effet le cation sodium contient six molécules d'eau alors que le cation potassium en possède que quatre.

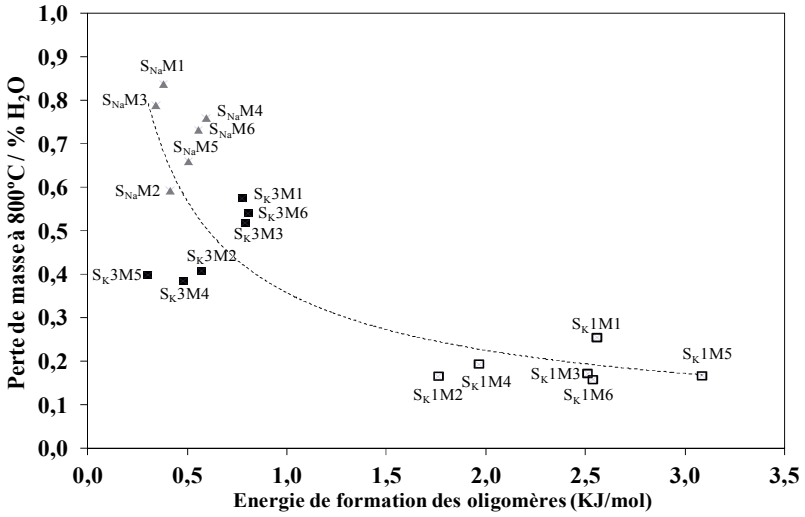

Figure 11 *: évolution de la perte de masse à 800 °C en fonction de l'énergie de formation des oligomères.*

Afin de mieux comprendre les différences observées par analyse thermique, des tests de porosimétrie par intrusion de mercure ont été réalisés sur neuf échantillons à base de trois

métakaolins de différentes réactivités M1, M2 et M5 et les trois solutions S_K1, S_K3 et S_{Na}. La variation de la porosité et de la taille des pores en fonction des caractéristiques structurales des métakaolins déterminées par RMN ^{27}Al sont présentées sur la **Figure 12**.

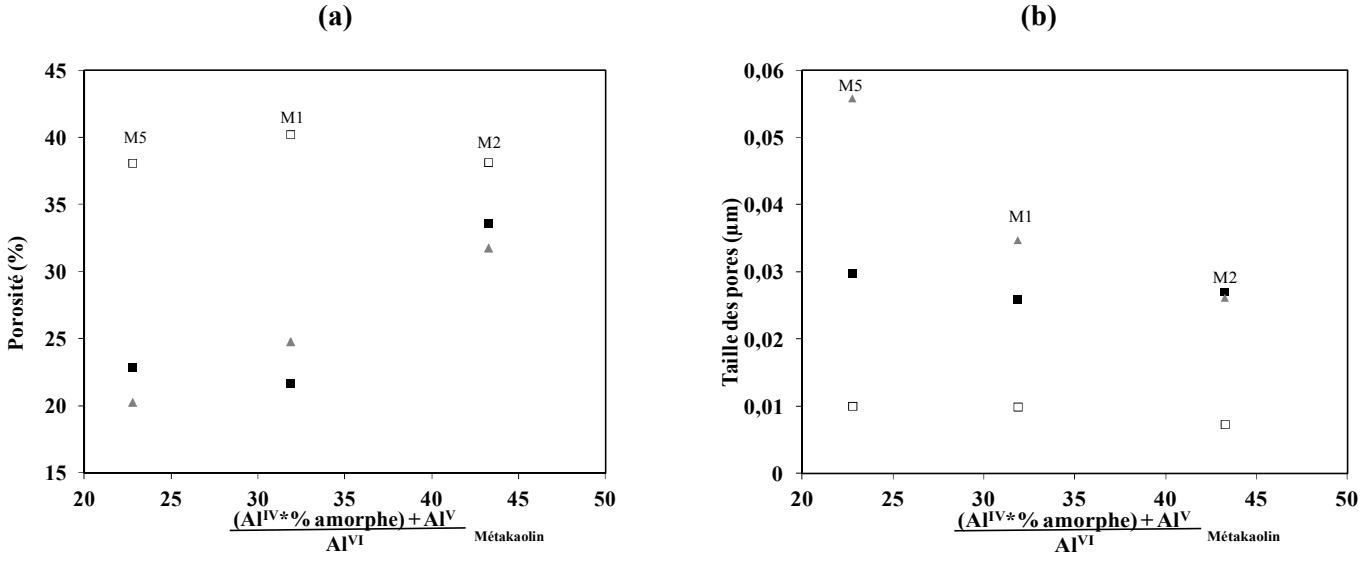

***Figure 12** : variation de **(a)** la porosité et de **(b)** la taille des pores en fonction des caractéristiques structurales des métakaolins (M1, M2 et M5) en présence des solutions (□) S_K1, (■) S_K3 et (▲) S_{Na}.*

Deux comportements sont notables à savoir : (i) les échantillons à base de la solution S_K1 de taux de porosité similaires (entre 38 et 40%) mais de tailles de pore différentes (0,007 et 0,01 µm respectivement pour S_K1M2 et pour S_K1M1 - S_K1M5) et (ii) les échantillons à base des solutions S_K3 et S_{Na} qui présentent des taux de porosité et des tailles de pores plus faibles mais variables selon le métakaolin utilisé. En effet, il est noté deux types de porosité l'une centrée vers 23% pour les métakaolins M1 et M5 et l'autre vers 32% pour M2. L'effet du cation alcalin est donc une fois encore souligné. En effet, en se référant à la littérature [14, 20], il a été démontré que l'utilisation d'une solution alcaline de potassium conduit à un géopolymère présentant une taille de pores plus faible et un nombre de pores plus élevé que pour un géopolymère à base de solution de sodium à cause des différence de taille et de mobilité entre les cations. Il semblerait par conséquent que la variation de la distribution et de la taille des pores résultent de différences de cinétique et de taux de géopolymérisation. Les espèces siliceuses dépolymérisées dans le cas des solutions S_K3 et S_{Na} induisent la formation de petits colloïdes répartis de façon homogène entrainant un taux élevé de polycondensation, ayant pour conséquence une faible porosité. Celle-ci est caractérisée par des pores de tailles

élevées qui ont coalescé induisant une densification de la structure [21]. Cependant, dans le cas des échantillons à base de la solution S_K1, la faible réactivité de la solution engendre un degré de densification moindre et l'existence de plusieurs réseaux. Ainsi, les colloïdes de plus grande taille sont formés induisant un taux de porosité plus élevé constitué de pores de petite taille.

Ces hypothèses ont été validées par des observations de microscopie électronique à transmission réalisées sur les échantillons S_K1M1 et S_K3M1 (**Figure 13)** présentant des différences de morphologie. L'échantillon S_K3M1, plus dense, est formé d'entités plus petites que l'échantillon S_K1M1 confirmant ainsi les résultats précédents.

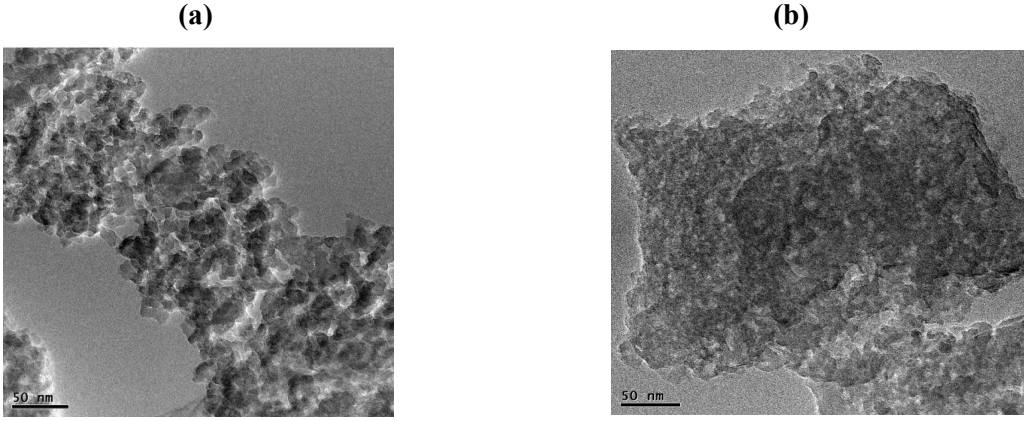

***Figure 13** : micrographies MET des échantillons **(a)** S_K1M1 et **(b)** S_K3M1.*

La réactivité des précurseurs engendre des variations à l'échelle nanométrique et influence la structure poreuse des matériaux géopolymères finaux.

2. Structure locale

Afin d'exacerber plus profondément l'influence des précurseurs sur la structure locale des matériaux géopolymères, les échantillons étudiés ont été analysés par spectroscopies RMN-MAS du ^{29}Si. Deux exemples de déconvolution des spectres obtenus pour les échantillons S_K1M2 et $S_{Na}M3$ sont présentés sur la **Figure 14 (A)**. Cinq contributions attribuées aux espèces riches en aluminium (type $Q^4(4Al)$ et $Q^4(3Al)$) et des espèces riches en silicium (type $Q^4(2Al)$, $Q^4(1Al)$ et $Q^4(0Al)$) [22] sont évidentes quel que soit l'échantillon. Une contribution supplémentaire a également été identifiée à -111 ppm dans certains échantillons (**Figure 14 (A.b)**), indiquant la présence d'acide silicique résultant d'un excès d'espèces siliceuses n'ayant pas réagi [23, 24].

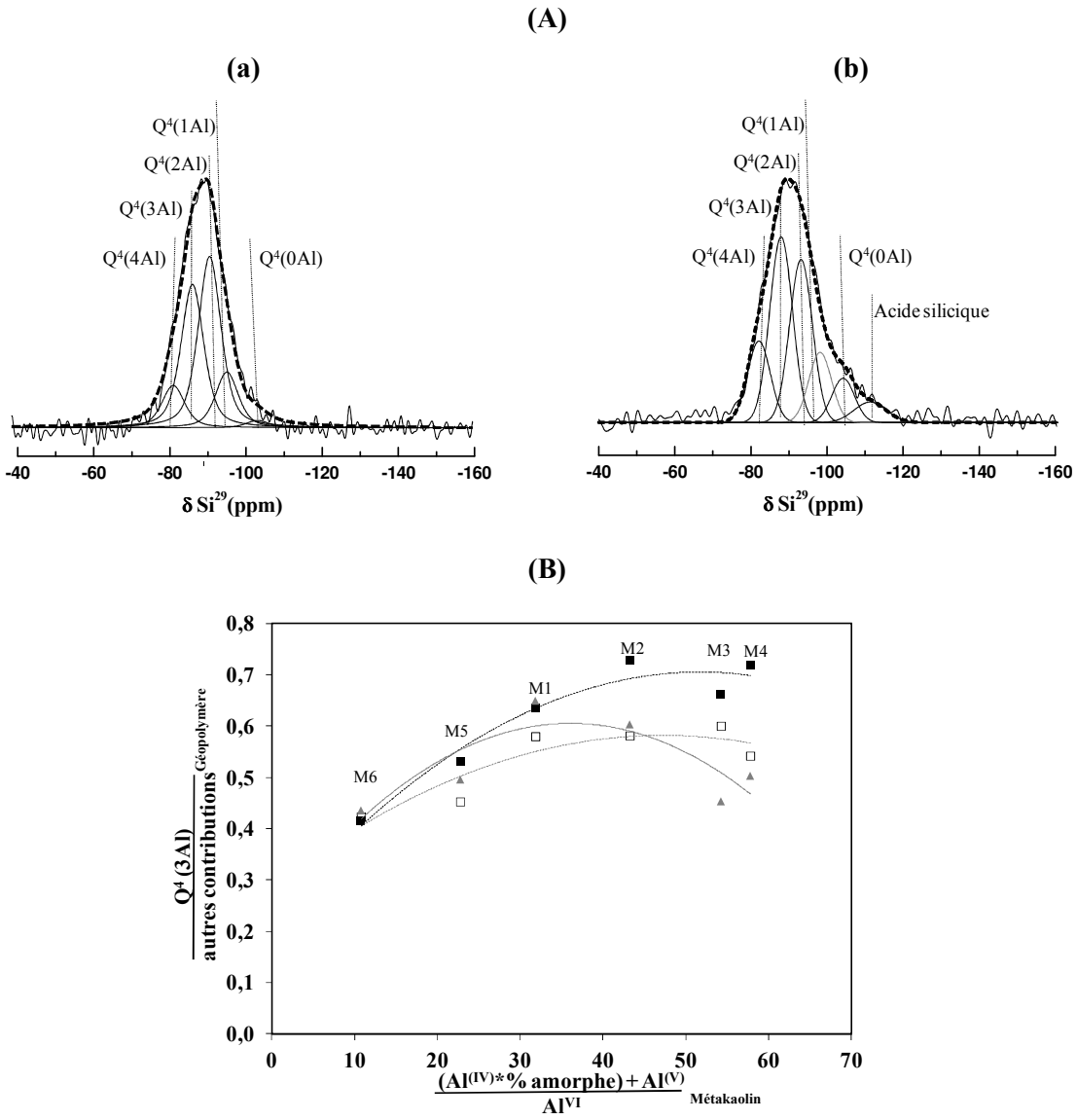

***Figure 14** : **(A)** exemples de déconvolution des spectres RMN-MAS du ^{29}Si des échantillons **(a, b)** S_K1M2 - $S_{Na}M3$ et **(B)** évolution du rapport ($Q^4(3Al)$ / autres contributions) en fonction de la réactivité du métakaolin en présence des solutions (□) S_K1, (■) S_K3 et (▲) S_{Na}.*

Les espèces $Q^4(3Al)$ étant caractéristiques de la phase géopolymère, elle sera prise comme référence par rapport aux autres contributions (**Annexe III.E**). Par conséquent, pour évaluer le taux de formation du réseau géopolymère par rapport aux autres réseaux potentiellement formés, la variation du rapport des proportions de la contribution relative à la phase géopolymère ($Q^4(3Al)$) par rapport aux autres contributions, a été tracée en fonction de la réactivité de métakaolin (**Figure 14 (B)**). Quelle que soit la solution d'activation utilisée, plus le métakaolin est réactif, plus la contribution liée au réseau géopolymère est favorisée. Pour les métakaolins les moins réactifs (M5 et M6), la faible disponibilité de l'aluminium réactif et

la présence de phases cristallines perturbent la formation du réseau géopolymère. Dans le cas des métakaolins très purs M3 et M4 (Si / Al = 1), il est noté une légère diminution du rapport Q^4(3Al) / autres contributions. Malgré leur réactivité élevée, ceci peut être expliquée par l'excès d'espèces siliceuses qui provoque la formation d'acide silicique entrainant ainsi la compétition entre les deux réseaux.

Les différences notées entre les différentes solutions soulignent encore la réactivité la plus élevée de la solution S_K3 comparée aux solutions S_K1 et S_{Na}. En effet, c'est la solution qui présente la meilleure capacité à favoriser la réaction de polycondensation et donc la formation du réseau géopolymère.

La réactivité des précurseurs contrôle les réseaux structuraux et le taux de formation de la phase géopolymère. Néanmoins, l'impact de la solution d'activation semble plus important que celui du métakaolin.

3. Propriétés mécaniques

Les différences structurales entre les matériaux géopolymères étudiés induisent des différences de propriétés mécaniques. Une corrélation a été établie entre le taux d'$Al^{(IV)}$ formé[1] et les contraintes spécifiques de compression[2] **(Figure 15 (a))**. Trois comportements différents ont été distingués en fonction de la réactivité des précurseurs utilisés :

- Pour l'échantillon S_K1M6, le taux de formation d'$Al^{(IV)}$ ne dépasse pas 62%, ce qui induit une faible valeur de contrainte en compression (18 $MPa.g^{-1}.cm^3$). Ceci peut être expliqué d'une part par la faible réactivité du métakaolin M6 en lien avec la présence de mullite tel que démontré précédemment et, d'autre part, par la faible réactivité d'attaque de la solution S_K1. Ces facteurs limitant la formation d'$Al^{(IV)}$, inhibent la formation d'une phase géopolymère homogène et diminuent donc la résistance mécanique des matériaux finaux.
- Pour les autres métakaolins, en présence de la même solution S_K1, la réactivité de la source aluminosilicate semble favoriser la formation d'$Al^{(IV)}$ (de 67% pour S_K1M1 à 72% pour S_K1M2) et améliore les propriétés mécaniques (de 20 $MPa.g^{-1}.cm^3$ pour S_K1M1 à 28

[1] quantité d'$Al^{(IV)}$ formée après 24 heures par rapport à la quantité d'$Al^{(IV)}$ initialement présente dans le métakaolin.

[2] σ / ρ avec ρ est la masse volumique des éprouvettes de compression.

MPa.g^{-1}.cm^3 pour S_K1M2). La contribution du quartz en tant que renfort est évidente dans le cas de l'échantillon S_K1M5 malgré la faible réactivité du métakaolin M5.

- Enfin, les échantillons à base de la solution S_K3 présentent des valeurs élevées de contrainte spécifique (entre 36 et 41 MPa.g^{-1}.cm^3) associées à des taux élevés de formation des $Al^{(IV)}$ (entre 70 et 80%) à l'exception de l'échantillon S_K3M6 (25 MPa. g^{-1}.cm^3). Ce résultat souligne à nouveau la capacité de cette solution à altérer les métakaolins et à favoriser la formation des $Al^{(IV)}$. De plus, cette solution engendre des comportements différents au niveau des phases cristallines présentes dans le métakaolin. En effet, contrairement au quartz qui peut renforcer la structure, la présence de la mullite perturbe la réaction de polycondensation, induisant une structure hétérogène diminuant la résistance mécanique des matériaux consolidés [25].

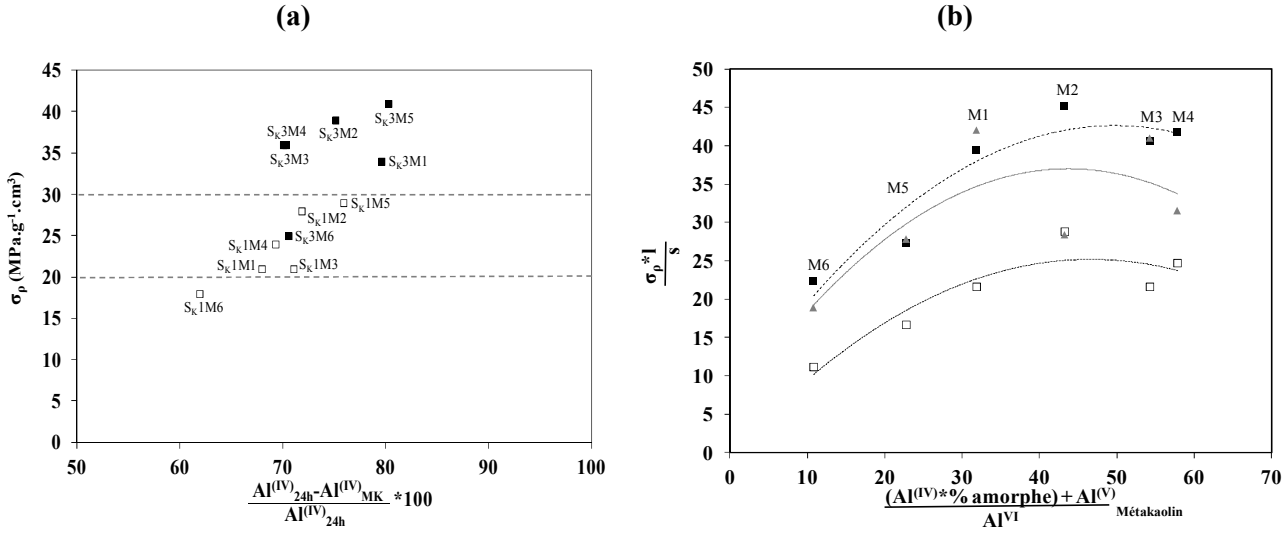

Figure 15 : *variation de la valeur de la contrainte spécifique en fonction du* ***(a)*** *taux de formation des Al $^{(IV)}$ et* ***(b)*** *des caractéristiques structurales des métakaolins en présence des solutions (□) S_K1, (■) S_K3 et (▲) S_{Na}.*

Afin de généraliser ces résultats, l'évolution des contraintes spécifiques de compression en tenant compte du rapport liquide sur solide (l/s) a été tracée en fonction des caractéristiques structurales des métakaolins pour les différents échantillons (**Figure 15. (b)**). La tendance observée est similaire à celle obtenue dans la **Figure 14. (B)**. Cela met en évidence une nouvelle fois la dépendance des propriétés mécaniques de la structure locale des matériaux géopolymères. Plus la solution est réactive (S_K1< S_{Na}< S_K3) et le métakaolin est réactif (M6< M5< M3< M4< M2) meilleures sont les contraintes à la compression. L'effet du rapport liquide sur solide (l/s) a été aussi mis en exergue. En effet, la quantité du liquide doit assurer

une maniabilité suffisante dans le mélange sans affaiblir la structure des matériaux finaux [26].

La réactivité des précurseurs régit le taux de formation de l'aluminium tetracoordinné, caractéristique de la phase géopolymère, et gouverne ainsi les propriétés mécaniques des matériaux consolidés.

VI. VALORISATION

Après avoir exacerbé les paramètres d'influence qui gouvernent le taux de polycondensation, le désordre structural et les propriétés d'usage des matériaux géopolymères, il paraissait intéressant d'extrapoler ces résultats, pour valoriser des matières premières aluminosilicates, exempt d'élément calcium, relativement moins chères et plus abondantes.

1. Recyclage des déchets géopolymères

Dans un contexte de développement durable et compte tenu de l'augmentation de la quantité de déchet potentiel de géopolymère pouvant être générée, leur recyclage a été initié dans le but d'une valorisation innovante et profitable. En effet, la réutilisation de ces déchets permet non seulement de les gérer, mais également de réduire la quantité des matières premières utilisées et par conséquent, minimiser le coût et préserver les ressources naturelles.

Cette partie (ACL 4 et ACL 5) est donc consacrée à l'étude de l'effet de l'intégration de déchet géopolymère broyé, par addition ou substitution dans deux différentes formulations (S_K1M1 et S_K3M1), sur le mécanisme de formation et les propriétés d'usage des matériaux finaux. Une étude de faisabilité a permis de retenir un pourcentage de 20% de déchet ajouté ou substitué au métakaolin M1, de façon à préserver l'aspect homogène, lisse et brillant caractéristiques des matériaux géopolymères. Ceci est confirmé par la concordance entre l'aspect des échantillons retenus et leur composition chimique dans le diagramme ternaire Si-Al-K/O, correspondant à la zone associée aux matériaux géopolymères relatif au métakaolin M1 (**Figure 16**).

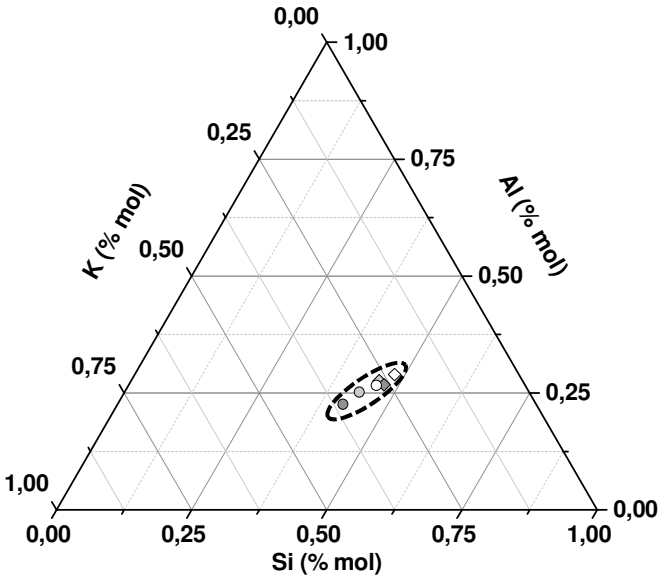

***Figure 16** : compositions chimiques des échantillons (◊) S_K1M1, (♦) $S_K1M1_{0,8}G_{0,2}$, (♦) $S_K1M1_{1,0}G_{0,2}$, (○) S_K3M1, (●) $S_K3M1_{0,8}G_{0,2}$ et (●) $S_K1M1_{1,0}G_{0,2}$ dans le diagramme ternaire Si-Al-K/O.*

Pour mieux comprendre l'effet de l'intégration de géopolymère broyé sur l'évolution structurale des différents échantillons étudiés, la variation des valeurs de déplacement de la position de la bande Si-O-M déterminées par spectroscopie infrarouge a été tracée en fonction du rapport solide/liquide (S/L) de chaque mélange. La référence est la valeur du rapport S/L de l'échantillon S_K1M1 (ayant le rapport S/L le plus faible) (**Figure 17**). En général, les valeurs de déplacement diminuent avec l'augmentation du rapport S/L. Ce ratio est plus élevé pour les échantillons à base de la solution S_K3 en raison de sa teneur en eau plus faible.

En présence de la solution S_K1, la substitution de métakaolin par la formulation recyclée de géopolymère n'a pas d'effet ni sur le rapport S/L (S/L=1) ni sur les valeurs de déplacement (47 et 44 cm^{-1} pour S_K1M1 et $S_K1M1_{0,8}G_{0,2}$). Cependant, l'insertion de géopolymère broyé induit l'augmentation du rapport S/L (S/L=1,47) et la diminution de la valeur de déplacement (27 cm^{-1} pour l'échantillon $S_K1M1_{1,0}G_{0,2}$). Les valeurs élevées de déplacement correspondant à des faibles rapports S/L traduisent la formation de plusieurs réseaux. Le faible rapport S/L (quantité de liquide élevée) favorise la mobilité des espèces et augmente par conséquent les nombres de liaisons et de réseaux formés mais limite la réaction de polycondensation [27]. Néanmoins, dans le cas de la solution S_K3, l'effet de géopolymère broyé et du rapport S/L est compensé par la réactivité élevée de la solution (28 et 24 cm^{-1} respectivement pour les mélanges $S_K3M1_{0,8}G_{0,2}$, $S_K3M1_{1,0}G_{0,2}$). Ce résultat confirme la capacité de cette solution à

gouverner le taux de la réaction quelles que soient les caractéristiques de la source aluminosilicate brute ou recyclée.

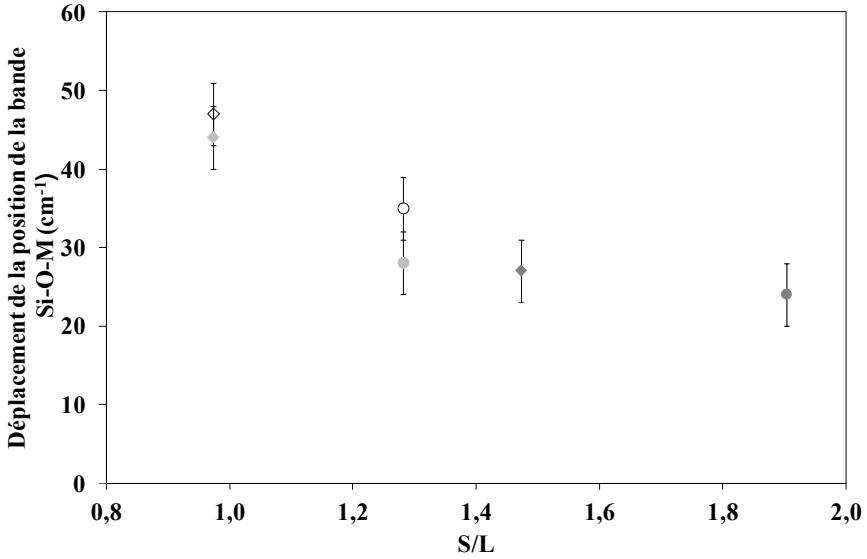

***Figure 17** : valeur de déplacement de la position de la bande Si-O-M en fonction du rapport solide / liquide (S/L) pour les échantillons (◊) S_K1M1, (◈) $S_K1M1_{0,8}G_{0,2}$, (◈) $S_K1M1_1G_{0,2}$, (○) S_K3M1, (●) $S_K3M1_{0,8}G_{0,2}$ et (●) $S_K1M1_1G_{0,2}$.*

L'influence de déchet géopolymère sur les propriétés mécaniques a été évaluée par des tests de compression. La variation des valeurs de contrainte de compression en fonction de la déformation pour les deux compositions est présentée dans la **Figure 18**. Quel que soit l'échantillon, un comportement élastique et une rupture fragile sont observés.

L'intégration de géopolymère broyé par addition ou par substitution induit une diminution de la valeur de contrainte de compression respectivement de 45 MPa pour S_K1M1 à 25 et 22 MPa pour $S_K1M1_{1,0}G_{0,2}$ et $S_K1M1_{0,8}G_{0,2}$ (**Figure 18 (a)**). Ce résultat est dû à la faible réactivité du géopolymère broyé comparé au métakaolin [28].

Cependant, dans le cas de la composition S_K3M1, l'addition de géopolymère broyé semble ne pas affecter les propriétés mécaniques (69 et 67 MPa pour S_K3M1 et $S_K3M1_{1,0}G_{0,2}$ respectivement). Par contre, la substitution induit une légère diminution des contraintes en compression (58 MPa pour $S_K3M1_{0,8}G_{0,2}$) **(Figure 18 (b))**. Ceci est lié à l'utilisation d'une solution alcaline plus réactive (S_K3). En effet, celle-ci est capable de contrebalancer la faible réactivité de géopolymère broyé et gouverner ainsi les propriétés mécaniques comme il a été démontré précédemment.

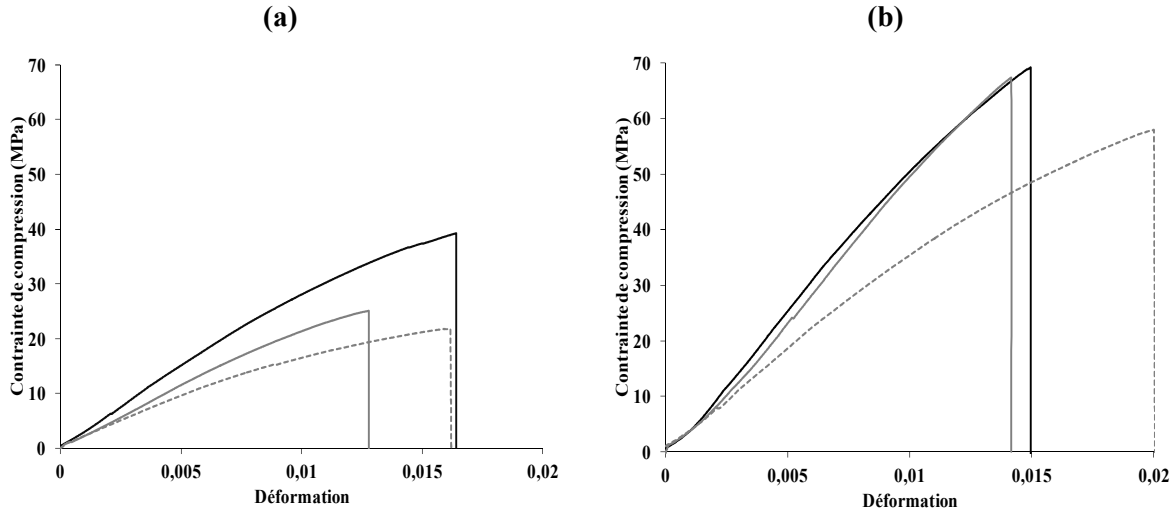

Figure 18 *: évolution des valeurs de contrainte de compression en fonction de la déformation pour les échantillons* ***(a)*** *(—)* S_K1M1*, (—)* $S_K1M1_{1,0}G_{0,2}$ *et (---)* $S_K1M1_{0,8}G_{0,2}$ *et* ***(b)*** *(—)* S_K3M1*, (—)* $S_K3M1_{1,0}G_{0,2}$ *et (---)* $S_K3M1_{0,8}G_{0,2}$*.*

Il est possible de réintégrer le déchet géopolymère par addition ou par substitution dans une formulation à hauteur de 20%. La faible réactivité d'un géopolymère recyclé peut être contrebalancée par la réactivité élevée de la solution activatrice.

2. Valorisation d'une argile tunisienne

La Tunisie est parmi les pays qui ont de nombreux gisements d'argile qui restent jusqu'à présent non entièrement exploités, tel que le gisement d'argile de Medenine situé au sud tunisien. L'évaluation de la possibilité de formuler des liants géopolymères à base de cette argile a fait l'objet des travaux de Essaidi et al. [29]. En continuité de ces travaux, cette partie (ACL3) vise à optimiser les formulations déjà établies et les propriétés d'usage correspondantes. Une étude de faisabilité a permis de sélectionner cinq mélanges qui ont été synthétisés à partir de métakaolin M3, d'argile calcinée Me ou de mélanges mixtes en présence de la solution S_K1. Le rapport Si/K de la solution varie de 0,4 à 0,7 (Annexe II-B).

Afin de comparer la réactivité des deux matières premières utilisées, leurs principales caractéristiques physicochimiques et structurales sont reportées dans le **Tableau 1**. La faible réactivité de l'argile Me comparée au métakaolin M3 a été mise en exergue par le rapport Si/Al élevé, la faible valeur de mouillabilité associée au pourcentage de phase amorphe et

compte tenu de sa composition minéralogique contenant des impuretés (quartz, hématite et illite).

***Tableau 1** : principales caractéristiques physicochimiques et structurales des sources aluminosilicates utilisées*

source aluminosilicate	M3	Me
Si/Al	1,00	2,33
phase amorphe (%)	98	25
mouillabilité (µL/g)	1010	600
composition minéralogique	Métakaolinite	Métakaolinite, quartz, illite, hématite

La différence de réactivité entre les deux précurseurs aluminosilicates laisse présager des différences structurales et microstructurales entre les différents matériaux de type liant géopolymère synthétisés.

Le diffractogramme relatif à l'échantillon $S_K1^{0,4}$Me (**Figure 19 (a)**) montre un léger dôme centré à environ 28° (2θ), caractéristique d'une légère amorphisation, et la persistance des phases cristallines, initialement présentes dans l'argile Me, telles que l'illite, le quartz et l'hématite. Cependant, l'augmentation du la proportion du métakaolin M3 (**Figure 19 (b, c, d, e**)) induit une augmentation de l'intensité du dôme amorphe et une diminution des intensités des phases cristallines. Cette variation indique une restructuration du matériau suite à l'augmentation de la quantité des espèces aluminosilicates plus disponibles.

En outre, pour une même proportion du métakaolin dans un mélange à base de solution alcaline de rapport molaire (Si/K) de 0,5 au lieu de 0,7 ($S_K1^{0,7}M3_{0,50}Me_{0,50}$ vs. $S_K1^{0,5}M3_{0,50}Me_{0,50}$), une amorphisation plus prononcée est notable. Ceci est dû à la réactivité plus élevée des espèces dépolymérisées libérées de la solution alcaline de rapport Si/K plus faible, favorisant ainsi la dissolution de la source aluminosilicate et donc la réaction de polycondensation.

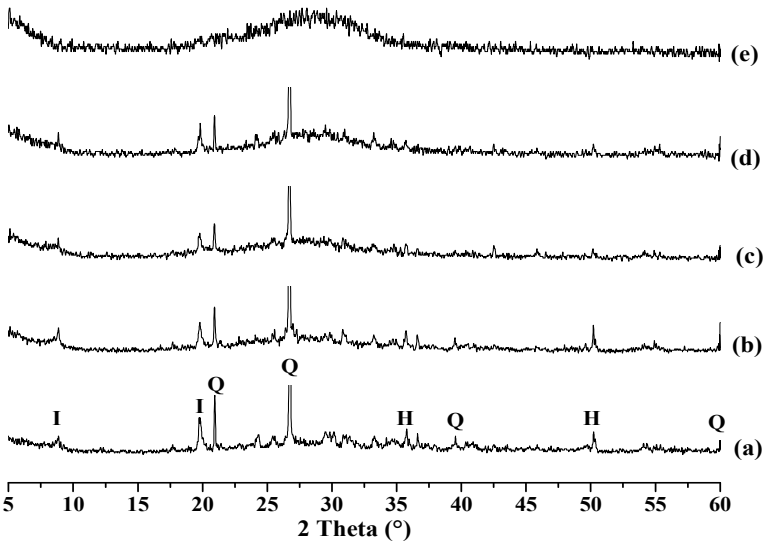

***Figure 19** : diffractogrammes des échantillons **(a)** $S_K1^{0,4}Me$, **(b)** $S_K1^{0,7}M3_{0,25}Me_{0,75}$, **(c)** $S_K1^{0,7}M3_{0,50}Me_{0,50}$, **(d)** $S_K1^{0,5}M3_{0,50}Me_{0,50}$ et **(e)** S_K1M3. PDF files (Q: Quartz (01-085-0865), I: Illite (00-009-0343), H: Hématite (00-003-0812)).*

Les micrographies MEB (**Figure 20**) confirment ces résultats. La faible réactivité de l'argile Me ($S_K1^{0,4}Me$), due au faible teneur en phase amorphe et à la présence accentuée des phases cristallines résistantes à l'attaque alcaline, induit une structure hétérogène. Une microstructure plus homogène, visible dans le cas de l'échantillon $S_K1^{0,7}M3_{0,50}Me_{0,50}$, résulte de la substitution de l'argile par le métakaolin intégré. Une meilleure densification et une homogénéisation de la structure sont notées pour l'échantillon $S_K1^{0,5}M3_{0,50}Me_{0,50}$ (**Figure 20 (c)**), confirmant l'impact plus important de la solution d'activation.

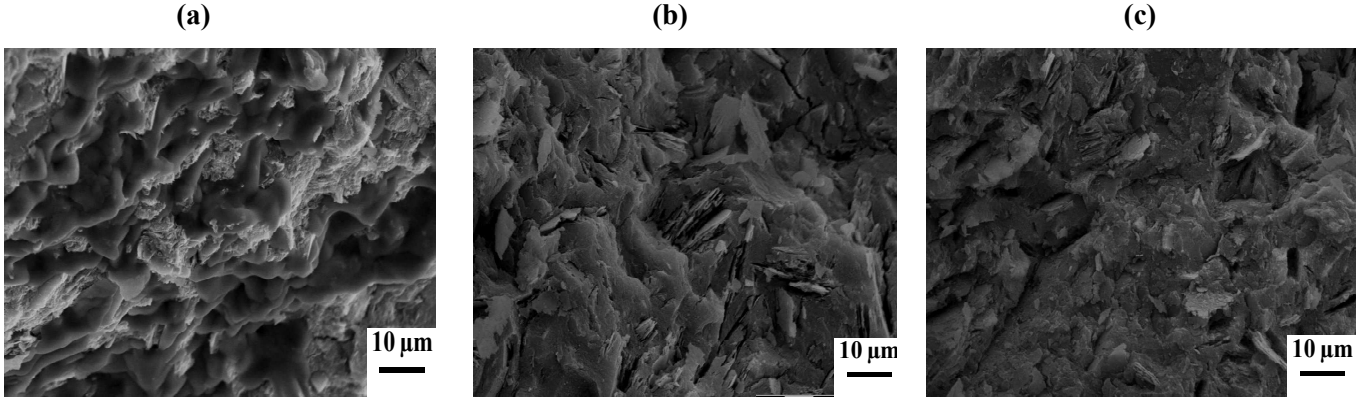

***Figure 20** : micrographies MEB* des échantillons **(a)** $S_K1^{0,4}Me$, **(b)** $S_K1^{0,7}M3_{0,50}Me_{0,50}$ *et* **(c)** $S_K1^{0,5}M3_{0,50}Me_{0,50}$.

Les différences structurales et microstructurales résultant des différences de composition chimique entre les mélanges étudiés influencent les propriétés mécaniques. Pour corréler les propriétés mécaniques et la composition chimique, l'évolution des valeurs de contrainte spécifique de compression et de module d'Young a été tracée en fonction du rapport molaire $n_{Si} / (n_K + n_{Al})$ dans la **Figure 21**.

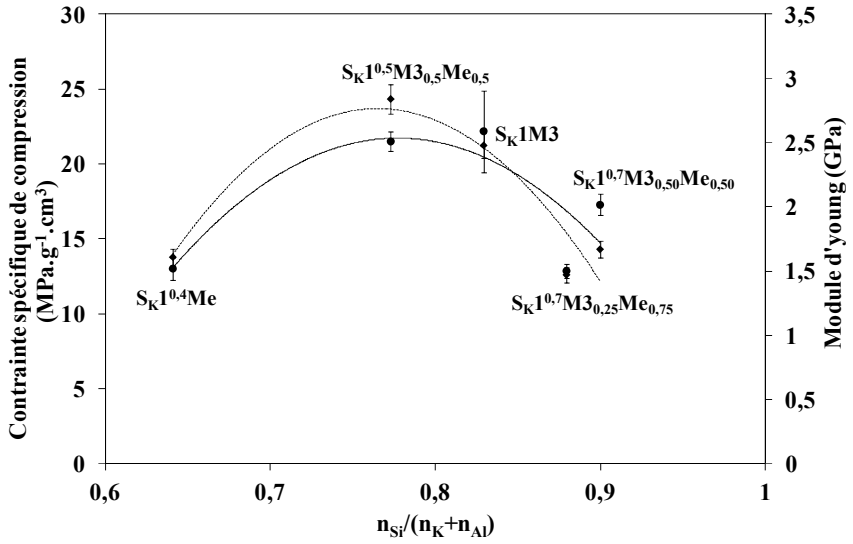

***Figure 21** : évolution des valeurs de contrainte spécifique de compression et de module d'Young en fonction du rapport molaire $n_{Si} / (n_K + n_{Al})$ pour les différents échantillons étudiés.*

Les valeurs de contrainte de compression et de module d'Young augmentent avec le rapport $n_{Si} / (n_K + n_{Al})$ jusqu'à une valeur optimale de 0,8 puis diminuent.

Les faibles propriétés mécaniques associées au faible rapport $n_{Si} / (n_K + n_{Al})$ dans le cas de l'échantillon $S_K1^{0,4}Me$, peut être expliqué par (i) la faible teneur en aluminium et en silicium réactifs dans l'argile Me et (ii) l'alcalinité trop forte de la solution d'activation (Si/K=0,4). Ces deux facteurs limitent la réactivité des précurseurs qui influence directement le taux de polycondensation de la réaction et les propriétés mécaniques, comme il a été démontré précédemment.

L'augmentation de la proportion de métakaolin et du rapport Si/K à 0,7 dans les mélanges $S_K1^{0,7}M3_{0,25}Me_{0,75}$ et $S_K1^{0,7}M3_{0,50}Me_{0,50}$ augmente la valeur du rapport $n_{Si} / (n_K + n_{Al})$ et améliore légèrement les propriétés mécaniques. Néanmoins, la diminution du rapport Si/K à 0,5 dans le cas de l'échantillon $S_K1^{0,5}M3_{0,50}Me_{0,50}$ induit une augmentation significative de la résistance mécanique comparable même à celle de l'échantillon de référence à base de métakaolin seul (S_K1M3). Ce résultat est en accord avec les données structurales et microstructurales.

En résumé, selon la proportion de la substitution de l'argile Me par le métakaolin M3 et le rapport Si/K de la solution, plusieurs réseaux peuvent être formés à savoir, un réseau de type géopolymère et un réseau silicaté intégrant les minéraux associés ne participant pas à la réaction de polycondensation, mais simplement collés par la solution alcaline.

Il est donc possible d'obtenir un matériau avec des propriétés mécaniques satisfaisantes à base de l'argile de Médenine, en substitution du métakaolin à hauteur de 50% avec une solution alcaline de rapport (Si/K=0,5). Ce résultat est important puisqu' il confirme le rôle de la réactivité des précurseurs et l'effet prépondérant de la solution alcaline.

VII. MODELE DE REACTIVITE

L'ensemble des résultats obtenus concernant les paramètres qui régissent la réactivité des matières premières, le mécanisme de formation, la structure et les réseaux finaux ont permis d'établir un modèle de réactivité, en fonction des matières premières utilisées (**Figure 22**). Trois solutions alcalines et trois métakaolins typiques ont été choisis pour représenter les différents scénarios envisageables modélisant les interactions, les mécanismes de formation, la structure poreuse et les réseaux susceptibles d'être formés :

- S_K1 représente la solution potassique peu réactive caractérisée par un taux d'eau élevé, une concentration en alcalin [M] et un nombre d'atomes d'oxygène non pontants faibles et une quantité importante d'espèces siliceuses sous forme de cycles.
- S_K3, une solution potassique très réactive caractérisée par un taux d'eau faible et une prépondérance des espèces dépolymérisées, des chaînes et des monomères.
- S_{Na}, une solution sodique réactive dont les différences de caractéristiques de cation alcalin (taille, hydration, diffusion) engendrent un comportement différent au contact de la source aluminosilicate.
- Le métakaolin M2 représente la source aluminosilicate très réactive ayant une valeur de mouillabilité, un taux d'amorphe et un taux d'Al^{IV} élevés en plus d'une quantité d'impuretés faible (muscovite, anatase quartz).
- Le métakaolin M5 représente la source aluminosilicate peu réactive et riche en impuretés telles que l'hématite, la calcite et le quartz.
- Le métakaolin M6 représente la source aluminosilicate peu réactive contenant la mullite et la muscovite.

(i) En présence d'une solution potassique peu réactive (cas de la solution S_K1) :

- La faible réactivité des espèces siliceuses provenant de la solution alcaline peut être contrebalancée par la réactivité élevée de la source aluminosilicate (cas du métakaolin M2), dont les espèces siliceuses et alumineuses passent facilement en solution. Cela permet de favoriser la dissolution et par suite la formation des oligomères. Le matériau final est majoritairement formé d'un **réseau géopolymère**, avec la possibilité de formation **d'acide silicique** résultant des espèces siliceuses qui n'ont pas réagi.
- La faible réactivité de la solution alcaline associée à la faible réactivité de la source aluminosilicate (cas des métakaolins M5 et M6), provoquent une dissolution incomplète et une formation lente des oligomères. Ceci implique la formation de **différents réseaux**, à savoir le réseau géopolymère et **les impuretés piégées au sein de la solution alcaline**. Les impuretés provenant de la source aluminosilicate montrent trois comportements différents: (i) les impuretés, telle que la muscovite, qui participent à la réaction c'est-à-dire qui peuvent être dissoutes, enrichissant le mélange réactif en espèces siliceuses et alumineuses, (ii) les impuretés inertes, tel que le quartz, qui ne participent pas à la réaction mais qui renforcent la structure du matériau final, (iii) les impuretés, telle que la mullite, qui perturbent la réaction à cause de leur résistance élevée à l'attaque alcaline, présentant donc une source de faiblesse dans le matériau final.

Quel que soit le métakaolin, la structure est constituée de **colloïdes de taille élevée** induisant **une porosité élevée et une taille de pore faible**.

(ii) En présence d'une solution potassique très réactive (cas de la solution S_K3) :

Les espèces réactives de la solution alcaline sont capables de favoriser le mécanisme de formation (dissolution, formation des oligomères et polycondensation), même à partir des espèces aluminosilicates les moins réactives. Un réseau géopolymère parfait est obtenu dans le cas de métakaolin réactif (M2). Pour les métakaolins, moins réactifs (M5 et M6), le réseau majoritaire final est de type géopolymère et le réseau minoritaire est à base d'impuretés. Ceci conduit à la formation de **colloïdes de petite taille**, donc la **porosité** résultante est **faible** (plus faible dans le cas de M5 et M6 comparée à M2) et **la taille de pore est élevée**.

(iii) En présence d'une solution sodique réactive (cas de la solution S_{Na}) :

La dissolution et la formation des oligomères sont favorisées quel que soit le métakaolin. Dans le cas du métakaolin M2, la diffusion plus faible du cation Na accentue la dissolution incongruente du métakaolin et l'encombrement stérique au sein du mélange. Par conséquent, le réseau résultant serait constitué par un réseau géopolymère plus désordonné. Alors que, différents réseaux sont formés dans le cas des métakaolins M5 et M6 avec une prédominance de réseau géopolymère. Les **colloïdes formés sont de petites tailles** ce qui engendre **une porosité faible et une taille des pores élevée** accentuée par la faible réactivité du métakaolin.

Ces différents mécanismes permettent de (i) contrôler la réaction de géopolymérisation et les réseaux structuraux résultant d'ordre local et de (ii) prédire ainsi les propriétés d'usage quelles que soient la source aluminosilicate et la solution alcaline.

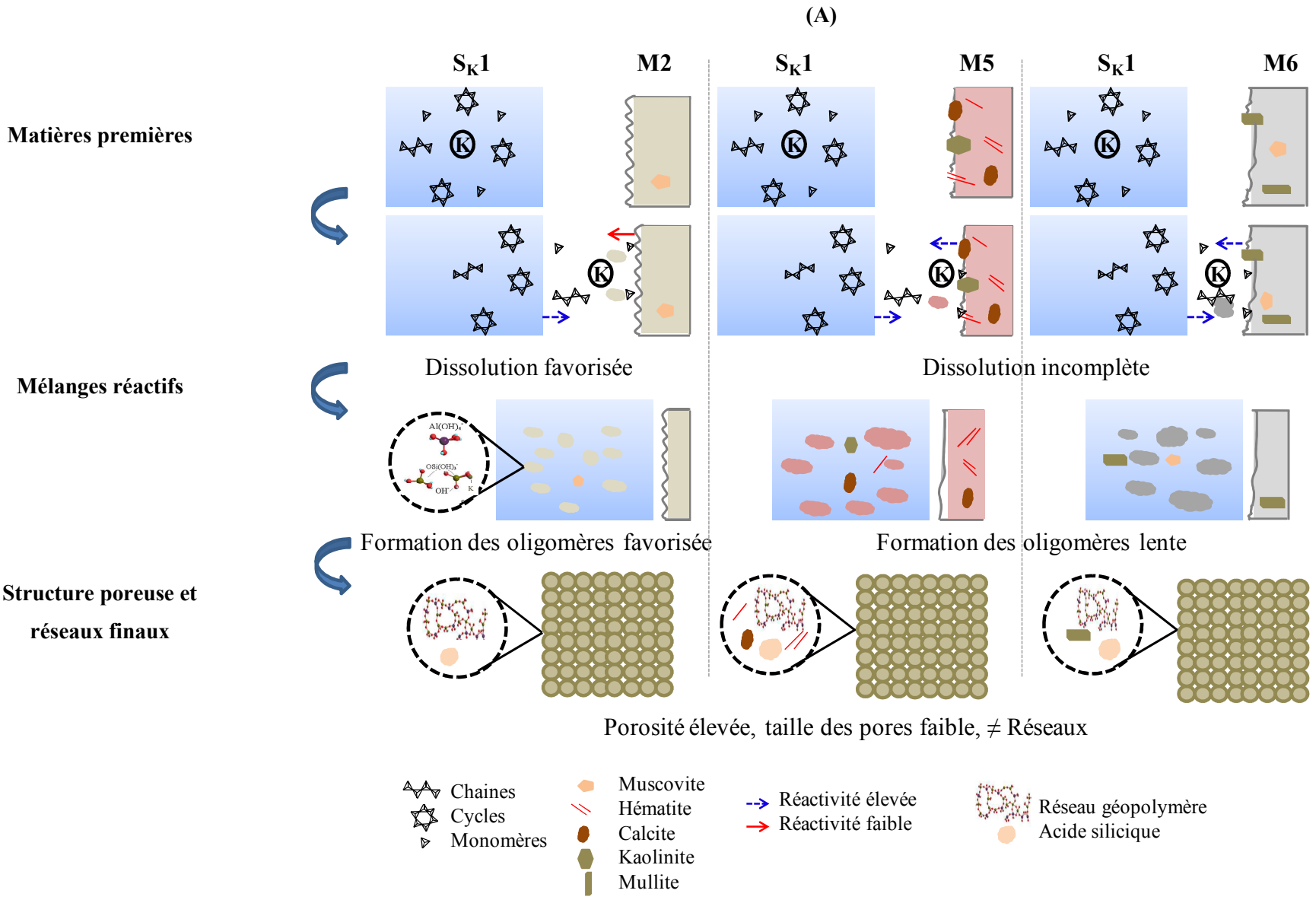
(A)
S_K1
M2
S_K1
M5
S_K1
M6
Matières premières
Mélanges réactifs
Structure poreuse et réseaux finaux
Dissolution favorisée
Dissolution incomplète
Formation des oligomères favorisée
Formation des oligomères lente
Porosité élevée, taille des pores faible, ≠ Réseaux
Chaines
Cycles
Monomères
Muscovite
Hématite
Calcite
Kaolinite
Mullite
Réactivité élevée
Réactivité faible
Réseau géopolymère
Acide silicique

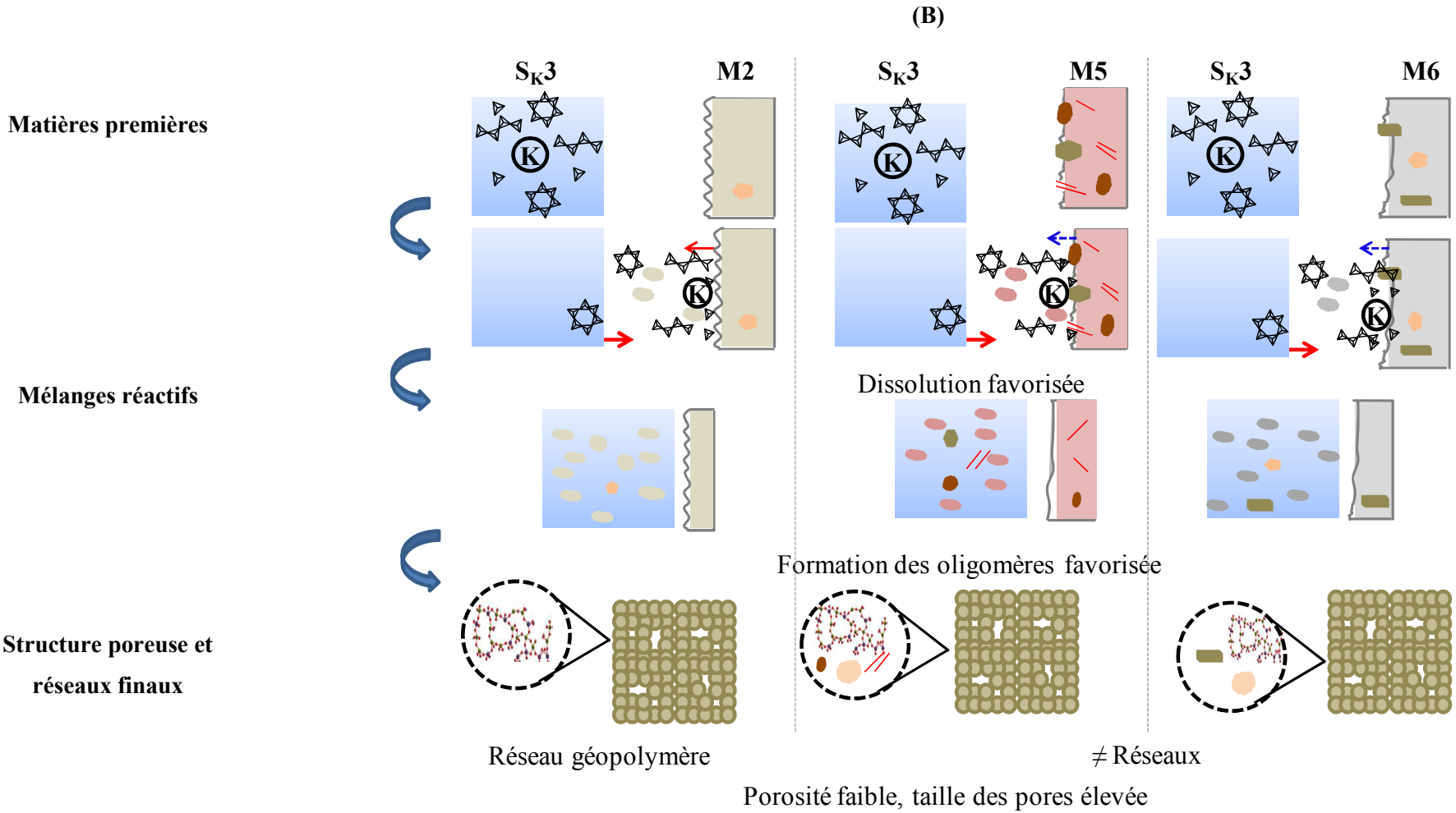
(B)
Matières premières
Mélanges réactifs
Structure poreuse et réseaux finaux
S_K3
M2
S_K3
M5
S_K3
M6
K
Dissolution favorisée
Formation des oligomères favorisée
Réseau géopolymère
≠ Réseaux
Porosité faible, taille des pores élevée

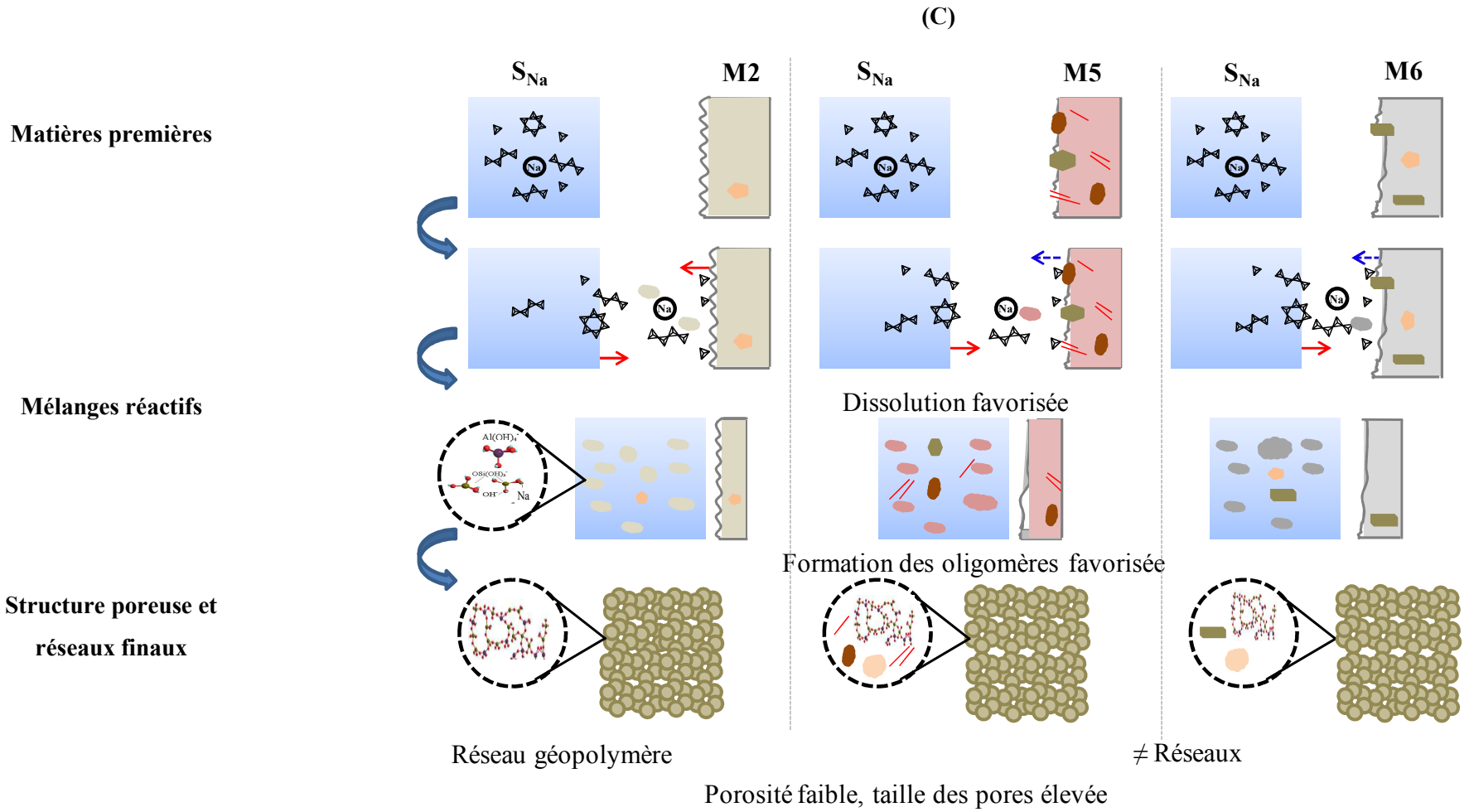

***Figure 22** : représentation schématique de la formation, de la structure poreuse et des réseaux finaux en fonction de la réactivité des matières premières M2, M5 et M6 en présence des solutions (A) S_K1 (B) S_K3 et (C) S_{Na}.*

VIII. BIBLIOGRAPHIE

[1] L.B. Jonathan, L.T. Garry, Anion Distributions in Sodium Silicate Solutions. Characterization by ^{29}Si NMR and Infrared Spectroscopies, and Vapor Phase Osmometry. J. Phys. Chem. B. 101 (1997) 10638-10644.

[2] M. Migliore, G. Corongiu, E. Clementi and G. C. Lie, Monte Carlo study of free energy of hydration for Li^+, Na^+, K^+, F^-, and Cl− with ab initio potentials. J. Chem. Phys, 88 (12) (1988) 7766-7771.

[3] E. Prud'homme, A. Autef, N. Essaidi, F. Michaud, B. Samet, E. Joussein, S. Rossignol Defining existence domains in geopolymers through their physicochemical properties. Appl. Clay. Sci. 73 (2013) 26-34.

[4] P.W.J.G. Wijnen, J.W Beelen, C.P.J Rummens, L.J.M Van de Ven, Van Santen RA Silica gel dissolution in aqueous alkali metal hydroxides studies by 29 Si –Nmr. J Non-Crystal. Solids 109 (1989) 85-94.

[5] W.J. Malfait, W.E. Halter, Y. Morizet, B. H. Meier, R. Verel, Structural control on bulk melt properties: Single and Double quantum 29Si NMR spectroscopy on alkali-silicate glasses, Geochimi. Cosmochim. Acta.71 (2007) 6002-6018.

[6] L. Vidal, E. Joussein, M. Colas, J. Cornette, J. Sanz, I. Sobrados, J.L. Gelet, J. Absi, SRossignol, controlling the reactivity of silicate solutions: an FTIR, Raman and NMR study Accepted in Colloid Surface A. doi:10.1016/j.colsurfa.2016.05.039.

[7] A. Autef, E. Joussein, A. Poulesquen, G. Gasgnier, S. Pronier, I. Sobrados, J. Sanz, S. Rossignol, Influence of metakaolin purities on potassium geopolymer formulation: The existence of several networks, J. colloids and interface Sci. 408 (2013) 43-53.

[8] X.X. Gao, A. Autef, E. Prud'homme, P. Michaud, E. Joussein, S. Rossignol, Synthesis of consolidated materials from alkaline solutions and metakaolin: Existence of domains in the Al-Si-K/O ternary diagram, J. Sol-Gel Sci. Technol. 65 (2) (2013) 220-229.

[9] F.A. Menon, M.F. Nuruddin, S. Khan, N. Shafiq, T. Ayub, Effect of sodium hydroxide concentration on fresh properties and compressive strength of self compacting geopolymer concrete, J. Eng. Sci. Technol. 8 (2013) 44-56.

[10] T. Melkior, S. Yahiaoui, D. Thoby, S. Motellier, V. Barthe`s. Diffusion coefficients of alkaline cations in Bure mudrock. Phys. Chem. Earth. 32 (2007) 453-462.

[11] A. Autef, E. Joussein, G. Gasgnier, S. Rossignol, Role of the silica source on the geopolymerization rate: A thermal analysis study, J. Non-Cryst. Solids. 366 (2013) 13-21.

[12] L. Weng, K. Sagoe-Crentsil, T. Brown, S. Song, Effects of aluminates on the formation of geopolymers, Mater. Sci. Eng. B 117 (2005) 163-168.

[13] Z. Zuhua, Y. Xiao, Z. Huajun, and C. Yue, Role of Water in the Synthesis of Calcined Kaolin-Based Geopolymer, Appl. Clay Sci., 43 [2] (2009) 218-23.

[14] P. Steins, Influence des paramètres de formulation sur la texturation et la structuration des géopolymères. Université de limoges, 2014.

[15] M. Migliore et al., Monte Carlo study of free energy of hydration for Li^+, Na^+, K^+, F^-, and Cl^- with ab initio potentials. J. Chem. Phys. 88 (1988) 7766-7771.

[16] F. Gouny, F. Fouchal, P. Maillard and S. Rossignol, Study of the Effect of Siliceous Species in the Formation of a Geopolymer Binder: Understanding the Reaction Mechanisms among the Binder, Wood, and Earth Brick, Ind. Eng. Chem. Res. 53 (2014) 3559-3565.

[17] P. S. Singh, M. Trigg, I. Burgar, T. Bastow, Geopolymer formation processes at room temperature studied by ^{29}Si and ^{27}Al MAS-NMR, Mater. Sci. Eng: A, 396 (2005) 392-402.

[18] M. R. Rowles, J. V. Hanna, K. J. Pike, M. E. SmithandB. H. O. Connor, ^{29}Si, ^{27}Al, ^{1}H and ^{23}Na MAS NMR Study of the Bonding Character in Aluminosilicate Inorganic Polymers, Appl. Magn. Reson. 32 (2007) 663-689.

[19] A. Favier, G. Habert, J.B. d'Espinose de Lacaillerie, N. Roussel, Mechanical properties and compositional heterogeneities of fresh geopolymer pastes, Cement Concrete Res. 48, 9-16 (2013).

[20] J.L. Bell, and W.M Kriven, Nanoporosity in Aluminosilicate, Geopolymeric Cements. Microscopy and Microanalysis, 10 (2004) 590-591.

[21] P. Duxson, J.L. Provis, G.C. Lukey, S.W. Mallicoat, W.M. Kriven, J.S.J. van Deventer, Understanding the relationship between geopolymer composition, microstructure and mechanical properties, Colloid. Surface A 269 (2005) 47-58.

[22] P. Duxson, J.L. Provis, G.C. Lukey , F. Separovic and J. S. J. van Deventer, 29Si NMR Study of Structural Ordering in Aluminosilicate Geopolymer Gels. Langmuir, 21 (7) (2005) 3028-3036.

[23]S.M. Chemtob, G.R. Rossman, J.F Stebbins, Natural hydrous amorphous silica: Quantitation of network speciation and hydroxyl content by ^{29}Si MAS NMR and vibrational spectroscopy. Am. Mineral. 97 (2012) 203-211.

[24] A. Autef, E. Prud'homme, E. Joussein, G. Gasgnier, S. Pronier, S. Rossignol, Evidence of a gel in geopolymer compounds from pure metakaolin, J. Sol-Gel Sci. Technol. 65 (2013) 220-229.

[25] L. Atmaja, H. Fansuri, A. Maharani, Crystalline phase reactivity in the synthesis of fly ash–based geopolymer, Indo. J. Chem. 11 (2011) 90-95.

[26] Z. Zuhua, Y. Xiao, Z. Huajun, C. Yue, Role of water in the synthesis of calcined kaolin-based geopolymer, Appl. Clay Sci. 43 (2009) 218-223.

[27] Y.M. Liew, H. Kamarudin, A.M. Mustafa Al Bakri, M. Bnhussain, M. Luqman, I. Khairul Nizar, C.M. Ruzaidi, C.Y. Heah, Optimization of solids-to-liquid and alkali activator ratios of calcined kaolin geopolymeric powder, Constr. Build. Mater. 37 (2012) 440-451.

[28] J. He, J. Zhang, Y.Yu, G. Zhang, The strength and microstructure of two geopolymers derived from metakaolin and red mud-fly ash admixture: a comparative study, Constr. Build. Mater. 30 (2012) 80-91.

[29] N. Essaidi, B. Samet, S. Baklouti, S. Rossignol, Feasibility of producing geopolymers from two different Tunisian clays before and after calcination at various temperatures, Appl. Clay Sci. 88-89 (2014) 221-227.

CHAPITRE IV

PUBLICATIONS

Publication 1 (ACL1)

A. Gharzouni, E. Joussein, S. Baklouti, S. Pronier, I. Sobrados, J. Sanz, S. Rossignol

"The effect of an activation solution with siliceous species on the chemical reactivity and mechanical properties of geopolymers"

J. Sol-Gel Sci. Technol.73 (2015) 250-259.

Les précurseurs sont des paramètres cruciaux qui influencent le mécanisme de géopolymérisation vu qu'ils gouvernent la cinétique de la réaction ainsi que les propriétés d'usage des matériaux finaux. Cette étude porte sur l'effet des solutions alcalines sur la formation des matériaux géopolymères. Pour le faire, plusieurs échantillons ont été synthétisés à partir d'un métakaolin et cinq solutions alcalines. Tout d'abord, les solutions ont été caractérisées par analyses thermique et thermogravimétrique (ATD-ATG), spectroscopie infrarouge et spectroscopie par résonance magnétique nucléaire (RMN de ^{29}Si). L'évolution structurale des géopolymères formés a été étudiée en utilisant la spectroscopie infrarouge. Les propriétés mécaniques ont été évaluées par des tests de compression. Les résultats obtenus ont mis en exergue une corrélation entre la composition chimique, le degré de dépolymérisation des solutions alcalines, la cinétique de la substitution des liaisons Si-O-Si par des liaisons Si-O-Al et la résistance à la compression. En effet, pour une source d'aluminosilicate donnée, la nature et la quantité des espèces siliceuses dans la solution d'activation induisent une différence de réactivité et conduisent, par conséquent, à la formation de différents réseaux qui contrôlent la cinétique de formation des géopolymères et leurs propriétés mécaniques.

J Sol-Gel Sci Technol (2015) 73:250–259
DOI 10.1007/s10971-014-3524-0

ORIGINAL PAPER

The effect of an activation solution with siliceous species on the chemical reactivity and mechanical properties of geopolymers

A. Gharzouni · E. Joussein · B. Samet · S. Baklouti · S. Pronier · I. Sobrados · J. Sanz · S. Rossignol

Received: 21 May 2014 / Accepted: 24 September 2014 / Published online: 2 October 2014

Abstract Precursors are critical parameters in geopolymerization mechanisms because they govern the reaction kinetics as well as the working properties of the final materials. This study focuses on the effect of alkaline solutions on geopolymer formation. Toward this end, several geopolymer samples were synthesized from the same metakaolin and various alkaline solutions. First, the solutions were characterized by thermogravimetric analysis as well as DTA–TGA, infrared spectroscopy, and MAS-NMR spectrometry. The structural evolution of the formed geopolymers was investigated using infrared spectroscopy. The measurement of mechanical strength was tested by compression. The results provide evidence of relationships between the chemical composition, the extent of depolymerization of the alkaline solutions, the kinetics of Si–O–Si bond substitution by Si–O–Al and the compressive strength. For a given aluminosilicate source, the nature and the quantity of siliceous species in the activation solution appear to lead to variation in the reactivity and, consequently, to the formation of various networks that control the kinetics of formation of geopolymers and their mechanical properties.

Keywords Si/K ratio · Alkaline solution · Depolymerization · Siliceous species · ^{29}Si MAS-NMR · TEM

A. Gharzouni · S. Rossignol (✉)
Sciences des Procédés Céramiques et Traitements de Surface (SPCTS), Ecole Nationale Supérieure de Céramique Industrielle, 12 rue Atlantis, 87068 Limoges Cedex, France
e-mail: sylvie.rossignol@unilim.fr

A. Gharzouni · B. Samet · S. Baklouti
Laboratoire de Chimie Industrielle, Ecole Nationale d'Ingénieurs de Sfax, 3038 Sfax, Tunisie

E. Joussein
Université de Limoges, GRESE EA 4330, 123 Avenue Albert Thomas, 87060 Limoges, France

S. Pronier
IC2MP, 40 Avenue du recteur Pineau, 86022 Poitiers, France

I. Sobrados · J. Sanz
Instituto de Ciencia de Materiales de Madrid, Consejo Superior de Investigaciones Científicas (CSIC), C/Sor Juana Inés de la Cruz, 3, 28049 Madrid, Spain

1 Introduction

The development of new economical construction materials with low energy consumption and good environmental compatibility remains a current global challenge. Geopolymer materials have garnered increasing interest because of their synthesis methods, high working performance [1], wide range of applications [2] and low environmental impact [3]. Their properties make them a promising alternative to ordinary Portland cement. Geopolymer binders are amorphous, three-dimensional materials that result from the activation of an aluminosilicate source, such as metakaolin, calcined clay or industrial waste activated by an alkaline solution at a temperature less than 100 °C [4]. The choice of precursors is a critical parameter in geopolymerization mechanisms because it governs the properties of the final materials.

The role of aluminosilicate precursors has been extensively studied. Previous studies have focused on the nature of the raw materials, the influence of the impurities [5] and the effect of the calcination temperature [6]. Metakaolin is the most commonly used raw material because of its high reactivity and purity [7]. Recently, Autef et al. [8] studied

different Metakaolin in terms of reactivity, dehydroxylation process, amount of imputities have proposed a model of material formation based on the properties of the metakaolin used. Their model highlights the role of metakaolin reactivity in the presence of an alkaline solution, where this activity leads to the formation of one or more networks. These nanostructure variations influence the mechanical properties of the obtained materials.

The activating solution has been the subject of several studies. The nature of the alkali cation affects the geopolymerization reaction and the working properties of the consolidated materials. Geopolymers based on potassium exhibit better thermal and mechanical properties because of the larger size of the potassium ion compared to that of the sodium ion [9]. The concentration of silicon in the activating solution (the Si/M^+ ratio, where $M^+ = Na^+$, K^+, …) plays an important role in the incorporation of alumina into the matrix [10].

Elucidation of the interaction of the alkaline solution with the aluminosilicate source requires that the structure of the silicate solution be defined. These products are manufactured by fusing silica with an alkali carbonate or sulfate at high temperatures. They have been widely studied; however, their chemistry has remained complex because of the variety of oligomeric silicate anion forms (monomer, linear, cyclic, prismatic, etc.) [11]. Infrared and ^{29}Si nuclear magnetic resonance spectroscopies (MAS NMR) contribute to the elucidation of the structure of silicate solutions. The structure is traditionally described with the notation Q^n [12] where Q represents the silicon atom coordinated to n bridging oxygen atoms and (4-n) non-bridging oxygen atoms in a tetrahedral environment.

Previous reports have demonstrated the existence of correlations between infrared wavenumber values and the Q^n units. Numerous infrared studies [13, 14] on silicate solutions have shown that bands located at approximately 1,060, 1080 and 1,165 cm^{-1} are attributable to the Si–O–Si asymmetric stretching generated by Q^2, Q^3 and Q^4 units, respectively.

Even if the aluminosilicate structure is understood, data concerning the role and reactivity of the silica alkaline solution in geopolymer synthesis is lacking. The aim of this work was to analyze five alkaline compositions based on different commercial silicate solutions with different initial Si/K molar ratios and to investigate their influence on the properties of the synthesized geopolymers.

2 Experimental

2.1 Sample preparation

Five commercial potassium silicate solutions supplied by Woellner® were denoted as S0, S1, S2, S3 and S4 and were used as starting solutions. Table 1 details the Si/K and Si/H_2O molar ratios of each solution.

Table 1 Nomenclature and characteristics of raw materials

Potassium silicate solutions		
Nomenclacture	Si/K	Si/H_2O
S0	1.56	0.05
S1	1.75	0.05
S2	1.52	0.09
S3	0.67	0.09
S4	0.45	0.10

Because a comparison of solutions with different parameters is difficult, the Si/K molar ratio of the five solutions was maintained at Si/K = 0.5. To maintain the Si/K ratios, we dissolved different amounts of potassium hydroxide pellets (VWR, 85.2 % pure) into the S0, S1, S2 and S3 solutions. For S4 solution, very fine and highly reactive amorphous silica (Aldrich, 99.9 % pure) was dissolved into the solution to increase the concentration of Si because of its low Si/K ratio (Si/K = 0.45). The obtained modified alkaline solutions were denoted S_m0, S_m1, S_m2, S_m3 and S_m4. Metakaolin M-1000, supplied by Imerys® and composed of 55 wt% SiO_2, 40 wt% Al_2O_3, 0.8 wt% ($K_2O + Na_2O$), 1.4 wt% Fe_2O_3, 1.5 wt% TiO_2 and 0.3 wt% (CaO + MgO), was used as aluminosilicate source. Syntheses were performed by mixing the metakaolin and the five modified alkaline solutions until obtaining homogenous geopolymer reactive mixtures. The compositions of the different mixtures are reported in Table 2. Then, samples were placed in cylindrical closed sealable polystyrene molds at room temperature (25 °C) for 7 days. The synthesized geopolymer materials were denoted as G0, G1, G2, G3 and G4.

2.2 Characterization

To characterize the starting and modified silicate solutions, differential thermal analyses (DTA) and thermogravimetric analyses (TGA) were performed in platinum crucibles using an SDT Q600 apparatus from TA Instruments in an atmosphere of flowing dry air (100 mL/min). The signals were measured with Pt/Pt-10 % Rh thermocouples. The different solutions were heated to 350 °C at a rate of 5 °C/min.

FTIR spectra were obtained on a Thermo Fisher Scientific 380 infrared spectrometer (Nicolet) using the attenuated total reflection (ATR) method. The IR spectra were recorded over a range of 400–4,000 cm^{-1} with a resolution of 4 cm^{-1}. The atmospheric CO_2 contribution was removed via a straight-line fit between 2,400 and 2,280 cm^{-1}. To monitor the geopolymer formation (G samples), software was used to acquire a spectrum (64

Table 2 Nomenclature and composition of the different prepared mixtures

Mixtures	Silicate solutions		KOH (wt%)	SiO_2 (wt%)	MK (wt%)	(Si*H_2O)/(K + Al)
G0	S0	50.7	10.3	–	39.0	0.81
G1	S1	50.7	10.3	–	39.0	0.83
G2	S2	48.4	14.4	–	37.2	0.71
G3	S3	53.7	5.1	–	41.3	0.68
G4	S4	55.6	–	1.6	42.8	0.64

scans) every 10 min for 13 h. For comparison, spectra were baseline corrected and normalized [15].

High-resolution MAS-NMR experiments were performed at room temperature on a Bruker AVANCE-400 spectrometer operating at 79.49 MHz (^{29}Si signal). The ^{29}Si (I = 1/2) MAS-NMR spectra were recorded after a π/2-pulse irradiation (4 μs) using a 500 kHz filter to improve the signal/noise ratio. In each case, 400 scans were collected. The time between acquisitions was set to 10 s to minimize saturation effects.

Compressive strengths were tested using a LLOYD EZ20 universal testing machine with a crosshead speed of 0.1 mm/min. The compressive tests were performed on ten samples for each composition. The values of compressive strength represent the average of the ten obtained values and are expressed in MPa. Test tubes used for the compression tests were cylindrical in shape with a diameter (Φ) of 15 mm and a height (h) of approximately 35 mm [16] and were aged for 7 days in a closed mold at room temperature.

Finally, the morphology and chemical composition of each phase of two representative geopolymer samples were characterized by transmission electron microscopy (TEM) using a TEM/STEM JEOL 2100 UHR microscope operated at 200 kV. The elementary particle composition was determined by energy-dispersive X-ray analysis (EDX). Samples were deposited onto a Cu grid.

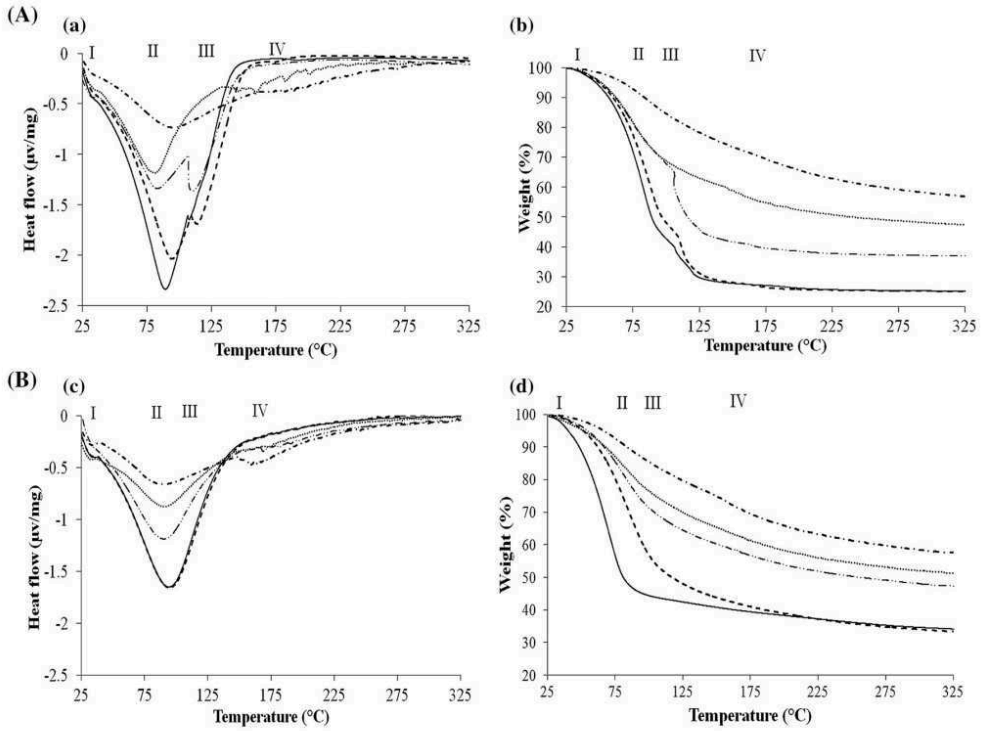

Fig. 1 DTA (*a*, *c*) -TGA (*b*, *d*) curves of (**A**) (*dashed line*) S0, (*solid line*) S1, (*line with double filled circle*) S2, (*filled circle*) S3 and (*line with single filled circle*) S4 starting solutions and (**B**) (*solid line*) S_m0, (*dashed line*) S_m1, (*line with double filled circle*) S_m2, (*filled circle*) S_m3 and (*line with single filled circle*) S_m4 modified solutions

3 Results and discussion

3.1 Characterization of alkaline silicate solutions

3.1.1 Starting solutions

A preliminary characterization was performed using thermal analyses, infrared spectroscopy and ^{29}Si MAS-NMR to compare the starting silicate solutions used. Figure 1A (a, b) present the heat flow and the weight loss of the five solutions (S0–S4) as a function of temperature from 25 to 325 °C. The perturbations of the heat-flow signal observed at approximately 125 °C do not indicate that the obtained signals are not representative of the samples because they are characteristic of phenomena caused by the ebullition of the solution [17].

Irrespective of the solution, several endothermic peaks at varying temperatures less than 200 °C are observed. In the case of S0, the first two peaks at approximately 40 °C (I) and 95 °C (II) correspond to a relatively high weight loss (56.7 %), which is attributed to the elimination of free and physically adsorbed water [18]. The third peak at 114 °C (III), which is associated with a smaller weight loss (14.9 %), is related primarily to the release of constitutional water. The fourth peak at 175 °C (IV) corresponds to a weight loss of 3.4 %, which may be due to reactions in the ionic liquid between the oligomers [19]. The S1 solution exhibited similar heat-flow and weight-loss profiles, which indicates that S0 and S1 have similar structures. This result was expected because the two solutions have the same Si/K molar ratio.

In the case of the S2 solution, the same phenomena are observed. The main difference is that the third endothermic peak is more pronounced and is accompanied by a greater weight loss (18.3 %). This greater weight loss can be explained by the size of the anions present in the solution, which is intimately linked to the concentration of Si, as previously demonstrated in the literature [20]. Indeed, S2 has a lower Si/K ratio and a higher concentration of Si compared to S1 and S0, which results in a greater average colloidal species. Thus, water can be easily trapped in the structure. This phenomenon is observed less often for S3 and S4 solutions, revealing that these solutions contain smaller species than the S0, S1 and S2 solutions. This hypothesis remains to be confirmed by ^{29}Si NMR.

Furthermore, differences were detected in the amount of water in the starting solutions. The water content, as evaluated from TGA curves, decreases in the order S0 (75 %) $\geq$ S1 (74.9 %) > S2 (63.1 %) > S3 (52.1 %) > S4 (43.9 %). These differences can be explained by the Si/K molar ratios, which decrease in the same order (Table 1). In fact, the increase in the amount of K_2O in the silicate solution promotes the formation of non-bridging oxygen. Consequently, the amount of water required during the manufacture of the corresponding geopolymers decreases.

Infrared spectroscopy was utilized to investigate the structure of each silicate solution. The infrared spectra recorded in the 4,000–1,400 cm^{-1} range are presented in Fig. 2Aa. Irrespective of the solution, the −OH and water bending vibrations are observed at approximately 3,300 and 1,650 cm^{-1}, respectively. The decrease in the intensities of these bands from S0 to S4 is in agreement with the

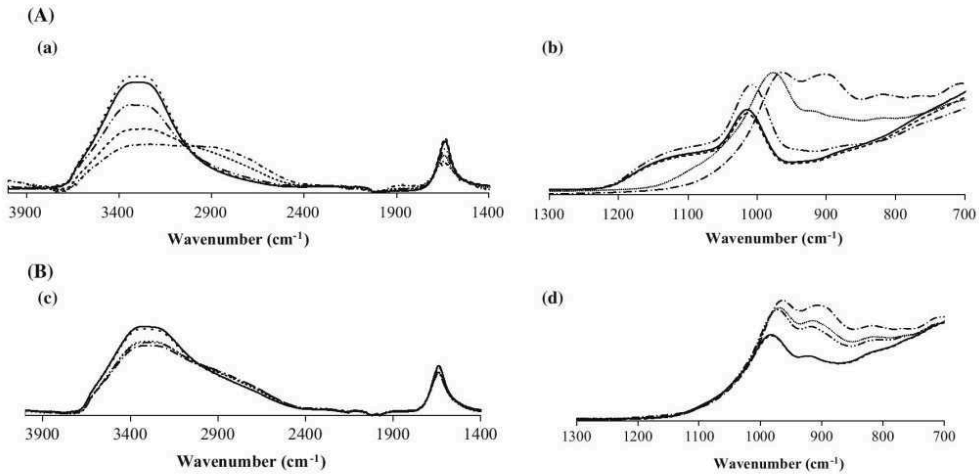

Fig. 2 FTIR spectra of (**A**) (*a*, *b*) (*dashed line*) S0, (*solid line*) S1, (*line with double filled circle*) S2, (*filled circle*) S3 and (*line with single filled circle*) S4 starting solutions and (**B**) (*c*, *d*) (*dashed line*) S_m0, (*solid line*) S_m1, (*line with double filled circle*) S_m2, (*filled circle*), S_m3 and (*line with single filled circle*) S_m4 modified solutions

Table 3 Main vibration bands of S0, S1, S2, S3, S4 starting silicate solutions

Band positions on silicate solutions spectra (cm^{-1})					Attribution
S0	S1	S2	S3	S4	
1,160	1,160	1,160	–	–	ν_{as} Si–O–Si (Q^4)
1,105	1,105	1,105	–	–	ν_{as} Si–O–Si (Q^3)
1,010	1,010	1,008	976	962	ν_{as} Si–O–Si (Q^2)
–	–	–	918	900	ν_{as} Si–O–Si (Q^1)
–	–	–	820	976	ν_{as} Si–O–Si (Q^0)

previously discussed thermal analysis results. These differences primarily suggest that the silicate solutions have variable compositions in terms of siliceous species. Figure 2Ab presents the infrared spectra of the solutions in the 1,300–700 cm^{-1} range to focus on the Q^n contributions of the siliceous species. The bands and their assignments are detailed in Table 3. The characteristic vibration bands of the Si–O–Si bond are located at approximately 1,200–1,000 cm^{-1} [21]. A comparison between the spectra provides evidence of the presence of various silicon environments. For the S0 and S1 solutions, the bands at 1,160, 1,105 and 1,010 cm^{-1} are asymmetric stretching vibrations characteristic of Si–O–Si (Q^4), Si–O–Si (Q^3) and Si–O–Si (Q^2), respectively [19]. The S2 spectrum exhibits a similar trend, with a slight shift to lower wavenumbers. In the case of the S3 and S4 solutions, only bands with characteristics of ν_{as} Si–O–Si (Q^2), ν_{as} Si–O–Si (Q^1) and ν_{as} Si–O–Si (Q^0) at approximately 976, 916 and 819 cm^{-1}, respectively, are observed. The Q^1 and Q^0 contributions appear to be more intense in the case of the S4 solution. Therefore, a decrease in the Si/K molar ratio of the silicate solution (Table 1) induces an increase in the formation of lower-order siliceous species (Q^1 and Q^0) to the detriment of higher-order species (Q^4, Q^3 and Q^2) [22].

The most efficient technique for providing additional details about the molecular structure is ^{29}Si MAS-NMR. The ^{29}Si NMR spectra of the starting solutions are plotted in Fig. 3a. The shifts at −72, −80, −88, −97 and −106 ppm are assigned to Q^0, Q^1, Q^2, Q^3 and Q^4, respectively [23]. Broad bands associated with Q^4, Q^3 and Q^2 species are observed in the spectra of the S0, S1 and S2 solutions. The broad peaks are mainly due to a continuous range in the number of bridging oxygen atoms, with distorted sites having bonding characteristics between those of the well-defined tetrahedra in a silicate crystal [24]. In the S3 and S4 solutions, Q^2, Q^1 and Q^0 predominate, whereas Q^4 is totally absent. Furthermore, the appearance of Q^2 and Q^1 cyclic species are observed [25]. Thus, the ^{29}Si NMR results indicate that the S0, S1 and S2 solutions are similar in structure and contain condensed siliceous species.

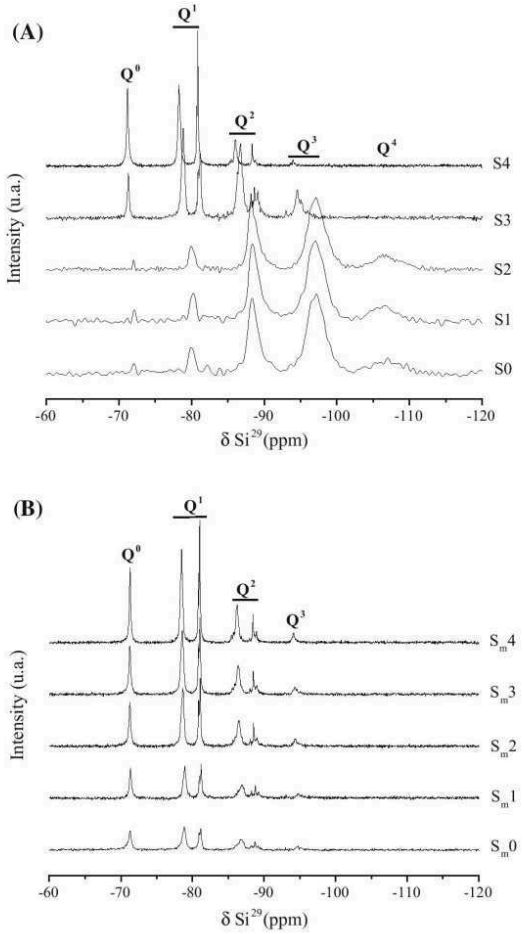

Fig. 3 Spectra of ^{29}Si MAS-NMR of (**A**) S0, S1, S2, S3 and S4 starting solutions and (**B**) S_m0, S_m1, S_m2, S_m3 and S_m4 modified solutions

However, the S3 and S4 solutions appear to be more depolymerized in comparison with the other solutions.

To confirm the thermal data, the amount of water in each solution, as estimated from the TGA analyses, is plotted as a function of the intensity ratio of the Q^2/Q^3 contributions determined by NMR and the number of non-bridging oxygen per tetrahedra (i.e., the NBO/T ratio), as calculated from the chemical composition of the starting solutions ($NBO/T = (2 \times K_2O)/SiO_2$) [26] (Fig. 4). As expected, the amount of water in the silicate solution decreases with an increase in depolymerized species (i.e., at a high Q^2/Q^3 ratio) following an increase of non-bridging oxygen.

In summary, the existence of several contributions to the Si–O–Si band in the silicate solutions can be linked to the Si/K molar ratio of the solution. In fact, as the Si/K ratio decreases, the solution becomes more depolymerized.

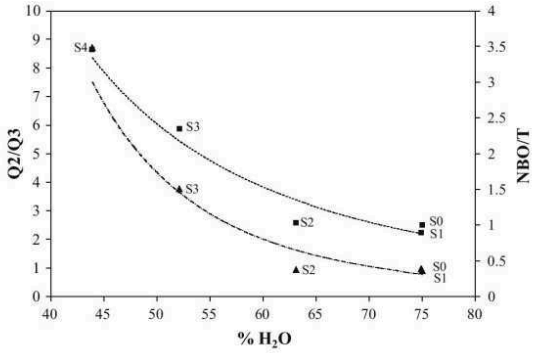

Fig. 4 Evolution of the amount of water, estimated from TGA analysis, in function of (*filled triangle*) the intensity ratio of the contributions Q^2/Q^3 determined by NMR and (*filled square*) the calculated number of non bridging oxygen per tetrahedra (NBO/T) for each starting solution

These results are in agreement with those obtained by Autef et al. [21], who studied different solutions prepared with various Si/K ratios by dissolution of amorphous silica in an alkali solution (water + KOH). The differences in terms of siliceous species and the degree of depolymerization between silicate solutions will induce different reactivities.

3.2 Modified solutions

A similar characterization was performed on the modified solutions ($S_m0 \rightarrow S_m4$). The DTA–TGA curves, plotted in Fig. 1b, show similar profiles and highlight few changes compared to the curves of the starting solutions. The same endothermic phenomena (I, II, IV) previously discussed are distinguished, except for the third peak at 115 °C (III), which is very weak and close to nonexistent. The intensities of the peaks and the weight loss were accompanied by decreases [S_m0 (66.2 %), S_m1 (67.0 %), S_m2 (53.4 %), S_m3 (52.1 %)]. These changes reveal that the addition of KOH in S0, S1, S2 and S3 causes dissociation of colloids that were initially present in the solution, which induces water consumption [27]. Hence, a smaller amount of water is released from the solutions. The trends in the heat-flow and weight-loss curves of S_m4 are the same as those observed for S4 because KOH was not added to the S4 solution. Solution S_m4 is already depolymerized because of its large amount of K_2O.

The infrared spectra of the modified solutions (Fig. 2B) show similar profiles. The relative absorbance of the νOH (3,300 cm^{-1}) and δH_2O (1,650 cm^{-1}) bands in the spectra of the S_m0 and S_m1 samples are slightly more intense than those in the spectra of the other solutions (Fig. 2Bc). This fact can be explained by the large amount of water in the S0 and S1 starting solutions. Furthermore, the decrease in the absorbance intensities relative to those observed in the spectra of the starting solutions (Fig. 2Bc) confirms the results obtained from thermal analysis (see below). At the same time, for the S_m0, S_m1 and S_m2 modified solutions, the band characteristic of asymmetric stretching vibrations of Si–O–Si (Q^4) disappeared, the band characteristic of Si–O–Si (Q^2) shifted from 1,015 to 980 cm^{-1} and new bands related to Si–O–Si (Q^1) and Si–O–Si (Q^0) appeared. In the case of the spectrum of S_m3, the band intensities of Si–O–Si (Q^1) and Si–O–Si (Q^0) increased compared to those in the spectrum of S3. Finally, the IR spectrum profile of S_m4 was the same as that of S4. Therefore, the nucleophilic attack by KOH breaks the Si–O–Si bonds to form Si–O–K bonds, which leads to the formation of non-bridging oxygen atoms and depolymerizes the solution [28].

To further assess the effect of the addition of KOH to the starting solutions, ^{29}Si NMR analysis was performed (Fig. 3b). The data highlight similarities between the siliceous species present in the modified solutions. Compared with the spectra of the initial solutions, those of the modified solutions exhibit narrower peaks, reflecting less distorted networks. The disappearance of the Q^4 species was also observed, as well as a strong decrease in the amount of Q^3 species and the appearance of Q^2 and Q^1 cyclic species, especially in the cases of S_m0, S_m1 and S_m2.

In conclusion, the type of siliceous species present in a potassium silicate solution depends on the Si/K ratio. Upon the addition of KOH, the bonds between the condensed silicon species in the initial silicate solution are destroyed. Hence, the amounts of potassium ions and free silicate species increase, leading to the formation of lower-order species, which are more reactive, as previously reported by Liabau [29].

3.3 Mixtures of alkaline solutions and metakaolin

To exacerbate the reactivity of the siliceous species present in the different alkaline solutions, five reactive mixtures were prepared using the same metakaolin M-1000. The structural evolution of the mixtures was followed by FTIR in ATR mode. Figure 5 shows the Q^2 shift as a function of time for the different mixtures. The evolution of the position of this band, located at approximately 980 cm^{-1}, indicates the substitution of Si–O–Si by Si–O–Al bonds and thereby reflects the reorganization of the network due to a geopolymerization reaction [8]. In addition, the slope of the curve in the beginning of the reaction is characteristic of the kinetics of this substitution [8]. For all samples, the position of the Q^2 band shifted toward lower wavenumbers over time. The initial band positions were similar for G0 (983 cm^{-1}) and G1 (984 cm^{-1}) and lower for G2 (972 cm^{-1}), G3 (970 cm^{-1}) and G4 (964 cm^{-1}). This fact

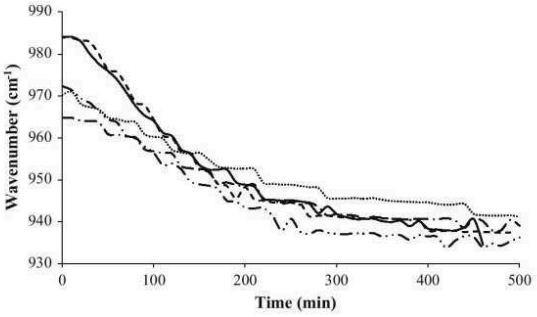

Fig. 5 Shift of Q^2 position from IR spectra versus the time (*dashed line*) G 0, (*solid line*) G1, (*line with double filled circle*) G2, (*filled circle*) G3 and (*line with single filled circle*) G4 reactive mixtures

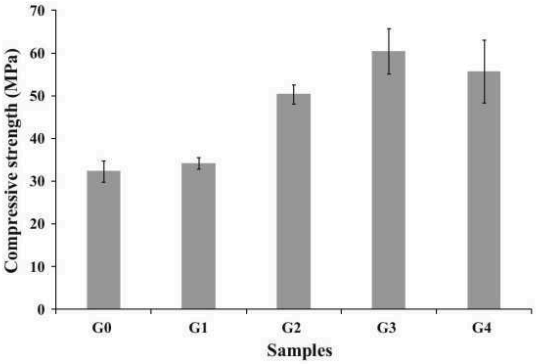

Fig. 6 Compressive strength of each sample after 7 days of ageing

can be explained by the presence of different amounts of non-bridging oxygen, which results in different extents of depolymerization between the alkali solutions despite the solutions having the same Si/K molar ratio.

The shift and the slope values for the five samples are reported in Table 4. These values are characteristic of aluminosilicate network formation. According to previous work [30], M-1000 is not pure metakaolin because of the presence of silicates such as quartz and mica. Moreover, the presence of these phases induces the combination of Si–O–M (M = Si, Al or K) from dissolved species and from the impurities of metakaolin. The IR spectra of the G0 and G1 geopolymer samples exhibit the greatest shift and slope values (shifts of 46 and 49 cm^{-1}, respectively; see Table 4). However, G2, G3 and G4 exhibit smaller slope and shift values, indicating differences between the networks formed in each sample. These differences may influence the working properties of the materials. To verify this hypothesis, the mechanical properties of the five consolidated materials were evaluated by subjecting the samples to compression for 7 days. The results are presented in Fig. 6. The materials exhibited compressive strength values greater than 32 MPa. The G3 sample exhibited the highest mechanical strength (approximately 60 MPa), followed by G4 (56 MPa) and G2 (50 MPa), whereas G0 and G1 exhibited the lowest compressive strengths (32 and 34 MPa, respectively). These results confirm the trends observed in the FTIR spectra.

Table 4 Values of the shift and the slope obtained by infrared spectroscopy for each sample

Sample	Shift (cm^{-1})	Slope (cm^{-1}/min)
G0	46	−0.21
G1	49	−0.21
G2	38	−0.14
G3	29	−0.09
G4	26	−0.09

3.4 Relationship between working properties of geopolymers and reactivity of the alkaline solutions

To correlate the mechanical properties of the geopolymers with the reactivity of the different solution compositions, the compressive strength values of the geopolymers were plotted as functions of the slopes obtained from the FTIR spectra (Fig. 7). The results show a relationship ($R^2 = 0.97$) between these two parameters. In fact, the smaller slopes observed in the spectra of the G3 and G4 samples indicate the slow kinetics of the Si–O–Si bond substitution by Si–O–Al, and these samples exhibit the best mechanical properties among the investigated samples. We obtained similar results in our previous work [30] on the role of metakaolin precursors, where we used highly

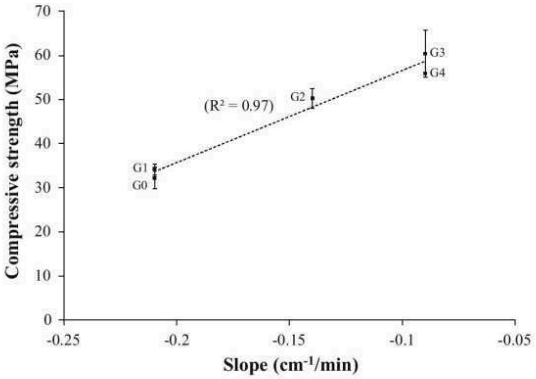

Fig. 7 Relation between the compressive strength and the slope for each sample. The *dash point* (*dashed line*) represents the linear regression line with $R^2 = 0.97$

reactive metakaolin. In the amorphous phase, Si and Al react easily in an alkaline medium, resulting in a smaller shift and slope; however, this configuration exhibits the highest compressive strength. The quickly released siliceous species reach speciation equilibrium and then react with the aluminous species because of their high reactivity. This reaction leads to the formation of a perfect geopolymer network, which enhances the mechanical properties of the final materials.

To more thoroughly evaluate this evolution, the compressive strength as well as the slope were plotted as functions of the ratio of intensities $\left[\left(Q^2/Q^3_{modifiedsolutions}\right)/\left(Q^2/Q^3_{startingsolutions}\right)\right]$ determined by ^{29}Si MAS-NMR. These plots reveal the influence of the extent of depolymerization of the starting solutions (Fig. 8). Two linear relationships are shown. For the lower $\left[\left(Q^2/Q^3_{modifiedsolutions}\right)/\left(Q^2/Q^3_{startingsolutions}\right)\right]$ ratios, better mechanical strengths and smaller slopes were observed, especially in the case of G2, G3 and G4. Indeed, the abundance of low-order species (Q^2 in this case) and, consequently, more extensively depolymerized starting solutions increases the reactivity of the mixture and leads to the rapid formation of small colloids that aggregate more rapidly to form the network [23].

The data suggest that correlation of the working properties and the reactivity of the mixtures to the chemical composition of the different synthesized materials is useful. Figure 9 presents the evolution of the compressive strength and the shift in the ratio (nSi*n H_2O)/(nK + nAl). Typically, the compressive strength decreased with increasing (nSi*n H_2O)/(nK + nAl), whereas the shift increased. The silicon and potassium availabilities differ between the five mixtures, which led to the variation in reactivity and, consequently, to the formation of various networks [31]. The G0 and G1 compositions are silicon-rich, which explains the amount of gel phase observed during the synthesis. In fact, an excess of siliceous species leads to polymerization and thus to the formation of a gel [32]. Competition between a Si-rich phase (gel) and a geopolymer phase weakened the structure. According to the literature [33], the mechanical properties of geopolymers depends on their water content. The large amounts of water in G0 and G1, which resulted from the high water content in the starting silicate solutions (S0 and S1, see Table 1), results in a greater amount of trapped water, which may also explain the comparatively worse compressive strengths of these samples. In the case of G2, G3 and G4, the larger amount of potassium and the accentuated presence of depolymerized species in the alkaline solution (Tables 1, 2) led to the formation of small, very reactive entities that quickly bridge Si and/or Al. This fact explains their relatively weak shift values and reveals the presence of two imbricated networks, which lead to an improvement in the mechanical strength of these samples. These explanations were validated by TEM investigations to provide additional structural information. The TEM micrographs of both compositions are presented in Fig. 10. They clearly highlight the differences in morphology between the G1 and G3 samples. Sample G3 contains smaller entities than sample G1, which confirms the previously discussed hypothesis. In summary, the extent of depolymerization of the activation solution and the chemical composition of the mixture are critical parameters that lead to nanostructural variations and govern the mechanical properties of the resulting geopolymers.

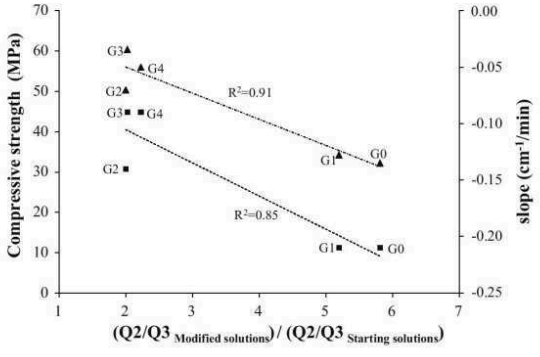

Fig. 8 Evolution of (*filled triangle*) the compressive strength and (*filled square*) the slope in function of the ratio of intensity $\left[\left(Q^2/Q^3_{modifiedsolutions}\right)/\left(Q^2/Q^3_{startingsolutions}\right)\right]$ determined by ^{29}Si MAS-NMR for each mixture

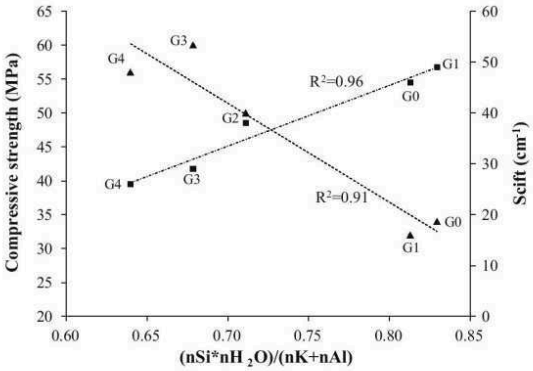

Fig. 9 Evolution of (*filled triangle*) the compressive strength and (*filled square*) the shift in function of the chemical compositions (nSi*nH_2O)/(nK + nAl) of each mixture

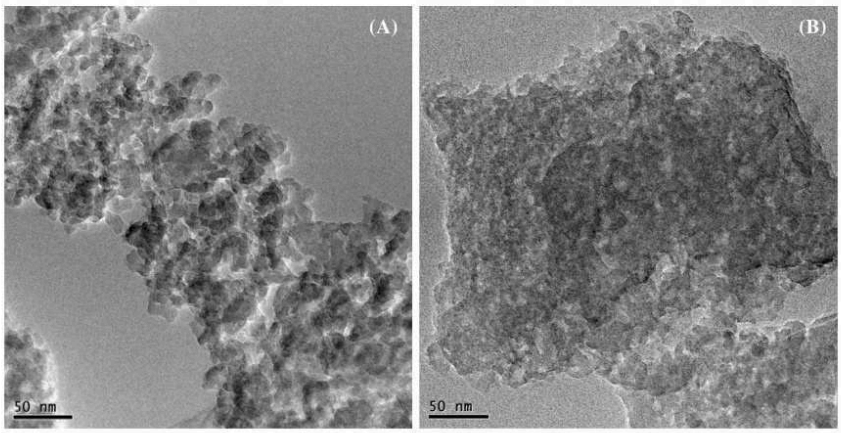

Fig. 10 TEM micrographs of (**A**) G1 and (**B**) G3 samples

4 Conclusion

Our elucidation of the geopolymerization reaction involved a comprehensive study of the precursors used. In the present work, the influence of the activating solution was demonstrated. Indeed, the Si/K ratio was observed to control the degree of depolymerization of the silicate solutions as well as the type and the amount of the siliceous species. Moreover, a relationship between the compressive strengths of geopolymers, the kinetics of Si–O–Si bond substitution by Si–O–Al, the chemical composition and the type of siliceous species in the alkaline solutions was demonstrated. In conclusion, depolymerized species are small and highly reactive, which enables the fast formation of oligomers and leads to better mechanical properties of the resulting geopolymers.

References

1. Van Jaarsveld JGS, Van Deventer JSJ, Lorenzen L (1999) The potential use of geopolymeric materials to immobilise toxic metals: part 1 Theory and applications. Miner Eng 10:659–669
2. Krivenko P (1997) Alkaline cements: terminology, classification, aspects of durability [C] Proceedings of the 10th International Congress on the Chemistry of Cement, Gothenburg, Sweden
3. Liew YM, Kamarudin H, Mustafa Al Bakri AM, Luqman M, Khairul Nizar I, Heah CY (2011) Investigating the possibility of utilization of kaolin and the potential of metakaolin to produce green cement for construction purposes. Aust J Basic Appl Sci 5:441–449
4. Davidovits J (2008) Geopolymer: Chemistry and Applications, 2nd edn. Institut Géopolymère, St-Quentin
5. Zibouche F, Kerdjoudj H, d'Espinose de Lacaillerie JB, Van Damme H (2009) Geopolymers from Algerian metakaolin. Influence of secondary minerals. Appl Clay Sci 43:453–458
6. Elimbi A, Tchakoute KH, Njopwouo D (2011) Effects of calcination temperature of kaolinite clays on the properties of geopolymer cements. Constr Build Mater 25:2805–2812
7. Zhang YJ, Li S, Wang YC, Xu DL (2012) Microstructural and strength evolutions of geopolymer composite reinforced by resin exposed to elevated temperature. J Non Cryst Solids 358:620–624
8. Autef A, Joussein E, Poulesquen A, Gasgnier G, Pronier S, Sobrados I, Sanz J, Rossignol S (2013) Influence of metakaolin purities on potassium geopolymer formulation: the existence of several networks. J Colloids Interface Sci 408:43–53
9. Duxson P, Provis JL, Lukey GC, Mallicoat SW, Kriven WM (2005) Understanding the relationship between geopolymer composition, microstructure and mechanical properties. Colloids Surf A 269:47–58
10. Duxson P, Fernandez-Jimenez A, Provis JL, Lukey GC, Palomo A, Van Deventer JSJ (2007) The effect of alkali and Si/Al ratio on the development of mechanical properties of metakaolin-based geopolymers. J Mater Sci 42:2917–2933
11. Swaddle TW (2001) Silicate complexes of aluminum (III) in aqueous systems. Coord Chem Rev 219:665–686
12. Engelhard G, Zeigan D, Jancke H, Hoebbel D, Weiker Z (1975) High resolution ^{29}Si NMR of silicates and Zeolites. Anorg Allg Chem 418:17–28
13. MacDonald SA, Schardt CR, Masiello DJ (2000) Dispersion analysis of FTIR reflection measurements in silicate glasses. J Non Cryst Solids 275:72–82
14. Matson W, Sharma SK, Philpotts JA (1983) The structure of high silica alkali-silicate glasses. A Raman spectroscopic investigation. J Non Cryst Solids 58:323–352
15. Prud'homme E, Michaud P, Joussein E, Clacens JM, Rossignol S (2011) Role of alkaline cations and water content on geomaterial foams: monitoring during formation. J Non Cryst Solids 357: 1270–1278
16. ASTM D1633 – 00, Standard test methods for compressive strength of molded soil cement cylinders, 2007
17. Haynes WM (2013) CRC handbook of chemistry and physics, 94th edn. CRC Press, Boca Raton, Florida
18. Langille KB, Nguyen D, Bernet JO, Veinot DE (1991) Mechanism of dehydration and intumescence of soluble silicates. I, Effect of silica to metal oxide molar ratio. J Mater Sci 26:695–703
19. Prud'homme E, Michaud P, Joussein E, Smith A, Peyratout C, Sobrados I, Sanz J, Rossignol S (2012) Geomaterial foams: role

assignment of raw materials in the network formation. J Sol–Gel Sci Technol 61(2):436–448
20. Jonathan LB, Garry LT (1997) Anion distributions in sodium silicate solutions. Characterization by ^{29}Si NMR and infrared spectroscopies, and vapor phase osmometry. J Phys Chem B 101:10638–10644
21. Autef A, Joussein E, Gasgnier G, Rossignol S (2013) Role of the silica source on the geopolymerization rate: a thermal analysis study. Ceram Eng Sci Proc 33:13–24
22. Goudarzi N (2013) Silicon-29 NMR spectroscopy study of the effect of tetraphenylammonium (TPA) as a template on distribution of silicate species on alkaline aqueous and alcoholic silicate solutions. Appl Magn Reson 44:469–478
23. Prud'homme E, Autef A, Essaidi N, Michaud F, Samet B, Joussein E, Rossignol S (2013) Defining existence domains in geopolymers through their physicochemical properties. Appl Clay Sci 73:26–34
24. Schmidt BC, Riemer T, Kohn SC, Holtz F (2001) Structural implications of water dissolution in haplogranitic glasses from NMR spectroscopy: influence of total water content and mixed alkali effect. Geochim Cosmochimi Acta 65:2949–2964
25. Wijnen PWJG, Beelen JW, Rummens CPJ, Van de Ven LJM, Van Santen RA (1989) Silica gel dissolution in aqueous alkali metal hydroxides studies by ^{29} Si–Nmr. J Non Cryst Solids 109:85–94
26. Halter WE, Morizet Y, Meier BH, Verel R (2007) Structural control on bulk melt properties: single and Double quantum ^{29}Si NMR spectroscopy on alkali-silicate glasses. Geochim Cosmochimi Acta 71:6002–6018
27. Schneider E, Stebbins JF, Pines A (1987) Speciation and local-structure in alkali and alkaline-earth silicate-glasses-constraints from Si-29 NMR-spectroscopy. J Non Cryst Solids 89:371–383
28. Bunker BC, Tallant DR, Headley TJ, Turner GL, Kirkpatrick R (1988) Structure of leached sodium borosilicate glass. Phys Chem Glasses 29:106
29. Liebau F (1985) Structural chemistry of silicates. Springer, Berlin
30. Autef A, Joussein E, Poulesquen A, Gasgnier G, Pronier S, Sobrados I, Sanz J, Rossignol S (2013) Role of metakaolin dehydroxylation in geopolymer synthesis. Powder Technol 250:33–39
31. Hajimohammadi A, Provis JL, Van Deventer JSJ (2011) The effect of silica availability on the mechanism of geopolymerisation. Cem Concr Res 41:210–216
32. Autef A, Prud'homme E, Joussein E, Gasgnier G, Pronier S, Rossignol S (2013) Evidence of a gel in geopolymer compounds from pure metakaolin. J Sol–Gel Sci Technol 65:220–229
33. Steveson M, Sagoe-Crentsil K (2005) Relationships between composition, structure and strength of inorganic polymers. J Mater Sci 40:2023–2036

Publication 2 (ACL2)

A. Gharzouni, E. Joussein, B. Samet, S. Baklouti, S. Rossignol, ,

"Effect of the reactivity of alkaline solution and metakaolin on geopolymer formation"

J. Non-Cryst. Solids. 410 (2015) 127-134.

Cette étude met en exergue l'effet de la réactivité de différents métakaolins et solutions alcalines sur la formation des géopolymères. Afin d'évaluer cet effet, plusieurs échantillons ont été synthétisés à partir de deux solutions alcalines et quatre métakaolins. L'évolution structurale des géopolymères au cours de la formation a été étudiée moyennant la spectroscopie IRTF et le suivi de la variation des valeurs de pH. Les propriétés mécaniques ont été évaluées par des essais de compression. Il ressort que le type et la quantité des espèces siliceuses et des atomes d'oxygène non pontants contrôlent la réactivité de la solution alcaline. L'effet de la réactivité du métakaolin est plus important lorsqu'il est activé avec une solution alcaline peu réactive. Cependant, l'effet des solutions alcalines très réactives est prépondérant. Par conséquent, le degré de dépolymérisation de la solution alcaline et la réactivité du métakaolin sont des paramètres cruciaux qui gouvernent la cinétique de la réaction de polycondensation et les résistances à la compression des matériaux géopolymères.

Journal of Non-Crystalline Solids 410 (2015) 127–134

Contents lists available at ScienceDirect

Journal of Non-Crystalline Solids

journal homepage: www.elsevier.com/ locate/ jnoncrysol

Effect of the reactivity of alkaline solution and metakaolin on geopolymer formation

A. Gharzouni [a,b], E. Joussein [c], B. Samet [b], S. Baklouti [b], S. Rossignol [a,*]

[a] Science des Procédés Céramiques et de Traitements de Surface (SPCTS), Ecole Nationale Supérieure de Céramique Industrielle, 12 rue Atlantis, 87068 Limoges Cedex, France
[b] Laboratoire de Chimie Industrielle, Ecole Nationale d'Ingénieurs de Sfax, 3038 Sfax, Tunisie
[c] Université de Limoges, GRESE EA 4330, 123 avenue Albert Thomas, 87060 Limoges, France

ARTICLE INFO

Article history:
Received 22 September 2014
Received in revised form 3 December 2014
Accepted 16 December 2014
Available online 20 December 2014

Keywords:
Metakaolin reactivity;
Alkaline solution;
Depolymerization;
pH value;
Polycondensation rate;
Mechanical strength

ABSTRACT

This paper focuses on the effects of alkaline solution reactivity and metakaolin properties on geopolymer formation. To examine these effects, several geopolymer samples were synthesized from two alkaline solutions and four metakaolins. The structural evolution of the formed geopolymers was investigated using FTIR spectroscopy and pH values during the material formation. The mechanical properties were measured using compression tests. The results show that the type and amount of siliceous species and non-bridging oxygen atoms control the alkaline solution reactivity. The effect of the metakaolin reactivity is more significant when it is activated with a poorly reactive alkaline solution. However, the alkaline solution governs the reaction when it is highly reactive. Therefore, the extent of depolymerization of the alkaline solution and the reactivity of metakaolin are crucial parameters that control the rate of polycondensation and the compressive strengths of geopolymer materials.

1. Introduction

Over the last decades, geopolymers have gained tremendous interest as a promising new class of binders that are environmentally friendly [1] and have good working properties [2]. These ecomaterials result from the activation of an aluminosilicate source using an alkaline solution at room temperature or slightly elevated temperature. The geopolymerization mechanism consists of the dissolution of reactive aluminosilicate precursors under the effect of the alkaline solution to form oligomers ($Si[OH]_4$ and $Al[OH]^-_4$) [3]. Then, a polycondensation reaction links the oligomers, which generates an amorphous three-dimensional network. A deeper comprehension of the geopolymerization mechanism and the parameters that can affect it is important to guarantee the widespread of geopolymer applications.

Considering that the used precursors (alkaline solution and aluminosilicate source) strongly affect the properties of geopolymer materials, numerous studies have focused on the nature of the raw materials. Although the use of common clays [4,5] and industrial waste [6,7] as aluminosilicate source has gained increasing interest, metakaolin remains the ideal and commonly used precursor because of its high purity, reactivity and potential low cost. The existing literature has addressed the effect of metakaolin impurities [8,9], calcination temperature [10], deshydroxylation degree of metakaolins and particle size distribution of metakaolin [11].

Recently, Autef et al. [12] highlighted the role of metakaolin reactivity in the presence of an alkaline solution that was prepared by dissolving KOH and amorphous silica in water. In fact, the metakaolin reactivity can generate the formation of one or several networks and lead to nanostructure variations that affect the mechanical properties of the obtained materials. A notably reactive metakaolin dissolves notably quickly and allows the formation of a perfect geopolymer network (a single geopolymer phase). For a notably pure metakaolin, where a small amount of kaolinite remains because of a non-complete dehydroxylation, the final material consists of a geopolymer network and layers that are coated with a silicate solution. However, with a metakaolin rich of impurities, the strengthened material consists of a geopolymer network, mica layers, a Si-rich phase and an Al-rich phase [12].

The type of alkali cation is also important. It was shown that geopolymers based on a mixture of potassium silicate and KOH exhibit higher mechanical properties than those based on sodium silicate and NaOH or potassium silicate/NaOH mixtures. In fact, the larger size of the potassium cation enhances the polycondensation reaction, which leads to a stronger network [13]. Moreover, in our previous work [14], we focused on the effect of different potassium-activating solutions on the same metakaolin. It was demonstrated [14] that the initial Si/K molar ratio of the silicate solution controls the nature and quantity of the siliceous species. In fact, when the Si/K ratio decreases, the solution becomes more depolymerized. The accentuated presence of depolymerized species in the alkaline solution leads to the formation of small, notably reactive entities that quickly bridge Si, which quickly forms of oligomers and

* Corresponding author.
E-mail address: sylvie.rossignol@unilim.fr (S. Rossignol).

http://dx.doi.org/10.1016/j.jnoncrysol.2014.12.021
0022-3093/

leads to better mechanical properties of the resulting geopolymers. In continuity of our previous work and regarding the lack of comparative studies on different metakaolin sources and alkaline solutions, this work aims to study the role of two potassium alkaline silicate solutions with different initial Si/K molar ratios in the presence of four metakaolins, which differ in terms of reactivity, and investigate their effect on the geopolymerization mechanism and the properties of the synthesized materials.

2. Experimental procedures

2.1. Raw materials and sample preparation

Two commercial potassium silicate solutions, which were denoted as S1 and S3 with Si/K molar ratios of 1.75 and 0.65 and pH values of 11.4 and 14, respectively, and four types of metakaolins (MR, MO, MQ and MP) (Table 1) were used to synthesize the geopolymer samples. To easily compare the two alkaline solutions, the Si/K molar ratio was maintained at Si/K = 0.5 by dissolving different amounts of potassium hydroxide pellets (VWR, 85.2% pure) into the two starting silicate solutions. Then, metakaolins were added. The obtained mixtures were placed in a closed sealable polystyrene mold at room temperature (25 °C). The nomenclature and the composition of the prepared mixtures are reported in Table 2. The samples were named S1MR, S3MR, S1MO, S3MO, S1MQ, S3MQ, S1MP and S3MP.

2.2. Sample characterization

High-resolution MAS-NMR experiments were performed on the alkaline solutions at room temperature on a Bruker AVANCE-400 spectrometer operating at 79.49 MHz (^{29}Si signal). The ^{29}Si (I = 1/2) MAS-NMR spectra were recorded after a π/2-pulse irradiation (4 μs) using a 500 kHz filter to improve the signal/noise ratio. In each case, 400 scans were collected. The time between acquisitions was set to 10 s to minimize saturation effects.

Fourier-transform infrared (FTIR) spectroscopy in ATR mode was used to investigate the structural evolution of the geopolymer mixtures. The FTIR spectra were obtained using a ThermoFisher Scientific Nicolet 380 infrared spectrometer. The IR spectra were gathered over a range of 400 to 4000 cm^{-1} with a resolution of 4 cm^{-1}. The atmospheric CO_2 contribution was removed with a straight line between 2400 and 2280 cm^{-1}. To monitor the geopolymer formation, a software was used to acquire a spectrum (64 scans) every 10 min for 13 h. For comparison, the spectra were baseline-corrected and normalized [15].

The pH values were measured using a Schott Instrument Lab860 pH-meter at 25 °C during the first 400 min of the geopolymer formation. A 2.4 g sample was immersed in 30 mL of osmosed water, which provided a solid to liquid ratio of 0.08 [16].

Differential thermal analysis (DTA) and thermogravimetric analysis (TGA) were performed on an SDT Q600 apparatus from TA Instruments in a flowing dry-air atmosphere (100 mL/min) in platinum crucibles. The signals were measured using Pt/Pt-10% Rh thermocouples. Milligrams of the material, in powder form, were placed in a platinum crucible. The analysis was performed from 30 to 1400 °C at 5 °C/min for the metakaolin raw materials and from 30 to 1350 °C at 20 °C/min for the consolidated geopolymer samples.

The compressive strengths were tested using a LLOYD EZ20 universal testing machine with a crosshead speed of 0.1 mm/min. The compressive tests were made on five samples for every composition. The compressive strength values represent the average of the five obtained values and were expressed in MPa. The samples were cylindrical in shape with a diameter (Φ) of 15 mm and a height (h) of approximately 30 mm, and they were aged for 7 days in a closed mold at room temperature. This method permit to predict the compressive strength of the final material from an early age.

Table 1
Characteristics of the different used metakaolins.

Metakaolin	MR	MO	MQ	MR
SiO_2 (wt.%)	55	55	53.3	52.4
Al_2O_3 (wt.%)	40	39	45.5	45.3
TiO2 (wt.%)	1.5	1.5	1.2	1
Fe_2O_3 (wt.%)	1.4	1.8	–	0.4
$K_2O + Na_2O$ (wt.%)	0.3	0.6	–	0.3
CaO + MgO (wt.%)	0.8	1	–	0.1
Si/Al	1.17	1.19	1.00	0.98
Wettability (μL/g)	570	1250	1010	1186

Table 2
Nomenclature, composition and compressive strength value of each sample.

Mixtures	Si/(K + Al)	Compressive strength (MPa)
S1MR	0.90	34 ± 1
S1MO	0.91	41 ± 2
S1MQ	0.82	30 ± 2
S1MP	0.81	38 ± 2
S3MR	0.84	60 ± 5
S3MO	0.85	61 ± 6
S3MQ	0.77	61 ± 3
S3MP	0.76	62 ± 5

3. Results

3.1. Raw-material investigation

3.1.1. Alkaline solutions

In our previous work [14], the used silicate solutions were extensively characterized before and after the addition of KOH by ^{29}Si NMR. The common used notation to describe a silicon tetrahedral environment, as established by Engelhard et al. [17], is Q^n where n and 4-n refer to the bridging and the non bridging oxygen atoms, respectively. Fig. 1 shows an example of ^{29}Si NMR spectrum relative to S1 silicate solution before addition of KOH. To identify the signal contributions, all spectra were deconvoluted. The chemical shifts and the percentages of the curve area are detailed in Table 3. Bands assigned to Q^0 (−72 ppm), Q^1 (−80 ppm), Q^2 (−88 ppm) and Q^3 (−97 ppm) and Q^4 (−106 ppm) [18] are observed in the case of S1 alkaline solution. The broadness and the high intensities of Q^4, Q^3 and Q^2 bands give evidence that S1 solution initially contained condensed siliceous (Fig. 1, Table 3). However, in S3 solution Q^2, Q^1 and Q^0 predominate in addition to the existence of Q^1 and Q^2 cyclic species. After the addition of KOH, similar contributions were observed and revealed less distorted networks where lower-order species predominate. According to the literature [19], the reactivity of

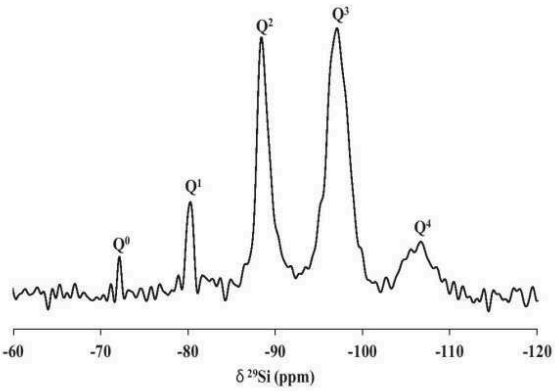

Fig. 1. ^{29}Si NMR spectrum of S1 silicate solution (before addition of KOH).

alkaline solutions is controlled by the amount of uncondensed species (Q^0 and Q^1) known to be more reactive than any other species. So, to highlight the difference in reactivity between the two alkaline solutions, the previous ^{29}Si NMR features were exploited to establish a quantitative comparison between the Q^0 and Q^1 contribution intensities and the number of non-bridging oxygen per tetrahedra (NBO/T = $(3*Q^1 + 2*Q^2 + Q^3)/100$) [20] as shown in Fig. 2. We have focused on Q^0 (monomer) and Q^1 (dimmer) species because the reactivity of alkaline solutions is controlled by the amount of uncondensed species (Q^0 and Q^1) known to be more reactive than the other species. At the beginning, in the starting solutions, it was noticed that the Q^0 and Q^1 intensities of the S3 solution (79.65 and 354.17, respectively) were obviously higher than the S1 solution (20.24 and 52.14, respectively). Furthermore, the NBO/T of S3 (2.47) is also higher compared to S1 (1.45). Thus, S3 (lower Si/K ratio of 0.65) is mainly composed by low-order species (Q^0 and Q^1). This result suggests that S3 solution is more depolymerized since it contains small and more reactive species [19,21]. However, the lack of Q^0 and Q^1 species, the absence of cyclic species and the small amount of non-bridging oxygen indicate that S1 is less depolymerized. This result is consistent with the work of Bass and Turner [22] who demonstrated that the high alkalinity of the solution promotes the formation of monomer dimer and cyclic trimer as shown for the S3 solution.

However, the addition of KOH increases the Q^0 intensity relative to S1 from 20.24 to 53.74 and the Q^1 intensity from 52.14 to 142.41. The NBO/T increases to 2.48. For S3, the Q^0 intensity increases from 79.65 to 86.59 when the NBO/T increases from to 2.47 to 2.57, but the Q^1 intensity slightly decreases from to 354.17 to 315.41. These results occur because KOH acts as a network modifier and breaks the bonds between the condensed silicon species in the starting silicate solution, which generates non-bridging oxygen atoms, enhances the formation of low-order species and increases the degree of depolymerization of the solution [14].

Despite the identical Si/K ratios of the two solutions (Si/K ratio = 0.5), there remain persistent differences. Indeed, a greater amount of Q^0 species and non-bridging oxygen is observed for the S3 solution. These differences make S3 more reactive than S1 because Q^0 is the most reactive among all Q^n [23].

3.1.2. Metakaolins

The main characteristics of the four metakaolins are reported in Table 1. Chemical data evidence that the four metakaolins contain different amounts of SiO_2, Al_2O_3 and impurities (Fe_2O_3, TiO_2, K_2O, Na_2O…). Furthermore, MR and MO exhibit higher Si/Al ratios (1.17 and 1.19, respectively) than MQ and MP (1 and 0.98, respectively). This fact can be explained, according to X-ray diffraction data obtained in a previous work [11], by the presence of accessory minerals for MR and MO, whereas MQ and MP are relatively more pure. In addition, the wettability value was proven to be a potential indicator of the metakaolin reactivity [11,12]. Thus, it was interesting to compare the wettability values of the studied metakaolins. Indeed, MO, MP and MQ have higher wettability values (1250 μL/g, 1186 μL/g and 1100 μL/g, respectively) whereas MR shows a lower wettability value (570 μL/g). These differences may occur because of the different deshydroxylation processes used in the metakaolin synthesis [11] and the crystallinity of initial kaolins. As a result, MO, MP and MQ can be more reactive in alkaline media than MR.

Table 3
Experimental parameters of the deconvoluted peaks of ^{29}Si NMR spectra for the different alkaline solutions (δ: chemical shift (ppm), %A: percentage of the area curve of contribution).

	Solutions							
	S1		S3		S1 + KOH		S3 + KOH	
Q^n	δ (ppm)	%A	δ (ppm)	%A	δ (ppm)	%A	δ (ppm)	%A
Q^0	−72.10	1.28	−71.32	6.72	−71.39	18.01	−71.30	16.10
Q^1	−80.21	6.57	−80.95	22.68	−81.01	25.40	−80.88	30.31
Q^1_{cyclic}	–	–	−81.27	14.19	−81.27	20.28	−81.04	22.20
Q^2	−88.43	25.02	−88.71	29.05	−88.30	18.64	−88.08	18.92
Q^2_{cyclic}	–	–	−89.18	13.07	−89.01	11.42	−89.06	8.02
Q^3	−97.06	52.99	−94.92	14.29	−94.85	6.27	−95.18	4.44
Q^4	−106.25	14.13	–	–	–	–	–	–

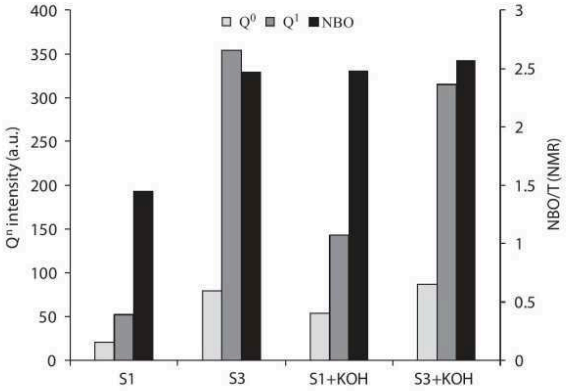

Fig. 2. Comparison between the Q^0 and Q^1 contribution intensities and the NBO/T for the silicate solutions before (S1 and S3) and after the addition of KOH (S1 + KOH and S3 + KOH).

To confirm this hypothesis, thermal analyses were performed on the metakaolin specimens. Fig. 3 presents the TGA curves of the four metakaolins as a function of temperature from 30 to 1400 °C. It appears that MO exhibits the highest weight loss (2.7%), which includes a first weight loss at approximately 100 °C and a second weight loss. The first weight loss corresponds to the elimination of physically adsorbed water, and the second weight loss can be attributed to the release of silica hydroxyl groups ($Si(OH_4)$), which suggests a higher reactive phase. For MR, in addition to the weight loss relative to the adsorbed water, two other weight losses are detected near 400–500 °C and 700 °C. These temperatures are closed to the temperature of dexhdroxylation of kaolinite (the transformation of kaolinite to metakaolinite) [24]. However, all the studied samples have been already dexydroxylated by thermal treatment. This fact reveals the persistence of residual kaolinite not fully deshydroxylated and accessory minerals such as micaeous clays in this metakaolin [11]. MQ and MP show lower weight loss (0.9% and 1.1%, respectively), which indicates the low impurity content in these metakaolins. This result is confirmed by XRD diffraction [11] since only traces of quartz and anatase were identified. Consequently, MO appears to be the most reactive species, followed by MP

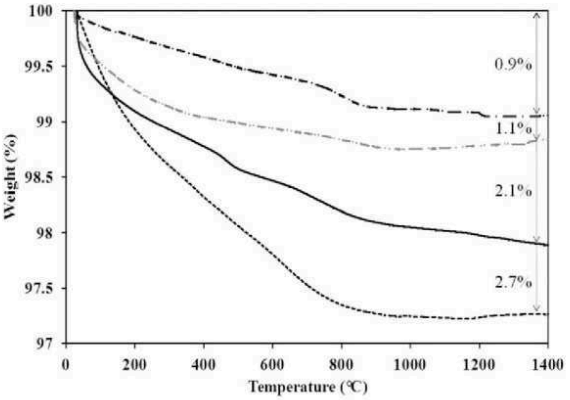

Fig. 3. TGA curves of (–) MR, (—) MO, (-•-) MQ and (-••-) MP metakaolin raw materials.

and MQ (pure metakaolins) and MR, which is consistent with the wettability value evolution.

3.2. Effect of the reactivity of the alkaline solution and metakaolins on the polycondensation rate

The behavior of the four types of metakaolins in the presence of two alkaline solutions was studied using FTIR spectroscopy in the ATR mode to monitor the structural evolution of the synthesized mixtures. This technique enables one to evaluate the substitution of the Si – O – Si bonds by Si – O – Al bonds, which is evidenced by the shift value and the kinetics of the reaction that is determined from the slope value [15].

Fig. 4 shows the evolution of the Q^2 position peak versus time for only S1MP and S3MP samples. The initial band position of S3MP (974 cm^{-1}) is lower than that of S1MP (987 cm^{-1}). This result can be explained with the presence of a higher amount of non-bridging oxygen and reactive species in the mixture that comes from the S3 alkaline solution in comparison with S1, as previously discussed. Furthermore, the shift value slightly increases from 24 cm^{-1} for S1MP to 30 cm^{-1} for S3MP. However, the slope values are notably similar (−0.10 cm^{-1}/min and −0.11 cm^{-1}/min for S1MP and S3MP, respectively). Thus, for MP metakaolin, the use of the S3 alkaline solution appears to slightly enhance the network reorganization without affecting the kinetics of the reaction.

Compared with the other studied samples, the Q^2 position shift versus the slope for all samples was plotted in Fig. 5. The S1MR sample exhibits the greatest shift and slope values (49 cm^{-1} and −0.20 cm^{-1}/min, respectively). However, the use of the S3 alkaline solution decreases the shift value to 29 cm^{-1} and the slope value to −0.1 cm^{-1}/min. For the MO metakaolin, the shift and the slope values are notably similar, and the variation of the alkaline solution appears not to affect the reaction. For MQ, small changes are detected with the use of S3. Indeed, the shift value slightly increases from 21 cm^{-1} for S1MQ to 27 cm^{-1} for S3MQ, and the slope decreases from −0.11 cm^{-1}/min to −0.09 cm^{-1}/min. The comparatively high shift and slope values observed for S1MR can be explained by a combination of Si – O – M (M = Si, Al or K) from dissolved species and the impurities of metakaolin as previously demonstrated. The weaker slope and shift values of S3MR mainly occur because of the reactivity of the S3 alkaline solution, which is more depolymerized than S1. Thus, highly reactive siliceous species, which are released from the S3 alkaline solution, reach speciation equilibrium and react with the aluminous species [14]. Indeed, it has been demonstrated that the monomeric silicate exchanges much more rapidly with aluminosilicate species than with any other silicate anions [25]. In addition, the geopolymerization reaction consequently involves the breaking of bridging-oxygen bonds with a higher number of non-bridging oxygen in the alkaline solution; hence, fewer bonds require hydrolysis before the species can be released [26]. Therefore, there are more available reactive species for geopolymerization in S3 because they are released more rapidly. For MO, MQ and MP, which are more reactive metakaolins, the effect of the alkaline solution appears negligible. The reactivity of the siliceous species that are released from the three metakaolin controls the kinetics of the substitution of Si – O – Si by Si – O – Al bonds and the network reorganization. In fact, the more reactive metakaolin corresponds to more favored and rapid oligomer formation.

In addition, previous studies [27] have shown that there are two areas according to the shift and slope values: For a shift less than 22 cm^{-1} and a slope above −0.1 cm^{-1}/min, the excess of siliceous species forms a gel. However, for a shift greater than 22 cm^{-1} and a slope below than −0.1 cm^{-1}/min, there is a formation of various networks. The intersection of the two areas appears to be characteristic of geopolymer materials. This fact was schematically represented in Fig. 5. All samples appear to be in the geopolymer area except S1MR, which presents different networks. These results are consistent with the previously discussed data in Fig. 4.

To further assess the effect of the alkaline solution and metakaolin on the polycondensation rate, the variation in pH value of different mixtures during the first 400 min of the formation was examined. The results are presented in Fig. 6. For the four metakaolins, the reactive mixture had different initial pH values: 12.8 (S1MR), 12.6 (S3MR), 11.5 (S1MO), 11.2 (S3MO), 11.9 (S1MQ), 11.5 (S3MQ), 12.2 (S1MP) and 11.7 (S3MP). For the same metakaolin, the use of S3 slightly decreases the initial pH value of the mixture. The measured pH value denotes the presence of alkaline species (silicium, aluminum or potassium) in solution. These nonreacting species result from the nonconsolidation of the samples. In the presence of S3 (highly reactive), the lower initial pH value can be explained by the fact that the species react easily and rapidly compared to S1. Consequently, less alkaline species are present in solution due to the fast formation of oligomers.

For S1MR (Fig. 6a), the pH value was substantially constant until 200 min and subsequently decreases to 11.5. However, in the case of S3MR (Fig. 6a), a rapid decrease to 10.8 was observed after 400 min. This reaction kinetics occurs because siliceous and/or aluminous species from micaeous clays, which are present in MR, are slowly and continuously released in the solution, which decreases the pH value but spontaneously delay the polycondensation reaction. S1MO and S3MO (Fig. 6b) exhibit a notably similar trend of decrease and reach 10.5 and 10.3, respectively. These values are close to the equilibrium constant $[Al(OH)_4^-)/Al(OH)_3]$, which indicates that there is no more charged aluminous species ($Al(OH)_4^-$) in the solution [28]. This result also reveals the material consolidation. For S1MQ (Fig. 6c), the pH value decreases in the first 30 min, increases and subsequently decreases

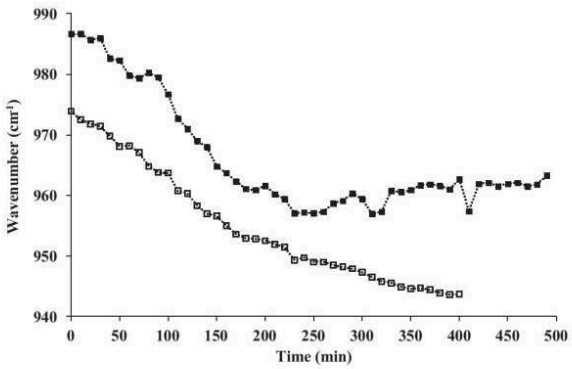

Fig. 4. Shift of Q^2 position from IR spectra versus the time at room temperature for (■) S1MP and (□) S3MP reactive mixtures.

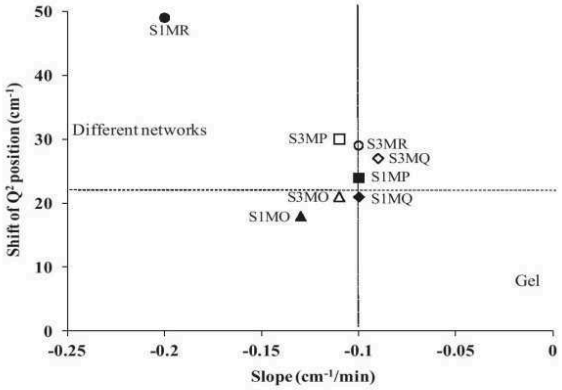

Fig. 5. Evolution of the Q^2 shift position in function of the slope value for (●) S1MR, (○) S3MR, (▲) S1MO, (△) S3MO, (♦) S1MQ, ( ) S3MQ, (■) S1MP and (□) S3MP samples.

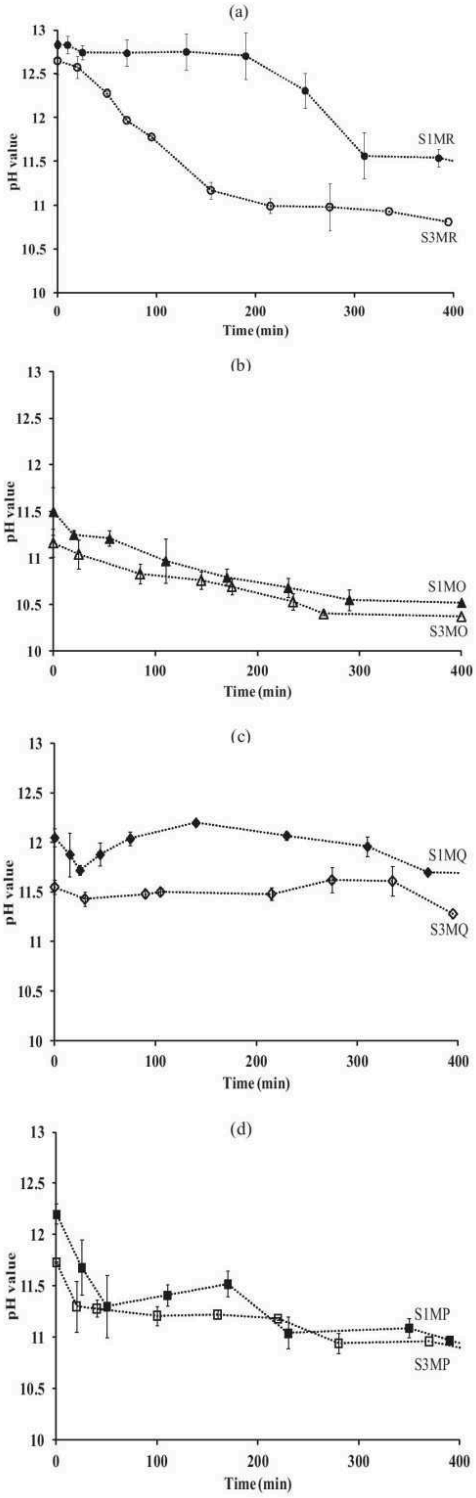

Fig. 6. Variation of the pH values along geopolymerisation measured in an aqueous media for (a) (●) S1MR, (○) S3MR, (b) (▲) S1MO, (△) S3MO, (c) (♦) S1MQ, ( ) S3MQ, and (d) (■) S1MP and (□) S3MP samples.

again after 170 min. A similar behavior of the pH value is shown in the case of S1MP after 50 min (Fig. 6d). However, it is less observed for S3MQ and S3MP most likely because of the competition between the formation of a geopolymer network and a Si-rich gel [20], which occurs because of the high purity of MQ and MP and their lower Si/Al ratios (1 and 0.98, respectively). The excess of siliceous species remains in the solution, which is responsible of the increase in pH. The use of the S3 solution with these two metakaolins (MQ and MP) appears to counterbalance the effect of excessive siliceous species of metakaolin and enhance the formation of the geopolymer phase in the detriment of the gel phase.

To clearly understand the effects of metakaolin and the alkaline solution reactivities on the polycondensation rate, a correlation between the FTIR and the pH value was established. Indeed, the slope and shift values obtained using FTIR were plotted in the function of consolidation time, when the pH value stabilizes, which indicates that there is no more species in the solution and consequently, the material is consolidated (Fig. 7). It is shown that the shift and slope values decrease when the consolidation time decreases. The S1MR sample shows the longest consolidation time (440 min), which is associated with the highest shift and slope values. Because of the impurities in the MR metakaolin, several interactions may occur among different phases in the mixture, which slows the oligomer formation and setting time. The use of the S3 solution decreases the shift and slope values as previously observed and the consolidation time to 395 min. For the remaining samples based on MO, MQ and MP, which are more reactive metakaolins, the use of S3 solution slightly decreases the consolidation time. Samples based on MQ and MP metakaolins show similar behaviors in terms of the shift, slope and consolidation time. However, S1MO and S3MO have the shortest consolidation time (290 and 265 min, respectively), which is consistent with the differences of reactivity among the metakaolins. The siliceous species, which are rapidly released from MO, easily react

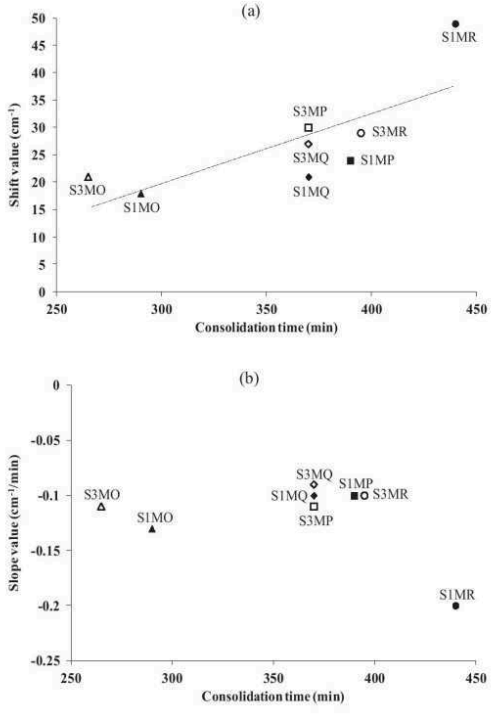

Fig. 7. Evolution of (a) the shift and (b) the slope values obtained by FTIR in function of the consolidation time estimated from the pH value following of the geopolymer reactive mixtures during formation.

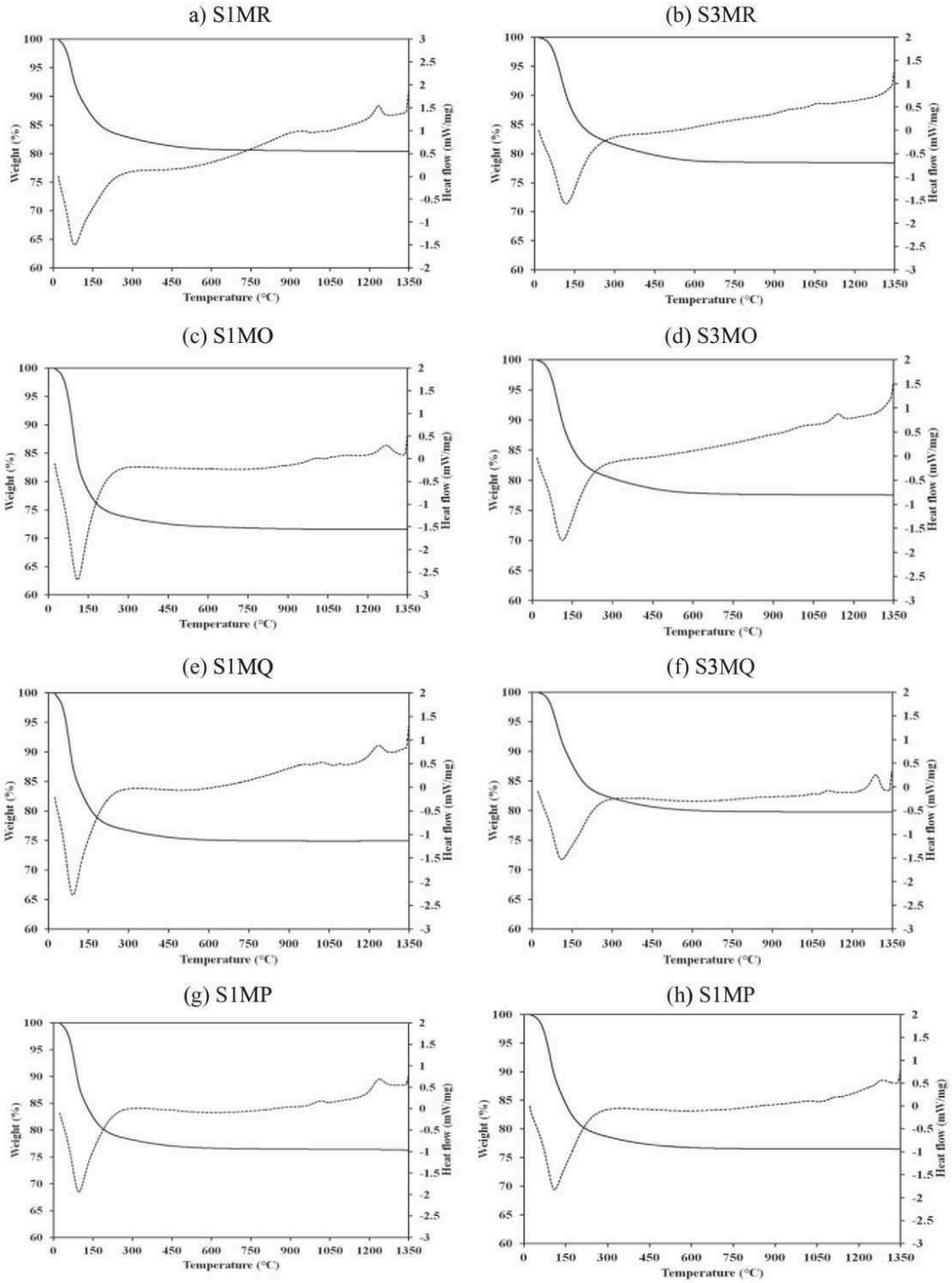

Fig. 8. Thermal curves of consolidated geopolymer samples (weight loss (solid line) and heat flow (dashed line)).

with the siliceous and/or aluminous species in the mixture. For MQ and MP, which are less reactive than MO according to the wettability values, the consolidation time is slower because the polycondensation reaction is disturbed by the formation of Si-rich gel.

Therefore, for a poorly reactive metakaolin (as observed for MR), the high reactivity of the alkaline solution may improve the polycondensation rate by a rapid formation of oligomers and as a result, the required time for consolidation is reduced. However, this effect is less important when more reactive metakaolins are used (MO, MQ and MP). In fact, the kinetics of the reaction and the consolidation time directly depend on the metakaolin reactivity.

3.3. Effect of the reactivity of the alkaline solution and metakaolins on the final properties of geopolymers

The various behaviors that are observed during the sample formation, which mainly occur because of the variations in metakaolin and alkaline solution reactivities, can affect the final properties of the synthesized materials. To verify this hypothesis, DTA-TG experiments were performed on the eight samples after 7 days of setting. The obtained thermal curves of the samples are shown in Fig. 8. Regardless of the sample, the TGA curves display two weight losses. Note that the major weight loss is observed below 250 °C, which indicates that the water in the geopolymer samples is mainly free and adsorbed water in small pores or in surface hydroxyl groups. The remaining weight loss at higher temperature can be attributed to more bound water, which results from the condensation of silanol or aluminol groups [29]. Samples with S1 solution exhibit increasing weight losses in the following order: S1MR (16.71%) < S1MP (21.71%) < S1MQ (22.75%) < S1MO (25.77%), which appears to be controlled by the metakaolin reactivity. More reactive metakaolin corresponds to more promoted and rapid oligomer formation, and water is trapped in the structure [12]. However, lower and closer weight losses are observed for samples with S3 solution (S3MR (17.54%), S3MO (18.86%), S3MQ (17.08%), S3MP (20.66%)) possibly because S3 has a lower initial water content than S1 [14]. Furthermore, regardless of the sample, the heat flow profiles show a large endothermic peak from 30 to 250 °C. Differences are detectable at higher temperatures (above 900 °C). When the S1 solution is used (Fig. 8a, c, e, g), regardless of the metakaolin, two exothermic peaks are observed at 1000 and 1200 °C, which denote the appearance of crystalline phases. According to the literature, these two peaks can be most likely assigned to the kalsilite and leucite formation at 1000 °C and 1200 °C, respectively [30]. Conversely, when S3 is used (Fig. 8b, d, f, h), the crystalline phases appear at higher temperatures. In order to identify precisely the crystalline phases those appear at higher temperatures, X-ray diffraction experiments were carried out on each sample after being heated at 1400 °C. An example of X-ray patterns obtained for S1M2 and S3M2 are presented in Fig. 9. From XRD patterns it is relatively easy to differentiate leucite from kalsilite phases using the pdf file (kalsilite $KAlSiO_4$; ICCD 00-048-1028, and Leucite $KAlSi_2O_6$; ICCD 01-071-1453). Whatever the samples studied, the recrystallization is effective and it is evidenced by the presence of leucite and kalsilite. However, some differences can be detected depending on the alkaline solution reactivity. For the S1 silicate solution, the XRD patterns after thermal treatment show the presence of leucite (dominant phase) with a little amount of kalsilite whatever the metakaolin used. In the case of the S3 silicate solution, which is more reactive, leucite and kalsilite are already present but the amount of kalsilite is comparatively higher (the intensity of such peak is higher). The presence and evolution of the phases in the geopolymers were also confirmed by ^{29}Si NMR MAS spectroscopy. Indeed, an increase of the peak area relative to kalsilite can be evidenced when S3 solution is used. Moreover, the difference observed in the XRD patterns confirms the DTA data and suggests that there are different network orders among the samples based on S1 and S3 solutions because the thermal properties are linked to the network order of silicon and aluminum in geopolymers [29]. Indeed, because of the reactivity

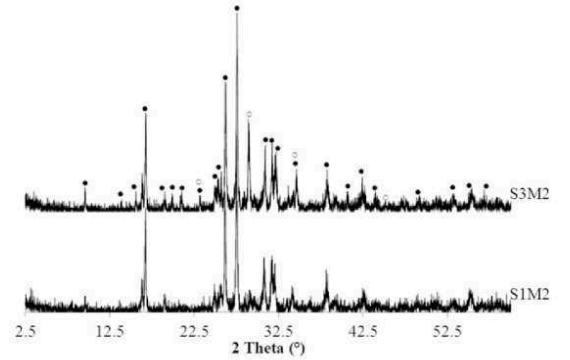

Fig. 9. X-ray patterns of S1M2 and S3M2 samples heated at 1400 °C (PDF files: ● $KAlSi_2O_6$ (01-071-1453) and ○ $KAlSiO_4$ (00-048-1028)).

of the species in S3, the formation of a more distorted geopolymer network is favored, which makes the S3-based samples more stable at high temperature and delays the recrystallization phenomenon.

4. Discussion

The various thermal behaviors of the samples, which translate into structural differences among the samples, affect the mechanical properties of the studied samples. To elucidate this effect, the mechanical strengths were evaluated by compression test after 7 days. The compressive strength values are reported in Table 2. Using the S1 alkaline solution, S1MO exhibited the highest mechanical strength (approximately 41 MPa), followed by S1MP, S1MR and S1MQ. However, for a highly depolymerized alkaline solution (S3), the compressive strengths are higher and notably similar (approximately 60 MPa) for the four metakaolins.

To understand the effect of the reactivity of raw materials on the mechanical properties of the final materials, the evolution of the compressive strength values was plotted as a function of the Si/K ratio multiplied by the weight loss between 30 and 250 °C, which is determined from the thermal analysis as shown in Fig. 10. It clearly appears that the compressive strength depends on the amount of water trapped in the structure. When S3 is used, higher and similar compressive strength values correspond to lower and similar (Si/K × weight loss), which indicates a lower amount of trapped water and confirms that the solution reactivity governs the mechanical properties. The effect of the metakaolin reactivity is more significant when we use S1, which is a less reactive

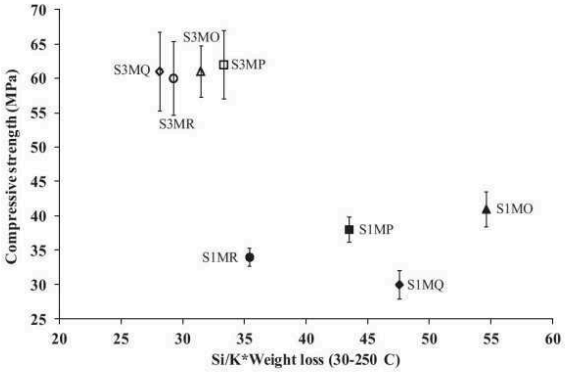

Fig. 10. Values of compressive strength obtained at 7 days in function of the parameter (Si/K*Weight loss (30–250 °C)) for each sample.

alkaline solution. The compressive strength values increase with increasing (Si/K × weight loss). For MR metakaolin, the coexistence of various networks leads to a heterogeneous structure and induces a decline of mechanical properties. The high reactivity of MO followed by MP leads to the formation of a geopolymer network, which yields the best mechanical properties. For MQ, the low compressive strength (30 MPa) can be explained by the presence of a gel as previously reported, which weakens the structure [12]. This result confirms that for a poorly reactive alkaline solution, the metakaolin reactivity controls the compressive strengths.

In summary, the obtained results show that the reactivity of metakaolin and the alkaline solution has crucial effects on the geopolymer formation and the working properties of the final materials.

5. Conclusion

This study focuses on the effect of the raw material reactivity on the geopolymer formation by elucidating the behavior of four different metakaolins in the presence of two potassium alkaline solutions. The results show that the polycondensation rate of the reactive geopolymer mixtures and the compressive strengths of the final materials strongly depend on the reactivity of metakaolin and the alkaline solution: (i) For a poorly reactive alkaline solution (low amount of Q^0 and non-bridging oxygen), the metakaolin reactivity is responsible for generating one or several networks, which control the geopolymerization reaction and subsequently affect the compressive strengths of synthesized materials.

(ii) When the alkaline solution is notably reactive (high amount of Q^0 and non-bridging oxygen), the depolymerized siliceous species enable a fast oligomer formation and, consequently govern the geopolymerization reaction and the final performances of the materials regardless of the properties of the used metakaolin.

Thus, it is possible to counter balance the reactivity of metakaolin by choosing the alkaline solution and vice versa.

References

[1] B.C. McLellan, R.P. Williams, J. Lay, A. van Riessen, G.D. Corder, Costs and carbon emissions for geopolymer pastes in comparison to ordinary portland cement, J. Clean. Prod. 19 (2011) 1080–1090.

[2] J. Davidovits, Geopolymer: Chemistry and Applications, 2nde édition Institut Géopolymère, St-Quentin, 2008.

[3] H. Xu, Geopolymerisation of Aluminosilicate Minerals(PhD Thesis) Department of Chemical Engineering, University of Melbourne, Australia, 2001.

[4] A. Buchwald, M. Hohmann, C. Kaps, The suitability of different clay resources in respect to form geopolymeric binders, 3rd Conference on Alkali-Activated Materials, Prag, 2007, pp. 137–148.

[5] N. Essaidi, B. Samet, S. Baklouti, S. Rossignol, Feasibility of producing geopolymers from two different Tunisian clays before and after calcination at various temperatures, Appl. Clay Sci. 88–89 (2014) 221–227.

[6] T.W. Cheng, J.P. Chiu, Fire-resistant geopolymer produced by granulated blast furnace slag, Min. Eng. 16 (2003) 205–210.

[7] N. Ye, J. Yang, X. Ke, J. Zhu, Y. Li, C. Xiang, H. Wang, L. Li, B. Xiao, Synthesis and characterization of geopolymer from Bayer red mud with thermal pretreatment, J. Am. Ceram. Soc. 97 (2014) 1652–1660.

[8] F. Zibouche, H. Kerdjoudj, J.B. d'Espinose de Lacaillerie, H. Van Damme, Geopolymers from Algerian metakaolin. Influence of secondary minerals, Appl. Clay Sci. 43 (2009) 453–458.

[9] A. Autef, E. Joussein, G. Gasgnier, S. Rossignol, Importance of metakaolin impurities for geopolymer based synthesis, Ceram. Eng. Sci. Proc. 34 (2014) 3–12.

[10] A. Elimbi, K.H. Tchakoute, D. Njopwouo, Effects of calcination temperature of kaolinite clays on the properties of geopolymer cements, Constr. Build. Mater. 25 (2011) 2805–2812.

[11] A. Autef, E. Joussein, A. Poulesquen, G. Gasgnier, S. Pronier, I. Sobrados, Role of metakaolin dehydroxylation in geopolymer synthesis, Powder Technol. 250 (2013) 33–39.

[12] A. Autef, E. Joussein, A. Poulesquen, G. Gasgnier, S. Pronier, I. Sobrados, J. Sanz, S. Rossignol, Influence of metakaolin purities on potassium geopolymer formulation: the existence of several networks, J. Colloid Interface Sci. 408 (2013) 43–53.

[13] D. Khale, R. Chaudhary, Mechanism of geopolymerization and factors influencing its development: a review, J. Mater. Sci. 42 (2007) 729–746.

[14] A. Gharzouni, E. Joussein, S. Baklouti, S. Pronier, I. Sobrados, J. Sanz, S. Rossignol, The effect of an activation solution with siliceous species on the chemical reactivity and mechanical properties of geopolymers, J. Sol–Gel Sci. Technol. (in press) 2014. http://dx.doi.org/10.1007/s10971-014-3524-0

[15] E. Prud'homme, P. Michaud, E. Joussein, J.M. Clacens, S. Rossignol, Role of alkaline cations and water content on geomaterial foams: monitoring during formation, J. Non-Cryst. Solids 357 (2011) 1270–1278.

[16] E. Prud'homme, P. Michaud, E. Joussein, J.M. Clacens, S. Rossignol, Durability of inorganic foam in solution: the role of alkali elements in the geopolymer network, Corros. Sci. 59 (2012) 213–221.

[17] G. Engelhard, D. Zeigan, H. Jancke, D. Hoebbel, Z. Weiker, High resolution ^{29}Si NMR of silicates and zeolites, Z. Anorg. Allg. Chem. 418 (1975) 17–28.

[18] M.T. Tognonvi, D. Massiot, A. Lecomte, S. Rossignol, J.P. Bonnet, Identification of solvated species present in concentrated and dilute sodium silicate solutions by combined ^{29}Si NMR and SAXS studies, J. Colloid Interface Sci. 352 (2010) 309–315.

[19] K.B. Langille, D. Nguyen, J.O. Bernet, D.E. Veinot, Mechanism of dehydration and intumescence of soluble silicates. I, effect of silica to metal oxide molar ratio, J. Mater. Sci. 26 (1991) 695–703.

[20] W.J. Malfait, W.E. Halter, Y. Morizet, B.H. Meier, R. Verel, Structural control on bulk melt properties: single and double quantum ^{29}Si NMR spectroscopy on alkali-silicate glasses, Geochim. Cosmochim. Acta 71 (2007) 6002–6018.

[21] N. Goudarzi, Silicon-29 NMR Spectroscopy Study of the Effect of Tetraphenylammonium (TPA) as a Template on Distribution of Silicate Species on Alkaline Aqueous and Alcoholic Silicate Solutions, Appl. Magn. Res. 44 (2013) 469–478.

[22] J.L. Bass, G.L. Turner, Anion distributions in sodium silicate solutions, characterization by ^{29}Si NMR and infrared spectroscopies, and vapor phase osmometry, J. Phys. Chem. B 101 (1997) 10638–10644.

[23] A. Autef, E. Joussein, A. Poulesquen, G. Gasgnier, S. Pronier, I. Sobrados, J. Sanz, S. Rossignol, Evidence of a gel in geopolymer compounds from pure metakaolin, J. Sol-Gel Sci. Technol. 65 (2013) 220–229.

[24] K.L. Konan, J. Soro, J.Y.Y. Andji, S. Oyetola, Gabrielle Kra, Etude comparative de la déshydroxylation/amorphisation dans deux kaolins de cristallinité différente, J. Soc. Ouest-Afr. Chim. 30 (2010) 29–39.

[25] M.R. North, T.W. Swaddle, Kinetics of silicate exchange in alkaline aluminosilicate solutions, Inorg. Chem. 39 (12) (2000) 2661–2665.

[26] C. Rees, G.C. Lukey, J.S.J. van Deventer, The microstructural characterization of geopolymers derived from fly ash and solid silicates, Geopolymer 2005 Proceedings, 2005, pp. 61–63.

[27] X.X. Gao, A. Autef, E. Prud'homme, P. Michaud, S. Basma, E. Joussein, S. Rossignol, Synthesis of consolidated materials from alkaline solutions and metakaolin: existence of domains in the Al–Si–K/O ternary diagram, J. Sol–Gel Sci. Technol. 65 (2013) 220–221.

[28] D. Landolt, Corrosion et Chimie de surface des métaux, 3 ème edition Press Polytechniques et Universitaires Romandes, Lausanne, 2003.

[29] P. Duxson, G.C. Lukey, J.S.J. van Deventer, Physical evolution of Na-geopolymer derived from metakaolin up to 1000 °C, J. Mater. Sci. 42 (2007) 3044–3054.

[30] V.F.F. Barbosa, K.J.D. MacKenzie, Synthesis and thermal behaviour of potassium sialate geopolymers, Mater. Lett. 57 (2003) 1477–1482.

Publication 3 (ACL3)

A. Gharzouni, E. Joussein, B. Samet, S. Baklouti, S. Rossignol,

"Addition of low reactive clay into metakaolin-based geopolymer formulation: Synthesis, existence domains and properties"

Powder Technol. 288 (2016) 212-220

Cette étude a été menée afin d'évaluer la réactivité d'une argile tunisienne, un métakaolin et des mélanges des deux en présence d'un milieu alcalin. Pour cela, les précurseurs aluminosilicates utilisés ont été caractérisés. Ensuite, plusieurs échantillons ont été synthétisés en faisant varier les proportions du métakaolin et d'argile dans le mélange, ainsi que le rapport molaire Si/K de la solution alcaline. Des corrélations entre (i) la cinétique de formation des mélanges synthétisés, suivie par spectroscopie IRTF, (ii) les propriétés mécaniques, évaluées par des tests de compression, et (iii) la composition chimique ont été mises en évidence. De plus, un modèle de réactivité a été proposé afin de schématiser les différents réseaux formés pour chaque échantillon. L'argile tunisienne, après traitement thermique, présente une certaine réactivité qui permet la formation des matériaux consolidés. Les minéraux associés présents dans l'argile, tels que l'hématite et l'illite, ne participent pas à la réaction de polycondensation et sont simplement collés par la solution alcaline. Cependant, l'augmentation de la proportion de métakaolin dans le mélange et la quantité plus importante des espèces dépolymérisées, provenant de la solution alcaline, favorisent le taux de polycondensation et les propriétés mécaniques des matériaux finaux. Les propriétés optimales sont obtenues pour un mélange de 50% d'argile tunisienne et 50% de métakaolin et un rapport Si/K de la solution alcaline de 0,50.

Powder Technology 288 (2016) 212–220

Contents lists available at ScienceDirect

Powder Technology

journal homepage: www.elsevier.com/locate/powtec

Addition of low reactive clay into metakaolin-based geopolymer formulation: Synthesis, existence domains and properties

A. Gharzouni [a,b], B. Samet [b], S. Baklouti [b], E. Joussein [c], S. Rossignol [a,*]

[a] Science des Procédés Céramiques et de Traitements de Surface (SPCTS), Ecole Nationale Supérieure de Céramique Industrielle, 12 rue Atlantis, 87068 Limoges Cedex, France
[b] Laboratoire de Chimie Industrielle, Ecole Nationale d'Ingénieurs de Sfax, 3038 Sfax, Tunisia
[c] Université de Limoges, GRESE EA 4330, 123 Avenue Albert Thomas, 87060 Limoges, France

ARTICLE INFO

Article history:
Received 5 May 2015
Received in revised form 16 October 2015
Accepted 6 November 2015
Available online 10 November 2015

Keywords:
Geopolymers
Clay
Metakaolin
Alkaline solution
Associated minerals
Gel
Si/K ratio

ABSTRACT

This paper investigates the addition of low reactive Tunisian clay into metakaolin-based geopolymer as a valorization way in alkaline media. To conduct this investigation, the aluminosilicate precursors used were primarily characterized. Then, several samples were prepared by varying the amounts of metakaolin and clay in the mixture as well as the Si/K molar ratio of the alkaline solution. Correlations between (i) the polycondensation rate of the synthesized mixtures, followed by FTIR spectroscopy; (ii) the working properties, evaluated by the compression test; and (iii) the chemical composition were established, and a model of reactivity was proposed to elucidate the different networks formed for each sample. It appears that the Tunisian clay, after heat treatment, exhibits some reactivity that allows for the formation of consolidated materials. The associated minerals present in the clay seem not to participate in the polycondensation reaction and are simply agglomerated by the alkaline solution. However, the increase of the proportion of metakaolin in the mixture and the depolymerized species in the alkaline solution may improve the polycondensation rate and the working properties of the final materials. The optimal properties were obtained for a mixture of 50% low reactive Tunisian clay and 50% metakaolin and a Si/K ratio of the alkaline solution of 0.50.

1. Introduction

Tunisia is among the countries that have numerous large clay deposits that remain not fully exploited [1]. So far, Tunisian clays have been largely used in the traditional ceramic industry [2,3]. More innovative recent applications include the evaluation of the pozzolanic activity of Tunisian clays [4], the preparation of a clay-based micro-porous filtration membrane [5,6]and the mineralization of organic compounds in waste waters [7]. A novel application, yet not largely studied, is the use of Tunisian clays as an aluminosilicate source for the synthesis of geopolymer or geomaterial-based materials. This seems to be a potentially profitable application that allows not only reducing the cost of the raw materials but also valorizing natural resources.

Geopolymers are a promising and innovative new class of binders generated from the activation of an aluminosilicate source with an alkaline solution [8]. Their formation implies the dissolution of aluminosilicate species in an alkaline environment to form an amorphous three-dimensional geopolymer network by polycondensation reactions. The geopolymerization process is strongly influenced by the nature of the raw materials used [9]. Furthermore, depending on the raw material, geopolymers can exhibit various properties such as high compressive strength, low shrinkage, acid resistance, fire resistance and low thermal conductivity [10]. The aluminosilicate source, metakaolin, is one of the most commonly used raw materials because of its purity and high reactivity [11,12,13]. Autef et al., [12,13] have studied the behavior of three commercial metakaolins, which differ in terms of reactivity, dehydroxylation process and the amount of impurities, in the presence of an alkaline solution. It was demonstrated that, depending on the metakaolin used, one or several geopolymer networks are formed that govern the working properties. Despite the extensive use of metakaolin, research on low-cost and more available materials has encouraged many investigators [14,15, 16,17,18] to turn to the use of common clays that display some reactivity that enables them to be suitable for producing geopolymer materials. Recently, two Tunisian clays, a kaolinitic clay from the region of Tabarka and an illito-kaolinitic clay rich in hematite from the region of Medenine, were tested as potential aluminosilicate precursors [15]. It appears that it is possible to obtain consolidated materials from fresh and calcined clays, although materials based on the calcined clays exhibit better mechanical strength. This fact highlights the effect of the heat treatment on the amorphization of clay minerals, and consequently, on the reactivity of the clay in an alkaline media.

Regardless of the aluminosilicate source, the alkaline solution plays an important role in the geopolymerization reaction [19]. In a previous work [20], the influence of the activating solution was elucidated.

* Corresponding author.
E-mail address: sylvie.rossignol@unilim.fr (S. Rossignol).

http://dx.doi.org/10.1016/j.powtec.2015.11.012
0032-5910/

Indeed, the Si/K molar ratio was observed to control the degree of depolymerization of the silicate solution as well as the type and the amount of the siliceous species. Moreover, depolymerized species are highly reactive, which enables the fast formation of oligomers and leads to better mechanical properties of the resulting geopolymers.

In summary, both the aluminosilicate source and alkaline solution are key parameters in the geopolymerization reaction. Regarding the variability of the raw materials that can be used, the effect of the reactivity of each precursor is not fully understood. The objective of this work is to define consolidated materials ternary existence domains based on metakaolin mixture with poorly reactive clay and alkaline solution as a tool to predict geopolymer formation and then valorization way of low reactive clay. Tunisian clay was used as low reactive raw materials corresponding potentially to a large amount of deposits around the world. Moreover, this study aims to deeper comprehension of the effect of the aluminosilicate source reactivity as well as the effect of the activation solution on the geopolymer formation, final structure and working properties in order to define the key parameters controlling the polycondensation reaction when using not pure precursors. In fine, for this, a comparative study of the physical and chemical properties of the various aluminosilicate sources used was established. Then, several samples were prepared by varying the proportion of calcined Tunisian clay and metakaolin and/or the Si/K ratio of the alkaline solution. The structural evolution of the reactive mixtures was monitored by FTIR spectroscopy. Finally, the consolidated materials were characterized by compression tests, X-ray diffraction, and SEM.

2. Experimental

2.1. Raw materials and sample preparation

Two types of clays were used in this study, kaolin supplied by Imerys (France) and low reactive red Tunisian clay from the region of Medenine situated in the South of Tunisia. The two clays were sieved at 80 μm and calcined for 4 h at 700 °C with a heating rate of 5 °C/min. The obtained materials were used as aluminosilicate sources to elaborate geopolymer samples and were denoted as Me and MK for Medenine clay and metakaolin, respectively (Table 1).

Geopolymer samples were prepared by dissolving potassium hydroxide pellets, supplied by VWR (Belgium) (85.2% pure), into a commercial potassium silicate solution (Si/K = 1.7) supplied by ChemLab (Belgium). Then, Me clay and/or MK were added. Samples were placed in a closed sealable polystyrene mold at room temperature (25 °C) according to the procedure previously established by Autef et al. [12].

Table 1
Chemical and physical properties of the two MK and Me aluminosilicate precursors used.

Aluminosilicate precursors		Metakaolin	Calcined Medenine clay
Nomenclature		MK	Me
Color		White	Red
SiO_2	(wt.%)	53.30	59.80
Al_2O_3		45.50	21.84
Fe_2O_3		–	7.56
TiO_2		1.20	1.05
$K_2O + Na_2O$		–	4.34
$CaO + MgO$		–	5.37
d_{50} (μm)		8	10
BET value (m^2/g)		8	29
Initial kaolinite amount* (%)		99	27
Amorphous phase** (%)		98	25
Wettability (μL/g)		1010	600

* Determined from TGA analysis.
** Determined from Rietveld.

The mixtures were denoted as $^{Si/K}GM^{mMe/mMK}$, where Si/K refers to the Si/K molar ratio of the alkaline solution and mMe and mMK are the masses of Me and MK, respectively, for a total of 12 g of aluminosilicate sources. For example, $^{0.70}G^{9/3}$ corresponds to a mixture composed of 9 g of Me and 3 g of MK with a Si/K molar ratio of the alkaline solution of 0.70.

2.2. Sample characterization

The chemical composition of the raw materials was determined using X-ray fluorescence (ARL 8400, XRF 386 software).

The particle size distributions of the clays were measured using a laser particle size analyzer (Mastersizer 2000). The powder is suspended by an air current flowing through a glass cell with parallel faces illuminated by a beam of laser light. The measurement is made at a pressure of 3 bars.

Powder BET surface areas were determined by N_2 adsorption at −195.85 °C using a Micrometrics Tristar II 3020 volumetric adsorption/desorption apparatus. Prior to the measurement, the samples were degassed at 200 °C under vacuum for 4 h.

The wettability value (μL/g) corresponds to the volume of water that can be adsorbed by one gram of powder until saturation.

X-ray diffraction patterns were acquired via X-ray diffraction (XRD) experiments on a Bruker-AXS D 5005 powder diffractometer using CuK α radiation (λKα = 0.154186 nm). The analytical range is between 5° to 60° (2θ) with a step of 0.04° and an acquisition time of 2 s for raw clays, and a dwell time of 0.5 s and a step size of 0.01° (2θ) for consolidated materials. JCPDS (Joint Committee Powder Diffraction Standard) files were used for phase identification.

FTIR spectra were obtained on a Thermo Fisher Scientific 380 infrared spectrometer (Nicolet) using the attenuated total reflection (ATR) method. The IR spectra were recorded over a range of 400 to 4000 cm^{-1} with a resolution of 4 cm^{-1}. The atmospheric CO_2 contribution was removed via a straight-line fit between 2400 and 2280 cm^{-1}. To monitor the geopolymer formation, software was used to acquire a spectrum (64 scans) every 10 min for 13 h. To enable comparison, the spectra were baseline corrected and normalized [21].

The compressive strengths were tested using a LLOYD EZ20 universal testing machine with a crosshead speed of 0.1 mm/min. The compressive tests were performed on ten samples for each composition. The values of compressive strength represent the average of the ten obtained values. The test tubes used for the compression tests were cylindrical in shape with a diameter (Φ) of 15 mm and a height (h) of approximately 30 mm [22] and were aged for 7 days in a closed mold at room temperature.

The morphology of the final materials was observed using a Philips XL30 scanning electron microscope (SEM) at 15 kV. An Au/Pd fine layer was deposited on the samples before the observations.

3. Results and discussion

3.1. Aluminosilicate precursors and feasibility of consolidated materials

3.1.1. Investigation of the aluminosilicate precursors

To elucidate the main differences between the two aluminosilicate sources used, a preliminary characterization was performed. Me and MK were extensively studied using various characterization techniques described by Essaidi et al. [15] and Autef et al. [12], respectively. Therefore, only the main physical and chemical characteristics as well as the mineralogical analysis of these two precursors will be briefly described in this study. The chemical compositions of the studied precursors are detailed in Table 1. It clearly appears that MK is very pure because it contains only SiO_2 and Al_2O_3 with a Si/Al molar ratio near 1 (the theoretical value for kaolinite is Si/Al = 1, traducing the purity of the metakaolin). However, Me has a high amount of silica (59.86%) and a lower alumina content (21.84%), for a Si/Al ratio near 2.4. The presence of impurities is also evidenced in the Fe_2O_3 content (7.56%), which was

expected from its red color. Moreover, the relatively high amounts of K_2O (3.92%) and MgO (2.24%) suggest the presence of illite clays. To confirm these hypotheses, X-ray diffraction (XRD) was performed. The mineralogical composition of Me after calcination (Fig. 1a) is mainly composed of quartz, illite and hematite. The kaolinite reflections disappear after heat treatment at 700 °C, which confirms that the temperature is sufficient to transform kaolinite into metakaolinite [23]. On the other hand, the diffractogram of MK (Fig. 1b) is typical of the metakaolin phase and exhibits a unique dome, characteristic of amorphous material, without other contributions, confirming the high purity of this metakaolin. These data are also validated by TGA analysis (data not shown) enabling the estimation of the initial kaolinite content (Table 1) and evidencing that MK is initially rich in kaolinite (99% of kaolinite before dehydroxylation). However, Tunisian clay contains only 27% kaolinite. XRD using the Rietveld method [24] provides quantitative information on the percentage of the amorphous phase in the two precursors. As expected, the amorphous phase is significantly more prevalent in the MK (98%) than in the Me (25%). These results are in accordance with the chemical and TGA analyses. Furthermore, Me and MK were characterized by BET analysis, wettability and size distribution (Table 1). The samples, after being sieved at 80 μm, have similar median diameters (d_{50}). The BET surface is higher in the case of Me (29 m^2/g) compared to MK (8 m^2/g) due to the presence of accessory phases such as illite, which is characterized by a large specific surface varying between 80 and 100 m^2/g [25]. The wettability value of MK is notably higher than Me. This fact can be explained by the structural differences between the two precursors. In fact, the amount of reactive phase (% amorphous phase) affects the adsorption process and consequently the affinity of the surface to water.

In summary, the different physical and chemical properties of the two precursors suggest different reactivities in an alkaline media. As expected, MK is more reactive than Me.

3.1.2. Feasibility of consolidated materials

Regarding the comparatively low content of the amorphous phase in Me clay (25%, Table 1), mixtures based on Me, MK and mixtures of both clays were studied. A preliminary study of the feasibility of consolidated materials was performed on 17 compositions with varying proportions of substitution of Me by MK (0, 3, 6, 9 and 12 g of MK within the 12 g of total aluminosilicate source) and the Si/K ratio of the alkaline solution (0.37, 0.50, 0.58 and 0.70). Fig. 2 represents all the synthesized compositions in a ternary diagram (wt.% Me–wt.% MK–wt.% alkaline solution). Based on their visual aspects and consolidated states, three types of materials can be distinguished: (i) stratified materials presenting different macroscopic phases, (ii) heterogeneous materials that are not consolidated and (iii) consolidated materials presenting a homogeneous structure. This is in accordance with the work of Gao et al. [26] examining the existence of domains of materials on a Si–Al–K ternary diagram including geopolymer, gel, sedimented and hardening materials depending on the Si/Al and Si/K ratios. For Si/K = 0.37, only the sample based on Me ($^{0.37}G^{12/0}$) is homogeneous. The substitution of Me with MK leads to the formation of heterogeneous materials ($^{0.37}G^{9/3}$, $^{0.37}G^{6/6}$, $^{0.37}G^{3/9}$ and $^{0.37}G^{0/12}$). This is due to the higher wettability value of MK compared to that of Me (Table 1). Therefore, the amount of reactive species coming out of the solution is not enough to completely alter the aluminosilicate source and trigger a polycondensation reaction. The particles are only coated by the alkaline solution. For the same reason, the substitution of Me by MK is feasible until 50% for Si/K = 0.70 ($^{0.70}G^{12/0}$, $^{0.70}G^{9/3}$ and $^{0.70}G^{6/6}$). For Si/K = 0.58, homogenous materials were obtained only for $^{0.58}G^{3/9}$ and $^{0.58}G^{0/12}$, while stratified materials exhibiting several layers are formed for the rest of the samples ($^{0.58}G^{12/0}$, $^{0.58}G^{9/3}$ and $^{0.58}G^{6/6}$). This fact can be explained by the excess of the alkaline solution and the deficiency of aluminate species available (low amount of aluminate species from Me), leading to the formation of alumino-silica gels with potassium [27] and an excess of alkaline solution floating on the surface. These materials hardened after several weeks, as the aluminum availability was proven to control the extent of the reaction and the hardening of the material [28]. Two extra compositions were tested for Si/K = 0.50 ($^{0.50}G^{9/3}$ and $^{0.50}G^{6/6}$) and lead to homogeneous consolidated materials.

In the following sections, only five compositions, exhibiting the best consolidated and homogeneous forms reported in Table 2, were selected for characterization. Two mixtures based on either MK or Me, denoted $^{0.58}G^{0/12}$ and $^{0.37}G^{12/0}$, respectively, were considered to be reference materials. In $^{0.70}G^{9/3}$ and $^{0.70}G^{6/6}$ materials, mixtures of Me and MK were used, and the Si/K molar ratio of the activating solution was fixed at 0.70. The impact of the Si/K molar ratio of the alkaline solution was investigated by varying this ratio from 0.70 in the $^{0.70}G^{6/6}$ material to 0.50 in the case of the $^{0.50}G^{6/6}$ sample. The appearance of a gel (transparent liquid) was observed on the surface of the $^{0.58}G^{0/12}$ and $^{0.70}G^{6/6}$ samples and, to a lesser extent, in the $^{0.70}G^{9/3}$ and $^{0.50}G^{6/6}$ materials. The same phenomenon was observed by Autef et al. [29] using a highly

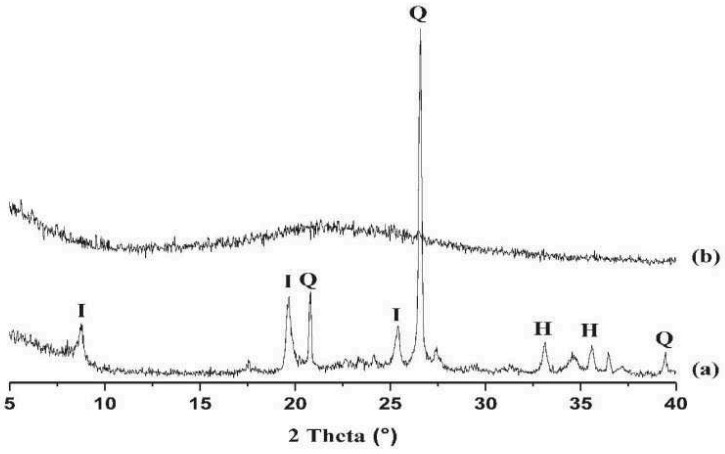

Fig. 1. XRD patterns of (a) Me clay and (b) MK after calcination at 700 °C. The main diffraction peaks are indexed according to the JCPDS files (Q: Quartz (04-008-7651), I: Illite (04-016-2976), H: Hematite (04-002-4944)).

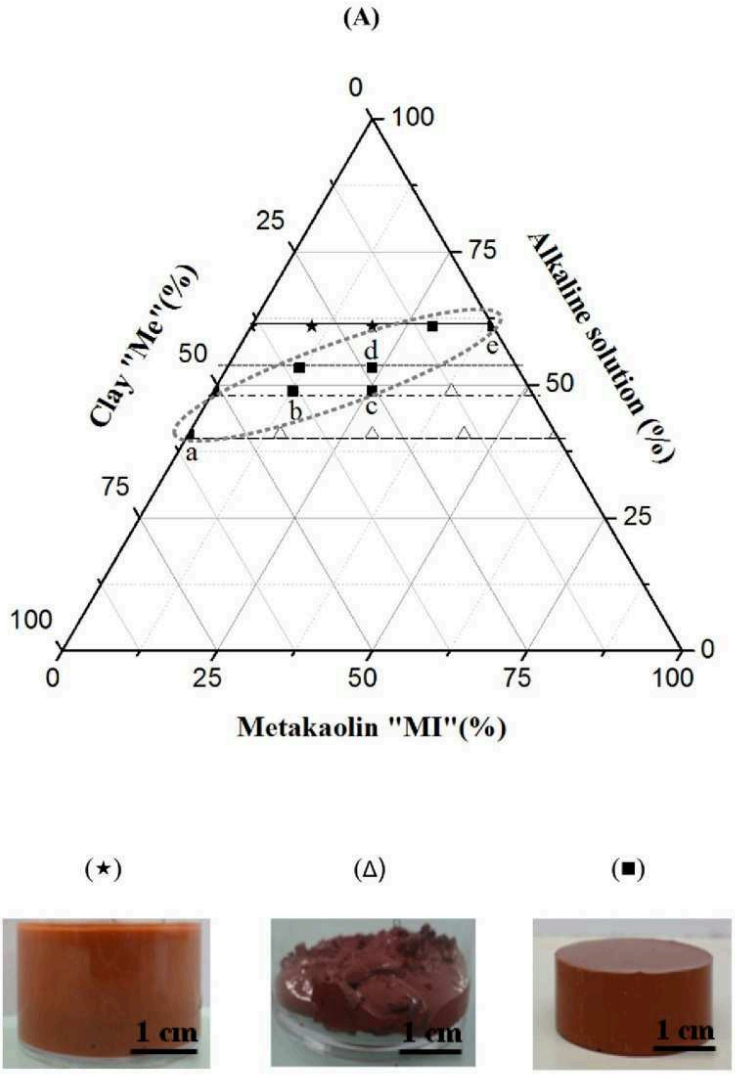

Fig. 2. Existence domains of synthesized mixtures on metakaolin "MK", clay "Me" and alkaline solution ternary for (—) Si/K = 0.58, (•••) Si/K = 0.50, (-•-) Si/K = 0.70 and (—) Si/K = 0.37 and different forms of: (★) stratified materials, (Δ) heterogeneous materials, (■) homogeneous consolidated materials (a, b, c, d, e were the compositions selected for characterization).

pure metakaolin and was explained by the siliceous species saturation of the solution leading to the formation of a gel. The differences observed in the amount of gel floating on the surface may be due to the proportion of MK in the mixture and the amount of water in the alkaline solution.

Table 2
Designation and composition of the selected geomaterial samples for characterization.

Sample	Si/K	Si/Al
$^{0.37}G^{12/0}$	1.1	1.5
$^{0.70}G^{9/3}$	2.0	1.5
$^{0.70}G^{6/6}$	2.6	1.4
$^{0.50}G^{6/6}$	1.7	1.4
$^{0.58}G^{0/12}$	2.1	1.4

3.2. Investigation of the selected compositions

3.2.1. Structural evolution

To assess the effect of the substitution of Me with MK as well as the impact of the activating solution, the structural evolution of the different synthesized mixtures was monitored by FTIR spectroscopy in ATR mode. Fig. 3A presents two infrared spectra recorded at 0 and 450 min, respectively, for the $^{0.50}G^{6/6}$ sample. A decrease of the H_2O bands located at 3255 and 1620 cm^{-1} and a shift of the Si–O–Si (Q^2) situated at 980 cm^{-1} [21] were detected over time. Hence, the polycondensation reaction induces a modification of the network and consequently a modification of the band vibration in the mixture.

Fig. 3B presents the Q^2 shift as a function of time for the $^{0.58}G^{0/12}$, $^{0.50}G^{6/6}$ and $^{0.37}G^{12/0}$ reactive mixtures. The evolution of the position of this band indicates the substitution of Si–O–Si by Si–O–Al bonds and therefore reflects a polycondensation reaction. The slope of the curve is characteristic of the kinetics of this substitution [12]. The initial band

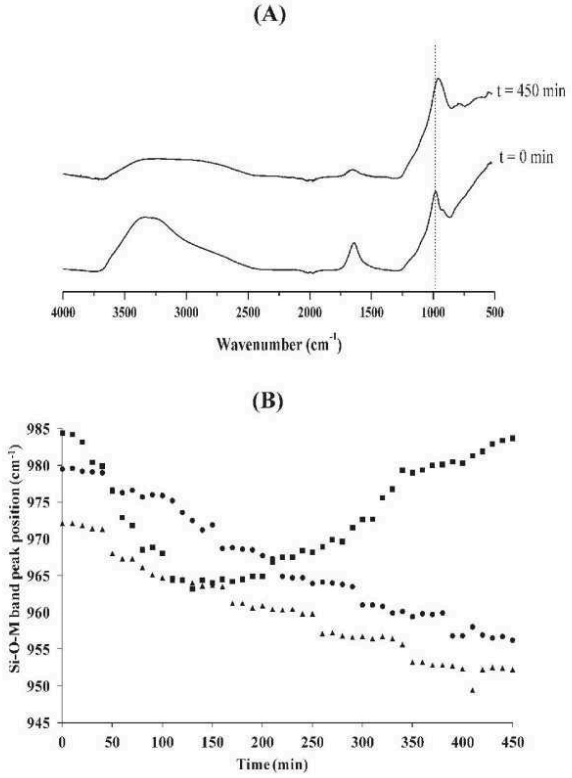

Fig. 3. (A) Example of infrared spectra recorded at t = 0 and t = 450 min for $^{0.50}G^{6/6}$ sample and (B) evolution of the shift of Si–O–M band position from IR spectra versus the time for (■) $^{0.58}G^{0/12}$, (●) $^{0.50}G^{6/6}$ and (▲) $^{0.37}G^{12/0}$ reactive mixtures.

positions are different for the three mixtures and decrease in the following order: $^{0.58}G^{0/12}$ (984 cm^{-1}), $^{0.50}G^{6/6}$ (979 cm^{-1}) and $^{0.37}G^{12/0}$ (972 cm^{-1}). This order seems to be imposed by the Si/K molar ratio of the alkaline solutions. In fact, the initial band positions decrease with the decrease of the Si/K molar ratio of the activating solution due to the increase of the number of non-bridging oxygen atoms [30]. $^{0.58}G^{0/12}$ and $^{0.50}G^{6/6}$ mixtures exhibit the same behavior. In fact, the position of the Q^2 band shifts toward lower wavenumbers over time. However, in the case of the $^{0.58}G^{0/12}$ mixture, the peak shifted back to higher wavenumbers after 200 min. This sudden increase can be explained by the appearance of Q^3 bonds. Indeed, the gel phase, observed during the synthesis, suggests that a polymerization reaction took place due to the siliceous species saturation of the solution [29].

To better understand the effect of the substitution of Me clay by MK as well as the effect of the Si/K ratio of the alkaline solution, the shift values for all the samples were plotted as a function of the $n_{Si}/(n_K + n_{Al})$ ratio presenting the chemical composition of the mixture (Fig. 5). The shift value tended to increase as the $n_{Si} / (n_K + n_{Al})$ ratio increased until approximately 0.77, at which point it decreased. It seems that from this value ($n_{Si} / (n_K + n_{Al}) = 0.77$), there is an excess of silica that perturbs the polycondensation reaction [31,32]. This explains the decrease of the shift values. Higher shift values are obtained in the cases of $^{0.50}G^{6/6}$ and $^{0.58}G^{0/12}$ (26 cm^{-1} and 21 cm^{-1}, respectively). These values indicate the possible formation of an aluminosilicate network. For the remaining samples, the lower shift values seem to be due to the competition of several networks perturbing the polycondensation reaction [12].

The different behaviors during geopolymerization detected by FTIR spectroscopy indicate differences between the networks formed in each sample. These differences may influence the working properties of the final materials.

3.2.2. Consolidated materials

The mechanical properties of the consolidated materials were evaluated by subjecting the samples to compression after 7 days aging. Compressive strength values as a function of the strain values for the $^{0.37}G^{12/0}$, $^{0.50}G^{6/6}$ and $^{0.58}G^{0/12}$ samples are presented in Fig. 5A. The curve shapes are characteristic of brittle materials [33]. The curves relative to the $^{0.50}G^{6/6}$ and $^{0.58}G^{0/12}$ samples displayed a more linear ascending part and more elastic deformation relative to $^{0.37}G^{12/0}$. However, $^{0.37}G^{12/0}$ (based on Me clay only) exhibited some plastic deformation. This may be due to the remaining associated minerals in this clay after heat treatment, especially the presence of illite, which induces high plasticity. Furthermore, Prud'homme et al. [27] have demonstrated that in similar types of materials (considered geopolymer composites) the presence of compounds such as quartz and dolomite act as reinforcements to the geopolymer matrix. These curves also permit the determination of the elastic modulus E (slope of the curve) of each sample. $^{0.50}G^{6/6}$ and $^{0.58}G^{0/12}$ samples exhibit the highest elastic modulus (2.8 and 2.5 GPa, respectively), while the elastic modulus of the $^{0.37}G^{12/0}$ sample is approximately 1.6 GPa. These values are in agreement with the literature [31,34]. Typical values for the elastic modulus of metakaolin-based geopolymers range from 1 GPa to 6 GPa.

To correlate the mechanical properties and the chemical compositions of the mixtures, the evolution of the specific mechanical strength values (σ/ρ, where ρ is the density of the specimens) as well as the elastic modulus were plotted versus $n_{Si} / (n_K + n_{Al})$ in Fig. 5B. Similar to the tendency observed in Fig. 4, the compressive strength value and the elastic modulus increased as the $n_{Si} / (n_K + n_{Al})$ ratio increased until an optimal value, at which point it decreased. The $^{0.58}G^{0/12}$ and $^{0.50}G^{6/6}$ samples exhibit the best mechanical properties, while the $^{0.37}G^{12/0}$, $^{0.70}G^{9/3}$ and $^{0.70}G^{6/6}$ samples displayed weaker compressive strength values because of the low content of the amorphous phase (i.e., reactive aluminosilicate phase) in Me clay [35]. These results are in agreement with the trends observed in the FTIR spectra discussed above. The associated minerals such as illite and hematite in Me clay did not participate in the polycondensation reaction and are simply coated by the alkaline solution (binder). This finding is in agreement with the work of Essaidi et al. [36], which highlights the role of hematite and its contribution to the polycondensation reaction using investigation materials based on metakaolin and iron oxide. It was demonstrated that the contribution of iron oxide seems to be negligible.

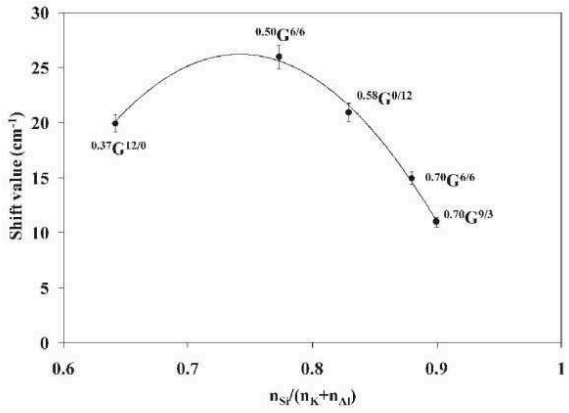

Fig. 4. Evolution of the shift value versus the chemical composition ($n_{Si} / (n_K + n_{Al})$) of the different mixtures.

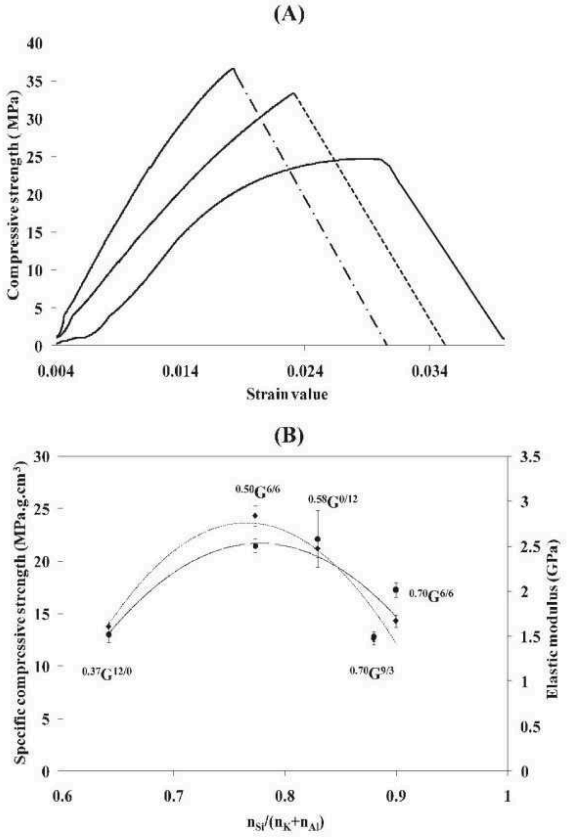

Fig. 5. (A) Compressive strength as a function of the strain value for (—) $^{0.37}G^{12/0}$, (-•-) $^{0.50}G^{6/6}$ and (---) $^{0.58}G^{0/12}$ samples and (B) evolution of (●) the specific compressive strength value and the (♦) elastic modulus versus the chemical composition (n_{Si} / ($n_K + n_{Al}$)) of the different mixtures.

The effect of the reactivity of the Si/K of the alkaline solution was also highlighted. In fact, the decrease of the Si/K molar ratio of a single aluminosilicate mixture (50% of Me clay, 50% of MK from 0.70 to 0.50 ($^{0.50}G^{6/6}$ vs. $^{0.70}G^{6/6}$)) sample caused a significant increase in the mechanical strength. In fact, as previously discussed, the Si/K ratio seems to control the degree of depolymerization of the silicate solutions. The depolymerized species, highly reactive, enables the fast formation of oligomers and therefore enhances the mechanical properties of the final materials [20,30].

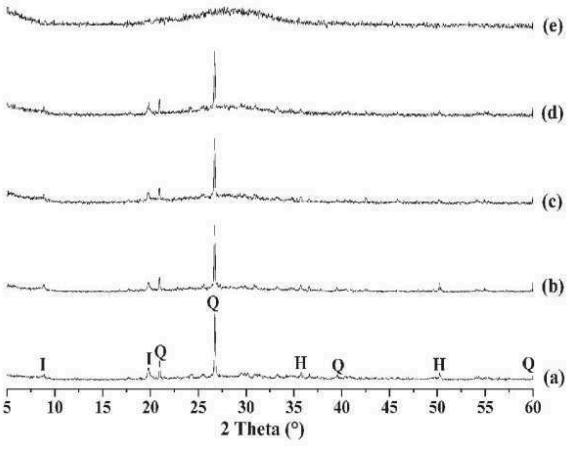

Fig. 6. X-ray patterns of (a) $^{0.37}G^{12/0}$, (b) $^{0.70}G^{9/3}$, (c) $^{0.70}G^{6/6}$, (d) $^{0.50}G^{6/6}$ and (e) $^{0.58}G^{0/12}$ samples at room temperature (JCPDS files; Q: Quartz (01-085-0865), I: Illite (00-009-0343), H: Hematite (00-003-0812)).

To validate these explanations, XRD diffraction was performed for all samples at room temperature (Fig. 6). The XRD patterns relative to the $^{0.37}G^{12/0}$ sample (Fig. 6a) evidence the presence of a minor dome centered at approximately 28° (2θ), characteristic of a slight amorphization, in addition to the persistence of the diffraction peaks attributed to crystalline phases such as illite, quartz and hematite, which are less subject to alkaline attack [37]. However, a slight increase in the intensity of the amorphous dome together with a slight decrease in the reflections related to the crystalline phases is noticeable in the cases of $^{0.70}G^{9/3}$ and $^{0.70}G^{6/6}$ (Fig. 6b, c). These changes are indicative of the restructuration of the material and are directly related to the increase of the MK content in the mixture, inducing the increase of the Si and Al species available, thereby favoring dissolution and network formation [38,39]. The same changes are more distinctive for the $^{0.50}G^{6/6}$ sample (Fig. 6d) and are due, in this case, to the reactivity of the depolymerized species released from the alkaline solution (with lower Si/K), as discussed previously, enhancing the partial dissolution of phases and the polycondensation reactions. Indeed, Sedmale et al. [40] demonstrated that highly alkaline conditions may cause slight structural changes in the illitic phase but do not destroy it completely. The changes are essentially associated with a decrease in the intensity of the diffraction peaks of illite. Finally, a typical broad dome characteristic of amorphous material centered at approximately 29° (2θ) [31] is effective for the $^{0.58}G^{0/12}$ sample (Fig. 6e), giving evidence to a complete alteration (and consumption) of the metakaolin. All these facts corroborate the formation of an amorphous compound resulting from a polycondensation reaction. The presence of secondary phases in Me clay appear not to perturb the reaction. However, the rate of the reaction is strongly related to the amount of metakaolin (reactive aluminosilicate species) in the mixture and the Si/K ratio of the alkaline solution (depolymerized alkaline species).

To obtain additional microstructural information, the SEM micrographs of the five compositions are presented in Fig. 7. In the case of $^{0.37}G^{12/0}$ (Fig. 7a), there appear unreacted particles coated by the alkaline solution, which leads to a comparatively heterogeneous structure and explains the inferior mechanical strengths obtained. The micrographs of $^{0.70}G^{9/3}$ (Fig. 7b) and $^{0.70}G^{6/6}$ (Fig. 7c) reveal mixtures of the microstructures of the geopolymer phase, gel and coated particles, depending on the amounts of the MK and Me clays in the mixture. The geopolymer phase seems to be favored in the $^{0.50}G^{6/6}$ sample (Fig. 7d). Finally, the micrograph of $^{0.58}G^{0/12}$ (Fig. 7e) clearly displays the microstructure of the amorphous geopolymer phase [26,31], which is in agreement with the XRD data and was expected due to the significant amorphous phase in MK clay, and thereby its high reactivity enhances the formation of a geopolymer phase.

In summary, the results of this study permit establishing a descriptive model of reactivity, schematically presented in Fig. 8. Indeed, depending on the proportion of the substitution of Me by MK and the Si/K ratio of the activating solution, it seems that three types of networks can be formed: (i) a geopolymer network, (ii) a coating phase agglomerating the associated minerals and finally, (iii) a gel phase rich in silicon. Me clay leads to the formation of a small geopolymer network in addition to a coating phase agglomerating the unreacted associated mineral such as illite and hematite. With MK metakaolin, the final material is composed of a geopolymer network associated with a Si-rich phase (gel). Strengthened materials based on mixtures of Me clay and MK metakaolin regroup into a geopolymer network, gel phase and associated minerals coated by the alkaline solution. It seems that for a proportion of substitution of 50% and a Si/K ratio of the alkaline solution of 0.50, the formation of a geopolymer network is favored.

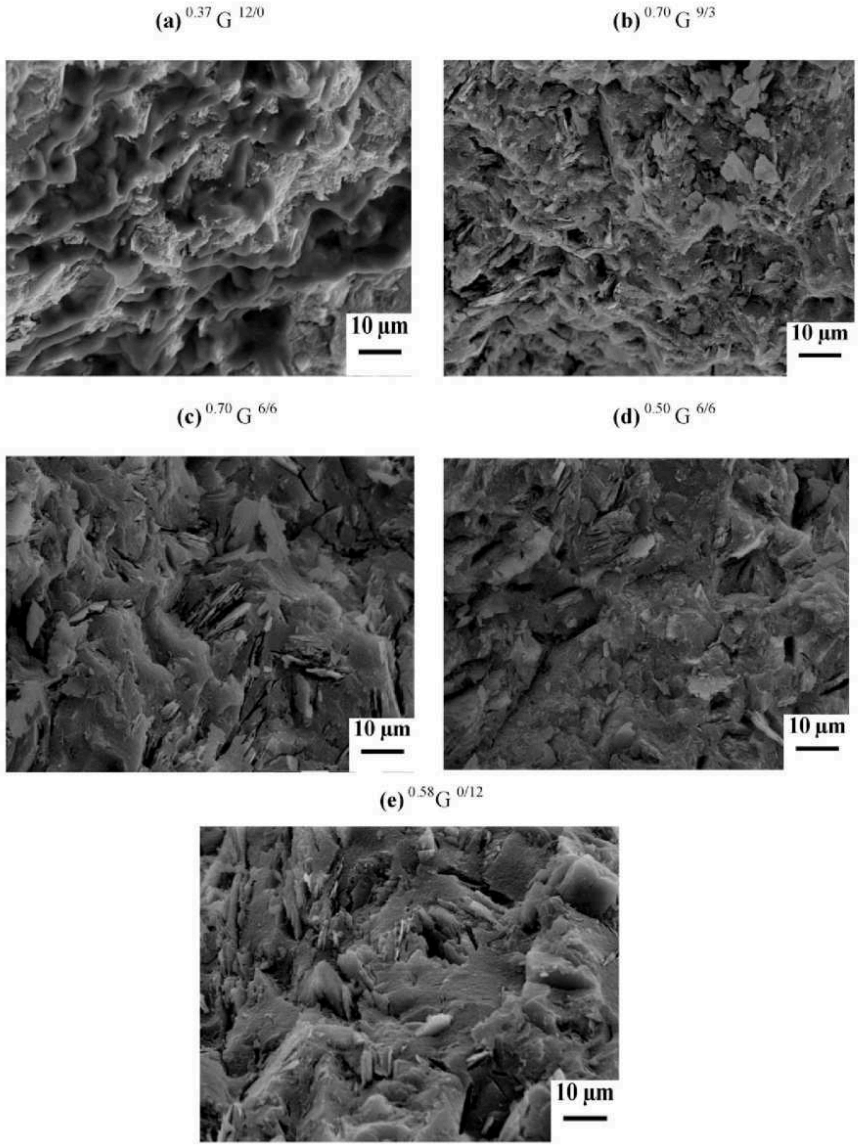

Fig. 7. SEM micrographs of the studied samples.

4. Conclusion

To reduce the cost of raw materials used in geopolymer applications and to valorize highly impure natural resources, some mixtures of low reactive Tunisian clay and metakaolin were investigated as aluminosilicate sources to elaborate geopolymer materials. The comparative characterization between the two precursors evidenced structural differences between them. Indeed, the metakaolin used is very pure and reactive, while the Tunisian clay is kaolinite poor but rich in impurities such as illite and hematite. Moreover, the feasibility of the consolidated materials was demonstrated based on the studied mixtures. The reactivity of the mixtures as well as the working properties were correlated with the chemical composition. It seems that the associated minerals in the Tunisian clay did not participate in the polycondensation reaction and remained simply agglomerated by the alkaline solution. The amount of metakaolin (amorphous phase) in the mixture is an important parameter because it enhances the formation of the geopolymer network and improves the final properties of the consolidated materials. The Si/K ratio of the alkaline solution is also a crucial parameter because it may control the nature and amount of the depolymerized species in the activating solution and consequently influences the polycondensation rate and the working properties of the final materials, regardless of the aluminosilicate source. The optimal properties were obtained for a proportion of substitution of Tunisian clay by metakaolin of 50% and a Si/K ratio of the alkaline solution of 0.50. From this study, it is demonstrated that low reactive clay can be added and valorized into metakaolin-based geopolymer formulation to obtain interesting consolidated material properties.

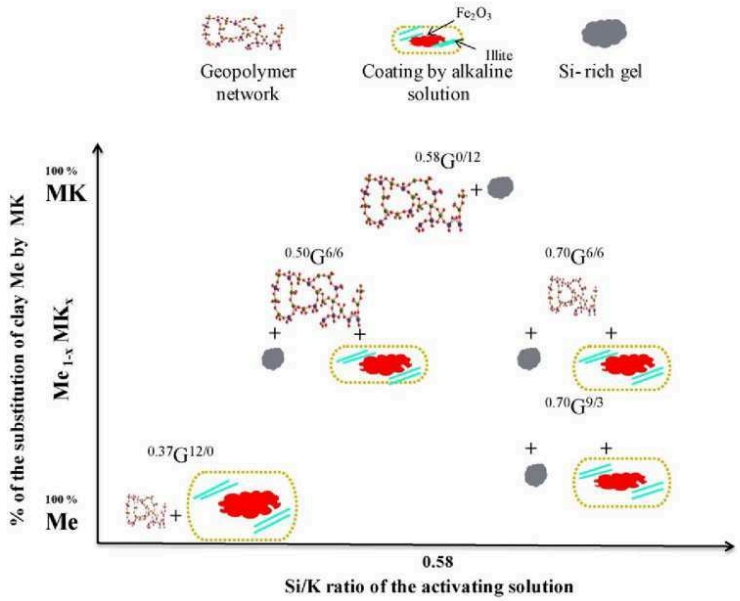

Fig. 8. Schematically model of the different networks formed from each mixture.

References

[1] H. Baccour, M. Medhioub, F. Jamoussi, T. Mhiri, A. Daoud, Mineralogical evaluation and industrial applications of the Triassic clay deposits, Southern Tunisia, Mater. Charact. 59 (2008) 1613–1622.

[2] M. Krichen, J.P. Bonnet, J. Bouaziz, S. Baklouti, Mineralogy and sintering mechanisms of a clay raw material from Kasrine (Tunisia), Silic. Ind. 74 (2009) 139–144.

[3] M. Krichen, S. Baklouti, J. Bouaziz, J.P. Bonnet, Sintering behavior of some Tunisian clay mixtures, Silic. Ind. 74 (2009) 289–291.

[4] A. Chakchouk, B. Samet, T. Mnif, Study on the potential use of Tunisian clays as pozzolanic material, Appl. Clay Sci. 33 (2006) 79–88.

[5] S. Fakhfakh, S. Baklouti, J. Bouaziz, Elaboration and characterization of low cost ceramic support membrane, Adv. Appl. Ceram. 109 (2010) 31–38.

[6] I. Hedfi, N. Hamdi, E. Srasra, M.A. Rodríguez, The preparation of micro-porous membrane from Tunisian kaolin, Appl. Clay Sci. 101 (2014) 574–578.

[7] H. Bel Hadjltaief, P. Da Costa, P. Beaunier, M.E. Gálvez, M. Ben Zina, Fe-clay-plate as a heterogeneous catalyst in photo-Fenton oxidation of phenol as probe molecule for water treatment, Appl. Clay Sci. 91–92 (2014) 46–54.

[8] J. Davidovits, Geopolymer: Chemistry and Applications, 2nde édition Institut Géopolymère, St-Quentin, 2008.

[9] D. Khale, R. Chaudhary, Mechanism of geopolymerization and factors influencing its development: a review, J. Mater. Sci. 42 (2007) 729–746.

[10] P. Duxson, A. Fernandez-Jimenez, J.L. Provis, G.C. Lukey, A. Palomo, J.S.J. Van Deventer, Geopolymer technology: the current state of the art, J. Mater. Sci. 42 (2007) 2917–2933.

[11] Y.J. Zhang, S. Li, Y.C. Wang, D.L. Xu, Microstructural and strength evolutions of geopolymer composite reinforced by resin exposed to elevated temperature, J. Non-Cryst. Solids 358 (2012) 620–624.

[12] A. Autef, E. Joussein, A. Poulesquen, G. Gasgnier, S. Pronier, I. Sobrados, J. Sanz, S. Rossignol, Role of metakaolin dehydroxylation in geopolymer synthesis, Powder Technol. 250 (2013) 33–39.

[13] A. Autef, E. Joussein, A. Poulesquen, G. Gasgnier, S. Pronier, I. Sobrados, J. Sanz, S. Rossignol, Influence of metakaolin purities on potassium geopolymer formulation: the existence of several networks, J. Colloid Interface Sci. 408 (2013) 43–53.

[14] A. Buchwald, M. Hohman, K. Posern, E. Brendler, The suitability of thermally activated illite/smectite clay as raw material for geopolymer binders, Appl. Clay Sci. 46 (2009) 300–304.

[15] N. Essaidi, B. Samet, S. Baklouti, S. Rossignol, Feasibility of producing geopolymers from two different Tunisian clays before and after calcination at various temperatures, Appl. Clay Sci. 88–89 (2014) 221–227.

[16] K.J.D. Mackenzie, S. Komphanchai, R. Vagane, Formation of inorganic polymers (geopolymer) from 2:1 layer lattice, J. Eur. Ceram. Soc. 28 (2008) 177–181.

[17] C. Ruiz-Santaquiteria, A. Fernández-Jiménez, J. Skibsted, A. Palomo, Clay reactivity: production of alkali activated cements, Appl. Clay Sci. 73 (2013) 11–16.

[18] S. Selmani, N. Essaidi, F. Gouny, S. Bouaziz, E. Joussein, A. Driss, A. Sdiri, S. Rossignol, Physical–chemical characterization of Tunisian clays for the synthesis of geopolymers materials, J. Afr. Earth Sci. 103 (2015) 113–120.

[19] P. Steins, Influence des Paramètres de Formulation sur la Texturation et la Structuration des GéopolymèresPhD thesis Université de Limoges, 2014.

[20] A. Gharzouni, E. Joussein, S. Baklouti, S. Pronier, I. Sobrados, J. Sanz, S. Rossignol, The effect of an activation solution with siliceous species on the chemical reactivity and mechanical properties of geopolymers, J. Sol-Gel Sci. Technol. 73 (2015) 250–259.

[21] E. Prud'homme, P. Michaud, E. Joussein, M. Clacens, S. Rossignol, Role of alkaline cations and water content on geomaterial foams: monitoring during formation, J. Non-Cryst. Solids 357 (2011) 1270–1278.

[22] ASTM D1633-00, Standard Test Methods for Compressive Strength of Molded Soil Cement Cylinders, 2007.

[23] B. Fabbri, S. Gualtieri, C. Leonardi, Modifications induced by the thermal treatment of kaolin and determination of reactivity of metakaolin, Appl. Clay Sci. 73 (2013) 2–10.

[24] M.E. Alves, Y.P. Mascarenhas, D.H. French, C.P.M. Vaz, Rietveld-based mineralogical quantitation of deferrified oxisol clays, Soil Res. 45 (2007) 224–232.

[25] S. Ferrai, A.F. Gualtieri, The use of illite clays in the production of stoneware tile ceramics, Appl. Clay Sci. 32 (2006) 73–81.

[26] X.X. Gao, A. Autef, E. Prud'homme, P. Michaud, B. Samet, E. Joussein, S. Rossignol, Synthesis of consolidated materials from alkaline solutions and metakaolin: existence of domains in the Al–Si–K/O ternary diagram, J. Sol-Gel Sci. Technol. 65 (2013) 220–221.

[27] E. Prud'homme, A. Autef, N. Essaidi, P. Michaud, B. Samet, E. Joussein, S. Rossignol, Defining existence domains in geopolymers through their physicochemical properties, Appl. Clay Sci. 73 (2013) 26–34.

[28] L. Weng, K. Sagoe-Crentsil, T. Brown, S. Song, Effects of aluminates on the formation of geopolymer, Mater. Sci. Eng. B 117 (2005) 163–168.

[29] A. Autef, E. Prud'homme, E. Joussein, G. Gasgnier, S. Pronier, S. Rossignol, Evidence of a gel in geopolymer compounds from pure metakaolin, J. Sol-Gel Sci. Technol. 65 (2013) 220–229.

[30] A. Gharzouni, E. Joussein, B. Samet, S. Baklouti, S. Rossignol, Effect of the reactivity of alkaline solution and metakaolin on geopolymer formation, J. Non-Cryst. Solids 410 (2015) 127–134.

[31] P. Duxson, G.C. Lukey, S.W. Mallicoat, W.M. Kriven, J.S.J. Van Deventer, Understanding the relationship between geopolymer composition, microstructure and mechanical properties, Colloids Surf. A Physicochem. Eng. Asp. 269 (2005) 47–58.

[32] A. Fernández-Jiménez, A. Palomo, I. Sobrados, J. Sanz, The role placed by the reactive aluminum content in the alkaline activation of fly ashes, Microporous Mesoporous Mater. 91 (2006) 111–119.

[33] J. He, J. Zhang, Y. Yu, G. Zhang, The strength and microstructure of two geopolymers derived from metakaolin and red mud–fly ash admixture: a comparative study, Constr. Build. Mater. 30 (2012) 80–91.

[34] J.L. Lawson, On the Determination of the Elastic Properties of Geopolymeric Materials Using Non Destructive Ultrasonic TechniquesPhD thesis Rochester institute of technology, 2008.

[35] M. Lizcano, A. Gonzalez, S. Basu, K. Lozano, M. Radovic, Effects of water content and chemical composition on structural properties of alkaline activated metakaolin-based geopolymers, J. Am. Ceram. Soc. 95 (2012) 2169–2177.

[36] N. Essaidi, B. Samet, S. Baklouti, S. Rossignol, The role of hematite in aluminosilicate gels based on metakaolin, Ceramics-Silikáty 58 (2014) 1–11.
[37] D. Carroll, H.C. Starkey, Reactivity of clay minerals with acids and alkalies, Clay Clay Miner. 19 (1971) 321–333.
[38] A. Hajimohammadi, J.L. Provis, J.S.J. van Deventer, The effect of silica availability on the mechanism of geopolymerisation, Cem. Concr. Res. 41 (2011) 210–216.
[39] C. Ruiz-Santaquiteria, A. Fernández-Jiménez, J. Skibsted, A. Palomo, Clay reactivity: production of alkali activated cements, Appl. Clay Sci. 73 (2013) 11–16.
[40] G. Sedmale, A. Korovkins, V. Seglins, L. Lindina, Application of chemical treated illite clay for development of ceramics products, IOP Conf. Series: Mater. Sci. Eng. 47 (2013) 012056.

Publication 4 (ACL4)

N. Essaidi, A. Gharzouni, L. Vidal, F. Gouny, E. Joussein, S. Rossignol

"Recycling of aluminosilicate waste: Impact onto geopolymer formation"

The European Physical Journal Special Topics, 224 (2015) 1707-1713

Les géopolymères sont des éco-matériaux innovants qui dérivent de l'activation d'une source d'aluminosilicate par une solution alcaline. Leurs propriétés d'usage dépendent directement des matières premières utilisées. Cette étude s'est focalisée sur l'évaluation de la possibilité d'obtenir des matériaux géopolymères avec les déchets du laboratoire. L'effet de ces ajouts sur les propriétés des géopolymères a été étudiée par spectroscopie IRTF et des essais mécaniques. Il a été mis en évidence que l'incorporation du déchet géopolymère induit un ralentissement de la réaction de polycondensation ainsi que la diminution de la résistance à la compression.

Recycling of aluminosilicate waste: impact onto geopolymer formation

N. Essaidi[1], A. Gharzouni[1], L. Vidal[1, 2], F.Gouny[1], E. Joussein[3] and S. Rossignol[1]

[1] Science des Procédés Céramiques et de Traitements de Surface (SPCTS) UMR 7315 CNRS, Ecole Nationale Supérieure de Céramique Industrielle, 12 rue Atlantis, 87068 Limoges Cedex, France.
[2] Groupe d'Etude des Matériaux Hétérogènes (GEMH), Ecole Nationale Supérieure de Céramique Industrielle, 12 rue Atlantis, 87068 Limoges Cedex, France
[3] Université de Limoges, GRESE EA 4330, 123 avenue Albert Thomas, 87060 Limoges, France.

Abstract

Geopolymers are innovative ecomaterials resulting from the activation of an aluminosilicate source by an alkaline solution. Their properties depend on the used raw materials. This paper focuses on the possibility to obtain geopolymer materials with aluminosilicate laboratory waste. The effect of these additions on the geopolymer properties was studied by FTIR spectroscopy and mechanical test. It was evidenced a slowdown of the polycondensation reaction as well as the compressive strength due to the addition of laboratory waste which decrease the Si/K ratio of mixture.

1 Introduction

Geopolymer materials have a lot of attention [1] as suitable binder because they are environmentally friendly and require less energy during their manufacturing process. These ecomaterials can be synthesized by the alkaline activation of aluminosilicates obtained from calcined clays, natural minerals and industrial wastes at room temperature. The properties of geopolymers are affected by two important factors which are the alkaline solution and the aluminosilicate source [2, 3]. Autef et al. [2, 4] highlighted that the purity and the reactivity of the metakaolin can lead to the formation of one or several networks which influence the working performances of the final material. Generally, for metakaolin-based geopolymers, the compressive strengths and Young's moduli ranged from 20 to 80 MPa and 2.5 to 5.5 GPa respectively [5]. In the case of fly ash based geopolymer, the compressive strength is about 61 MPa and the Young's modulus is 2.9 GPa [6].

Recently, economical and environmental demands encourage waste recycling in order to reduce the consumption of natural resources. Taking this into account, some studies focused on recycled aggregates incorporation in the geopolymer materials [7, 8, 9]. Indeed, Sata et al. [7] compared materials obtained with natural and recycled coarse aggregates. They proved that recycled aggregates could be reused to make pervious geopolymer concretes. However, a loss in compressive strength was observed.

In this context, the aim of the current study is to investigate the influence of laboratory waste addition on geopolymer formation in order to minimize the cost and to focus on the life cycle of material. For this, different amounts of laboratory waste were added to geopolymer reactive mixture. The synthesized materials were characterized by FTIR spectroscopy and compression tests.

2 Experimental Part

2.1 Raw materials and sample preparation

The experimental protocol of geopolymer synthesis is described in Fig.1 [10]. The alkaline solution was obtained by dissolving potassium hydroxide pellets (VWR, 85.2% pure) in a commercial potassium silicate solution in order to maintain the $Si/K_{solution}$ molar ratio to 0.58. Then, laboratory aluminosilicate waste, previously crushed and sieved through 80 µm, and metakaolin were added. The waste proportion ranged from 10 to 30% of total mass. The reactive mixtures were placed in open polystyrene molds at room temperature. Samples are denoted as G^x, where x refers to the percentage of laboratory waste added. For example, G^{20} corresponds to a geopolymer with 20% of waste.

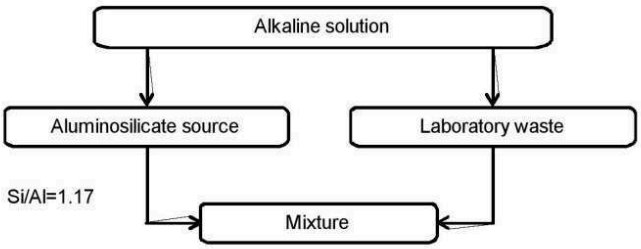

Fig.1. Synthesis protocol of geopolymer samples.

2.2 Technical characterization

Fourier-transform infrared (FTIR) spectroscopy in ATR mode was used to investigate the structural evolution of the geopolymer mixtures. The FTIR spectra were obtained using a ThermoFisher Scientific Nicolet 380 infrared spectrometer. The IR spectra were gathered over a range of 400 to 4000 cm^{-1} with a resolution of 4 cm^{-1}. The atmospheric CO_2 contribution was removed with a straight line between 2400 and 2280 cm^{-1}. To monitor the geopolymer formation, a software was used to acquire a spectrum (64 scans) every 10 minutes for 250 minutes. For comparison, the spectra were baseline-corrected and normalized [10].

The compressive strengths were tested using a LLOYD EZ20 universal testing machine with a crosshead speed of 0.1 mm/min. The compressive tests were made on five samples for every composition. The samples were cylindrical in shape with a diameter (Φ) of 15 mm and a height (h) of approximately 30 mm, and were aged for 7 days in an open mold at room temperature. The compressive strength values represent the average of the obtained values and were expressed in MPa.

3 Results and Discussion

3.1 Feasibility of consolidated material

A preliminary feasibility study of consolidated materials with different amounts of laboratory waste was carried out. The initial composition G^0 was based on the Prud'homme et al studies [11]. Then, the laboratory waste was progressively added to the mixture up to 30%. The obtained materials were consolidated, homogeneous and show a geopolymer feature (Fig.2a). The different compositions are reported in Si-Al-K ternary diagram (Fig.2b). Previous studies [12] have evidenced the existence of various domains which are (A) geopolymer, (B) hardening material, (C) sedimented material and (D) gel. Whatever the amount of laboratory waste added, the studied compositions are still located in the

geopolymer domain. To understand the effect of aluminosilicate laboratory waste addition on geopolymer formation, FTIR spectroscopy and mechanical test were performed.

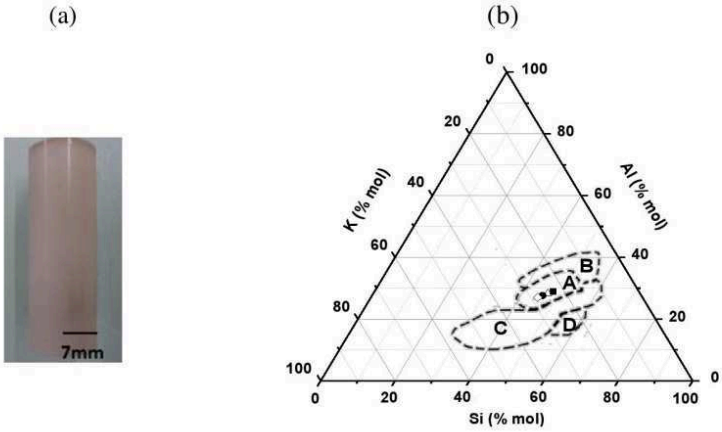

Fig.2. (a) Photo of G^{20} geopolymer (Ø = 14 mm) and (b) position of the different G^x compositions with x = (■) 0, (Δ) 10, (●) 20 and (◊) 30% of laboratory waste. The various domains correspond to (A) geopolymer, (B) hardening material, (C) sedimented material and (D) gel.

3.2 Effect of laboratory waste addition on the polycondensation rate

The various compositions were followed by FTIR spectroscopy. Examples of the obtained spectra for G^0 composition are shown in Fig.3a. For the spectra at t=0 min, the bands at 3200 and 1640 cm^{-1} were attributed to ν_{OH} and δ_{OH} respectively. The bands assigned to Si-O-M bonds (M=Si, Al, K) were located in the 1100-950 cm^{-1} range [11]. Over the time, the decrease of OH bands and the shift of Si-O-M band indicate the dissolution of metakaolin by the basic environment [13] and the occurrence of polycondensation reaction leading to the formation of specific networks [11, 14, 15].

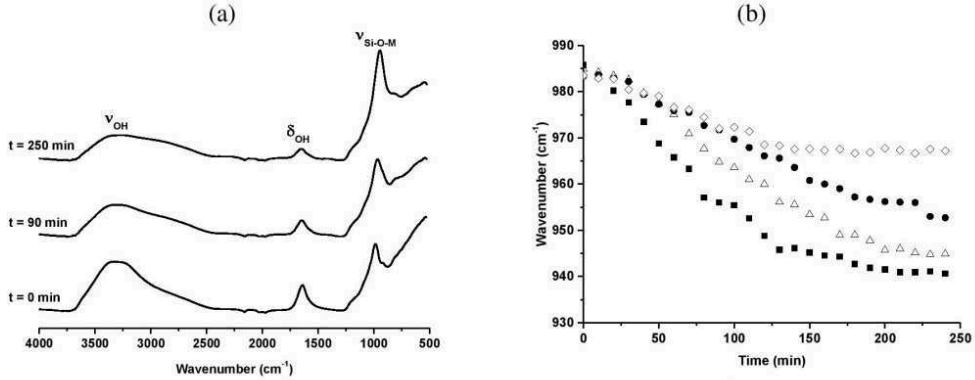

Fig.3. (a) In situ FTIR spectra obtained at t = 0, 90 and 250 min and (b) Q^2 position versus time for the G^x samples with x = (■) 0, (Δ) 10, (●) 20 and (◊) 30% of laboratory waste added.

The displacement of the Si-O-M band versus time was plotted in Fig.3b for all samples. The slope at the beginning of the curve gives information about the kinetic of the reaction [11]. The displacement and the slope values relative to G^0 composition were approximately 45

reactivity of the mixture and alters the structure, then the mechanical properties of formed materials. These results are in accordance with FTIR analysis.

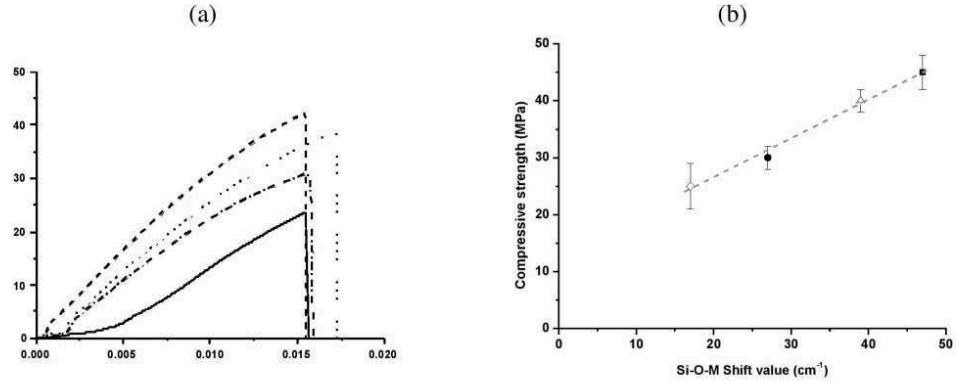

Fig.4. (a) Variation of compressive strength versus strain for G^x reactive mixture with x = (---) 0, (···) 10, (-·-) 20 and (—) 30% of laboratory waste added and (b) evolution of the shift value as a function of the compressive strength for (■) G^0, (Δ) G^{10}, (●) G^{20} and (◊) G^{30}.

4 Conclusion

This study evidenced the possibility of re-using aluminosilicate laboratory waste to synthesize consolidated materials. It was shown that the laboratory waste addition influences the polycondensation rate as well as the mechanical strength, still acceptable to consolidated materials. The low reactivity of these incorporated materials disturbs the geopolymerization reactions and lead to the formation of different networks. These networks induce the presence of some weaknesses into the final material due to a lower Si/K ratio in the mixture. However, this hypothesis needs to be confirmed by microstructural characterization in further work.

5 Acknowledgment

The authors thank the Limousin council and the FEDER for financing this study.

6 References

[1] J.S.J. Van Deventer, J.L. Provis, P. Duxson, Miner. Eng. **29**, 89 (2012)

[2] A. Autef, PhD thesis, University of Limoges, 2013

[3] A. Gharzouni, E. Joussein, S. Baklouti, S. Pronier, I. Sobrados, J. Sanz, S. Rossignol, J. Sol-Gel Sci. Technol. Article in press (2014)

[4] E. Prud'homme, P. Michaud, E. Joussein, A. Smith, C. Peyratout, I. Sobrados, J. Sanz, S. Rossignol, J. Sol-Gel Sci. Technol. **61**, 436 (2012)

[5] P. Duxson, J.L. Provis, G.C. Lukey, S.W. Mallicoat, W.M. Kriven, J.S.J. Van Deventer, Colloids Surf. A. **269**, 47 (2005)

[6] E. Ul Haq, S. Kunjalukkal Padmanabhan, A. Licciulli, Ceram. Int. **40**, 2965 (2014)

[7] V. Sata, A. Wonsga, P. Chindaprasirt, Constr. Build. Mater. **42**, 33 (2013)

[8] X.S. Shi, F.G. Collins, X.L. Zhao, Q.Y. Wang, J. Hazard. Mater. **237-238**, 20 (2012)

[9] A.R.M. Ridzuan, M.M. Al Bakri Abdullah, M.F. Arshad, M.F. Mohd Tahir, A.A. Khairulniza, Mater. Sci. Forum **803**, 194 (2014)

[10] E. Prud'homme, P. Michaud, E. Joussein, J.M. Clacens, S. Rossignol, J. Non-Cryst. Solids. **357**, 1270 (2011)

[11] E. Prud'homme, PhD thesis, University of Limoges, 2011

[12] X.X. Gao, A. Autef, E. Prud'homme, P. Michaud, E. Joussein, S. Rossignol, J. Sol-Gel Sci. Technol. **65**, 220 (2013)

[13] W.K.W. Lee, J.S.J. Van Deventer, Langmuir **19**, 8726 (2003)

[14] C.A. Ress, J.L. Provis, G.C. Luckey, J.S.J. Van Deventer, Langmuir **23**, 8170 (2007)

[15] C.A. Ress, J.L. Provis, G.C. Luckey, J.S.J. Van Deventer, Langmuir **23**, 9076 (2007)

[16] J. He, J. Zhang, Y. Yu, G. Zhang, Constr. Build. Mater. **30**, 80 (2012)

[17] P. Duxson, J.L. Provis, G.C. Lukey, S.W. Mallicoat, W.M. Kriven, J.S.J. Van Deventer, Colloids Surf. A **269**, 47 (2005)

[18] A. Autef, E. Joussein, G. Gasgnier, S. Rossignol, J. Non-Cryst. Solids **358**, 2886 (2012)

[19] A. Autef, E. Joussein, G. Gasgnier, S. Rossignol, Ceram. Eng. Sci. Proc. **34**, 3 (2014)

.

6

Publication 5 (ACL5)

A. Gharzouni, L.Vidal, N. Essaidi, E. Joussein, S. Rossignol,

"Recycling of geopolymer waste: Influence on geopolymer formation and mechanical properties"

Materials and Design 94 (2016) 221-229.

Les géopolymères sont des nouveaux liants minéraux résultant de l'activation d'une source aluminosilicate par une solution alcaline. Ces liants sont économiques et respectueux de l'environnement car ils ont l'avantage de la réutilisation des déchets recyclés et des sous-produits industriels comme des sources aluminosilicates. Dans ce contexte, cette étude met l'accent sur l'incorporation des déchets géopolymères dans différentes formulations et leur effet sur la formation des géopolymères et les propriétés finaux des matériaux synthétisés. Pour cela, les déchets géopolymères ont été tout d'abord caractérisés. Trois compositions, qui différent de la solution alcaline utilisée et de la quantité de métakaolin ajoutée, ont été étudiées. Une étude de faisabilité a permis de retenir un pourcentage de 20% de déchet ajouté ou substitué au métakaolin pour obtenir des matériaux géopolymères. En outre, il a été montré que l'incorporation des déchets de géopolymère perturbe la réaction de polycondensation qui dépend fortement du rapport solide/liquide et du rapport Si/K de la solution alcaline. De plus, des corrélations ont été démontrées entre les résistances à la compression et la composition chimique des différents échantillons. Enfin, il a été prouvé que la faible réactivité des déchets géopolymères peut être compensée par l'utilisation d'une solution alcaline très réactive ou par l'augmentation de la quantité de métakaolin dans le mélange.

Materials and Design 94 (2016) 221–229

Contents lists available at ScienceDirect

Materials and Design

journal homepage: www.elsevier.com/locate/matdes

Recycling of geopolymer waste: Influence on geopolymer formation and mechanical properties

A. Gharzouni [a], L. Vidal [a], N. Essaidi [a], E. Joussein [b], S. Rossignol [a,*]

[a] Univ Limoges, CNRS, ENSCI, SPCTS, UMR7315, F-87000 Limoges, France
[b] Univ Limoges, GRESE, EA 4330, F-87000 Limoges, France

ARTICLE INFO

Article history:
Received 18 November 2015
Received in revised form 8 January 2016
Accepted 9 January 2016
Available online 12 January 2016

Keywords:
Recycling
Geopolymer waste
Alkaline solution
Metakaolin
Mechanical properties
Reactivity

ABSTRACT

Geopolymers are new binders resulting from the activation of an aluminosilicate source by an alkaline solution. These binders are economically and environmentally profitable since they have the advantage of reusing recycled waste and industrial by-products as aluminosilicate sources. In this context, this paper focuses on the geopolymer wastes incorporation in different formulations and their effect on geopolymer formation and the properties of the final materials. For this purpose, the geopolymer wastes were at first characterized. Three compositions differing in the used alkaline solution and the amount of metakaolin added were investigated. A feasibility study allowed retaining 20% as the waste percentage added or substituted to the metakaolin to still obtain geopolymer materials. Moreover, it was shown that the incorporation of the geopolymer waste may disturb the polycondensation rate which was proven to strongly depend on the solid to liquid ratio and the Si/K ratio of the alkaline solution. Finally, relationships were demonstrated between the compressive strengths and the chemical compositions of the different samples. The low reactivity of geopolymer waste can be compensated with the use of highly reactive alkaline solution or the increase of the amount of metakaolin in the mixture.

1. Introduction

In recent years, the growth of waste production associated with the awareness of the environmental problems and the need of sustainable development make waste management a priority [1]. Recycling has drawn great interest as a way to solve waste problems, reduce environmental pollutions and preserve natural resources. For example, the glasses are reused in glass or enamel compositions as cullet and allow lowering the energy and the raw material consumption [2]. Others examples are concretes or ceramics which are crushed and used as aggregates in new concretes [3,4]. In this context, geopolymer materials are a new class of binders having the advantage of using industrial byproducts and recycled waste. These binders are generated from the activation of an aluminosilicate source with an alkaline solution [5,6]. Their formation implies the dissolution of aluminosilicate species in an alkaline environment to form an amorphous three-dimensional geopolymer network by polycondensation reaction. Based on such a unique structure, geopolymers may exhibit good mechanical, chemical and thermal properties making them a promising alternative for a variety of applications [7]. Diverse industrial by-products were proven to be suitable for producing geopolymer materials such as fly ash [8,9], furnace slag [9,10,11], red mud [12], mine waste mud [13], waste concrete [14] and construction and demolition waste [15]. He et al., [12] established a comparative study between two types of geopolymers based on metakaolin and a mixture of red mud and fly ash. The lower strength obtained for a mixture of red mud and fly ash sample were attributed to the reactivity of the raw materials. The final materials were composed of a geopolymer binder and unreacted phases present as inactive fillers. This fact was also evidenced by Komnitsas et al. [15], in the case of construction and demolition waste-based geopolymers. Indeed, they observed a heterogeneous matrix containing grains of various sizes and attributed this to the partial reaction of the initial concrete. Similarly, Gao et al. [16], demonstrated that the compressive strength firstly increased up to 20% of fly ash content and then decreased as the fly ash content increased into metakaolin-slag blends.

Nazari and Sanjayan [17] proved the possibility of producing geopolymers using aluminum and cast iron slags. They highlight that the silica to alumina ratio is the most important parameter governing the mechanical properties. Onutai et al. [18] evidenced that 40 wt.% of Al waste content in geopolymer mixture lead to a dense structure and therefore optimal compressive strength. Moreover, investigation study about the influence of different types of aggregates, such as lime stone, schist and granite, on the properties of geopolymeric mine waste mud binder was undertaken. It was demonstrated that the aggregate dimensions affect the tensile strength. Ferone et al. [19] have shown the suitability of calcined clay sediments for geopolymer synthesis and evidenced the role of heat treatment temperature on the reactivity. In addition to that, the immobilization of heavy metals in municipal solid waste incineration fly ash based geopolymer was evidenced [20]. The mechanical properties

* Corresponding author.
E-mail address: sylvie.rossignol@unilim.fr (S. Rossignol).

http://dx.doi.org/10.1016/j.matdes.2016.01.043
0264-1275/

and microstructure of the resulting materials were directly linked to the alkaline solution dosage and the Si/Al molar ratio. According to these studies, there are different remaining problems to consider. Indeed, the authors evidenced that the use of wastes implies a decrease of the compressive strength, a contamination coming from the wastes and the low reactivity of these materials. In order to improve the results, it seems to be necessary to determine the optimum amount of wastes for the addition or the substitution of raw materials.

So far, as extensive research on geopolymer has been conducted, the generation of geopolymer waste increases. In this context, an innovative use of geopolymer waste is their incorporation in different geopolymer formulations which is in accordance with the "cradle to cradle" concept. Moreover, reusing these geopolymers allow reducing the amount of raw materials used. Recycling of waste and their use as aluminosilicate sources seems to be profitable since it economical and environmental benefits, leading to greener manufacturing and global sustainable development. Recent investigations using recycling aggregates produced in laboratory point out to the fact that the use of fine recycled aggregates must not exceed 30%, otherwise the performance could be at risk [14]. Current recycled aggregates have particles of impurities such as soil, plastics, wastepaper wood, metals and organic matter. Organic matter leads to lower mechanical performance and lower concrete durability. Moreover, Park and Noguchi [21] studied concrete containing metal impurities and it was found that aluminum caused performance degradation.

The present work aims to evaluate the suitability of using crushed geopolymer in addition or substitution of metakaolin to produce geopolymers materials. For this, the used raw materials were characterized. Then, the feasibility of consolidated materials was evaluated. Several samples were prepared by varying the proportion of geopolymer waste. The structural evolution of the reactive mixtures was monitored by FTIR spectroscopy. Finally, the consolidated materials were characterized by compression tests.

2. Experimental part

2.1. Raw materials and sample preparation

The consolidated materials were prepared by mixing the metakaolin (MK) and the geopolymer, crushed and sieved at 80 μm, in an alkaline solution (AS) as described in Fig. 1 [22,23]. The reactive mixtures were placed in open polystyrene molds at room temperature for 7 days. Three formulations, differenced by the amount of metakaolin and the starting silicate solution were studied. The two silicate solutions, denoted as S1 and S3, differ in terms of the Si/K molar ratio (1.7 for S1and 0.7 for S3) and the water contents (79% for S1 and 59% for S3) [24,25].

For each composition, the effect of the substitution of an amount of metakaolin (MK) by crushed geopolymer (CG) or the addition of this compound was investigated. So, three sets are synthesized. Samples were synthesized either by adding the crushed geopolymer to metakaolin or substituting an amount of metakaolin by crushed geopolymer. Samples are denoted as $^{x,Si}G^{y}$ or $^{x,Si}G^{Sy}$ where x refers to the quantity of metakaolin, Si is the type of the used silicate solution, y the percentage of crushed geopolymer added to the mixture and ^{Sy} the percentage of crushed geopolymer which substitutes an amount of metakaolin mass. For example $^{12,S1}G^{S20}$ refers to the geopolymer obtained from the substitution of 20% of 12 g of metakaolin by crushed geopolymer using S1 as a silicate solution. The nomenclature and the composition of the samples analyzed are presented in the Table 1.

2.2. Technical characterization

The chemical composition of the precursors was determined using X-ray fluorescence (XRF). This technique allows the quantification of the atomic elements.

The particle size distributions of the raw materials were measured using a laser particle size analyzer (Mastersizer 2000). The mixture contained 1 g of aluminosilicate precursor in 20 ml of water, mixed by ultrasound to eliminate any aggregation. The measured particle sizes are in the range 0.05–880 μm. Additionally, the concentration of the solution should not be too large (obscuration < 35%).

Powder BET surface areas were determined by N_2 adsorption at −195.85 °C using a Micrometrics Tristar II 3020 volumetric adsorption/desorption apparatus. Prior to the measurement, the samples were degassed at 200 °C under vacuum for 4 h.

Bulk density was measured by pycnometer method. Numerically, it represents the mass per unit volume of matter. The SI unit of density is kg/m^3.

The wettability (water demand) of a powder is the volume of water that can be absorbed by 1 g of powder until saturation. This quantity depends directly on the particle size, the specific surface and the morphology of powder. One gram of powder is weighted and then deposited on a glass slide. Using a micropipette, the water is added to the powder (microlite by microlite) until visual saturation of the granular.

The pH values were measured using a Schott Instrument Lab860 pH-meter at 25 °C during the first 400 min of the geopolymer formation. A 2.4 g sample was immersed in 30 mL of osmosed water, which provided a solid to liquid ratio of 0.08 [26].

The mineral phases were identified by powder X-ray diffraction (XRD) with a BRUKERAXS D8 Advance powder diffractometer using CuKα radiation (λKα = 0.154186 nm). The analytical range used was between 5° and 70° with a step size of 0.04° and an acquisition time of 2 s. JCPDS (Joint Committee Powder Diffraction Standard) files were used for phase identification.

Fourier-transform infrared (FTIR) spectroscopy in ATR mode was used to investigate the structural evolution of the geopolymer mixtures. The FTIR spectra were obtained using a ThermoFisher Scientific Nicolet

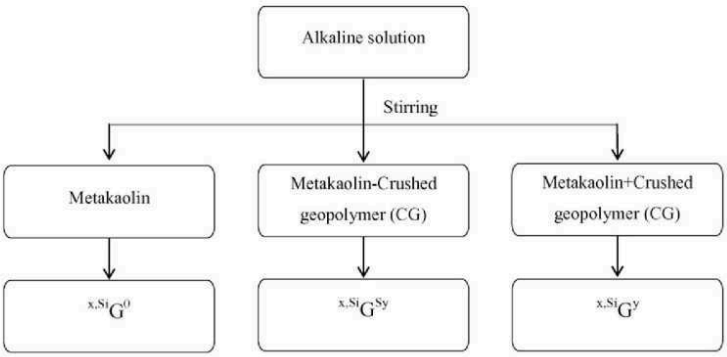

Fig. 1. Synthesis protocol of the various consolidated samples.

Table 1
Nomenclature and compositions of the different studied mixtures.

Set	Nomenclature	Mass of metakaolin (g)	Solution type	% geopolymer waste	Si/Al	Si/K
1	$^{12,S1}G^0$			0	1.66	2.09
	$^{12,S1}G^{20}$	12	S1	20		
	$^{12,S1}G^{S20}$			20	1.76	1.80
2	$^{12,S3}G^0$			0	1.72	1.67
	$^{12,S3}G^{20}$	12	S3	20		
	$^{12,S3}G^{S20}$			20	1.84	1.45
3	$^{20,S1}G^0$			0	1.41	3.09
	$^{20,S1}G^{20}$	20	S1	20		
	$^{20,S1}G^{S20}$			20	1.45	2.63

380 infrared spectrometer. The IR spectra were gathered over a range of 400 to 4000 cm^{-1} with a resolution of 4 cm^{-1}. The atmospheric CO_2 contribution was removed with a straight line between 2400 and 2280 cm^{-1}. To monitor the geopolymer formation, a software was used to acquire a spectrum (64 scans) every 10 min for 13 h. For comparison, the spectra were baseline-corrected and normalized.

The compressive strengths were tested using a LLOYD EZ20 universal testing machine with a crosshead speed of 0.1 mm/min. The compressive tests were made on five samples for every composition. The compressive strength values represent the average of the five obtained values and were expressed in MPa. The samples were cylindrical in shape with a diameter (Φ) of 15 mm and a height (h) of approximately 30 mm, and they were aged for 7 days in an open mold at room temperature.

3. Results

3.1. Raw materials characterization

The properties of the geopolymers are strongly influenced by the raw materials used for their synthesis. In this study, the raw materials used in the preparation of the samples, such as the metakaolin (MK) and various crushed geopolymers (CG), are characterized using several methods.

The Si/K and Si/Al molar ratios and physical data of the precursors, such as the specific surface, the D_{50} (particle size) and the wettability values are reported in Table 2. The Si/Al ratio is deduced from their chemical composition. It is about 1.17 for MK whereas for the $^{12,S1}CG^0$, $^{12,S3}CG^0$ and $^{20,S1}CG^0$ crushed geopolymers, these ratios are 1.66, 1.72 and 1.41 respectively. These higher values for CG compared to MK are due to the additional silicon provided by the silicate solution. In the case of $^{20,S1}CG^0$, the lower value can be explained by the higher amount of metakaolin. The Si/K ratio is about 2.09, 1.67 and 3.09 for $^{12,S1}CG^0$, $^{12,S3}CG^0$ and $^{20,S1}CG^0$ respectively. These differences are related to the Si/K molar ratio of the alkaline solution (0.58, 0.51 and 0.47 for $^{12,S1}CG^0$, $^{12,S3}CG^0$ and $^{20,S1}CG^0$ respectively), to the different silicate solutions used (S1 or S3) and to the various metakaolin contents (12 or 20 g).

The d_{50} values of $^{12,S1}CG^0$, $^{12,S3}CG^0$ and $^{20,S1}CG^0$ are 5.9, 3.6 and 3.6 μm respectively while MK has a slightly greater D_{50} of approximately 10 μm. According to the BET measurements, the $^{12,S1}CG^0$ exhibits the highest specific surface area (125 m^2/g) followed by $^{12,S3}CG^0$ and $^{20,S1}CG^0$ which have similar specific surface areas (≈53 m^2/g). MK has the lowest specific surface area (17 m^2/g). The wettability values are 611, 523, 744 and 758 μl/g for $^{12,S1}CG^0$, $^{12,S3}CG^0$, $^{20,S1}CG^0$ and MK respectively. The bulk densities of these precursors are 2.24, 2.15, 2.35 and 2.63 g/cm^3 for $^{12,S1}CG^0$, $^{12,S3}CG^0$, $^{20,S1}CG^0$ and MK respectively. These values are almost similar. The crushed geopolymers $^{12,S1}CG^0$, $^{12,S3}CG^0$ and $^{20,S1}CG^0$ indicate a pH value of about 11 which is the common pH value of geopolymer materials in compliance with the work of Aly et al. [27]. The metakaolin has a pH value of 7 [28]. The measured pH value denotes the presence of alkaline species in solution released from geopolymers. The physicochemical characterizations have shown similar results for the three CG samples. The main differences are due to the different chemical composition of the starting geopolymer materials. This may also be indicative of various amorphous phase contents in the three samples.

To validate this hypothesis, XRD analyses were performed. The resulting XRD patterns (Fig. 2) display a broad peak characteristic of an amorphous material and peaks relative to crystalline phases such as quartz, muscovite and anatase. These phases present in the crushed geopolymer are explained by the fact that there were not altered as in metakaolin. The shift of the amorphous dome position between MK ($2\theta \approx 23°$) and the crushed geopolymer ($2\theta \approx 30°$) indicates the dissolution of SiO_4 and AlO_4 tetrahedra in alkaline solution [29]. Furthermore, the amorphous dome is more pronounced for $^{12,S1}CG^0$ evidencing higher amorphization in comparison with the other precursors. This phenomenon explained the higher BET value obtained for this sample.

All these distinct data suggest that the various precursors (metakaolin and crushed geopolymers) might have different reactivities in the alkaline solution and therefore on the feasibility of consolidated materials based on these precursors.

3.2. Feasibility of consolidated materials

In order to evaluate the feasibility of consolidated materials using crushed geopolymer, several formulations were synthesized. Three compositions denoted as $^{12,S1}G^0$, $^{12,S3}G^0$ and $^{20,S1}G^0$ were considered as reference materials. They differ in terms of the amount of metakaolin (12 g of metakaolin for $^{12,S1}G^0$ and $^{12,S1}G^0$, $^{12,S3}G^0$ vs 20 g for $^{20,S1}G^0$) and the type of the solution as detailed in Table 1.

Then, for each composition, a set of samples was synthesized either by addition or substitution of crushed geopolymer up to 100% of metakaolin's mass. Based on their visual aspects and consolidated states, the domains of feasibility of consolidated materials as well as geopolymers were defined in function of the amount of crushed geopolymer in the mixture and the Si/K molar ratio of the activating solution in Fig. 3(A).

For the first set ($^{12,S1}G^y$), the Si/K molar ratio of the alkaline solution is about 0.58. The consolidated materials were obtained until 90% of crushed geopolymer substituting the metakaolin. Above this value, sedimented materials showing different layers were obtained. Indeed, the crushed geopolymer remains in the bottom layer and the excess of solution is in the upper layer. This fact suggests differences in reactivity between the metakaolin and the crushed geopolymer in an alkaline media. On the other hand, when crushed geopolymer is added to the mixture, consolidated materials were obtained up to 50% of crushed geopolymer. Above this percentage, there is an excess of aluminosilicate

Table 2
Physical and chemical properties of the raw materials.

Raw materials	Molar ratios		D_{10} (μm)	D_{50} (μm)	D_{90} (μm)	BET value (m^2/g)	pH value	Wettability w (μl/g)	Bulk density (g/cm^3)
	Si/Al	Si/K							
MK	1.17	–		10.0		17	7.92	758	2.63
$^{12,S1}G^0$	1.66	2.09	2.0	5.9	15.1	125	10.67	611	2.24
$^{12,S3}G^0$	1.72	1.67	1.3	3.6	9.3	54	10.61	523	2.15
$^{20,S1}G^0$	1.41	3.09	1.3	3.6	9.6	51	10.83	744	2.35

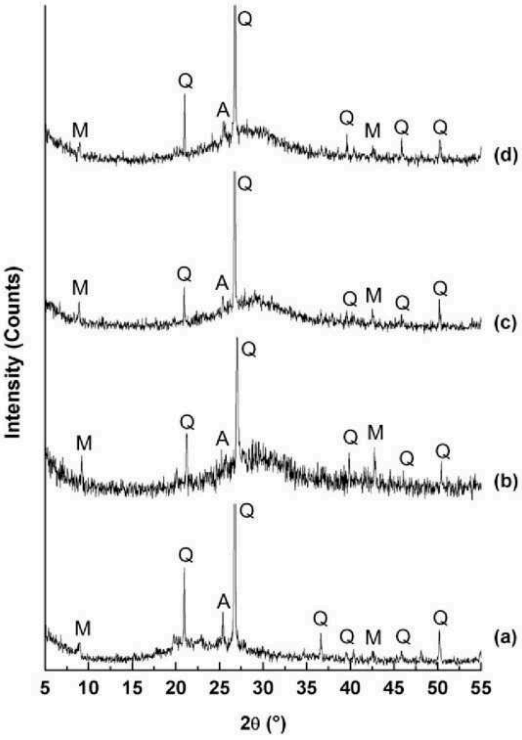

Fig. 2. XRD patterns of raw materials (a) MK, (b) $^{12,S1}G^0$, (c) $^{12,S3}G^0$, and (d) $^{20,S1}G^0$. Q: quartz, M: muscovite, and A: anatase.

source. The amount of species coming out from the solution is not enough to wet and completely alter the aluminosilicate source to initiate a polycondensation reaction. The materials exhibiting geopolymer features, homogenous and brilliant aspect were only obtained up to 50% of crushed geopolymer substituting the metakaolin or added to the mixture. For the second set ($^{12,S3}G^y$), with a Si/K molar ratio of 0.51, 50% of crushed geopolymer for both substitution and addition permit to obtain consolidated materials. The percentage of substitution is lower than the first set ($^{12,S1}G^y$) regarding the lower water content in S3 starting solution. Taking this fact into account, above 50% of crushed geopolymer, there is not enough silicate to dissolve the entire aluminosilicate source. In fact, the water content in silicate solutions is known to play a crucial role during and after synthesis since it affects the viscosity and the workability during mixing as well as the structure and the properties of the materials [30]. Indeed, the increase of the water content in the solution leads to the polymerization of the silicate species which will have an influence on the polycondensation reactions. The geopolymer zone extends only to 40% and 25% of crushed geopolymer for substitution and addition respectively. For the last set ($^{20,S1}G^y$), with a Si/K molar ratio of 0.47, consolidated materials are feasible up to 50% of substitution of metakaolin by crushed geopolymer and only up to 20% of addition. The percentage of addition is lower than the two others sets because the reference composition ($^{20,S1}G^0$) was already charged in metakaolin compared to $^{12,S1}G^0$ and $^{12,S3}G^0$ samples.

Furthermore, it is noticed that the feasibility of consolidated and geopolymer materials increases as the Si/K molar ratio of the alkaline solution increases. In fact, it was demonstrated that the Si/K molar ratio controls the nature and the amount of siliceous species present in the solution. The increase of this ratio from 0.35 to 0.60 leads to the formation of oligomers to the detriment of monomers and the increase of the non-bridging oxygen atom (NBO). According to Autef et al. [31],

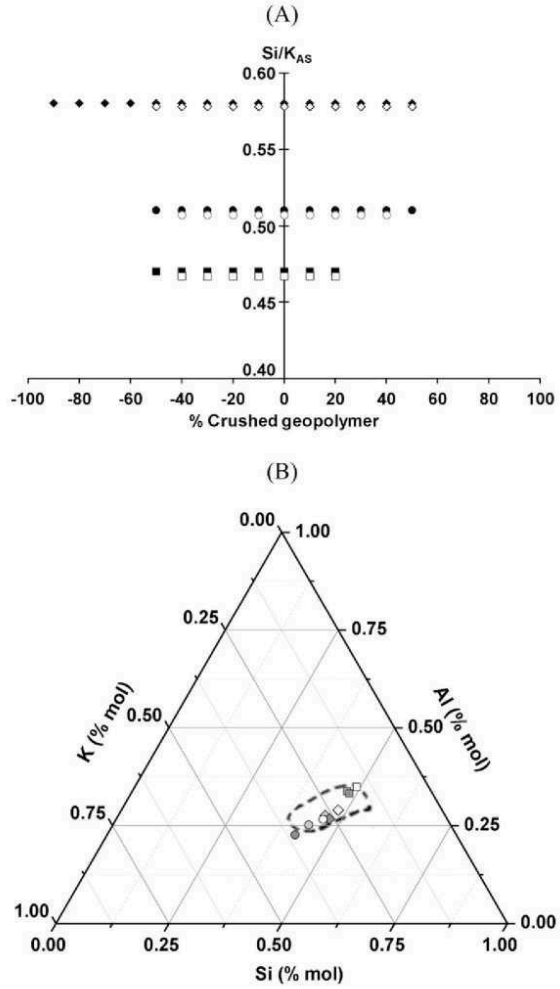

Fig. 3. (A) Feasibility domains for (♦) $^{12,S1}G^y$, (●) $^{12,S3}G^y$ and (■) $^{20,S1}G^y$ and geopolymer domains for (◊) $^{12,S1}G^y$, (○) $^{12,S3}G^y$ and (□) $^{20,S1}G^y$ and (B) position of the different compositions (◊) $^{12,S1}G^0$, (⧫) $^{12,S1}G^{20}$, (⧫) $^{12,S1}G^{S20}$, (○) $^{12,S3}G^0$, (●) $^{12,S3}G^{20}$, (●) $^{12,S3}G^{S20}$, (□) $^{20,S1}G^0$, (■) $^{20,S1}G^{20}$, (■) $^{20,S1}G^{S20}$ on the Si—Al—K/O ternary.

an increase of the Si/K ratio from 0.35 to 0.60 favors the formation of the geopolymer phase. This fact was explained by a decrease of the connectivity of the silicate anions and, consequently, inhibits the network polymerization due to the very high alkalinity of the solution. In the following sections, to exacerbate the effect of addition and substitution of crushed geopolymer on the polycondensation rate and the working properties of the final materials, only the compositions ($^{12,S1}G^0$, $^{12,S1}G^{20}$ and $^{12,S1}G^{S20}$), ($^{12,S3}G^0$, $^{12,S3}G^{20}$ and $^{12,S3}G^{S20}$) and ($^{20,S1}G^0$, $^{20,S1}G^{20}$ and $^{12,S1}G^{S20}$) were chosen for characterization.

To validate the previously discussed data, the chosen samples were reported in Al–Si–K–O ternary diagram as presented in Fig. 3(B). According to previous work [32], it was evidenced the existence of various domains depending on the Si/Al and Si/K molar ratios which are (A) geopolymer, (B) hardening material, (C) sedimented material and (D) gel. It was confirmed that all samples, for both addition and substitution of 20% of crushed geopolymer, were located in the geopolymer zone.

In order to investigate the effect of aluminosilicate waste on geopolymer formation, FTIR spectroscopy and mechanical tests were performed.

3.3. Characterization of selected compositions

3.3.1. Effect of the crushed geopolymer on the polycondensation rate

The formation of the geopolymer was the result of a geopolymerization reaction involving the restructuration of material which could be followed by FTIR spectroscopy. Example of the spectra obtained at different time for $^{12,S1}G^0$ sample are shown in Fig. 4(A). All the spectra exhibit the contributions at 3200 and 1640 cm^{-1} attributed to the ν_{OH} and δ_{OH} respectively. A broad band is also observed in the 1100–950 cm^{-1} range and is assigned to the Si—O—M (M = Si, Al) bond. Over time, the intensity of the ν_{OH} and δ_{OH} bands gradually decreases whereas the Si—O—M contribution shifts towards lower wavenumber. This variation reveals a polycondensation reaction and is characteristic of the formation of a specific network [33,34]. The evolution of Si—O—M band position versus time is plotted in Fig. 4(B). A displacement of this band to lower wavenumber is noticed. Indeed, the Si—O—M peak position shifts from 969 cm^{-1} to 940 cm^{-1} during 250 min. This is in agreement with the literature data [29] and it evidences the dissolution of the metakaolin species by the basic environment. Furthermore, the shift value denotes the replacement of Si—O—Si by Si—O—Al bonds during the geopolymerization and the calculated slope value at the beginning of the curve gives information about the kinetic of the reaction.

In order to understand the effect of the presence of crushed geopolymer in the mixture, the displacement of the Si—O—M band versus time for all samples was plotted in Fig. 5. All the samples show a shift of Si—O—M band to lower wavenumber. The initial peak positions are similar for the $^{12,S1}G^y$ and $^{20,S1}G^y$ samples (986 and 980 cm^{-1} respectively) whereas it is lower for $^{12,S3}G^y$ mixtures (969 cm^{-1}). This difference is explained by the different initial alkaline solutions. Indeed, the similar initial peak position for $^{12,S1}G^y$ and $^{20,S1}G^y$ geopolymers are due to the use of S1 solution contrary to $^{12,S3}G^y$ sample. These two solutions have different silicate species as shown by Gharzouni et al. [24,25]. Then, for $^{12,S1}G^y$ mixtures (Fig. 5(A)), the addition of CG implies a diminution of the shift value (from 47 to 27 cm^{-1} for $^{12,S1}G^0$ and $^{12,S1}G^{20}$ samples respectively) slowing down the polycondensation reactions. This fact may reveal a low or non-reactivity of the CG. Indeed, according to previous work [15], the presence of low or non-reactive species provided by the waste disrupts the exchanges between reactive aluminous and siliceous

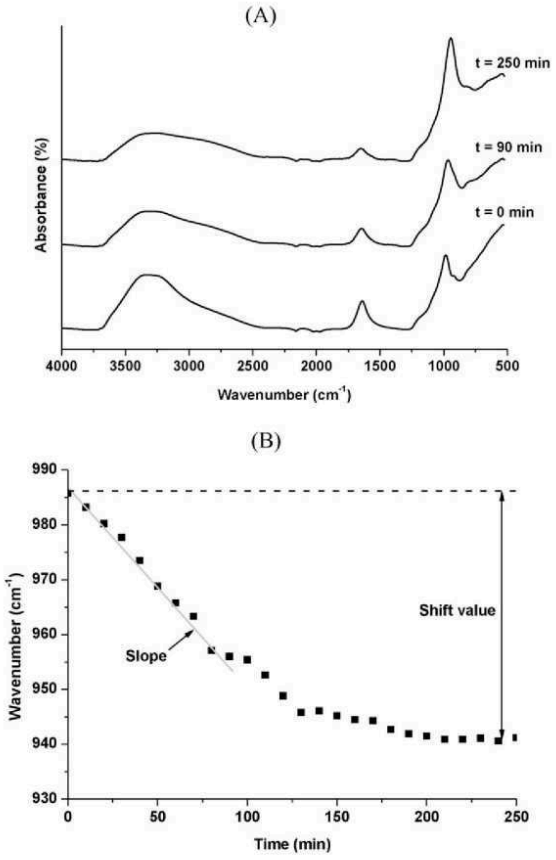

Fig. 4. In situ FTIR spectra obtained at t = 0, t = 90 and t = 250 min for the (A) $^{12,S1}G^0$ and (B) Q^2 position shift and slope from IR spectra versus time for the $^{12,S1}G^0$ sample.

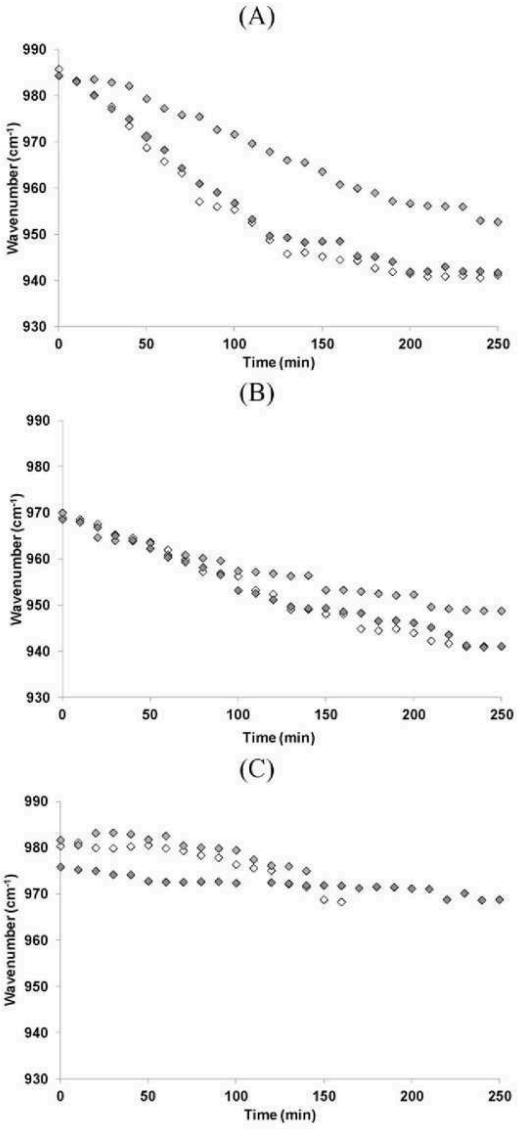

Fig. 5. Evolution of the shift of Q^2 position from FTIR spectra versus time for (A) $^{12,S1}G^X$, (B) $^{12,S3}G^X$ and (C) $^{20,S1}G^{SX}$ reactive mixtures with x = (◇) 0, (◈) 20 and (◈) S20% of crushed geopolymer.

species leading to a slowdown of the reactions. In the case of $^{12,S3}G^{y}$ samples (Fig. 5(B)), the addition of CG has no effect on the shift values (28 and 29 cm^{-1} for $^{12,S3}G^{0}$ and $^{12,S3}G^{20}$ mixtures respectively). The unchanged values observed are due to the fact that the alkaline solution governs the reactions. In fact, Gharzouni et al. [25] demonstrated that, when S3 is used, close shift values were observed for four metakaolins differing in terms of reactivity. Consequently, S3 solution governs the reactivity of the mixtures regardless the metakaolin properties. The addition of crushed geopolymers in the $^{20,S1}G^{y}$ mixtures (Fig. 5(C)) lead to weak variations of the shift values (21 and 13 cm^{-1} for $^{20,S1}G^{0}$ and $^{20,S1}G^{20}$ geopolymers respectively). In this case, the slight decrease of the shift values evidences that the effect of the presence of CG is associated to the influence of the high amount of metakaolin in these compositions. Some authors [26,35] showed that a high amount of metakaolin leads to a lack of reactive silicate species to completely react with the MK. A geopolymerization reaction took place but the attack of the MK being incomplete, the final material may exhibit a geopolymer network with unreacted MK particles. This is the phenomenon observed for the $^{20,S1}G^{0}$ sample. When CG is added, the reactions are also incomplete and the final material may contain unreacted CG and MK particles in a geopolymeric matrix.

Contrary to the addition, the substitution of an amount of metakaolin by crushed geopolymer does not have a significant effect on the various samples. For the $^{12,S1}G^{S20}$ sample, the unchanged shift values (44 cm^{-1} instead of 47 cm^{-1} for $^{12,S1}G^{0}$ mixture) may be explained by the low or non-reactivity of the waste. Indeed, the CG has a limited effect on the polycondensation degree of the network according to Gao et al. [16]. The authors showed that the substitution of a small amount of slag by fly ash leads to unchanged infrared band position and attributed this to the small influence of fly ash inclusions on the networks. Then, for the $^{12,S3}G^{y}$ set, the unchanged shift values (28 and 35 cm^{-1} for $^{12,S3}G^{0}$ and $^{12,S3}G^{S20}$ samples) may be due to the fact that the alkaline solution governs the geopolymerization reactions as it was observed for the addition. For the $^{20,S1}G^{y}$ samples, the shift values are also unchanged (21 and 16 cm^{-1} for $^{20,S1}G^{0}$ and $^{20,S1}G^{S20}$ samples) and this phenomenon could be explained by the low or non-reactivity of the waste as well as the small amount of CG substituting the metakaolin as previously seen. All these data evidenced a more pronounced effect of the geopolymer waste on the $^{12,S1}G^{y}$ mixtures. For the other two compositions, the limited effect of the waste is attributable at the use of a highly reactive solution or the higher amount of metakaolin.

The evolution of the shift versus the slope values calculated for all the samples is presented in Fig. 6. Different zones were determined depending on the shift and slope values [36]. For a slope and a shift higher than −0.10 cm^{-1}/min and 22 cm^{-1} respectively, there is the coexistence of several networks. The existence of a gel was determined for a shift and a slope lower than 22 cm^{-1} and −0.10 cm^{-1}/min respectively. Then, the junction of these two zones seems to be characteristic of geopolymer materials. According to the shift and slope values, different types of networks were identified for the studied samples [37]. All the samples from the $^{12,S1}G^{y}$ set are located in the zone were several networks coexists whereas the mixtures from the $^{12,S3}G^{y}$ and $^{20,S1}G^{y}$ sets are placed in the geopolymer domain. These results are in accordance with the previously discussed results and with the works of Gharzouni et al. [25]. However, for the first set ($^{12,S1}G^{y}$), the $^{12,S1}G^{0}$ sample is far from the geopolymer zone and the $^{12,S1}G^{20}$ mixture is closer to the geopolymer domain (decrease of the shift and slope values). The addition of CG seems to modify the behavior of the mixture and to lead to the presence of several networks different from those in the $^{12,S1}G^{0}$ sample. This fact may be explained by the low or non-reactivity of the waste which disrupts and slows down the exchanges between the reactive species during the geopolymerization process [22]. For the second and third set ($^{12,S3}G^{y}$ and $^{20,S1}G^{y}$), the $^{12,S3}G^{0}$, $^{12,S3}G^{20}$, $^{20,S1}G^{20}$ and $^{20,S1}G^{0}$ samples are located in the geopolymer zone. As it was seen previously, the waste addition does not seem to have a significant effect on the behavior of these materials. For the $^{12,S3}G^{y}$ set, this phenomenon is

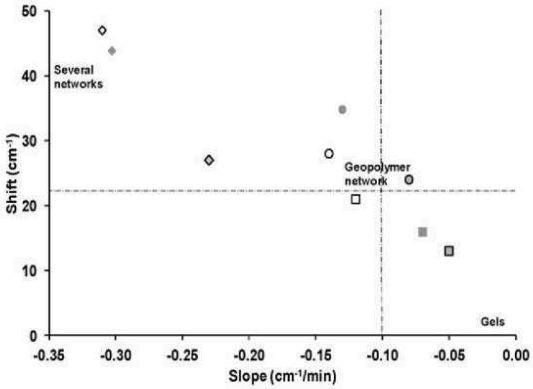

Fig. 6. Evolution of the shift versus the slope for different compositions (◇) $^{12,S1}G^{0}$, (◆) $^{12,S1}G^{20}$, (◆) $^{12,S1}G^{S20}$, (○) $^{12,S3}G^{0}$, (●) $^{12,S3}G^{20}$, (●) $^{12,S3}G^{S20}$, (□) $^{20,S1}G^{0}$, (■) $^{20,S1}G^{20}$ and (■) $^{20,S1}G^{S20}$ samples.

explained by the reactions governed by the alkaline solution. For the $^{20,S1}G^{y}$ set, the behavior is due to the high amount of MK in the reactive mixture. In fact, Liew et al. [35] showed that for a high quantity of metakaolin, the polycondensation reactions are incomplete. According to this, for the $^{20,S1}G^{20}$ sample, the effect of the CG may be associated to the influence of the amount of MK. Whatever the considered set, the substitution of an amount of MK by CG has no significant effect on the behavior of the different mixtures. Indeed, the $^{12,S1}G^{S20}$, $^{12,S3}G^{S20}$ and $^{20,S1}G^{S20}$ samples are located close to the reference samples ($^{12,S1}G^{0}$, $^{12,S3}G^{0}$ and $^{20,S1}G^{0}$ respectively). According to Gao et al. [16], the behavior of the three samples with substitution may be explained by the small amount of MK substituted by the waste which has a weak influence on the reactions.

So, the effect of the crushed geopolymer on the polycondensation rate can be counterbalanced by the use of a reactive alkaline solution or by the increase of the amount of metakaolin in the mixture. These differences in reactivity suggest the existence of variations on the mechanical properties of these compositions.

3.3.2. Effect of on geopolymer waste the mechanical properties

The influence of crushed geopolymer on the mechanical properties was evaluated by compressive test. The variation of compressive strength values as a function of strain for the three sets is illustrated in Fig. 7(A). Regardless of the sample, the obtained curves exhibited a linear variation characteristic of elastic regime followed by a slight plastic deformation and a brittle failure. The compressive strength value of samples, considered as reference, increased from 45, 68 to 76 MPa ± 0.2 for $^{12,S1}G^{0}$, $^{12,S3}G^{0}$ and $^{20,S1}G^{0}$ respectively. It is noticed, firstly, that the increase of the metakaolin amount from $^{12,S1}G^{0}$ to $^{20,S1}G^{0}$ seems to improve the mechanical properties. Then, the $^{20,S1}G^{0}$ display the highest compressive strength because it contains a high amount of metakaolin [38].

In the case of the addition 20% of crushed geopolymer and compared to reference samples, for the first set ($^{12,S1}G^{20}$), the compressive strength value decreases to 30 MPa ± 0.2. However, the mechanical properties of the second set ($^{20,S3}G^{20}$) are quite identical while 20% is added (about 70 MPa ± 0.2). The $^{20,S1}G^{20}$ has a compressive strength of 65 MPa ± 0.2 which is lower than $^{20,S1}G^{0}$. Consequently, it seems that the addition of crushed geopolymer decreases the compressive strength value especially for the first and third set. The loss of strength can be due to the non- or poor reactivity of the geopolymer crushed compared to metakaolin in an alkaline environment. This behavior is in agreement with the literature [12,39] since the aluminosilicate source based on metakaolin and crushed geopolymer as filler has been modified. The close values of mechanical properties for the second set ($^{12,S3}G^{20}$), can

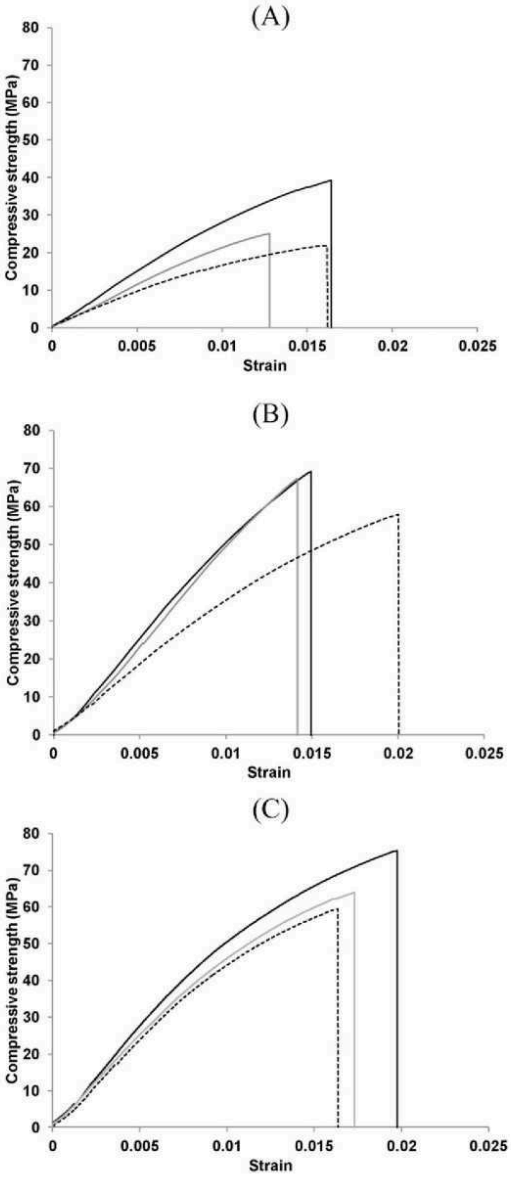

Fig. 7. Variation of compressive strength as a function of strain for (A) $^{12,S1}G^{x}$, (B) $^{12,S3}G^{Sx}$ and (C) $^{20,S1}G^{x}$ reactive mixtures with x = (—) 0, (---) 20, and (−) S20 of crushed geopolymer added.

be related to the use of highly reactive alkaline solution (S3) which govern the working properties as it was proved by Gharzouni et al. [25].

In the case of metakaolin substitution by crushed geopolymer, the compressive strength values decrease to (25, 60 to 62 MPa ± 0.2) for $^{12,S1}G^{S20}$, $^{12,S3}G^{S20}$ and $^{20,S1}G^{S20}$ respectively revealing that the mechanical properties decreased also with the substitution of metakaolin by crushed geopolymer. For the ($^{20,S1}G^{20}$ and $^{20,S1}G^{S20}$) compositions, the similar values are in relation with the crushed geopolymer source of aluminosilicate in presence of alkaline solution. Indeed, the $^{20,S1}G^{20}$ behaves as a geopolymer containing reinforcements in which the reactivity metakaolin is slowed in the presence of the alkaline solution, while for the $^{20,S1}G^{S20}$ sample, although metakaolin rate is lower, the alkaline solution allows dissolution which also leads to further enhanced geopolymer.

From these data, both the addition and the substitution of metakaolin by the crushed geopolymer diminish the compressive strength of the obtained materials.

4. Discussion

In order to understand the effect of crushed geopolymer incorporation in the different compositions on the polycondensation rate, the shift values were plotted versus the solid to liquid ratio (S/L) of each mixture normalized by the S/L of $^{12,S1}G^{0}$ sample (exhibiting the lowest S/L ratio) in Fig. 8(A). Typically, the shift values decreased with increasing the solid to liquid ratio (S/L). This ratio increased from 0.97 for $^{12,S1}G^{0}$ to 1.28 for $^{12,S3}G^{0}$ due to the lower water content in S3 solution and to 2.11 in the case of $^{20,S1}G^{0}$ higher amount of metakaolin in the case of $^{20,S1}G^{0}$. Whatever the composition, the substitution of metakaolin by crushed geopolymer maintains the same S/L ratio which explains the close obtained shift values (47 and 44 cm^{-1} for $^{12,S1}G^{0}$ and $^{12,S1}G^{S20}$ having a S/L ratio of about 0.97). However, the addition of crushed geopolymer increases the amount of aluminosilicate source and therefore increases the S/L ratio which corresponds to lower shift values compared to the reference compositions (27 cm^{-1} for $^{12,S1}G^{20}$ having a S/L ratio of 1.47). High shift values corresponding to low S/L suggest the existence of higher number of bonds between dissolved species and impurities of metakaolin engendering the formation of several networks as has been previously demonstrated by Autef et al. [37]. In fact, the high amount of activating liquid increases the mobility of species and, hence, facilitates the interaction between them. Liew et al. [35] have shown that low S/L

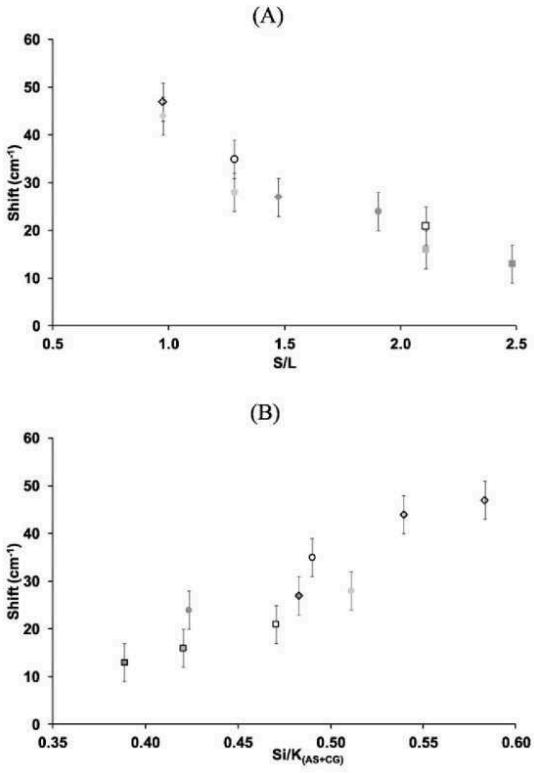

Fig. 8. Evolution of the shift values versus (A) the solid to liquid ratio (S/L) and (B) the Si/K molar ratio of the alkaline solution for (◇) $^{12,S1}G^{0}$, (◆) $^{12,S1}G^{20}$, (◆) $^{12,S1}G^{S20}$, (○) $^{12,S3}G^{0}$, (●) $^{12,S3}G^{20}$, (●) $^{12,S3}G^{S20}$, (□) $^{20,S1}G^{0}$, (■) $^{20,S1}G^{20}$ and (■) $^{20,S1}G^{S20}$ samples.

ratio favors the dissolution rate. However, it prevents the polycondensation rate because the diffusion of dissolved species is difficult. On the other hand, the relatively lower shift values corresponding to high S/L ratios indicate that the increase of the amount of solid in the mixture reduce the mobility of species at the interface charged region [40] leading to the formation of a unique network. Consequently, in addition to controlling the workability of the mixture, the S/L ratio is a crucial parameter which governs the type of formed networks in the resulting materials. To thoroughly understand this evolution, the shift values were plotted as function of the Si/K molar ratio of the activating solution in Fig. 8(B). The shift value decreases as the Si/K molar ratio decreases. The substitution of metakaolin by CG and in a greater extent the CG addition decreases the Si/K molar ratio of the activating solution due to the additional amount of potassium species released from crushed geopolymer causing therefore the decrease of the shift values. This fact can be explained by different extent of depolymerization of alkaline solution after the CG incorporation. In fact, the decrease of the Si/K ratio increases the depolymerization of the solution by increasing the number of non-bridging oxygen and the amount of low order siliceous species (Q^0 and Q^1) known to be more reactive than the other species [41]. Less depolymerized solution (high Si/K) induces the combination of Si—O—M (M = Si, Al or K) from dissolved species and from the impurities of metakaolin leading to high shift values and formation of different networks as discussed previously. In contrast, the decrease of the Si/K ratio increases the depolymerization of the solution by increasing the number of non-bridging oxygen and the amount of low order siliceous species (Q^0 and Q^1) known to be more reactive than the other species. The quickly released siliceous species reach speciation equilibrium and then react with the aluminous species because of their high reactivity inducing low shift values and formation of a geopolymer network. However, it should be mentioned that a very high alkalinity can act negatively on the polymerization due to lower connectivity between silicate anions.

To correlate the mechanical properties with the chemical compositions of the different samples, the specific compressive strength values were plotted versus the $(nSi/nK)_{AS}/(nSi/nAl)_{CG\ +\ MK}$ molar ratio in Fig. 9. Whatever the composition, the specific compressive strength values decreases with the decrease of $(nSi/nK)_{AS}/(nSi/nAl)_{CG\ +\ MK}$ molar ratio as a result of the CG incorporation by addition or by substitution. Using S1 alkaline solution, a linear relationship is observed between $^{12,S1}G^{y}$ and $^{20,S1}G^{y}$ series of samples evidencing the decrease of the compressive strength values with the decrease of aluminum availability. This finding is in accordance with the literature [30,42]. In fact, a strong correlation between the chemical composition and the mechanical properties was demonstrated. With a low Si/Al ratio, the geopolymer exhibits a weak porous structure. However, the increase of the Si/Al ratio leads to an homogenous microstructure and hence an increase in strength. For $^{12,S3}G^{y}$ samples, S3 alkaline solution seems to govern the compressive strengths. This fact can be explained by the differences in the distribution of silicon atoms and potassium availability between the two solutions inducing different reactivities [43]. Reactive released siliceous species from S3 solution [25] react quickly with the aluminous species leading to the formation of a perfect geopolymer network which enhance the mechanical properties of the strengthened materials.

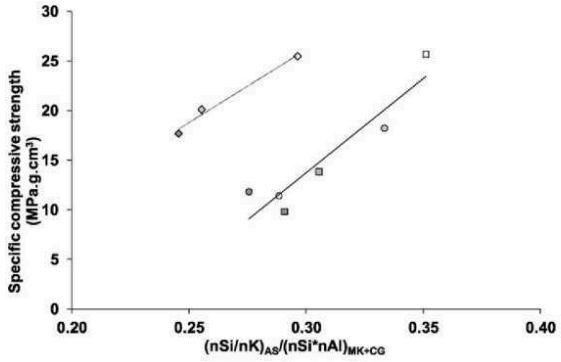

Fig. 9. Evolution of the specific compressive strength values versus the chemical composition $((nSi/nK)_{AS}/(nSi/nAl)_{(CG\ +\ MK)}$ for (◇) $^{12,S1}G^{0}$, (◆) $^{12,S1}G^{20}$, (◉) $^{12,S1}G^{S20}$, (○) $^{12,S3}G^{0}$, (●) $^{12,S3}G^{20}$, (●) $^{12,S3}G^{S20}$, (□) $^{20,S1}G^{0}$, (■) $^{20,S1}G^{20}$ and (■) $^{20,S1}G^{S20}$ samples.

5. Conclusion

This study evidenced the possibility of recycling geopolymer wastes to synthesize new geopolymer materials. Three compositions differing in the used alkaline solution and the amount of metakaolin were investigated. The geopolymer wastes characterization has evidenced different physico-chemical properties suggesting different reactivities in contact with an alkaline solution. A feasibility study allowed determining the waste amount which could be added or substituted to the metakaolin to obtain geopolymer materials. 20% of geopolymer waste was the retained percentage of both addition and substitution. Furthermore, it was shown that the incorporation of the geopolymer waste may hinder the polycondensation rate and decreases the mechanical strengths of the final materials due to its low or non-reactivity. Indeed, correlations were established on one hand, between the polycondensation rate and solid to liquid ratio ($1.41 \le S/L \le 1.72$) and Si/K molar of the alkaline solution and on the other hand, between the compressive strengths and the chemical compositions of the different samples. Nevertheless, the effect of geopolymer waste incorporation can be counterbalanced with the use of a highly reactive alkaline solution or the increase of the amount of metakaolin in the mixture.

References

[1] L.A. Guerrero, G. Mass, W. Hogland, Solid waste management challenges for cities in developing countries, Waste Manag. 33 (2013) 220–232.
[2] M. Ruth, P. Dell'Anno, An industrial ecology of the US glass industry, Res. Policy 23 (3) (1997) 109–124.
[3] M. Gomes, J. De Brito, Structural concrete with incorporation of coarse recycles concrete and ceramic aggregates: durability performance, Mater. Struct. 42 (5) (2009) 663–675.
[4] A. Gonzalez-Corominas, M. Etxeberria, Properties of high performance concrete made with recycled fine ceramic and coarse mixed aggregates, Constr. Build. Mater. 68 (2014) 618–626.
[5] P. Duxson, A. Fernández-Jiménez, J.L. Provis, G.C. Lukey, A. Palomo, J.S.J. van Deventer, Geopolymer technology: the current state of the art, J. Mater. Sci. 42 (2007) 2917–2933.
[6] J. Davidovits, Geopolymer: Chemistry and Applications, second ed. Institut Géopolymère, St-Quentin, 2008.
[7] C.A. Rees, J.L. Provis, G.C. Lukey, J.S.J. van Deventer, The mechanism of geopolymer gel formation investigated through seeded nucleation, Colloids Surf. A 318 (2008) 97–105.
[8] W.D.A. Rickard, R. Williams, J. Temuujin, A.v. Riessen, Assessing the suitability of the three Australian fly ashes as an aluminosilicate source for geopolymers in high temperature applications, Mater. Sci. Eng. A 528 (2011) 3390–3397.
[9] F. Messina, C. Ferone, F. Colangelo, R. Cioffi, Low temperature alkaline activation of weathered fly ash: influence of mineral admixtures on early age performance, Constr. Build. Mater. 86 (2015) 169–177.
[10] I. Ismail, S.A. Bernal, J.L. Provis, R. San Nicolas, S. Hamdan, J.S.J. van Deventer, Modification of phase evolution in alkali-activated blast furnace slag by the incorporation of fly ash, Cem. Concr. Compos. 45 (2014) 125–135.
[11] H. Xu, W. Gong, L. Syltebo, K. Izzo, W. Lutze, I.L. Pegg, Effect of blast furnace slag grades on fly ash based geopolymer waste forms, Fuel 133 (2014) 332–340.
[12] J. He, J. Zhang, Y. Yu, G. Zhang, The strength and microstructure of two geopolymers derived from metakaolin and red mud-fly ash admixture: a comparative study, Constr. Build. Mater. 30 (2012) 80–91.
[13] F. Pacheco-Torgal, J. Castro-Gomes, S. Jalali, Investigations about the effect of aggregates on strength and microstructure of geopolymeric mine waste mud binders, Cem. Concr. Res. 37 (6) (2007) 933–941 (Cem. Concr. Res. 37(6) (2007) 933-941).
[14] L. Evangelista, J. de Brito, Mechanical behaviour of concrete made with fine recycled concrete aggregates, Cem. Concr. Compos. 29 (5) (2007) 397–401.
[15] K. Komnitsas, D. Zaharaki, A. Vlachou, G. Bartzas, M. Galetakis, Effect of synthesis parameters on the quality of construction and demolition wastes (CDW) geopolymers, Adv. Powder Technol. 26 (2) (2015) 368–376.
[16] X. Gao, Q.L. Yu, H.J.H. Brouwers, Reaction kinetics, gel character and strength of ambient temperature cured alkali activated slag–fly ash blends, Constr. Build. Mater. 80 (2015) 105–115.

[17] A. Nazari, J.G. Sanjayan, Synthesis of geopolymer from industrial wastes, J. Clean. Prod. 99 (2015) 297–304.
[18] S. Onutai, S. Jiemsirilers, P. Thavorniti, T. Kobayashi, Aluminium hydroxide waste based geopolymer composed of fly ash for sustainable cement materials, Constr. Build. Mater. 101 (2015) 298–308.
[19] C. Ferone, B. Liguori, I. Capasso, F. Colangelo, R. Cioffi, E. Cappelletto, R. DiMaggio, Thermally treated clay sediments as geopolymer source material, Appl. Clay Sci. 107 (2015) 195–204.
[20] L. Zheng, W. Wang, Y. Shi, The effects of alkaline dosage and Si/Al ratio on the immobilization of heavy metals in municipal solid waste incineration fly ash-based geopolymer, Chemosphere 79 (6) (2010) 665–671.
[21] W. Park, T. Noguchi, Influence of metal impurity on recycled aggregate concrete and inspection method for aluminum impurity, Constr. Build. Mater. 40 (2013) 1174–1183.
[22] N. Essaidi, A. Gharzouni, L. Vidal, F. Gouny, E. Joussein, S. Rossignol, Recycling of aluminosilicate waste: impact onto geopolymer formation, Eur. Phys. J. 224 (2015) 1707–1713.
[23] N. Essaidi, L. Vidal, F. Gouny, E. Joussein, S. Rossignol, Recycled geopolymer on new formulations, Ceram. Eng. Sci. Proc. 36 (8) (2015) 49–60.
[24] A. Gharzouni, E. Joussein, B. Samet, S. Baklouti, S. Pronier, I. Sobrados, J. Sanz, S. Rossignol, The effect of an activation solution with siliceous species on the chemical reactivity and mechanical properties of geopolymers, J. Sol-Gel Sci. Technol. 73 (2015) 250–259.
[25] A. Gharzouni, E. Joussein, B. Samet, S. Baklouti, S. Rossignol, Effect of the reactivity of alkaline solution and metakaolin on geopolymer formation, J. Non-Cryst. Solids 410 (2015) 127–134.
[26] E. Prud'homme, P. Michaud, A. Smith, C. Peyratout, I. Sobrados, J. Sanz, S. Rossignol, Geomaterial foams: role assignment of raw materials in the network formation, J. Sol-Gel Sci. Technol. 61 (2) (2012) 436–448.
[27] Z. Aly, E.R. Vance, D.S. Perera, J.V. Hanna, C.S. Griffith, J. Davis, D. Durce, Aqueous leachability of metakaolin-based geopolymers with molar ratios of Si/Al = 1.5–4, J. Nucl. Mater. 378 (2) (2008) 172–179.
[28] E. Moulin, P. Blanc, D. Sorentino, Influence of key cement chemical parameters on the properties of metakaolin blended, Cem. Concr. Compos. 23 (2001) 463–469.
[29] E. Prud'homme, P. Michaud, E. Joussein, J.M. Clacens, S. Rossignol, Role of alkaline cations and water content on geomaterial foams: monitoring during formation, J. Non-Cryst. Solids 357 (2011) 1270–1278.
[30] M. Lizcano, A. Gonzalez, S. Basu, K. Lozano, M. Radovic, Effects of water content and chemical composition on structural properties of alkaline activated metakaolin-based geopolymers, J. Am. Ceram. Soc. 95 (7) (2012) 2169–2177.
[31] A. Autef, E. Joussein, G. Gasgnier, S. Rossignol, Effect of alkaline solutions Si/K ratio on mechanical properties of geomaterial components, Ceram. Eng. Sci. Proc. 35 (8) (2014) 29–38.
[32] X.X. Gao, A. Autef, E. Prud'homme, P. Michaud, E. Joussein, S. Rossignol, Synthesis of consolidated materials from alkaline solutions and metakaolin: existence of domains in the Al–Si–K/O ternary diagram, J. Sol-Gel Sci. Technol. 65 (2) (2013) 220–229.
[33] C.A. Rees, J.L. Provis, G.C. Lukey, J.S.J.v. Deventer, Attenuated total reflectance Fourier transform infrared analysis of fly ash geopolymer gel aging, Langmuir 23 (15) (2007) 8170–8179.
[34] C.A. Rees, J.L. Provis, G.C. Lukey, J.S.J.v. Deventer, In situ ATR-FTIR study of the early stages of fly ash geopolymer gel formation, Langmuir 23 (17) (2007) 9076–9082.
[35] Y.M. Liew, H. Kamarudin, A.M. Mustafa Al Bakri, M. Bnhussain, M. Luqman, I. Khairul Nizar, C.M. Ruzaidi, C.Y. Heah, Optimization of solids-to-liquid and alkali activator ratios of calcined kaolin geopolymeric powder, Constr. Build. Mater. 37 (2012) 440–451.
[36] F. Gouny, F. Fouchal, P. Maillard, S. Rossignol, Study of the effect of siliceous species in the formation of a geopolymer binder: understanding the reaction mechanisms among the binder, wood, and earth brick, Ind. Eng. Chem. Res. 53 (9) (2014) 3559–3569.
[37] A. Autef, E. Joussein, A. Poulesquen, G. Gasgnier, S. Pronier, I. Sobrados, J. Sanz, S. Rossignol, Influence of metakaolin purities on potassium geopolymer formulation: the existence of several networks, J. Colloid Interface Sci. 408 (2013) 43–53.
[38] P. Duxson, J.L. Provis, G.C. Lukey, S.W. Mallicoat, W.M. Kriven, J.S.J. Van Deventer, Understanding the relationship between geopolymer composition, microstructure and mechanical properties, Colloids Surf. A 269 (1–3) (2005) 47–58.
[39] X.S. Shi, F.G. Collins, X.L. Zhao, Q.Y. Wang, Mechanical properties and microstructure analysis of fly ash geopolymeric recycled concrete, J. Hazard. Mater. 237-238 (2012) 20–29.
[40] F.K. Crundwell, The mechanism of dissolution of the feldspars: part I. Dissolution at conditions far from equilibrium, Hydrometallurgy 151 (2015) 151–162.
[41] F. Liebau, Structural Chemistry of Silicates, first ed. Springer-Verlag, Berlin, Germany, 1985.
[42] J.S.J. Van Deventer, J.L. Provis, P. Duxson, Technical and commercial progress in the adoption of geopolymer cement, Miner. Eng. 29 (2012) 89–104.
[43] A.S. Brykov, V.V. Danilov, E.Y. Aleshunina, State of silicon in silicate and silica-containing solutions and their binding properties, Russ. J. Appl. Chem. 81 (10) (2008) 1717–1721.

Publication 6 (ACL6)

A. Gharzouni, I. Sobrados, E. Joussein, S. Baklouti, S. Rossignol

"Control of polycondensation reaction generated from different metakaolins and alkaline solutions"

Cement and concrete composite, submitted

L'objectif de la présente étude est de contrôler la réaction de polycondensation de différents matériaux géopolymères élaborés à partir de six métakaolins et deux solutions alcalines de potassium ayant différentes réactivités. Dans un premier temps, la caractérisation des métakaolins a révélé que la réactivité augmente avec l'augmentation du degré de pureté, de la phase amorphe et de la valeur de la mouillabilité (demande en eau). Dans un second temps, la formation des géopolymères a été étudiée. L'analyse thermique in situ a permis de démontrer que la disponibilité des espèces dissoutes diminue l'énergie nécessaire à la formation des oligomères à environ 1,8 kJ/mol. En revanche, une solution alcaline très réactive favorise la dissolution et diminue l'énergie à environ 0,6 kJ/mol, même dans le cas des métakaolins faiblement réactifs. En outre, les études par spectroscopie IRTF in situ ont révélé que les impuretés du métakaolin sont responsables de la formation de plusieurs réseaux. Cependant, la formation d'un seul réseau de type géopolymère est favorisée dans le cas d'une solution alcaline très réactive. En outre, des informations structurales ont été fournies par RMN de l'aluminium (^{27}Al) in situ. En effet, il a été prouvé que la réactivité du métakaolin et la réactivité des solutions alcalines permettent l'augmentation des taux de conversion de l'$Al^{(VI)}$ et $Al^{(V)}$ en $Al^{(IV)}$, qui dépassent 80% dans le cas de la solution alcaline très réactive. Les meilleures valeurs de résistance à la compression (> 60 MPa) ont été obtenues pour des taux de conversion élevés.

CONTROL OF POLYCONDENSATION REACTION GENERATED FROM DIFFERENT METAKAOLINS AND ALKALINE SOLUTIONS

1. A. Gharzouni[1, 2], I. Sobrados[3], E. Joussein[4], S. Baklouti[2], S. Rossignol[1]

[1] Science des Procédés Céramiques et de Traitements de Surface (SPCTS), Ecole Nationale Supérieure de Céramique Industrielle, 12 rue Atlantis, 87068 Limoges Cedex, France.

[2] Laboratoire de Chimie Industrielle, Ecole Nationale d'Ingénieurs de Sfax, université de Sfax, 3038 Sfax, Tunisie.

[3] Instituto de Ciencia de Materiales de Madrid, Consejo Superior de Investigaciones Científicas (CSIC), C/Sor Juana Inés de la Cruz, 3, 28049 Madrid, Spain.

[4] Université de Limoges, GRESE EA 4330, 123 avenue Albert Thomas, 87060 Limoges, France.

■ corresponding author: sylvie.rossignol@unilim.fr, tel.: 33 5 87 50 25 64

Metakaolin	*Alkaline solution*	*Kinetics*
Oligomer formation	*^{27}Al NMR*	*Mechanical strength*

Abstract

The purpose of the present study is to control the polycondensation reaction of various geopolymer samples based on six metakaolins and two potassium alkaline solutions with different reactivities. At first, metakaolin characterization revealed three levels of reactivity, which increase essentially with the increase of purity degree, amorphous phase and wettability value. Then, the formation of geopolymer samples was investigated. In situ thermal analysis showed that depending on the metakaolin surface reactivity, the availability of dissolved species decreases the energy required for oligomer formation to approximately 1.8 KJ/mol. However, a highly reactive alkaline solution favors the dissolution and decreases this energy to approximately 0.6 KJ/mol, even in the case of low-reactive metakaolins. In addition, in situ

FTIR spectroscopy revealed that the metakaolin impurities are responsible for the generation of several networks. However, the geopolymer network is favored in the case of a highly reactive alkaline solution. Further, structural information was given by in situ ^{27}Al NMR. It was proven that the reactivity of metakaolin and, more significantly, the reactivity of alkaline solutions ensure higher conversion rates of $Al^{(VI)}$ and $Al^{(V)}$ species to $Al^{(IV)}$, which may reach 80%. Better compressive strengths (>60 MPa) were obtained for high conversion rates.

1. Introduction

Under increasing necessity to develop new construction materials that are environmentally friendly, low-energy-consuming and cost-efficient, geopolymer materials appear as competitive alternative mineral binders. Geopolymers can be defined as three-dimensional amorphous materials derived from the activation of an aluminosilicate source (metakaolin, clays, fly ash, blast furnace slag) by an alkaline solution (silicate solution and alkali hydroxide). Research questions about these materials have been diverse, including the formation mechanism, working properties and potential applications. Metakaolin was extensively used as an ideal precursor for fundamental studies aiming to explore the kinetics, reaction mechanism and properties of geopolymer materials. In this context, Granizo et al. [1] have demonstrated that the degree of the reaction is closely related to the metakaolin specific surface and the volume of the activating solution. As a result, the mechanical strength increases with decreasing activator volume and increasing alkali concentration. Furthermore, Wang et al. [2] summarized the reaction process as first, the dissolution of the metakaolin surface layer by NaOH solution and then, the polymerization of aluminosilicate species under the effect of monomer, dimer and oligomer species of the silicate solution. They also mentioned that the colloid reaction mainly takes place at the surface of the microflake of the metakaolin particles. Moreover, many authors have tried to explore the geopolymer formation mechanism using different characterization techniques. Provis et al. [3], considered it difficult to separate each step of the reaction from the other because they are occurring simultaneously and rapidly. Despite this fact, they succeeded in modeling the reaction kinetics using in situ energy dispersive X-ray diffraction. Other authors have used more accurate structural analysis, such as NMR experiments. For instance, Rahier et al. [4] studied the reaction kinetics and mechanism using modulated temperature differential scanning calorimetry and dynamic mechanical analysis. They also explored the possibility of ^{27}Al and ^{29}Si NMR to follow the molecular changes during the material synthesis. They found that geopolymers

result from complex combined reactions. Indeed, the decrease of OH^- concentration at the beginning of the reaction leads to the formation of an intermediate aluminosilicate species that evolutes afterwards to a geopolymer. Recently, Favier et al. [5]conducted a heteronuclear liquid NMR study to observe the chemical evolution of the interstitial phase during geopolymerization and correlate it with the evolution of the elastic modulus of the geopolymer paste. An ^{1}H NMR study was also carried out to characterize the geopolymerization process of a metakaolin-based geopolymer. The geopolymerization process, in the early age, was described as a succession of an induction period, an acceleration period, a deceleration period and finally, a stabilization period [6]. Differential thermal analysis (DTA) and thermogravimetric analysis (TGA) during formation have also been useful in determining the geopolymerization rate [7]. The geopolymer samples were maintained at 70°C for two hours. According to the obtained heat flow curve and associated weight losses, four zones were defined, denoting different reactions: first, the reorganization of species; then, the dissolution of metakaolin, followed by the oligomer formation; and finally, the polycondensation reaction. Despite the existing background models describing the geopolymerization reaction, the mechanism is still the subject of research because it is strongly dependent on the raw materials used. Thus, it is interesting to assess the influence of raw precursor reactivity on the structural evolution of geopolymer materials and its final properties. For this, elucidation of the structural changes as the reaction of geopolymerization proceeds in function of various metakaolins and alkaline solutions seems to be profitable.

In this paper, the control of the polycondensation reaction will be investigated. The effect of aluminates species from different metakaolins will be studied because they are thermodynamically limiting factors for the polycondensation reaction [8]. The role of silicate species is also important and depends on the alkali cation. Two potassium silicate solutions differing in terms of reactivity were used to exacerbate the effect of alkaline solution reactivity on reaction kinetics. The geopolymer formation was probed by differential thermal analysis and thermogravimetric analysis (DTA-TGA), FTIR spectroscopy and ^{27}Al NMR. Then, the mechanical properties of the strengthened materials were evaluated by compression tests.

2. Experimental

2.1. Raw materials and sample preparation

Geopolymer samples were synthesized using six metakaolins (named M1 through M6) (Table 1) and two commercial potassium silicate solutions denoted as S1 and S3 with Si/K molar ratios of 1.75 and 0.65. Potassium hydroxide pellets (VWR, 85.2% pure) were dissolved into the two starting silicate solutions to maintain the Si/K molar ratio at 0.5. Then, metakaolins were added.

Table 1 Chemical and physical properties of raw metakaolins

Metakaolins	M1	M2	M3	M4	M5	M6
Si/Al	1.17	1.19	1.00	0.98	1.44	1.33
d_{50} (µm)	10	6	8	6	20	26
BET value (m^2/g)	17	22	8	17	18	6
Wettability (µL/g)	760	1250	1010	1186	530	670
Amorphous phase	63	87	98	98	64	59
Heating process	Rotary	Flash	Oven	Flash	Flash	Flash

The obtained mixtures were placed in a closed sealable polystyrene mold at room temperature (25°C). The nomenclature and the composition of the prepared mixtures are reported in Table 2.

Table 2 Nomenclature and composition of the studied samples.

Mixtures	Si/Al
S1M1	1.56
S1M2	1.60
S1M3	1.34
S1M4	1.33
S1M5	1.67
S1M6	1.63
S3M1	1.68
S3M2	1.73
S3M3	1.45
S3M4	1.44
S3M5	1.76
S3M6	1.74

2.2. Sample characterization

The chemical composition of the raw materials was determined using X-ray fluorescence (ARL 8400, XRF 386 software).

X-ray diffraction patterns were acquired via X-ray diffraction (XRD) experiments on a Bruker-AXS D 5005 powder diffractometer using CuK α radiation (λKα=0.154186 nm). The analytical range is between 5° and 55° (2θ), with a step of 0.04° and an acquisition time of 2 s for raw metakaolins powder. JCPDS (Joint Committee Powder Diffraction Standard) files were used for phase identification. The amorphous phase for each metakaolin was determined using the Rietveld method [9].

The particle size distributions of the clays were measured using a laser particle size analyzer (Mastersizer 2000). The powder is suspended by an air current flowing through a glass cell with parallel faces illuminated by a beam of laser light. The measurement is made at a pressure of 3 bars.

Powder BET surface areas were determined by N_2 adsorption at -195.85°C using a Micrometrics Tristar II 3020 volumetric adsorption/desorption apparatus. Prior to the measurement, the samples were degassed at 200°C under vacuum for 4 h.

The wettability value (µL/g) corresponds to the volume of water that can be adsorbed by one gram of powder before saturation.

Fourier-transform infrared (FTIR) spectroscopy in ATR mode was used to investigate the structural evolution of the geopolymer mixtures. The FTIR spectra were obtained using a ThermoFisher Scientific Nicolet 380 infrared spectrometer. The IR spectra were gathered over a range of 400 to 4000 cm-1 with a resolution of 4 cm-1. The atmospheric CO2 contribution was removed with a straight line between 2400 and 2280 cm-1. To monitor the geopolymer formation, software was used to acquire a spectrum (64 scans) every 10 minutes for 13 hours. For comparison, the spectra were baseline-corrected and normalized [10].

Differential thermal analysis (DTA) and thermogravimetric analysis (TGA) were performed on an SDT Q600 apparatus from TA Instruments in an atmosphere of flowing dry air (100 mL/minute) in platinum crucibles. The signals were measured with Pt/Pt–10%Rh thermocouples. Thermal analysis was conducted during the formation of the consolidated materials using the thermal cycle previously established by Autef et al. [7]. The fresh reactive mixtures were maintained at 50°C for two hours.

High-resolution NMR experiments were performed at room temperature on a Bruker AVANCE-400 spectrometer, operating at 104.26 MHz (^{27}Al signal). MAS experiments were carried out for metakaolins powder samples, which were spun at 10 KHz. The number of

scans was 400 [11]. For fresh geopolymer reactive mixtures, ^{27}Al NMR in static mode was used. It is well known that ^{27}Al is a quadrupolar nuclei (spin I>1/2), which means that there is an asymmetric charge distribution in the nucleus due to the non-symmetry of protons and neutrons. The difficulty of quadrupolar nuclei involves a quick relaxation in the liquid state and a broadening at the first and second order in a solid state [12]. The energy levels are shifted by the quadrupolar interaction, which may limit the quantitative determination of the populations [13]. However, in the liquid state, quadrupolar interaction can be neglected, as previously reported by Favier [14]. The synthesized mixtures were deposed in a zirconia rotor (Ø= 4 mm). A solution of AlCl3 was used as a reference. The ^{27}Al (I = 5/2) NMR spectra were recorded after π/8 pulse irradiation (1.5 μs) using a 1-MHz filter to improve the signal/noise ratio. In each case, 400 scans were collected. The time between acquisitions was set at 10 s.

The compressive strengths were tested using a LLOYD EZ20 universal testing machine with a crosshead speed of 0.1 mm/min. The compressive tests were performed on ten samples for every composition. The samples were cylindrical in shape, with a diameter of 15 mm and a height of approximately 30 mm, and were aged for 7 days in a closed mold at room temperature.

3. Results and Discussion

3.1. Raw metakaolin characterization

To elucidate the main differences between the six used metakaolins, the mineralogical compositions were determined by X-ray diffraction. The resulting XRD patterns are reported in Fig. 1.

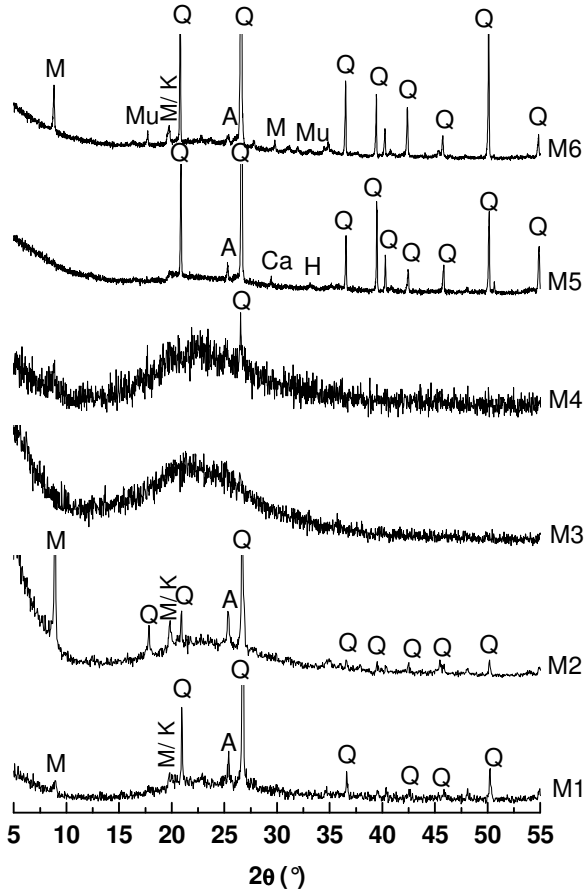

Fig. 1. XRD patterns of the raw metakaolins. The main diffraction peaks are indexed according to the JCPDS files (Q: Quartz (01-083-2465), K: Kaolinite (00-012-0447), M: Muscovite (00-003-0849), A: Anatase (01-071-1166), H: Hematite (01-079-1741), Ca: Calcite (00-005-0586), Mu: Mullite (01-089-2814)).

Whatever the metakaolin, a broad reflection in the 2θ ≈ 20° range is observed, characteristic of the typical metakaolin amorphous structure. M1 and M2 show the presence of peaks relative to crystalline phases, such as quartz, residual kaolinite, muscovite and anatase. In the case of M3 and M4, the dome is more pronounced, denoting high structural disorder and a large amount of amorphous phases. Only traces of quartz were identified in M4. For M5 and M6, the impurity content is higher. Quartz, anatase, calcite and hematite were detected in M5 metakaolin. The presence of hematite was expected from the pinkish color of this metakaolin. M6 is characterized by the presence of mullite in addition to quartz, muscovite, kaolinite and anatase. The presence of mullite can be explained by the over-calcination of particles when passing near the flame in the case of the flash calcination process as previously detailed by San Nicolas et al. [15] and Cyr et al. [16]. Thus, the studied metakaolins present different mineralogical phases denoting different purity degrees.

Furthermore, the main physical and chemical characteristics of the six metakaolins are reported in Table 1. M1 and M2 have Si/Al molar ratios of approximately 1.17 and 1.19, respectively. M3 and M4 exhibit Si/Al ratios close to 1 (1 and 0.98, respectively), revealing high purity (pure theoretical metakaolin having a Si/Al ratio = 1). However, M5 and M6 have the highest Si/Al ratios (1.44 and 1.33, respectively). This fact is in accordance with the previously discussed mineralogical data. The grain size of each metakaolin was also determined. The d_{50} varies from 6 μm in the case of M4 to 26 μm for M6. The difference in the median diameter from a metakaolin to another can be explained by the different heating process and pre-treatment [17]. Indeed, all metakaolins were heated at 750°C but with various processes, as detailed in Table 1. It was demonstrated that the rotary process lead to massive aggregates of particles (the case of M1, for example). However, the flash process produces finer particles with lower agglomeration [18] (the case of M2, for example). The high d_{50} observed in the cases of M5 and M6, despite being heated with the flash process, may be due to the high amounts of accessory minerals, such as quartz. The specific surface area (S_{BET}) is also an important parameter to study because it controls the dissolution rate of metakaolin [19]. Regardless of metakaolin, the specific surface area values are between 6 and 22 m^2/g, which is in accordance with the literature [20, 21]. M1 and M4 present similar S_{BET} values of approximately 17 m^2/g. M2 and M5 exhibit higher S_{BET} values (22 and 18 m^2/g, respectively), whereas M3 and M6 have weaker values (8 and 6 m^2/g, respectively). The differences of specific surface area between the six studied metakaolins denote the different structures of the particles [17]. It should also be mentioned that a high specific surface is not always an indicator of high reactivity. Fabri et al. [17] mentioned that the dehydroxylation lead to the formation of porous grains. The very small pores can be entered by nitrogen but not by water molecules. Thus, even if the specific surface area is high in this case, the reactive surface is low. That is why the research of another parameter controlling the reactivity is necessary. Recently, Autef et al. [11] demonstrated that the wettability value may be a good indicator of reactivity. Thus, it was interesting to compare the wettability values of the studied metakaolins. M1, M6 and M5 show lower wettability values (760, 670 and 530 μL/g, respectively), whereas, M2, M4 and M3 exhibit high wettability values (1250, 1186 and 1091 μL/g, respectively). These differences are linked to different parent kaolins crystallinity and various dehydroxylation processes [11]. Finally, the amorphous phase content differs for each metakaolin. As expected, the most pure metakaolins (M2, M3 and M4) present the most amorphous phases content (> 87%) compared to the others one.

For deeper comprehension of the structural differences between the raw metakaolins, ^{27}Al MAS-NMR experiments were performed. The obtained spectra are presented in Fig. 2. A. All samples exhibit typical ^{27}Al MAS-NMR spectra of metakaolin, showing three main types of components, at approximately 60, 31 and 1 ppm, which are assigned to tetrahedral ($Al^{(IV)}$), pentahedral ($Al^{(V)}$) and octahedral aluminum ($Al^{(VI)}$), respectively [22, 23, 24, 25]. To facilitate the exploitation of these data, the obtained spectra were deconvoluted. For example, Fig. 2. B shows three deconvoluted spectra corresponding to M4, M5 and M6. The obtained data concerning the chemical shifts and the percentages of the curve area of the various contributions ($Al^{(IV)}$, $Al^{(V)}$ and $Al^{(VI)}$) relative to the different metakaolins are given in Table 4. A. Broad signals (bands 1, 2, 3 and 4 in Fig. 2.B) with a Full-width at half maximum (FWHM) varying between 25 and 40 are associated to metakaolin and reflect the disorder of the structure. However, narrower peaks (band 5, 6, 7 and 8 in Fig. 2.B.b, c) indicate the presence of more crystallized phases. Indeed, a contribution at approximately 2 ppm (FWHM≈10) relative to 6 coordinated aluminums of muscovite can be detected in all samples (Fig. 2.B.b and c) except M4 (Fig. 2.B.a) and M3 (data not shown). Furthermore, the deconvolution of the M6 spectrum (Fig. 2.B.c) shows the presence of three additional contributions: two peaks at 53.94 and 66.67 ppm (FWHM≈15) that can be assigned to $Al^{(IV)}$ and a peak for $Al^{(VI)}$ at 1.52 ppm (FWHM≈9) revealing the presence of mullite [25, 26] in this metakaolin. This finding is in a good agreement with the XRD data. It also permits distinguishing between tetrahedral aluminum coming from impurities (muscovite and mullite) and tetrahedral aluminum relative to metakaolin, which will be the more reactive phase for geopolymerization applications.

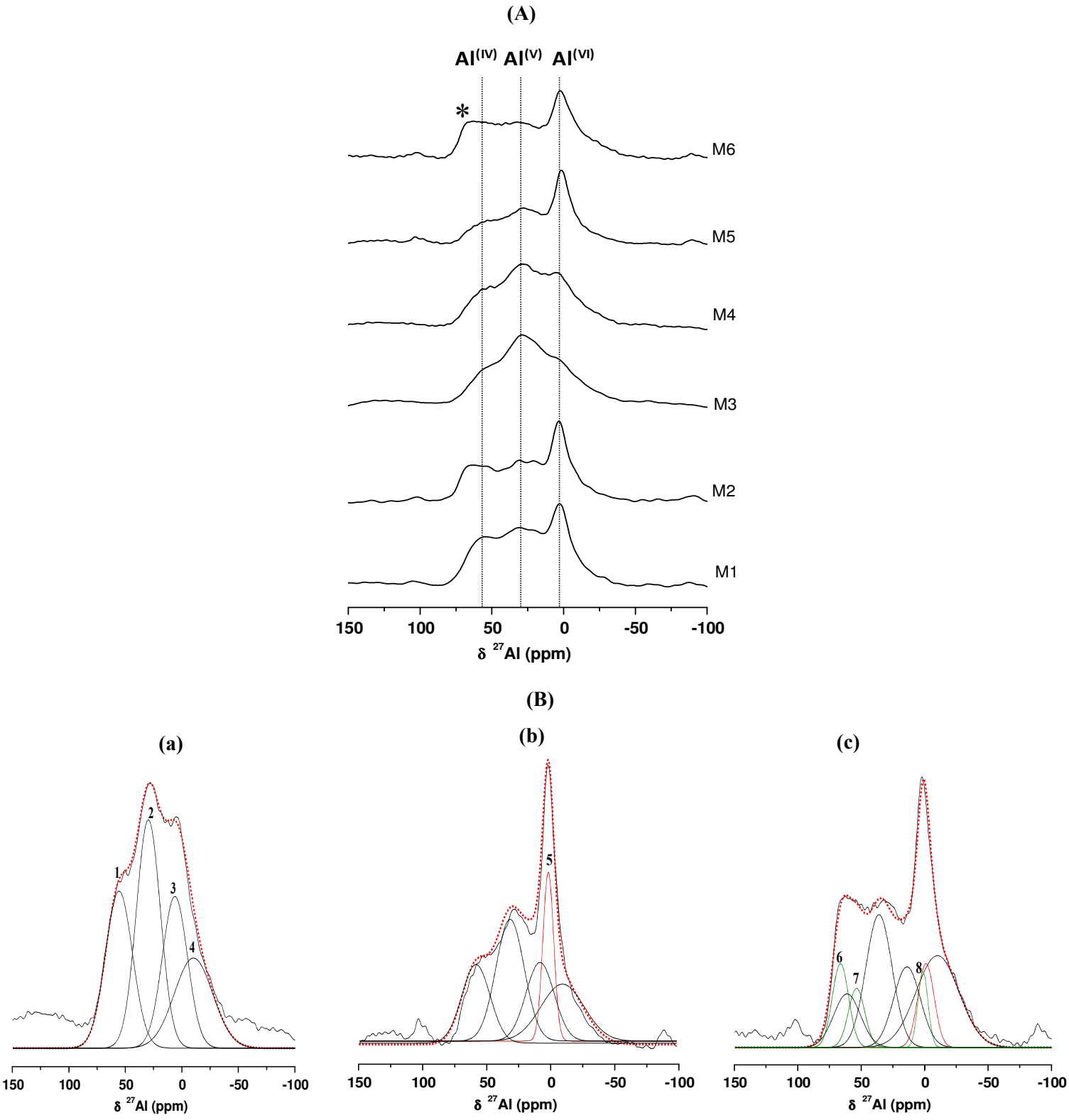

Fig. 2. (A) ^{27}Al NMR spectra of the raw metakaolins (* $Al^{(IV)}$ of mullite) and **(B)** examples of deconvoluted spectra relative to (a) M4, (b) M5 and (c) M6 (The bands 1, 2, 3, 4 are attributed to $Al^{(IV)}$, $Al^{(V)}$, $Al^{(VI)}$ of metakaolin, respectively, band 5 is associated to $Al^{(VI)}$ of muscovite, and bands 6, 7 and 8 correspond to $Al^{(IV)}$ and $Al^{(VI)}$ of mullite).

Table 4 ^{27}Al NMR data of the various species for **(A)** raw metakaolins and **(B)** geopolymer reactive mixtures at different times of the reaction.

(A)

Metakaolins	Percentage of the area curve of contribution (%)		
	$Al^{(IV)}$ ≈ 60 ppm	$Al^{(V)}$ ≈ 31 ppm	$Al^{(VI)}$ ≈ 1 ppm
M1	18.6	43.4	38.0
M2	21.1	35.7	43.2
M3	24.3	31.3	44.4
M4	24.9	32.3	42.8
M5	18.4	28.6	53.0
M6	24.3	22.8	52.9

(B)

Mixtures	S1M4			S3M4		
	Percentage of the area curve of contribution (%)					
Time (h)	$Al^{(IV)}$		$Al^{(VI)}$	$Al^{(IV)}$		$Al^{(VI)}$
	≈70 ppm	≈60 ppm	≈10 ppm	≈70 ppm	≈60 ppm	≈10 ppm
0	11.3	24.0	64.7	14.0	19.6	66.5
2	12.2	31.5	56.4	15.1	33.2	51.7
6	2.6	71.9	25.5	2.2	72.8	25.0
24	0.0	95.7	4.3	6.1	83.9	10.0
Mixtures	S1M5			S3M5		
	Percentage of the area curve of contribution (%)					
Time (h)	$Al^{(IV)}$		$Al^{(VI)}$	$Al^{(IV)}$		$Al^{(IV)}$
	≈70 ppm	≈60 ppm	≈10 ppm	≈70 ppm	≈60 ppm	≈10 ppm
0	17.8	26.8	55.4	6.9	27.0	66.1
2	4.6	43.4	52.0	7.5	48.4	44.1
6	6.0	71.6	22.4	0.0	92.3	7.7
24	8.9	76.3	14.8	0.0	93.2	6.8

In the light of the starting metakaolin characterization results, it appears that M2 and M4, followed by M1, have higher wettability values, specific surface areas and reactive tetrahedral aluminum phases, which make them more reactive than the other metakaolins. M3 is very pure and shows interesting properties, but the low specific surface area may likely decrease its reactivity in an alkaline medium. M5 and M6 are the more impure metakaolins and show similar properties. Nevertheless, M5 seems to be more reactive than M6 because it has a higher specific surface area. In summary, the reactivity of metakaolins, which means the

ability to release aluminates and silicates species in the alkaline solution, decreases in the order: M2 > M4 > M3 > M1 > M5 > M6.

These hypotheses need to be confirmed in the next sections. Moreover, the effect of the reactivity of metakaolins in the presence of two alkaline solutions, differing in terms of reactivity, on the geopolymer formation and final properties will be exacerbated.

3.2. Monitoring geopolymer formation

3.2.1. In situ thermal analysis

In the interest of understanding the influence of the starting precursors reactivity on the geopolymerization reaction, twelve reactive mixtures, based on the previously characterized metakaolins (from M1 to M6) and two alkaline solutions (S1 and S3), were prepared and studied by thermal analysis at 50°C for two hours. Fig. 3.A presents a typical example of obtained heat flow and weight loss curves for the S1M4 sample during 120 min of formation. An endothermic peak, associated with a weight loss of 33%, indicates the occurrence of the different stages of the various reactions. Based on the work of Autef et al. [7], four zones can be distinguished according to the inflexion points of the first derivate of the heat flow as schematized in Fig. 3.B. (a, b, c, d for S1M1, S3M1, S1M2 and S3M2, respectively). The first zone corresponds to the reorganization of species to reach speciation equilibrium.

The second zone is representative of metakaolin dissolution. Zone 3 is attributed to oligomer formation, and finally, zone 4 is associated with polycondensation reaction. In this study, we have focused on the effect of the reactivity of used precursors on oligomer formation (zone 3). Extra information can be deduced from thermal analysis curves, such as the time of the beginning of the oligomer formation stage (Fig. 3.B.a) and the energy required for this stage as determined from the heat flow peak area in zone 3.

Examples of the obtained heat flow and first derivate of heat flow profiles during the first 50 min of the reaction are given in Fig. 3. B for S1M1, S3M1, S1M2 and S3M2 mixtures. Similar trends are observed permitting delimitation of the four zones as detailed above.

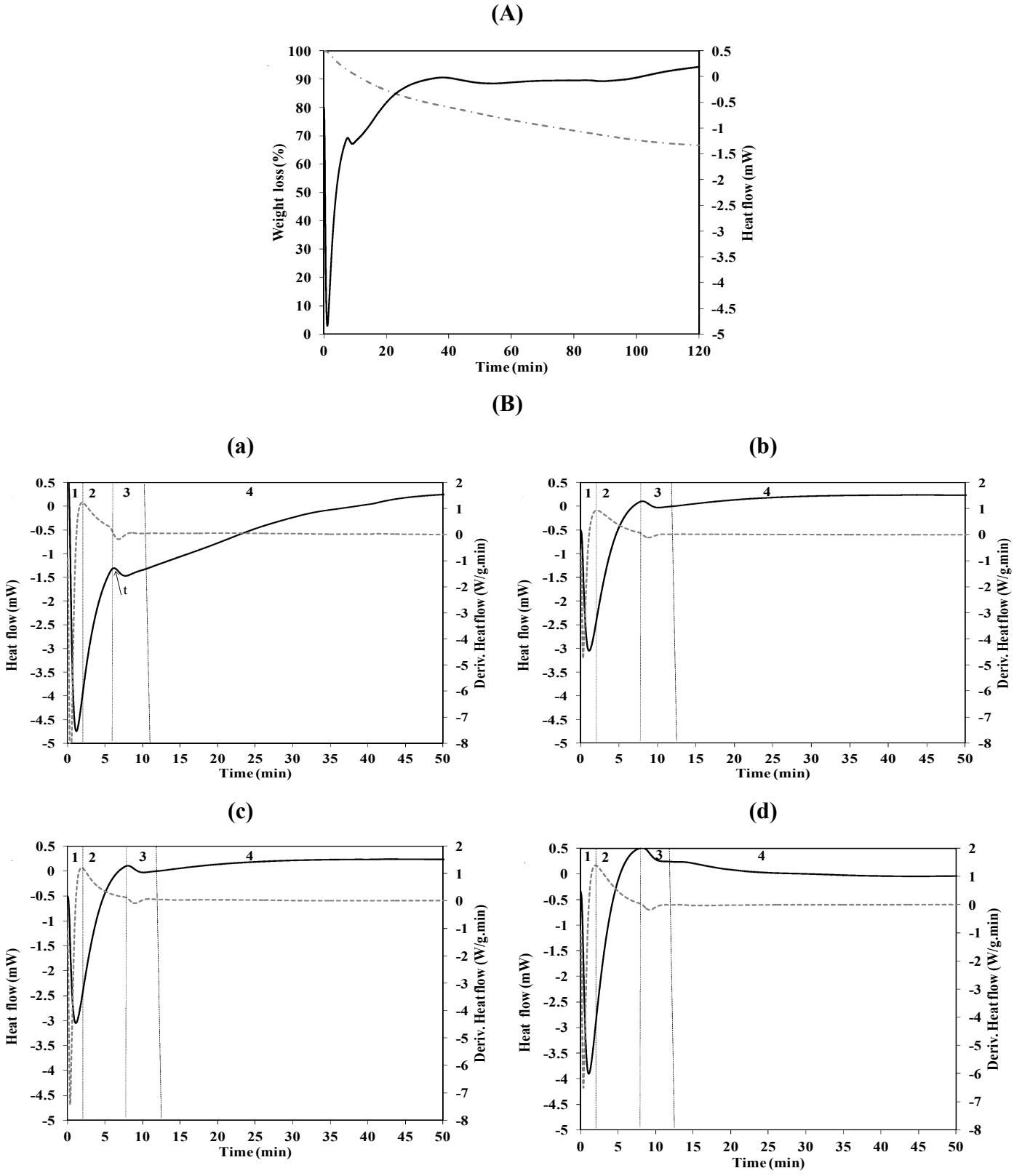

Fig. 3. (A) Typical example of thermal analysis curves and weight loss during 120 min of formation at 50°C spectra obtained for S1M4 sample and **(B)** definition of different zones of the reaction for (a) S1M1, (b) S3M1, (c) S1M2 and (d) S3M2 (t=time of beginning of zone 3).

Table 3 summarizes the obtained times and energy values deduced from heat flow curves for each studied sample. Differences are visible depending on the metakaolin and/or the alkaline solution.

Table 3 Beginning time of oligomer formation (t) and energy required for this stage of the reaction (E) determined from heat flow curves of studied samples.

Mixtures	t (min)	E (KJ/Mol)
S1M1	6.4	2.6
S1M2	8.6	1.8
S1M3	6.5	2.5
S1M4	7.8	2.0
S1M5	6.4	3.1
S1M6	6.5	2.5
S3M1	8.3	0.8
S3M2	8.7	0.6
S3M3	8.7	0.8
S3M4	7.9	0.5
S3M5	7.2	0.3
S3M6	8.8	0.8

To compare the different samples, the evolution of the energy as a function of the nAl/t ratio was plotted in Fig. 4, where nAl represents the amount of aluminum responsible for oligomer formation. Regardless of the sample, the energy seems to decrease with a decrease of nAl/t. For S1, a less reactive solution, differences between samples can be considered as a function of the used metakaolin. Indeed, the energy decreases as the nAl/t ratio decreases and as the reactivity of the metakaolin increases. Moreover, the oligomer formation seems to begin earlier (at $t \approx 6.4$ min) for less reactive metakaolins (M1, M3, M5 and M6) compared to M2 and M4 (at 7.8 min and 8.6 min for S1M4 and S1M2, respectively). This fact can be explained by the incomplete dissolution of these metakaolins (zone 2) due to their lower ability to release aluminates and silicates species and higher stability of impurities, such as mullite, for example, in M6, in an alkaline medium [27]. As a consequence, despite oligomer formation beginning earlier, the lower availability of reactive aluminate and silicate species limits the oligomerization, and more energy is necessary in this stage of formation. However, in the case of more reactive metakaolins, better dissolution is ensured, and the oligomer formation is favored by the high availability and reactivity of the released aluminate and silicate species. This finding is in accordance with the study of Weng et al. [19], which

highlights the role played by aluminate speciation and $[Al(OH)_4]^-$ ion distribution in promoting geopolymer formation.

For S3, a more reactive solution, no significant difference can be detected between the samples. Indeed, the time varies between 7.2 min and 8.8 min, while the energy is between 0.3 KJ/mol and 0.8 KJ/mol. These values are lower than those of the samples based on S1. The role of the high reactivity of the S3 solution is evident. The small depolymerized siliceous species released from this solution are able to enhance oligomer formation and counterbalance the low reactivity of metakaolins [28].

As a result, it appears that the different stages of the reaction, particularly the oligomer formation, directly depend on the reactivity of the metakaolin as well as the alkaline solution. The surface reactivity of the metakaolin controls the dissolution rate. Thus, the availability of dissolved species influences the kinetics and the energy required for oligomer formation. A highly reactive alkaline solution is able to ensure better dissolution even for low-reactivity metakaolins, which, consequently, favors the oligomer formation. More structural data are required to apprehend the effect of precursors on the reaction rate and the formed networks.

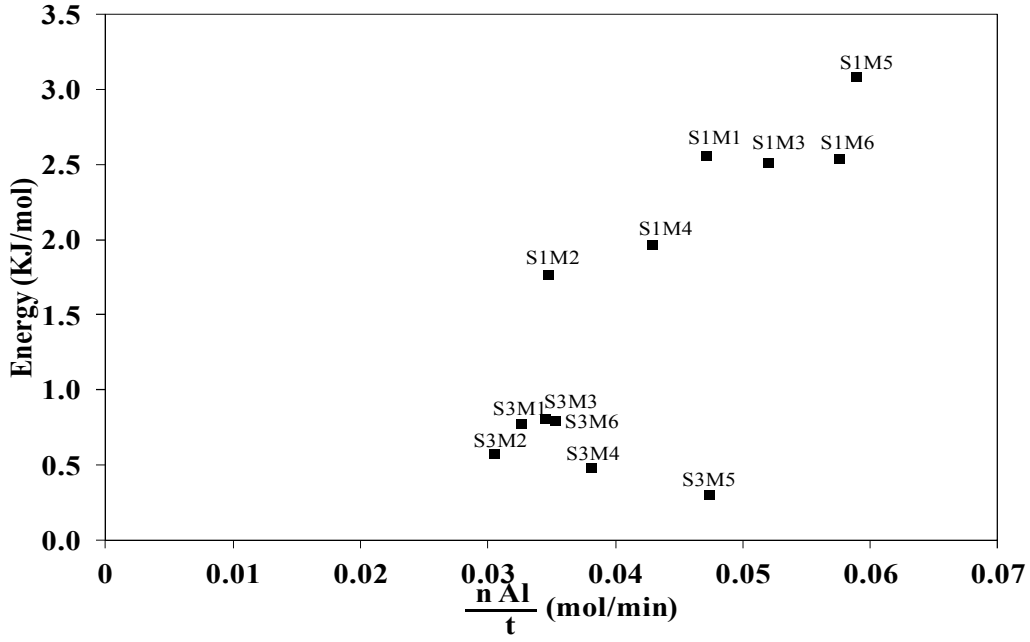

Fig. 4. Evolution of the energy in function of nAl/t ratio for each mixture based on various metakaolins and solutions

3.2.2. In situ FTIR spectroscopy

For deeper structural information on the influence of the starting precursors on the reaction rate and the formed networks, ATR-FTIR spectroscopy experiments were performed on the

twelve reactive mixtures. This technique has recently shown good potential for monitoring the geopolymer formation at an early age of the reaction [12, 29]. Fig. 5.A gives an example of the FTIR spectral change between t = 0 and t = 400 min for the S3M4 sample.

(A)

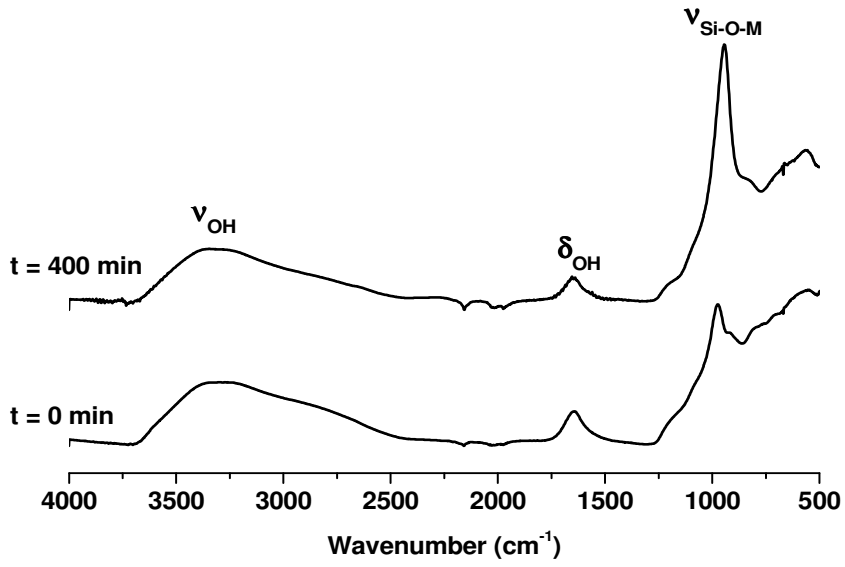

(B)

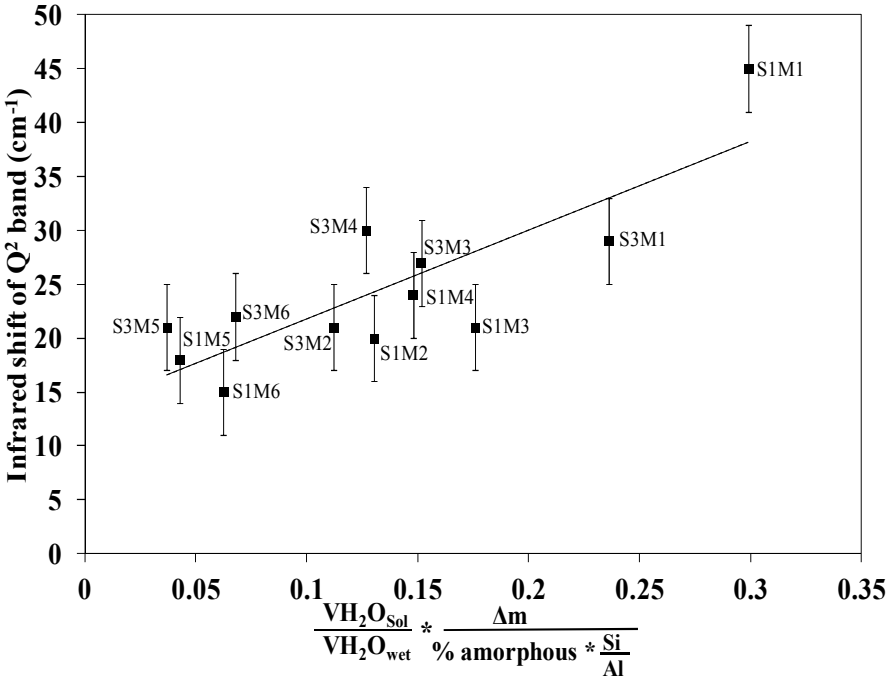

Fig. 5. (A) Example of in situ FTIR spectra obtained at t = 0 and t = 400 min for S3M4 sample and **(B)** evolution of the Q^2 shift position in function of $(VH_2O_{sol}/VH_2O_{wet})*(\Delta m/(\%\ amorphous*Si/Al))$

The spectra exhibit two contributions at 3200 and 1640 cm^{-1}, attributed to ν_{OH} and δ_{OH}, respectively. A broad band is also observed in the 1100-950 cm^{-1} range and is assigned to the Si-O-M (M = Si, Al) bond. The main change observed over time is the decrease of the intensity of the ν_{OH} and δ_{OH} bands and the shift of the Si-O-M contribution towards lower wavenumbers. This change reveals the occurrence of a polycondensation reaction. The evolution of the Si-O-M band position versus time can be plotted, and the slope at the beginning of the curve can be calculated. The shift value denotes the replacement of Si-O-Si by Si-O-Al bonds during the geopolymerization, and the slope value gives information about the kinetics of the reaction [9, 10].

Fig. 5.B shows the shift values versus $(VH_2O_{sol}/VH_2O_{wet})*(\Delta m/(\%\ amorphous*Si/Al))$, which represents the ratio of the volume of water supplied by the solution to the volume necessary to wet the metakaolin (calculated according to the wettability values in Table 1) multiplied by $(\Delta m/(\%\ amorphous*Si/Al))$, denoting the reactive properties of the metakaolin. Δm is the non-dehydroxylated kaolinite content determined from thermal analysis of the starting metakaolins [12]. Whatever the sample, the shift value increases with $(VH_2O_{sol}/VH_2O_{wet})*(\Delta m/(\%\ amorphous*Si/Al))$. Different behaviors are observed: higher $(VH_2O_{sol}/VH_2O_{wet})*(\Delta m/(\%\ amorphous*Si/Al))$ corresponds to higher shift values in the case of the S1M1 sample. A large shift value (45 cm^{-1}) denotes the formation of different networks, as has been demonstrated in previous work [9, 28]. Indeed, when the M1 metakaolin is activated by S1, a less reactive solution, the volume of water supplied by the solution is largely higher than the volume necessary to wet the metakaolin. This fact enables easier species diffusion, as previously demonstrated by thermal analysis during formation, and increases the extent of crosslinking between them. Thus, several networks are formed. The use of S3, a more reactive solution, with the same metakaolin decreases the shift value to 29 cm^{-1} for S3M3. Thus, S3 enhances the formation of a geopolymer phase in detriment to the other networks [28]. Regardless of the used solution, M2, M3 and M4 exhibit similar shift values varying from 22 to 30 cm^{-1}. These values are characteristic of the formation of a geopolymer phase [9, 30]. These three metakaolins are characterized by a high initial kaolinite amount, then an amorphous phase and wettability values and Si/Al ratios close to 1. Furthermore, the volume of water supplied by the solution seems to be optimal to wet the metakaolin and initiate the reaction. The water volume is important because it controls the driving forces for polymerization [3]. Consequently, the reactivity of the metakaolin and/or alkaline solution favors the formation of a geopolymer network.

In the case of M5 and M6, which are less pure metakaolins, weaker shift values are obtained, especially in presence of S1 (18 cm^{-1} and 15 cm^{-1} for S1M5 and S1M6, respectively). S3 increases these values to 21 cm^{-1} and 22 cm^{-1} for S3M5 and S3M6, respectively. This result is indicative of the formation of a minor geopolymer phase blocked with impurities, such as mullite for M6 and hematite for M5. In fact, these impurities do not participate in the polycondensation reaction and are coated by the alkaline solution [31].

Thus, regardless of the solution, the metakaolin properties control the nature of the formed networks. The impurity content is also an important factor because of their high resistance to alkaline attack. The role of the alkaline solution consists of favoring the geopolymer network towards other possible formed networks. To ensure full comprehension of the reaction rate, NMR analysis is necessary.

3.2.2. In situ ^{27}Al static NMR

For more detailed structural information about the geopolymer formation depending on the starting precursors' reactivity, the twelve reactive mixtures were studied by ^{27}Al static NMR at different times of the formation (0, 2, 6 and 24 hours). Examples of the obtained spectra for the S1M4, S3M4, S1M5 and S3M5 samples are presented in Fig. 6. The obtained data concerning the chemical shifts and the percentages of the curve area of the different contributions are detailed in Table 4B. Irrespective of the mixture, it was noticed that the spectra are immediately different from those of the starting metakaolins when there is contact with the alkaline solution (from t=0 h). Indeed, metakaolins show very broad peaks due to the disorder of the structure. However, for geopolymer reactive mixtures, the peaks become noticeably narrower, indicating a higher degree of structural order [32]. Moreover, the spectra show a dominant phase at approximately 60 ppm, which is characteristic of $Al^{(IV)}$, and a minor broad peak at approximately 17 ppm, corresponding to $Al^{(VI)}$ [33]. In fact, when the metakaolin is mixed with the alkaline solution, an increase of the contribution's area relative to $Al^{(IV)}$ to the detriment of the disappearance of $Al^{(V)}$ and a remarkable decrease of $Al^{(VI)}$ initially present in the metakaolin are observed. These changes indicate the rapid and strong interaction between the two precursors. As time progresses, the peak relative to $Al^{(IV)}$ broadens, denoting the formation of a geopolymer network, and the intensity of the peak relative to $Al^{(VI)}$ decreases, revealing the dissolution of metakaolin. However, $Al^{(V)}$, which is initially present in the metakaolin, was not observed in any spectra. The disappearance of

$Al^{(V)}$ indicates that it was rapidly consumed due to its high reactivity linked to its strained coordination, as has been previously demonstrated in the literature [19, 34]

The amount of $Al^{(VI)}$ that is still observed in the ^{27}Al spectra of geopolymers even after 24 hours is due to unreacted metakaolin, especially as $Al^{(VI)}$ is more stable and more difficult to dissolve than $Al^{(V)}$ and $Al^{(IV)}$ [23, 32, 35]. Moreover, differences can be distinguished between the percentages of the area curves of the different contributions (Table 4B) as a function of the used metakaolins and alkaline solutions. For example, the use of S3 instead of the S1 solution increases the percentage of $Al^{(IV)}$ species at 24 h from 81.1 to 83.9% for the M4 metakaolin and from 76.4 to 93.2% for the M5 metakaolin and at the same time decreases the percentage of $Al^{(VI)}$ species from 11.9 to 10.6% and from 14.8 to 6.8% in the case of M4 and M5, respectively. Thus, S3 seems to ensure an easier and more rapid conversion of $Al^{(IV)}$, $Al^{(V)}$ and $Al^{(VI)}$ of metakaolins into $Al^{(IV)}$ in the geopolymer mixture than S1. This fact is more prominent when S3 is combined with a poor-reactivity metakaolin (M5 in this case). These results are in agreement with DTA and FTIR data and confirm that the structural evolution of the geopolymer reactive mixture is strongly dependent on the reactivity of the starting precursors. The role of the aluminosilicate source is related to the availability of reactive aluminate species (especially $Al^{(IV)}$ and $Al^{(V)}$) initially present in the starting metakaolins, while the influence of the reactivity of the alkaline solution is more important because reactive species released from a highly reactive alkaline solution are more able to attack even poor-reactivity aluminosilicate species to form a geopolymer phase.

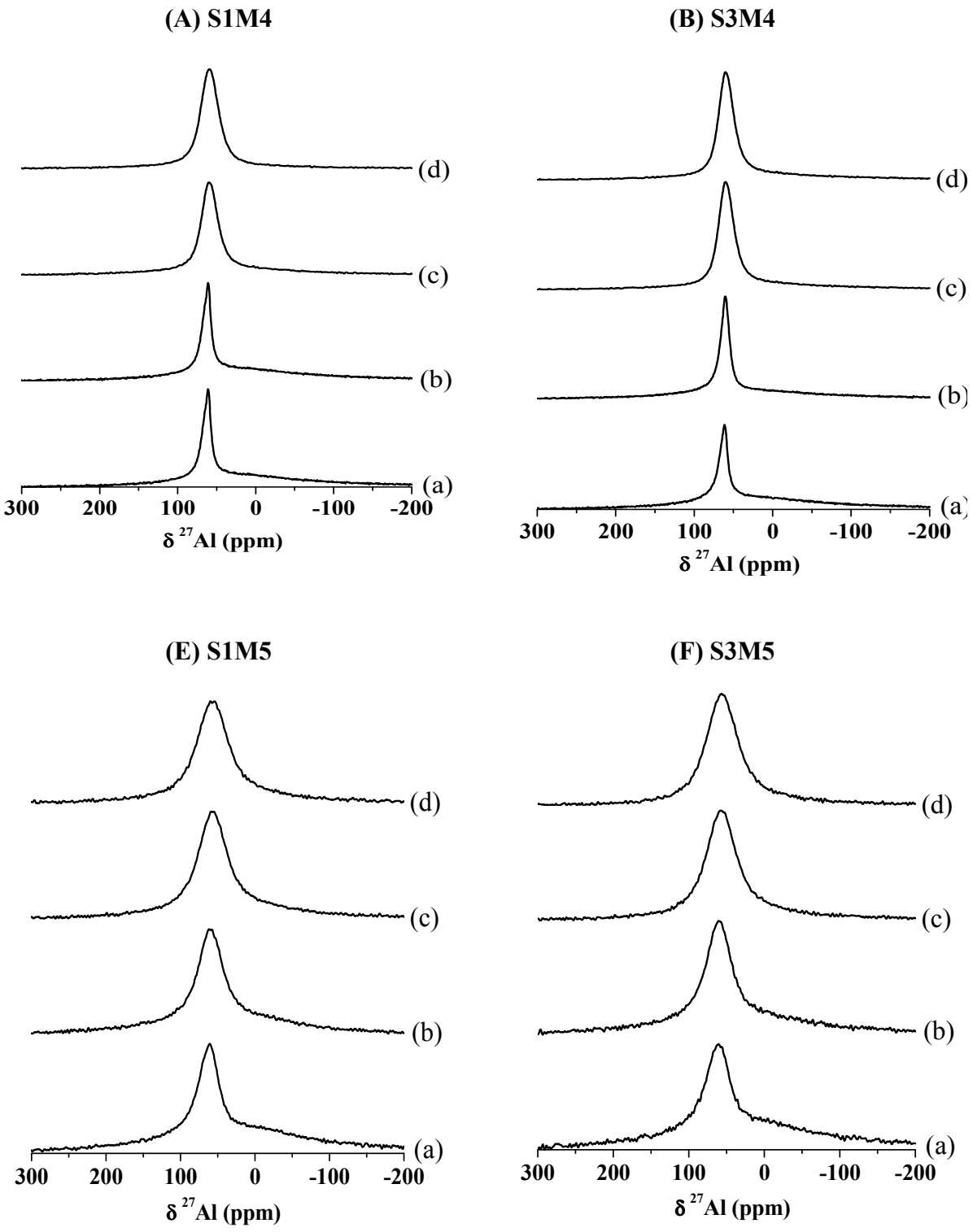

Fig. 6. Recorded ^{27}Al NMR spectra in static mode at (a) 0, (b) 2, (c) 6 and (d) 24 hours of formation for (A) S1M4, (B) S3M4, (C) S1M5 and (C) S3M5 studied samples.

3.3. Impact of the metakaolin and alkaline solution on the mechanical properties of the geopolymer

The various behaviors of the samples detected by thermal analysis, FTIR and NMR experiments during the formation translate to different polycondensation rates depending on the reactivity of the raw materials used and suggest different mechanical properties. To elucidate this effect, the mechanical strengths were evaluated by compression tests. Then, a correlation was established between the $Al^{(IV)}$ formation rate (the difference between the amount of $Al^{(IV)}$ formed after 24 hours in the geopolymer samples and the amount of $Al^{(IV)}$ initially present in the starting metakaolin) and compressive strength data as shown in Fig. 7.

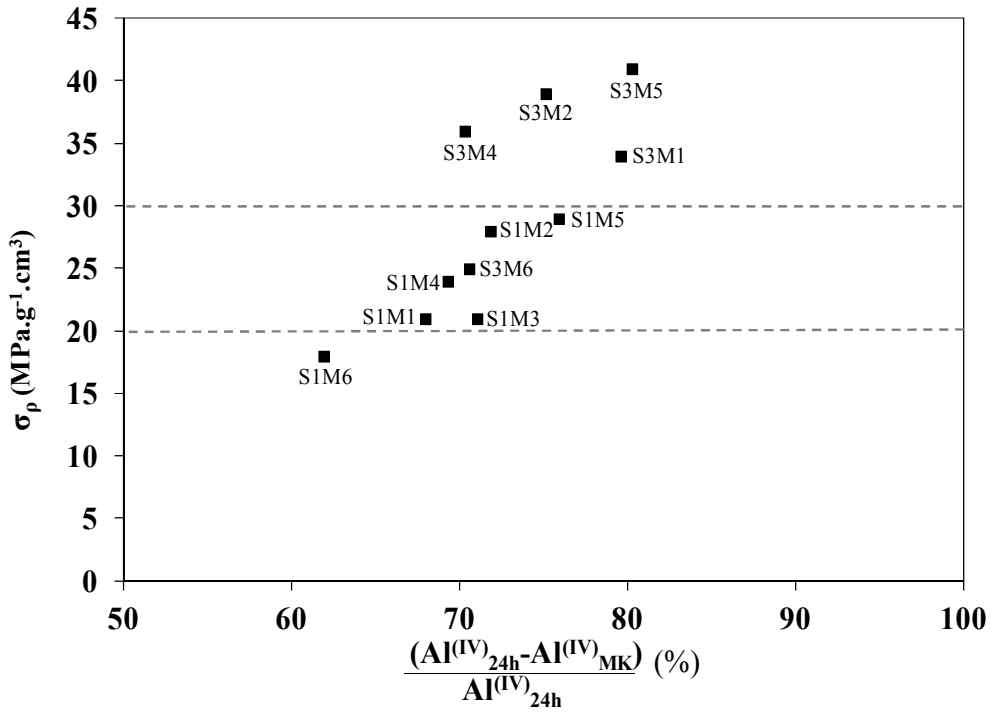

Fig. 7. Evolution of the compressive strength values in function of the $Al^{(IV)}$ formation rate.

Regardless of the sample, it is noted that better compressive strengths correspond to higher $Al^{(IV)}$ formation rates. Moreover, three different behaviors, depending on the reactivity of the used precursors, can be distinguished, as schematized in Fig. 7. For the S1M6 sample, the $Al^{(IV)}$ formation rate did not exceed 62%, leading to the weakest specific compressive strength value (18 $MPa.g^{-1}.cm^3$). This fact can be explained by, on one hand, the low surface reactivity of metakaolin. Indeed, M6 has low metakaolin content, reactive $Al^{(IV)}$ and surface area, as detailed previously. On the other hand, the low attack reactivity of the alkaline solution S1

[28] may prevent the formation of $Al^{(IV)}$ species and consequently not allow total alteration of the metakaolin. All of these factors inhibit the formation of a homogenous geopolymer phase and therefore decrease the mechanical strength.

The M1, M2, M3, M4 and M5 metakaolins in the presence of the same solution, S1, lead to a higher formation rate of $Al^{(IV)}$, which rises from 67 to 76%, and increase the specific compressive strength values from 20 to 30 $MPa.g^{-1}.cm^3$. Thus, the high metakaolin reactivity favors the geopolymer phase and allows the improvement of mechanical strengths. Nevertheless, the S1M5 sample exhibits higher compressive strength despite the low reactivity of the metakaolin. This result can be explained by the high amount of quartz in this metakaolin, which is known to reinforce the geopolymer matrix and increase the strength by providing additional silicon to form Si-O-Si bonds [7, 36].

Finally, for samples using the S3 solution, high formation rates (between 70 and 80%) were associated with high specific compressive strength values (between 36 and 41 $MPa.g^{-1}.cm^3$), except for the S3M6 sample (25 $MPa.g^{-1}.cm^3$). This is due to reactive siliceous species released from the S3 solution being able to ensure a higher metakaolin attack degree traduced in this case due to the greater formation rate of $Al^{(IV)}$. The contribution of quartz as a reinforcement is evident in the case of S3M5. Nevertheless, the weak compressive strength observed in the case of S3M6 is due to the low reactivity of this metakaolin in addition to the presence of mullite. In counter of quartz, crystalline phases such as mullite are known to have higher stability in alkaline media, which may hinder the polycondensation reaction, increase the heterogeneity of the sample and consequently decrease the mechanical strength.

4. Conclusion

The study of the effect of precursors with different reactivity may contribute to better control of the quite complex geopolymerization mechanism. That is why a comparative study of the formation of various samples based on six different metakaolins and two potassium alkaline solutions with different reactivity was established. At first, metakaolin characterization permits classifying the metakaolins into three groups: most, medium and least reactive depending on the impurity content, amorphous phase and wettability value. This result was later verified by monitoring the formation of geopolymer samples by several techniques. In situ thermal analysis reveals that the energy required for oligomer formation in the case of a highly reactive alkaline solution is approximately 0.6 KJ/mol regardless of the

metakaolin, while the energy is approximately 1.8 KJ/mol for a highly reactive metakaolin in the presence of a low-reactivity alkaline solution. These results were confirmed by in situ FTIR spectroscopy. The metakaolin properties are responsible for the generation of one or several networks. A highly reactive alkaline solution favors the geopolymer network towards other possible formed networks. In situ ^{27}Al NMR measurements supply detailed structural information about the reaction rate of the different mixtures. The role of the aluminosilicate source is related to the availability of $Al^{(IV)}$ and $Al^{(V)}$ in the starting metakaolins, while the role of the reactivity of the alkaline solution is to ensure an easier and more rapid conversion of species, and therefore, the reaction rate can reach 80%. Finally, a correlation was demonstrated between NMR data during formation and the compressive strength of consolidated materials.

Finally, the obtained results indicated the effect of the reactivity of the precursors on the kinetics and rate of the polycondensation reaction, which is a powerful tool to control the geopolymer formation and final properties and adapt them to potential applications.

Acknowledgments

The authors gratefully acknowledge Pr. Jesus Sanz for NMR experiments at the Institute of Materials Science in Madrid.

References

[1] M.L. Granizo, M.T.B. Varela, S. Martinez-Ramirez, Alkali Activation of Metakaolins: Parameters Affecting Mechanical, Structural and Microstructural Properties, Mater. Sci. 42 (2007) 2934-2943.

[2] H. Wang, H. Li, F. Yan, Synthesis and mechanical properties of metakaolinite-based geopolymer, Colloid. Surface 268 (2005) 1-6.

[3] J.L. Provis, J.S.J. van Deventer, Geopolymerisation kinetics. 2. Reaction kinetic modelling, Chem. Eng. Sci. 62 (2007) 2309-2317.

[4] H. Rahier, J. Wastiels, M. Biesemans, R. Willlem, G. Van Assche, B. Van Mele, Reaction mechanism, kinetics and high temperature transformations of geopolymers, Mater. Sci. 42 (2007) 2982-2996.

[5] A. Favier, G. Habert, N. Roussel, J. d'Espinose de Lacaillerie, A multinuclear static NMR study of geopolymerisation, Cem. Concr. Res. 75 (2015) 104–109.

[6] M. Xia, H. Shi, X. Guo, Probing the structural evolution during the geopolymerization process at an early age using proton NMR spin-lattice relaxation, Mater. Lett. 136 (2014) 222-224.

[7] A. Autef, E. Joussein, G. Gasgnier, S. Rossignol, Role of the silica source on the geopolymerization rate: A thermal analysis study, J. Non-Cryst. Solids. 366, 2013, 13–21.

[8] J.L. Provis, P. Duxson, G.C. Lukey, J.S.J. van Deventer, Statistical Thermodynamic Model for Si/Al Ordering in Amorphous Aluminosilicates, *Chem. Mater.* 17 (2005) 2976–2986.

[9] A. Autef, E. Joussein, A. Poulesquen, G. Gasgnier, S. Pronier, I. Sobrados, J. Sanz, S. Rossignol, Influence of metakaolin purities on potassium geopolymer formulation: The existence of several networks, J. Colloids and Interface Sci. 408 (2013) 43–53.

[10] E. Prud'homme, P. Michaud, E. Joussein, J.M. Clacens, S. Rossignol, Role of alkaline cations and water content on geomaterial foams: Monitoring during formation, J. Non-Cryst. Solids 357 (2011)1270-1278.

[11] A. Autef, E. Joussein, A. Poulesquen, G. Gasgnier, S. Pronier, I. Sobrados, Role of metakaolin dehydroxylation in geopolymer synthesis, Powder Technol. 250 (2013) 33-39.

[12] D. Iuga, C. Morai, Z. Gan, D.R. Neuville, L. Cormier, D. Massiot, NMR Heteronuclear Correlation between Quadrupolar Nuclei in Solids, J. Am. Chem. Soc. 127 (2005) 11540-11541.

[13] P.P. Man and J. Klinowski, Quantitative Determination of Aluminium in Zeolites by Solid-state 27AI N.m.r.Spectroscopy, J. Chem. Soc. Chem. Comm. 19 (1988) 1291-1294.

[14] A. Favier, Mécanisme de prise et rhéologie de liants géopolymères modèles, PhD thesis, University of Paris-Est, 2013.

[15] R. San Nicolas, M. Cyr, G. Escadeillas, Characteristics and applications of flash metakaolins, Appl. Clay Sci. 83–84 (2013) 253-262.

[16] M. Cyr, M. Trinh, B. Husson, G. Casaux-Ginestet, Effect of cement type on metakaolin efficiency, Cem. Concr. Res. 64 (2014) 63-72.

[17] B. Fabbri, S. Gualtieri , C. Leonardi, Modifications induced by the thermal treatment of kaolin and determination of reactivity of metakaolin, Appl. Clay Sci. 73 (2013) 2-10.

[18] V. Medri, S. Fabbri, J. Dedecek, Z. Sobalik, Z. Tvaruzkova, A. Vaccari, Role of the morphology and the dehydroxylation of metakaolins on geopolymerization, Appl. Clay Sci. 50 (2010) 538-545.

[19] L. Weng, K. Sagoe-Crentsil, T. Brown, S. Song, Effects of aluminates on the formation of geopolymers, Mater. Sci. Eng. B 117 (2005) 163–168.

[20] K.L. Konan, J. Soro, J.Y.Y. Andji, S. Oyetola, G. Kra, Etude comparative de la déshydroxylation/amorphisation dans deux kaolins de cristallinité différente, J. Soc. Ouest-Afr. Chim. 30 (2010) 29-39.

[21] J. Guyot, Mesure des surfaces spécifiques des argiles par adsorption, Ann. Argon, 20 (1969) 33-359.

[22] I.W.M. Brown, K.J.D. Mackenzie, M.E. Bowden, R.H. Meinhold, Outstanding Problems in the Kaolinite-Mullite Reaction Sequence Investigated by 29Si and 27Al Solid-state Nuclear Magnetic Resonance: 11, High-Temperature Transformations of Metakaolinite, J. Am. Ceram. Soc. 68 (1985) 298-301.

[23] P. Duxson, G.C. Lukey, F. Separovic, J.S.J. van Deventer, Effect of alkali cations on Aluminum incorporation in geopolymeric gels, Ind. Eng. Chem. Res. 44 (2005) 832-839.

[24] M.R. Rowles, J.V. Hanna, K.J. Pike, M.E. Smith, B.H.O. Connor, 29Si,27Al, 1H and 23Na MAS NMR Study of the Bonding Character in Aluminosilicate Inorganic Polymers, Appl. Magn. Reson. 32 (2007) 663-689.

[25] J. Sanz, J. Madani, M. Serratos, J.S. Moya, S. Aza, Aluminum-27 and Silicon-29 Magic-Angle Spinning Nuclear Magnetic Resonance Study of the Kaolinite-Mullite Transformation J. Am. Ceram. Soc. 71 (1988) 418-421.

[26] H. He, J. Guo, J. Zhu, P. Yuan , C. Hu, 29Si and 27Al MAS NMR spectra of mullites from different kaolinites, Spectrochim. Acta A-M 60 (2004) 1061–1064.

[27] A. Fernandez-Jimenez, A.G. de la Torre, A. Palomo, G. Lopez-Olmo, M.M. Alonso, M.A.G. Aranda, Quantitative determination of phases in the alkaline activation of fly ash. Part II: Degree of reaction, Fuel 85 (2006) 1960-1969.

[28] A. Gharzouni, E. Joussein, B. Samet, S. Baklouti, S. Rossignol, Effect of the reactivity of alkaline solution and metakaolin on geopolymer formation, J. Non-Cryst. Solids. 410 (2015) 127-134.

[29] C.A. Rees, J.L. Provis , G.C. Lukey , J.S.J. van Deventer, In situ ATR-FTIR study of the early stages of fly ash geopolymer gel formation, Langmuir 17 (2007) 9076-9082.

[30] F. Gouny, F. Fouchal, P. Maillard and S. Rossignol, Study of the Effect of Siliceous Species in the Formation of a Geopolymer Binder: Understanding the Reaction Mechanisms among the Binder, Wood, and Earth Brick, Ind. Eng. Chem. Res. 53 (2014) 3559-3565.

[31] A. Gharzouni, E. Joussein, B. Samet, S. Baklouti, S. Rossignol, Addition of low reactive clay into metakaolin-based geopolymer formulation: Synthesis, existence domains and properties, Powder Technol. 288 (2016) 212-220.

[32] J. Davidovits, Structural characterization of geopolymeric materials with X-ray diffractometry and MAS-NMR spectrometry. Geopolymer ’88 –First European Conference on Soft Mineralurgy, Compeigne, France, Universite de Technologie de Compeigne, 1988.

[33] R.A. Fletcher, K.J.D. MacKenzie, C.L. Nicholson, S. Shimada, The composition range of aluminosilicate geopolymers, J. Eur. Ceram. Soc. 25 (2005)1471-1477.

[34] J.V. Walther, Relation between rates of aluminosilicate mineral dissolution, pH, temperature, and surface charge Am. J. Sci. 7 (1996), 296-693.

[35] P. Duxson, J.L. Provis, G.C. Lukey, S.W. Mallicoat, W.M. Kriven, J.S.J. van Deventer, Understanding the relationship between geopolymer composition, microstructure and mechanical properties, Colloid. Surface A 269 (2005) 47-58.

[36] L. Atmaja, H. Fansuri, A. Maharani, Crystalline phase reactivity in the synthesis of fly ash–based geopolymer, Indo. J. Chem. 11 (2011) 90-95.

Publication 7 (ACL7)

A. Gharzouni, I. Sobrados, E. Joussein, S. Baklouti, S. Rossignol

"Predictive tools to control the structure and the properties of metakaolin based geopolymer materials"

Colloids and surface A, accepted

Les géopolymères sont des liants minéraux innovants. Ces matériaux sont en cours de développement afin de mieux comprendre le mécanisme de la formation, la structure locale et les propriétés d'usage finales. L'objectif de cette étude est de déterminer des outils prédictifs permettant de contrôler la réaction de géopolymérisation. Tout d'abord, il a été déterminé les paramètres responsables de la réactivité des matières premières. D'une part, la distribution et la connectivité des espèces siliceuses contrôlent la réactivité des solutions alcalines. En ce qui concerne les métakaolins, le rapport molaire Si/Al, la valeur de la mouillabilité, la teneur en phase amorphe et la quantité d'aluminium tétraèdrique réactif sont responsables de la réactivité du métakaolin. En outre, il a été prouvé que les domaines d'existence des matériaux géopolymères dans le diagramme ternaire Si-Al-O/M dépendent de la réactivité des matières premières. L'analyse thermique pendant et après la formation donne des informations sur la quantité d'eau consommée lors de la réaction et piégée dans la structure finale, ainsi que sur l'énergie nécessaire à la formation des oligomères. Cette énergie est directement liée à la réactivité des matières premières. La distribution et la taille des pores sont également influencées par la réactivité des matières premières. L'utilisation des précurseurs réactifs, et plus particulièrement des solutions alcalines réactives, induisent un taux de densification plus élevé et, par conséquent, un taux de porosité plus faible et des tailles des pores plus élevées. En outre, les résultats de la spectroscopie RMN de ^{29}Si ont mis en évidence que les précurseurs réactifs favorisent la formation du réseau géopolymère. Ceci induit l'amélioration de la résistance mécanique, tandis que la compétition entre différents réseaux est source de faiblesse.

PREDICTIVE TOOLS TO CONTROL THE STRUCTURE AND THE PROPERTIES OF METAKAOLIN BASED GEOPOLYMER MATERIALS

A. Gharzouni[1, 2], I. Sobrados[3], E. Joussein[4], S. Baklouti[2], S. Rossignol[1]

[1] Science des Procédés Céramiques et de Traitements de Surface (SPCTS), Ecole Nationale Supérieure de Céramique Industrielle, 12 rue Atlantis, 87068 Limoges Cedex, France.

[2] Laboratoire de Chimie Industrielle, Ecole Nationale d'Ingénieurs de Sfax, université de Sfax, 3038 Sfax, Tunisie.

[3] Instituto de Ciencia de Materiales de Madrid, Consejo Superior de Investigaciones Científicas (CSIC), C/Sor Juana Inés de la Cruz, 3, 28049 Madrid, Spain.

[4] Université de Limoges, GRESE EA 4330, 123 avenue Albert Thomas, 87060 Limoges, France.

■ corresponding author: sylvie.rossignol@unilim.fr, tel.: 33 5 87 50 25 64

Metakaolin	Alkaline solution	porosity
Oligomer formation	^{29}Si NMR	Mechanical strength

Abstract

Geopolymers are innovative mineral binders which still under research development in order to better understand the formation mechanism, the local structure and the final working properties. The aim of this study is to give predictive tools permitting to control the geopolymerisation reaction. At first it is important to determine the parameters responsible of raw materials reactivity. For alkaline solutions, the siliceous species distribution and connectivity control the reactivity. Concerning metakaolins, the Si/Al molar ratio, the wettability value, the amorphous phase content and the amount of reactive tetrahedral aluminium are responsible of metakaolin reactivity. The reactivity of raw materials was proven to determine the geopolymer existence domains in the Si–Al–M/O ternary diagram. Thermal analysis during and after curing give informations about the amount of water

consumed during the reaction and trapped in the final structure as well as the energy required for oligomer formation which seem to be directly related to raw materials reactivity. The pores distribution and size are also influenced by raw materials reactivity. Reactive precursors especially reactive alkaline solution induce higher densification rate and therefore lower degree of porosity and larger pore size. Furthermore, reactive precursors favor the formation of geopolymer network which was evident by ^{29}Si NMR. The increase of geopolymer phase in the structure improves the mechanical strength while the competition of different networks is source of weakness.

2. Introduction

Geopolymers are amorphous aluminosilicate binders synthesized by the activation of an aluminosilicate source by an alkaline solution at atmospheric pressure and a temperature below than 100 °C [1]. The term "geopolymer" was introduced in 1978 by the French chemist Joseph Davidovits to designate their inorganic character and their structure similar to polymers. Geopolymers are formed by a three-dimensional network of SiO_4 and AlO_4 tetrahedra. The alkali cation M^+ compensates the deficit of charge created by the substitution of Si^{4+} by Al^{3+}. There is a wide range of potential and existing applications for geopolymers. Nevertheless, deeper fundamental research on the parameters governing the mechanism of formation and the working properties are still required.

The role played by silicium, aluminum and alkali cation on geopolymer formation and properties was extensively discussed. Recently, Gao et al, [2] have examined the influence of the Si, Al and K contents from a metakaolin and two potassium silicate solutions (commercial and laboratory made) on geopolymer existing domains in Si-Al –K/O ternary diagram. Four types of materials were obtained including geopolymers, gel, sedimented and hardened materials. Moreover, the effect of Si/Al ratio was extensively studied. It was demonstrated that it influences the dissolution of the aluminosilicate source and therefore the availability of silicium and aluminium. Weng et al., [3] have focused on the mechanisms of Al speciation and the distribution of $[Al(OH)4]^-$ ions depending on the metakaolin properties. They have highlighted the effect of aluminates not only on geopolymer formation by promoting polycondensation reaction but also on improving mechanical properties of strengthened materials. Duxon et al., [4] have shown that samples with a Si/Al molar ratio > 1.65 exhibit higher compressive strength and Young's modulus. Above this value, the mechanical properties decrease due to higher amount of non reacted species.

In addition to that, the alkaline solution is also a crucial parameter in geopolymer formation. Taking into account the differences in size and hydration properties [5], the alkali cations may engender variations on the reaction rate and the final properties of consolidated materials. In fact, Na cation is known to facilitate aluminosilicate source dissolution. However, K cation has the advantage of ensuring higher condensation rate and more disordered structure [6, 7]. As a result, potassium-based geopolymers have shown better compressive strength than sodium-based one. Moreover, it was also demonstrated that the compressive strengths increase with increasing concentration of the NaOH solution from 4 to 12 mol. L^{-1} [8].

Water also influences the geopolymer formation. It was evident that water facilitates the dissolution of the aluminosilicate source and favors the ion transfer and therefore the polycondensation reaction. However, it was shown that low solid to liquid ratio that means high water content accelerates the dissolution but perturbs the polycondensation reaction. The impact of water on the mechanical properties was also studied. In final geopolymer materials, water was found to be predominantly as free water (about 60 %) and the rest is interstitial and structural bounded water [9, 10]. Zuhua et al., [11] have demonstrated that higher water content induces higher pore volume and low mechanical strength. However, lower water content lead to denser structure with higher mechanical strength.

The existing literature emphasis the dependence of geopolymer materials of used raw materials. However, there is a strong requirement to identify tools to control the formation, the structure and the working properties of these materials. That is a why a deeper comprehension of raw materials is necessary.

In this topic, the main objectives of the present work are (i) to identify the parameter governing raw materials reactivity, (ii) to establish predictive tools to determine the nature of obtained materials from the chemical composition of any mixture and finally (iii) to exacerbate the influence of raw materials reactivity on local structure and mechanical properties of obtained geopolymers. To achieve these objectives, different metakaolins and alkaline solutions were studied and their reactivity rates were evaluated by physical, chemical and structural characterization. Then, numerous formulations were tested in order to identify the geopolymer existing domains in the Si-Al-M/O ternary diagram. The influence of raw materials on the local structure was determined by differential thermal analysis and thermogravimetric analysis (DTA-TGA), mercury intrusion porosimetry (MIP) and ^{29}Si

NMR. The impact on the mechanical properties of the strengthened materials was evaluated by compression tests.

2. Experimental

2.1. Raw materials and sample preparation

Geopolymer samples were synthesized using six metakaolins (named M1 through M6) (Table 1) and three commercial silicate solutions provided by woellner (i) Two potassium silicate solutions named S_K1, S_K3 with different Si/K molar ratio (1.7 and 0.7, respectively) and (ii) a sodium silicate solution named S_{Na} with Si/Na molar ratio of 1.7. Potassium and sodium hydroxide pellets (VWR, 85.2% and 97.0% pure) were dissolved into the starting silicate solutions to maintain the Si/M (with M= K or Na) molar ratio at 0.5 and 0.7 for potassium and sodium silicate solutions respectively. Then, metakaolins were added. The obtained mixtures were placed in a closed sealable polystyrene mold at room temperature (25°C).

2.2. Sample characterization

X-ray diffraction patterns were acquired via X-ray diffraction (XRD) experiments on a Bruker-AXS D 5005 powder diffractometer using CuK α radiation (λKα=0.154186 nm). The analytical range is between 5° and 55° (2θ), with a step of 0.04° and an acquisition time of 2 s for raw metakaolins powder. JCPDS (Joint Committee Powder Diffraction Standard) files were used for phase identification. The amorphous phase for each metakaolin was determined using the Rietveld method [12].

The wettability value (µL/g) corresponds to the volume of water that can be adsorbed by one gram of powder before saturation.

High-resolution NMR experiments were performed on alkaline solutions, metakaolins and consolidated geopolymers at room temperature using a Bruker AVANCE-400 spectrometer, operating at 104.26 MHz for ^{27}Al signal and 79.49 MHz for ^{29}Si signal. The ^{29}Si (I = 1/2) NMR spectra were recorded after a π/2-pulse irradiation (4 µs) using a 500 kHz filter to improve the signal/noise ratio. In each case, 400 scans were collected. The time between acquisitions was set to 10 s to minimize saturation effects. Powder samples were spun at 10 KHz.

Differential thermal analysis (DTA) and thermogravimetric analysis (TGA) were performed on an SDT Q600 apparatus from TA Instruments in an atmosphere of flowing dry

air (100 mL/minute) in platinum crucibles. The signals were measured with Pt/Pt–10%Rh thermocouples. Thermal analysis was conducted during the formation of the consolidated materials using the thermal cycle previously established by Autef et al. [13]. The fresh reactive mixtures were maintained at 50°C for two hours then heated to 800°C.

Mercury intrusion porosimetry tests (MIP) were carried out using a porosimeter Micromeritics Autopore IV 9510 able to detect a pore diameter varying between 360 µm and 3 nm and an intrusion and extrusion mercury volume of 0.1 µL. The mercury pressure gradually increases from 0.0007 to 413.6854 MPa. The geopolymer sample was previously placed in an oven at 50 °C for 12 hours in order to eliminate the water that may prevent the intrusion of mercury into the porous network [14]. Then, tests were performed in two steps: At first, the low pressure step to remove gases, fill the samples with mercury and perform the test with a pressure of 345 kPa. Then, the high pressure step with a pressure that may attain 414 MPa [7].

The compressive strengths were tested using a LLOYD EZ20 universal testing machine with a crosshead speed of 0.1 mm/min. The compressive tests were performed on ten samples for every composition. The samples were cylindrical in shape, with a diameter of 15 mm and a height of approximately 30 mm, and were aged for 7 days in a closed mold at room temperature.

3. Results and Discussion

3.1 Evaluation of raw precursors reactivity

3.1.1 Alkaline solutions

Knowledge of the properties and the structure of the used alkaline solution is primordial in order to understand their interaction with metakaolins. In this study, three different potassium and sodium silicate solutions were investigated. The main characteristics of the solutions are summarized in Table 1.

Table 1. Nomenclature and characteristics of the various studied solutions

Nomenclature	Cation	Si/M	% water	density
S_K1	K	1.7	79	1.18
S_K3		0.7	59	1.51
S_Na	Na	1.7	64	1.36

The solutions have different water content and densities in the following order S_K1 (79%, 1.18) < S_{Na} (64%, 1.36) < S_K3 (59%, 1.51). Despite having the same Si/M ratio, S_{Na} exhibits

lower water content and it is denser than S_K1. This is due to the difference of the alkali cation. To further visualize the differences between the studied solutions, ^{29}Si NMR measurements were performed on solutions before and after addition of of alkali hydroxide (MOH avec M = K or Na). The obtained ^{29}Si NMR spectra, presented in Fig. 1, show different siliceous species distribution between the solutions. S_K1 solution (Fig. 1 (A a)) is mainly composed of condensed siliceous species Q^2, Q^3 and Q^4 at -88, -97 and -106 ppm respectively and minor small depolymerized species Q^0 and Q^1 at -72, -80 ppm respectively [15]. However, S_K3 solution (Fig. 1 (A b)) with lower Si/K (Si/K=0.7) has a different structure characterized by the absence of Q^4, the predominance of Q^1 and Q^0 and the presence of cyclic species (Q^{2c} and Q^{3c}) situated at approximately -81 and -89 ppm [16]. The S_{Na} silicate solution (Fig. 1 (A c)) exhibits similar silicate species distribution as $S_K1$which can be explained by the fact that they have the same Si/M molar ratio (Si/M=1.7). Regardless of the solution, the addition of alkali hydroxide (Fig. 1 (B)) causes the predominance of low order (Q^0 and Q^1) and cyclic species (Q^{2c} and Q^{3c}) highlighting the depolymerization of silicate solutions. A similar degree of depolymerization seems to occur for sodium silicate solution but with higher Si/M molar ratio (Si /M=0.7) compared to potassium solutions. Nevertheless, it should be noticed that slight differences can be detected between potassium (Fig. 1 (B d and e)) and sodium silicate solutions (Fig. 1 (B f)) especially for cyclic species. Furthermore, a Raman investigation [17] has demonstrated differences of monomer, oligomer and rings depending on the Si/M molar ratio and the nature of cation.

Thus, the alkali cation acts as a network modifier by breaking the bonds between the condensed siliceous species in the silicate solution generating higher amount of non-bridging oxygen atoms. The use of Na cation instead of K cation induces the same phenomenon but for higher Si/M.

As a result, the silicate structure is controlled by the Si/M molar ratio. The decrease of this ratio favors the formation of small and depolymerised species. This finding is in accordance with literature [18,19,20]. Nevertheless, the differences of cation characteristics (size, hydration shell and diffusion) engender some structural differences between the solutions

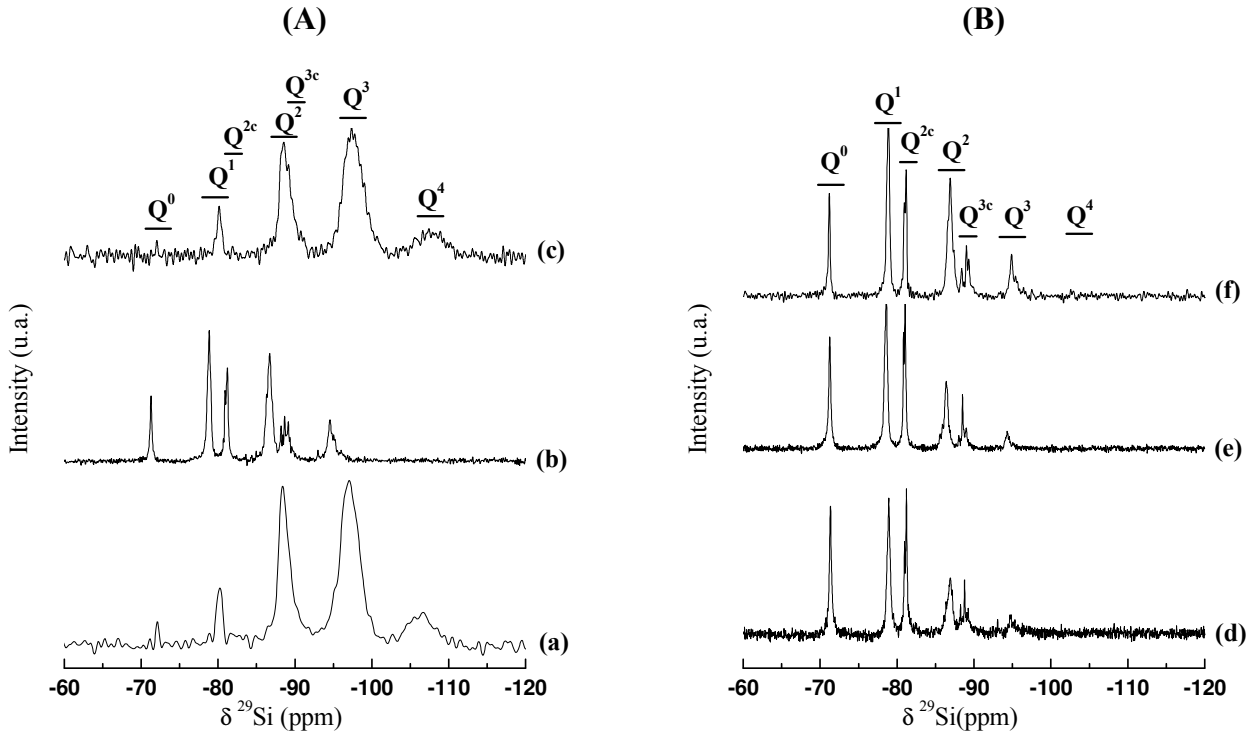

Fig. 1. ^{29}Si NMR Spectra of (A) starting silicate solutions (a) S_K1, (b) S_K3 and (c) S_{Na} and (B) solutions after addition of alkali hydroxide (d) S_K1, (e) S_K3 and (f) $S_{Na.}$

3.1.2. Metakaolins

A comparative study of the six used metakaolins is detailed in previous work [21]. That is why only the main characteristics are summarized in Table 2.

Table 2. Chemical and physical properties of raw metakaolins

Metakaolins	M1	M2	M3	M4	M5	M6
Si/Al	1.17	1.19	1.00	0.98	1.44	1.33
Wettability (µL/g)	760	1250	1010	1186	530	670
Amorphous phase (%)	63	87	98	98	64	59
Al^{IV} (%)	18.6	21.1	24.3	24.9	18.4	9.3

The Si/Al, the wettability value, amorphous phase (determined by XRD Rietveld) and reactive tetrahedral aluminum are crucial parameters that influence the aluminosilicate source reactivity [22,23,24]. For this reason, the reactivity rate determined from chemical and structural data were plotted for each metakaolin in Fig. 2. M4, M3, M2 and M1, have higher reactivity rates (chemical and structural data) and ratios indicating lower Si/Al molar ratios (≤

1.2), higher wettability values (≥ 760 µL/g), amorphous phase (≥ 63) and reactive tetrahedral aluminum (≥ 19 %). Nevertheless, M5 and M6 exhibit lower ratios denoting higher Si/Al molar ratio, lower wettability values, amorphous phase and reactive tetrahedral aluminum which make them less reactive. According to these results, an estimation of metakaolin reactivity was established in the following reactivity order: M4 ≥ M3 ≥ M2 > M1 > M5 > M6. This estimation will be verified by studying the behavior of the metakaolins in presence of different alkaline solutions.

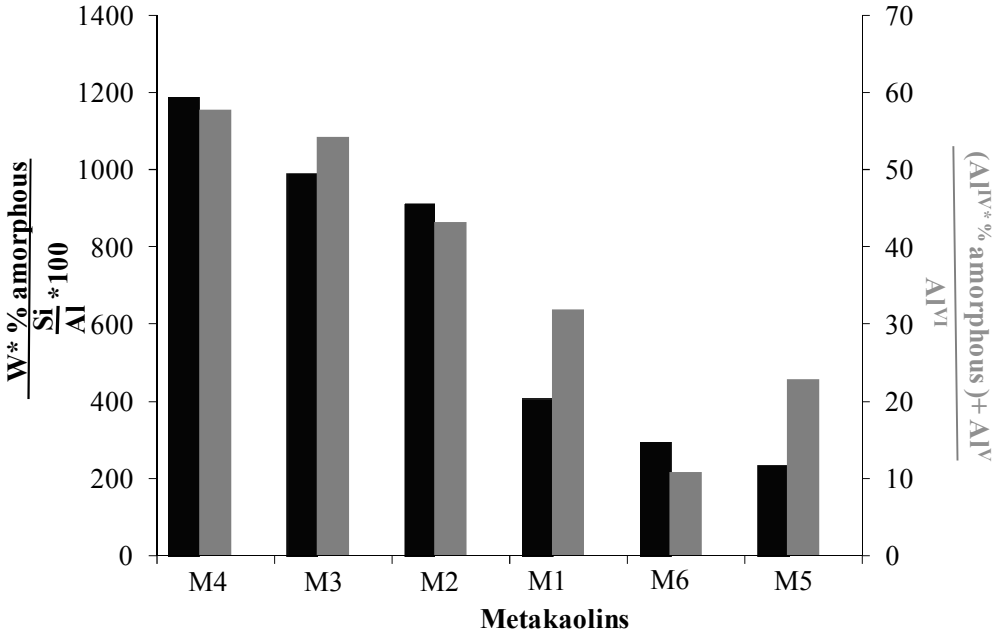

Fig. 2. Evaluation of metakaolin reactivity depending on chemical data (■) $\frac{W*\%\ \text{amorphous}}{\frac{Si}{Al}*100}$ and structural data (■) $\frac{(Al^{IV}*\%\ \text{amorphous})+Al^{V}}{Al^{VI}}$.

3.2. Effect of raw precursors on geopolymer existing domains in Si-Al-M/O ternary diagram

A feasibility study was undertaken in order to determine the geopolymer existence domains in the Si–Al–M/O ternary diagram. For this, 36 compositions for each metakaolin and alkaline solution were synthesized. Then, the obtained materials were classified based on their visual aspect and consolidation state onto geopolymer, hardened, sedimented and gel materials. The excess of alkaline solution or the deficiency of metakaolin leads to the formation of sedimented materials with different layers. The excess of siliceous species is responsible of the formation of gel materials (transparent and plastic). The hardened materials (consolidated but not homogenous and brilliant) generally result from either an excess of metakaolin or very high alkalinity of the solution. A geopolymer material is characterized by

an homogenous brilliant and smooth aspect and a rapid consolidation (≤ 24 h). The geopolymer region was defined for each metakaolin and alkaline solution as schematized in Fig. 3.

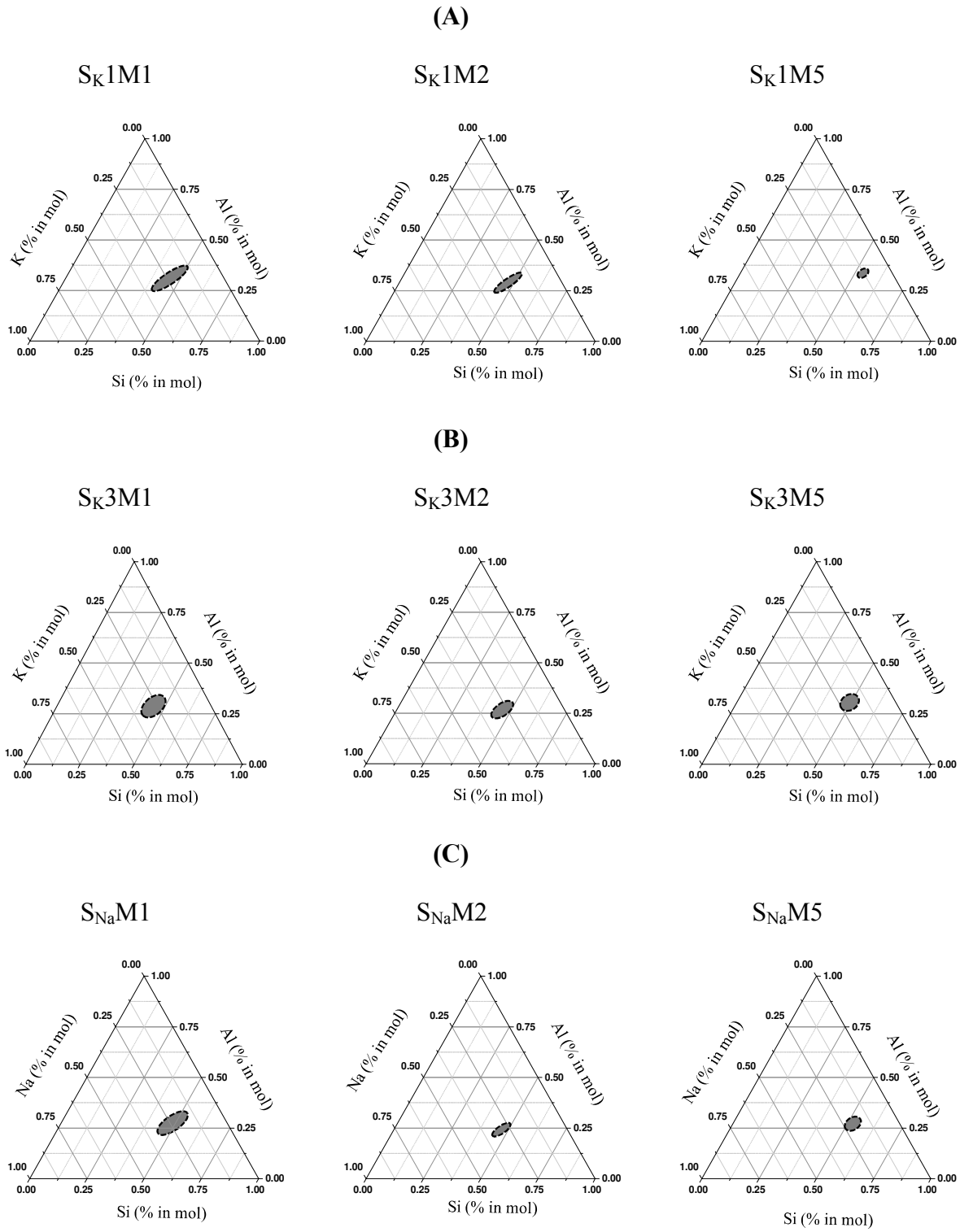

Fig. 3. Examples of the geopolymer existence domains in the Si-Al-M/O ternary for M1, M2 and M5 metakaolins in presence of (A) S_K1, (B) S_K3 and (C) S_{Na} alkaline solutions.

Whatever the used raw material, the geopolymer zones are quite small. For S_K1 (Fig. 3 (A)), M1 and M2 exhibit similar geopolymer zones with 1.22<Si/K<3.44 and 1.38 <Si/Al< 1.56 for M1 and 1.59 <Si/K< 2.84 and 1.47 <Si/Al< 1.60 for M2. Differences can be observed especially for less reactive metakaolin M5. The geopolymer zone is very limited and shifted to higher Si/Al (1.63 <Si/K< 1.67 and 3.98 <Si/Al <5.35). This fact can be explained by the low amount of reactive aluminates available in this metakaolin. So, it was necessary in this case to increase the proportion of metakaolin (% Al).

For S_K3 (Fig. 3 (B)), quite similar geopolymer zones are observed even for M5 (1.31 <Si/K <1.39 and 1.82< Si/Al< 2.11). The low reactivity of metakaolin is compensated by the high reactivity of the alkaline solution.

For S_{Na} (Fig. 3 (C)), the geopolymer zone relative to M2 is smaller (1.38 <Si/Na <1.87 and 1.98 <Si/Al< 2.10). This fact can be explained by the high viscosity of S_{Na} [25] and the high wettability of M2 which will reduce the workability of the mixture and therefore the faisability of geopolymer materials especially that no extra water was added. The water content in the mixture comes only from the activation solution.

To facilitate the exploitation of these data, the aluminum to alkali concentration ratio variation domain in relation with the sphere of cation movement in the mixture ($[Al]*d_{M-O}/[M]$) was delimited for each metakaolin and alkaline solution in Fig. 4. The M−O bond distance (d_{M-O}) varies from 2.43 to 2.81 for sodium and potassium silicate solutions respectively [26]. Three similar behaviors are evident defining aluminum to alkali concentration ratio variation depending on the initial characteristics of the activating solutions. Close aluminum to alkali concentration ratios permitting the formation of geopolymer materials were found for S_K3 and S_{Na} solutions, whereas in the case of S_K1, the concentrations ratio are shifted to higher values. This fact demonstrates that it is possible to identify aluminum and alkali concentrations variation area permitting the formation of geopolymers. For highly reactive solutions S_K3 and S_{Na}, the kinetic of geopolymerization is favored. In contrast, for S_K1, the reaction seems to be slower and require a larger amount of aluminum to take place especially in the case of less reactive metakaolins (M5 and M6). The slight difference between S_{Na} and S_K3 are related to the difference in viscosity and in cyclic species as previously discussed. Fast curves are relative to highly reactive saturation zones for metakaolins with (W*% amorphous)/((Si/Al)*100)> 700. Conversely, slow curves correspond to low ratios and are in relation with heterogeneous precipitation zones.

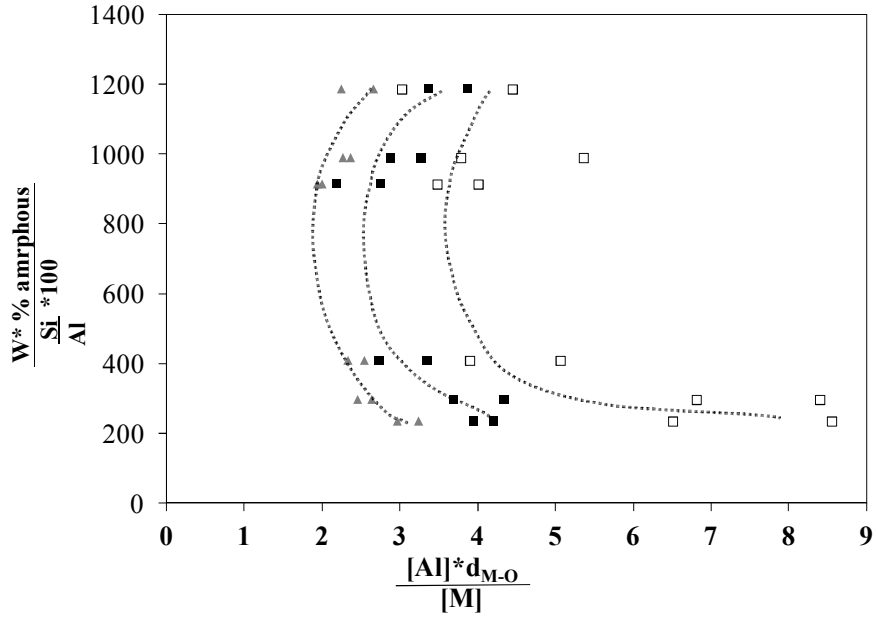

Fig. 4. Concentrations ratio variation domain ([Al]* d_{M-O})/ [M] permitting the obtaining of geopolymer materials for each metakaolin ($\frac{W*\%\ amorphous}{\frac{Si}{Al}*100}$) in presence of (□) S_K1, (■) S_K3 and (▲) S_{Na}.

3.3. Effect of precursors reactivity on water status and porous structure

After defining geopolymer existing domains in Si-Al-M/O ternary diagram from the different metakaolins and alkaline solutions. Eighteen compositions (one composition of every ternary diagram) were chosen for further study. The nomenclature and the composition of the prepared mixtures are reported in Table 3. Thermal analysis experiments were performed for all samples. Fig. 5 (A) presents a typical example of heat flow and weight loss curves during formation at 50°C for 120 min (zone I) and heating at 800°C (zone II) for $Si_{Na}M1$ sample. The first zone is characterized by an endothermic peak associated with a weight loss of 6.5 % in this case which corresponds to the loss of water during the different reactions of geopolymer formation. According to previous work [13], this stage includes the reorganization of species, the metakaolin dissolution, the oligomer formation and polycondensation reaction. Moreover, it is possible to determine the energy required for oligomer formation from the heat flow curve [21].The quantification of this energy is indicative of the kinetics of interactions between the species in solution. The second zone is also characterized by a large endothermic peak associated with a total weight loss (27.6 %) which corresponds to the remained water in the geopolymer samples. This water is in major

part (24.8 %) free and interstitial water (removed at approximately 250°C) and in a smaller part (2.8 %) hydroxyl water [9, 27].

Fig. 5 (B a) shows the evolution of the (weight loss $_I$ / % H_2O) ratio versus the energy required for oligomer formation for all samples. The weight loss during formation (weight loss $_I$) is divided by the initial water content in the mixture (% H_2O) because the water content differ from a sample to another depending on the used activating silicate solution and the proportion of the metakaolin in the mixture. So, the weight loss $_I$ / % H_2O ratio gives informations about the amount of released water during formation taking into account the initial water content of the mixture. The weight loss $_I$ / % H_2O ratio decreases as the energy decreases. It is clear that samples with S_K1 require more energy to form oligomers (from 1.8 to 3.1 KJ/mol for S_K1M2 and S_K1M5 respectively, and have higher weight loss $_I$ / % H_2O ratios (from 0.74 to 0.89 for S_K1M1 and S_K1M6, respectively). Some differences can be also noticed in function of the metakaolin reactivity. The more reactive is the metakaolin, the lower is the energy (3.1 KJ/mol for S_K1M5 vs 1.8 KJ/mol for S_K1M2). This is not the case for samples based on S_K3 and S_{Na} which exhibit similar and lower energy (from 0.3 to 0.8 KJ/mol for $S_{Na}M3$ and S_K3M1 respectively) and lower weight loss $_I$ / % H_2O ratios (from 0.41 to 0.66 for S_K3 and from 0.20 to 0.34 for S_{Na}). This result can be explained by the higher initial water content and low reactivity of S_K1 solution compared to S_K3 and S_{Na}. Indeed, higher initial water content leads to greater amount water to be removed [28]. Even if the higher initial water content will firstly facilitate the dissolution of metakaolin and the hydrolysis of dissolved aluminates and silicate species, it will then hinder or delay the oligomer formation and the polycondensation [11] which may justify the higher required energy for oligomer formation. The higher amount of released water gives evidence of lower consumed water during the reaction and therefore lower formation rate due to low reactivity of siliceous species coming from S_K1 (luck of reactive siliceous species (Q^1 and Q^0) and non bridging oxygen atoms).

For S_K3, the lower energy and associated weight loss $_I$ / % H_2O are due to lower initial water content and higher reactivity of siliceous species. The lower connectivity between small siliceous species favors the availability of hydroxide ions OH^- [20] and therefore accelerates the oligomer formation.

Finally, the behavior of mixtures based on S_{Na} is almost due to the difference of size and properties of alkali cation. In fact, Na^+ ion is smaller and has a higher charge density than K^+ ion. Furthermore the free energy of hydration Na^+ ions is higher than K^+ which makes the

removal of water more difficult in the case of sodium compared to potassium [28, 29]. This fact gives an explanation of the lower weight loss $_{I}$ / % H_2O.

Fig. 5 (B b) shows the evolution of the weight loss $_{II}$ / % H_2O ratio after heating at 800°C. A reverse trend is observed. The weight loss $_{II}$ / % H_2O ratio decreases as the energy increases. In other words, more the kinetics of formation is faster, more water remains entrapped in the pores or bonded to the geopolymer network. Higher water amount weight (loss $_{II}$ / % H_2O) remains in samples based on S_{Na} compared to those based on S_K3 and S_K1. This result is in accordance with the literature and can be explained by the differences between the two alkali cations hydration shell. Indeed, The Na^+ ions are more hydrated and have a more stable hydration shell compared to K^+ ions due to their smaller size. That means that Na^+ is more able to attract the water molecules than K^+ [30, 31]. As a consequence, once the reaction is completed, higher amount of water remains entrapped in the pores or bonded to the geopolymer network.

Table 3. Nomenclature, composition and specific compressive strength values of the studied samples.

Mixtures	Si/Al	liquid/solid (l/s)	Specific compressive strength (σ_ρ)
S_K1M1	1.56	1.03	21
S_K1M2	1.60	1.03	28
S_K1M3	1.34	1.03	21
S_K1M4	1.33	1.03	24
S_K1M5	1.67	0.57	29
S_K1M6	1.56	0.62	18
S_K3M1	1.68	1.16	34
S_K3M2	1.73	1.16	39
S_K3M3	1.45	1.16	35
S_K3M4	1.44	1.16	36
S_K3M5	1.76	0.66	41
S_K3M6	1.74	0.89	25
S_{Na}M1	1.90	1.05	40
S_{Na}M2	1.95	1.05	27
S_{Na}M3	1.63	1.05	39
S_{Na}M4	1.63	1.05	30
S_{Na}M5	1.89	0.62	45
S_{Na}M6	1.59	0.82	23

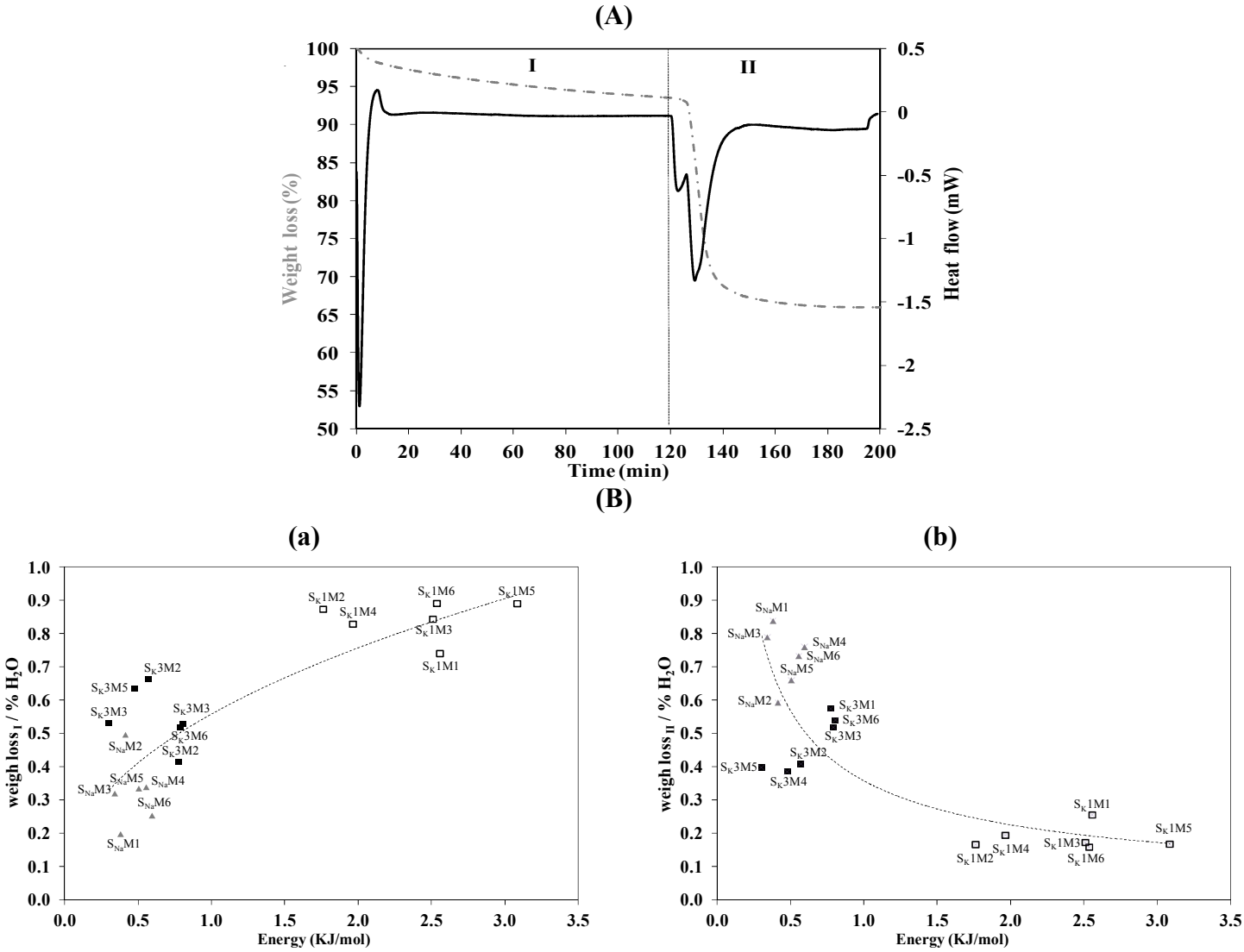

Fig. 5. Example of heat flow and weight loss curves during formation at 50°C for 120 min (Zone I) and heating at 800°C (zone II) for $S_{Na}M1$ sample and **(B)** evolution of the weight loss **(a)** during formation and **(b)** heating versus the energy required for oligomer formation for all samples.

The differences observed by thermal analysis suggest difference in pore structure and distribution. That is why the pore structure of nine samples based on three metakaolins with different reactivity (M1, M2 and M5) and the three solutions S_K1, S_K3 and S_{Na} was determined by MIP measurements (Table 4). Two types of behaviors are observed : (i) samples based on S_K1 solution exhibiting similar porosities (between 38 and 40%) but different pore sizes (0.007 and 0.01 µm for S_K1M2 and S_K1M1 - S_K1M5 respectively) and (i) samples based on S_K3 and S_{Na} solutions having lower porosities and smaller pore sizes that

vary depending on the used metakaolin. Indeed, two types of porosity are noted: one centered at around 23% for M1 and M5 metakaolins and the other at about 32% for M2 metakaolin. The effect of alkali cation is once again highlighted and it is in accordance with literature. In fact, it was demonstrated that the use of a potassium alkaline solution leads to the formation of geopolymer having a smaller pore size and a greater number of pores than geopolymer based on sodium solution because of the difference in size and mobility between the two cations [32, 33]. It seems therefore that the variation in the pores distribution and size result from the different kinetics and rates of geopolymerization between the samples. Depolymerized siliceous species in the case of S_K3 and S_{Na} solutions permit the formation of small colloids homogeneously distributed inducing a high polycondensation rate and low porosity. The high pore size can be explained by the agglomeration of small pores resulting from the densification of the structure [4]. However, in the case of the samples based on the S_K1 solution, the low reactivity of the solution causes a lower degree of densification and the existence of several networks. Thus, larger colloids are formed inducing a higher degree of porosity and lower pore size.

Table 4. Porosity and pore size values determined from MIP measurement for different samples.

Mixtures	Porosity (%)	Pore size (µm)
S_K1M1	40.23	0.010
S_K1M2	38.14	0.007
S_K1M5	38.09	0.010
S_K3M1	21.62	0.026
S_K3M2	33.55	0.027
S_K3M5	22.86	0.029
S_{Na}M1	24.78	0.035
S_{Na}M2	31.77	0.026
S_{Na}M5	20.27	0.056

3.4 Effect of precursors on the structural ordering of final geopolymer

^{29}Si MAS-NMR experiments were performed on geopolymer samples. Two examples of the results of deconvolution of the spectra are presented in Fig. 6 (A) for S_K1M2 and S_{Na}M3

samples. Table 5 provides deconvolution details about the chemical shifts, the assignment and the percentages of the contributions areas for all samples

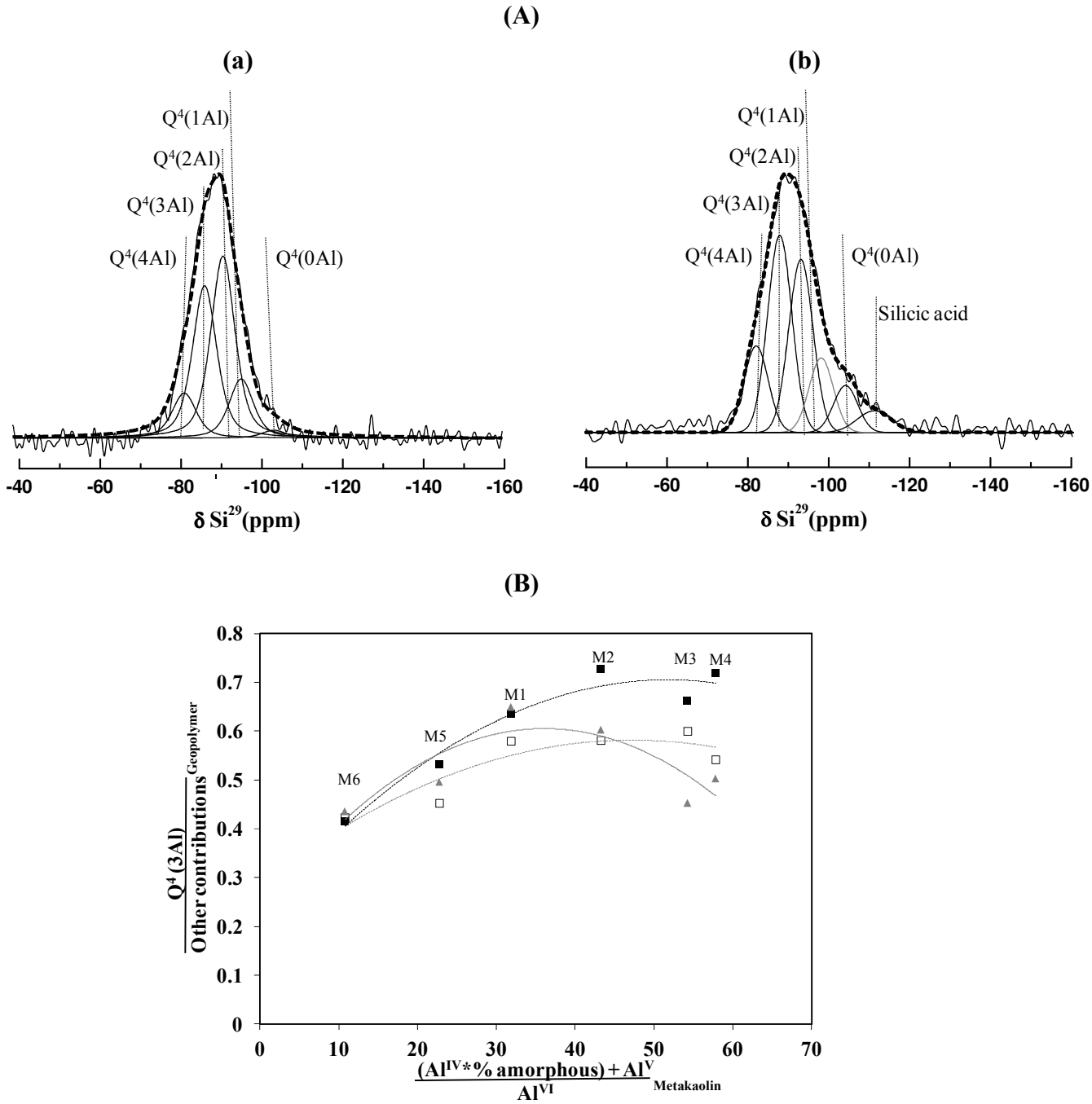

Fig. 6. (A) Examples of ^{29}Si MAS-NMR spectra and its deconvolution for **(a)** S_K1M2 and **(b)** S_{Na}M3 samples and **(B)** evolution of the contributions area ratio ($\frac{Q^4\,(3Al)}{\text{Other contributions}}$) of geopolymer samples based on (□) S_K1, (■) S_K3 and (▲) S_{Na} solutions in function of the metakaolin reactivity ($\frac{(Al^{IV}*\%\,\text{amorphous}) + Al^{V}}{Al^{VI}}$).

Table 5. Deconvolution details about the chemical shifts, the assignment and the percentages of the contributions areas for all samples

Contribution / Sample	Mulitte (-79 ppm)	Q^4 (4Al) (-84 ppm)	Q^4 (3Al) (-89 ppm)	Q^4 (2Al) (-94 ppm)	Q^4 (1Al) (-99 ppm)	Q^4 (0Al) (-104 ppm)	Silicic acid (-111 ppm)
S_K1M1	-	20.0	36.7	27.5	11.7	4.1	-
S_K1M2	-	25.6	36.8	23.0	7.9	2.7	4.1
S_K1M3	-	23.3	37.5	20.0	9.2	5.0	5.0
S_K1M4	-	18.4	35.1	19.1	11.5	-	15.9
S_K1M5	-	20.2	31.1	23.1	8.7	8.1	8.7
S_K1M6	1.9	18.6	29.7	20.5	14.9	5.2	9.3
S_K3M1	-	20.0	38.8	30.4	7.7	3.2	-
S_K3M2	-	22.2	42.1	23.6	9.9	2.2	-
S_K3M3	-	26.1	39.8	23.1	5.5	3.4	2.1
S_K3M4	-	26.0	41.8	22.0	7.8	2.4	-
S_K3M5	-	20.4	34.7	29.6	8.2	2.0	5.1
S_K3M6	2.8	18.7	29.4	26.6	15.5	5.5	1.6
S_{Na}M1	-	23.9	39.3	23.1	11.9	1.8	-
S_{Na}M2	-	24.6	37.6	23.7	11.8	2.3	-
S_{Na}M3	-	21.2	31.2	25.5	12.0	3.5	6.8
S_{Na}M4	-	22.9	33.5	20.5	13.6	2.4	7.1
S_{Na}M5	-	19.1	33.2	23.9	14.9	1.9	7.2
S_{Na}M6	1.2	12.3	30.3	30.8	15.6	3.3	6.6

Q^n(mAl) is the adopted nomenclature with n is the polymerization degree of the silicon tetrahedra and m the amount of aluminium substitution per silicon tetrahedron [34]. Five typical components at -84,-89, -94, -99 and -104 ppm (± 1 ppm) were evident whatever the sample and can be assigned to Q^4(4Al), Q^4(3Al), Q^4(2Al), Q^4(1Al) and Q^4(0Al) respectively [35]. The peak at around -79 was present only for samples based on M6 metakaolin which initially contains mullite [21]. An extra peak was also found in some samples (Fig. 6 (A b), Table 5) at -111 ppm denoting the presence of silicic acid [36] resulting from an excess of non reacted siliceous species. Q^4(2Al) and Q^4(1Al) in contrary to Q^4(4Al) and Q^4(3Al) are Si-rich components that give evidence that the reaction is not completed. However, Q^4(3Al) is the characteristic peak of geopolymer phase. That is why it will be considered as a reference.

In order to evaluate the degree of formation of geopolymer network in detriment of other potential formed networks, the evolution of the contributions area ratio $\frac{Q^4\,(3Al)}{\text{Other contributions}}$ of geopolymer samples in function of the metakaolin reactivity was plotted in Fig. 6 (B).

Whatever the used activating solution, the $\frac{Q^4\,(3Al)}{\text{Other contributions}}$ ratio increase with the increase of $\frac{(Al^{IV}*\%\,\text{amorphous})+ Al^{V}}{Al^{VI}}$ ratio. A slight decrease is noted for M3 and M4 metakaolins. Consequently, more the metakaolin is reactive more the geopolymer network is favored. For less reactive metakaolins (M5and M6), the low availability of reactive aluminium [24] and the presence of crystalline phases (Quartz , mullite) resistant to alkaline attack perturbate the formation of geopolymer network. Very pure metakaolins M3 and M4 (Si/Al = 1) show lower ratios despite their high reactivity due the excess of siliceous species which causes the formation of silicic acid which enter in competition with the geopolymer network.

Higher $\frac{Q^4\,(3Al)}{\text{Other contributions}}$ ratios were obtained in the case of S_K3 alkaline solution especially with more reactive metakaolins (from 0.63 to 0.73 for S_K3M1 and S_K3M2 respectively) while M5 and M6 show lower ratios (0.53 and 0.42 for S_K3M5 and S_K3M6 respectively). This result confirms the higher reactivity of S_K3 and its capacity to favor polycondensation and enhance geopolymer network formation. Samples based on S_K1 and S_{Na} exhibit similar and lower $\frac{Q^4\,(3Al)}{\text{Other contributions}}$ ratios varying from 0.42 to 0.62 for S_K1M6 and S_K1M3 respectively and from 0.44 to 0.65 for $S_{Na}M6$ and $S_{Na}M1$ respectively.

The structural differences resulting from the use of different alkaline solutions emphasize once again the higher reactivity of S_K3 solution compared to S_K1 and S_{Na} solutions. Indeed, this solution has the best ability to promote the polycondensation reaction and thus the formation of the geopolymer network.

3.4. Effect of precursors on the geopolymer mechanical properties

Structural differences between the studied geopolymer materials suggest differences in the resulting mechanical properties. The evolution of the obtained specific compressive strength values multiplied by the liquid to solid ratio ($\sigma\rho$*l/s) versus the metakaolin reactivity rate determined from structural data ($\frac{(Al^{IV}*\%\,\text{amorphous})+ Al^{V}}{Al^{VI}}$) is presented in Fig. 7. Similar trends are observed as obtained in Fig. 6 (B) highlighting the dependence of the mechanical properties of the raw materials properties. The compressive strength increases with the increase of alkaline solution and metakaolin reactivity. Samples based on S_K3 and S_{Na} exhibit

similar and higher compressive strength values compared to samples based on S_K1. This result was expected since the geopolymer network is more favored using S_K3 and S_{Na}. The slight decrease of mechanical strength observed in the case of M3 and M4 metakaolins is due to the competition between the formed silicic acid and the geopolymer network. That means that the geopolymer phase formation ($Q^4(3Al)$) has an important effect on the mechanical strength but is not the only influencing factor. The effect of solid liquid ratio (l/s) was also highlighted. Indeed, the amount of liquid must provide sufficient workability of the mixture without weakening the structure of the final materials.

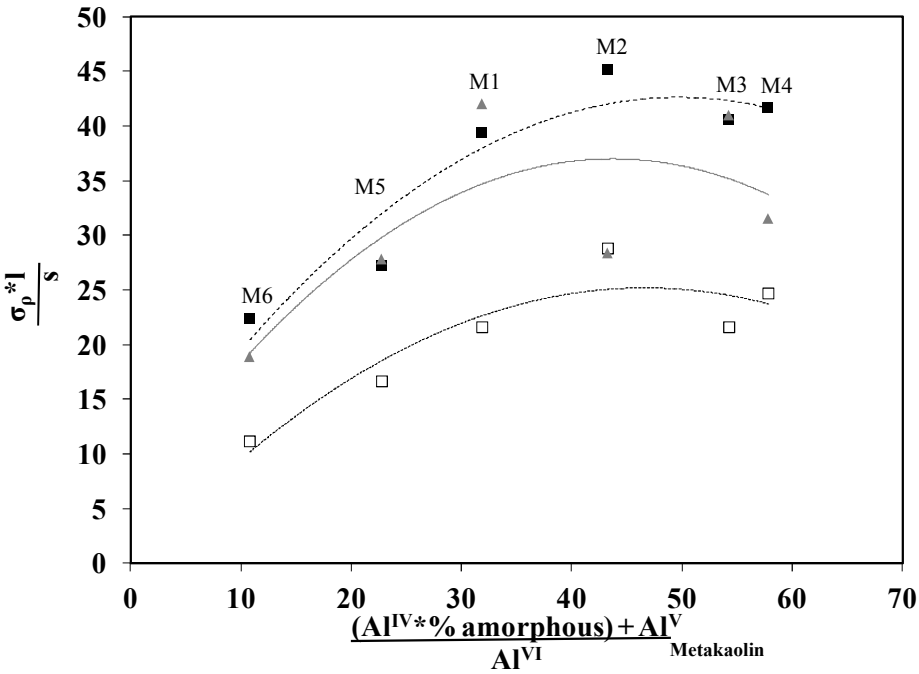

Fig. 7. Evolution of the specific compressive strength (σ_{ρ}*l/s) in function of the metakaolin reactivity ($\frac{(Al^{IV} * \%\ amorphous) + Al^{V}}{Al^{VI}}$) for samples based on (□) S_K1, (■) S_K3 and (▲) S_{Na} solutions.

4. Conclusion

This study was conducted in order to define the key parameters that govern the formation, the structure and the working properties of geopolymer materials synthesized from different metakaolins and alkaline solutions. Control of geopolymerization reaction requires a deeper knowledge of the structure and the reactivity of raw materials. For this, three alkaline solutions which differ in terms of alkali cation (M= Na or K), Si/M molar ratio and water content were at first investigated by ^{29}Si NMR. The reactivity rate of alkaline solutions was evaluated depending on the amount of small depolymerized species and cyclic species.

Concerning metakaolins, physical, chemical and structural characterizations have demonstrated that the Si/Al molar ratio, the wettability value, the amorphous phase content and the reactive tetrahedral aluminium are the key parameters controlling its reactivity. Then, a feasibility study was undertaken in order to determine the geopolymer existence domains in the Si–Al–M/O ternary diagram. It was found that the feasibility of geopolymer is linked to the nature of used raw precursors and the alkali and aluminum concentration. Furthermore, thermal analysis has permitted to demonstrate that the use of reactive precursors especially a reactive alkaline solution reduce the energy necessary to oligomer formation. Moreover, the initial water content and cation hydration characteristics influence the amount of water consumed during the reaction and trapped in the final structure. The different kinetics and rates of geopolymerization affect also the pores distribution and size. The high reactivity of the precursors induces higher densification degree. Thus, smaller entities are formed inducing a lower degree of porosity and larger pore size. ^{29}Si NMR experiments corroborate these results and give evidence that higher reactive precursors favor preferentially the formation of geopolymer phase in detriment of other networks which increase significantly the mechanical properties of the final materials.

Acknowledgments

The authors gratefully acknowledge Pr. Jesus Sanz for NMR experiments at the Institute of Materials Science in Madrid.

References

[1] J. Davidovits, Geopolymer: Chemistry and Applications, 2nde édition, Institut Géopolymère, St-Quentin, 2008.

[2] X.X. Gao, A. Autef, E. Prud'homme, P. Michaud, S. Basma, E. Joussein, S. Rossignol, Synthesis of consolidated materials from alkaline solutions and metakaolin: existence of domains in the Al-Si-K/O ternary diagram, J. Sol-Gel Sci. 65 (2013) 220-221.

[3] L. Weng, K. Sagoe-Crentsil, T. Brown, S. Song, Effects of aluminates on the formation of geopolymers, Mater. Sci. Eng. B. 117 (2005) 163–168.

[4] P. Duxson, J.L. Provis, G.C. Lukey, S.W. Mallicoat, W.M. Kriven, Understanding the relationship between geopolymer composition, microstructure and mechanical properties, Colloids Surf. A. 269 (2005) 47-58.

[5] J.P. Jolivet, Condensation des cations en solution aqueuse-Chimie de surface des oxydes, dans De la solution à l'oxyde, Savoirs actuels, InterEditions / CNRS Editions, 17, Paris, 1994.
[6] P. Duxson, J.L. Provis, G.C. Lukey, F .Separovic, J.S.J Van Deventer, 29Si NMR Study of Structural Ordering in Aluminosilicate Geopolymer Gels, Langmuir. 21 (2005) 3028-3036.
[7] Z. Peng, K.Vance, A. Dakhane, R. Marzke, N. Neithalath. Microstructural and 29Si MAS NMR spectroscopic evaluations of alkali cationic effects on fly ash activation. Cement Concrete Comp. 57 (2015) 34-43.
[8] H. Wang, H. Li, F. Yan, Synthesis and mechanical properties of metakaolinite-based geopolymer Colloids and Surfaces A: Physicochemical and Engineering Aspects 268 (2005) 1–6.
[9] D. S. Perera, E. R. Vance, K. S. Finnie, M. G. Blackford, J. V. Hanna, D. J. Cassidy, and C. L. Nicholson, Disposition of Water in Metakaolinite-Based Geopolymers, Ceram. Trans. 185 (2005) 225–36.
[10] M. Lizcano, A. Gonzalez, S. Basu, K. Lozano, and M. Radovic, Effects of Water Content and Chemical Composition on Structural Properties of Alkaline Activated Metakaolin-Based Geopolymers. J. Am Ceram Soc. 95 (2012) 2169–2177.
[11] Z. Zuhua, Y. Xiao, Z. Huajun, and C. Yue, Role of Water in the Synthesis of Calcined Kaolin-Based Geopolymer, Appl. Clay Sci. 43 (2009) 218–23.
[12] A. Autef, E. Joussein, A. Poulesquen, G. Gasgnier, S. Pronier, I. Sobrados, J. Sanz, S. Rossignol, Influence of metakaolin purities on potassium geopolymer formulation: The existence of several networks, J. Colloids and Interface Sci. 408 (2013) 43–53.
[13] A. Autef, E. Joussein, G. Gasgnier, S. Rossignol, Role of the silica source on the geopolymerization rate: A thermal analysis study, J. Non-Cryst. Solids. 366 (2013) 13–21.
[14] C. Galle, Effect of drying on cement-based materials pore structure as identified by mercury intrusion porosimetry - A comparative study between oven-, vacuum-, and freeze-drying, Cem. Concr. Res. 31 (2001) 1467-1477.
[15] P.W.J.G. Wijnen, J.W Beelen, C.P.J Rummens, L.J.M Van de Ven, Van Santen RA Silica gel dissolution in aqueous alkali metal hydroxides studies by 29 Si –Nmr. J Non-Crystal. Solids 109 (1989) 85-94.
[16] C.T.G Knight, R.J Kirkpatrick, E. Oldfield, Two-dimensional silicon-29 nuclear magnetic resonance spectroscopic study of chemical exchange pathways in potassium silicate solutions Journal of Magnetic Resonance (1969) 78, 1988, 31–40.

[17] L. Vidal, E. Joussein, M. Colas, J. Cornette, J. Sanz, I. Sobrados, J.L. Gelet, J. Absi, S. Rossignol, controlling the reactivity of silicate solutions: an FTIR, Raman and NMR study Accepted in Colloid Surface A. doi:10.1016/j.colsurfa.2016.05.039

[18] L.B. Jonathan, L.T. Garry, Anion Distributions in Sodium Silicate Solutions. Characterization by 29Si NMR and Infrared Spectroscopies, and Vapor Phase Osmometry. J Phys Chem B 101(1997) 10. 638-10644.

[19] A. Gharzouni, E. Joussein, B. Samet, S. Baklouti, S. Rossignol, Effect of the reactivity of alkaline solution and metakaolin on geopolymer formation, J. Non-Cryst. Solids. 410 (2015) 127-134.

[20] P. Steins, Influence des paramètres de formulation sur la texturation et la structuration des géopolymères, thèse de doctorat, université de Limoges, 2014.

[21] A. Gharzouni, I. Sobrados, E. Joussein, S. Baklouti, S. Rossignol Control of polycondensation reaction generated from different metakaolins and alkaline solutions; submitted to cement and concrete composite.

[22] A. Autef, E. Joussein, A. Poulesquen, G. Gasgnier, S. Pronier, I. Sobrados, J. Sanz, S. Rossignol, Influence of metakaolin purities on potassium geopolymer formulation: The existence of several networks, J. Colloids and Interface Sci. 408 (2013) 43–53.

[23] A. Gharzouni, E. Joussein, B. Samet, S. Baklouti, S. Rossignol, Effect of the reactivity of alkaline solution and metakaolin on geopolymer formation, J. Non-Cryst. Solids. 410 (2015) 127-134.

[24] L. Weng , Kwesi Sagoe-Crentsil, Trevor Brown, Shenhua Song, Effects of aluminates on the formation of geopolymers Materials Science and Engineering: B. 117 (2005) 163–168.

[25] F.A. Menon, M.F. Nuruddin, S. Khan, N. Shafiq, T. Ayub, Effect of sodium hydroxide concentration on fresh properties and compressive strength of self compacting geopolymer concrete, J. Eng. Sci. Technol. 8 (2013) 44 – 56.

[26] J. Mähler and I. Persson, A Study of the Hydration of the Alkali Metal Ions in Aqueous Solution Inorg. Chem. 51 (2012) 425–438.

[27] C E. White, J. L. Provis, T. Proffen, and J. S. J. V. Deventer, The Effect of Temperature on the Local Structure of Metakaolin-Based Geopolymer Binder: A Neutron Pair Distribution Function Investigation, J. Am. Ceram. Soc. 93 [10] (2010) 3486–3492.

[28] C. Kuenzel, L. Vandeperre, S. Donatello, A. R. Boccaccini, C. R. Cheeseman, Ambient temperature drying shrinkage and cracking in metakaolin-based geopolymers, J. Am. Ceram. Soc. 95 (2012) 3270-3277.

[29] M. Migliore, G. Corongiu, E. Clementi and G. C. Lie, Monte Carlo study of free energy of hydration for Li+, Na+, K+, F−, and Cl− with ab initio potentials. J. Chem. Phys, 88 (12) (1988) 7766-7771.

[30] L. Degrève, S.M Vechi, C.Q Junior, The hydration structure of the Na+ and K+ ions and the selectivity of their ionic channels, Biochimica et Biophysica Acta (BBA) - Bioenergetics 1274 (1996) 149–156.

[31] J.G.S. van Jaarsveld, J.S.J. van Deventer, G.C. Lukey, The effect of composition and temperature on the properties of fly ash- and kaolinite-based geopolymers. Chem. Eng. J. 89 (2002) 63–73.

[32] J.L Bell and W.M Kriven, Nanoporosity in Aluminosilicate, Geopolymeric Cements. Microsc. Microanal. 10 (2004) 590-591.

[33] P. Steins, Influence des paramètres de formulation sur la texturation et la structuration des géopolymères. Ph.D. thesis. University of limoges, 2014.

[34] S.L.A. Valcke, P. Pipilikaki, H. R. Fischer, M H. W. Verkuijlen, E. R. H. van Eck, FT-IR and 29Si-NMR for evaluating aluminium–silicate precursors for geopolymers, Mater. Struct. 48 (2015) 557–569.

[35] P. Duxson, J.L. Provis, G.C. Lukey , F. Separovic and J. S. J. van Deventer, 29Si NMR Study of Structural Ordering in Aluminosilicate Geopolymer Gels. Langmuir, 21 (7) (2005) 3028–3036.

[36] S.M. Chemtob, G.R. Rossman, J.F. Stebbins, Natural hydrous amorphous silica: Quantitation of network speciation and hydroxyl content by 29Si MAS NMR and vibrational spectroscopy. Am. Mineral. 97 (2012) 203−211.

Acte de congrès 1 (ACTI1)

A. Gharzouni, E. Joussein, S. Baklouti, S. Rossignol

"Effect of the Reactivity of the Alkaline Solution and the Metakaolin on the Geopolymer Formation"

Advances in Science and Technology, 92 (2014) 20-25

Advances in Science and Technology Vol. 92 (2014) pp 20-25
Online available since 2014/Oct/31 at www.scientific.net

doi:10.4028/www.scientific.net/AST.92.20

Effect of the reactivity of the alkaline solution and the metakaolin on the geopolymer formation

Ameni Gharzouni[1, 3], Emmanuel Joussein[2], Samir Baklouti[3],

Sylvie Rossignol[1*]

[1]Groupe d'Etude des Matériaux Hétérogènes (GEMH-ENSCI) Ecole Nationale Supérieure de Céramique Industrielle, 12 Rue Atlantis, 87068 Limoges Cedex, France

[2]Université de Limoges, GRESE, EA 4330, 123 Avenue Albert Thomas, 87060 Limoges, France
[3]Laboratoire de Chimie Industrielle, Ecole Nationale d'Ingénieurs de Sfax, 3038, Sfax, Tunisie

[*] sylvie.rossignol@unilim.fr

Keywords: alkaline solutions, metakaolins, FTIR spectroscopy, pH following, geopolymer, mechanical properties.

Abstract. The choice of precursors is a key parameter in the geopolymerization mechanism since it governs the kinetic of the reaction as well as the working properties of the final materials. This study focuses on the effect of the alkaline solution reactivity and metakaolin properties on the geopolymer formation. For this purpose, several geopolymer samples were synthesized from two alkaline solutions and three metakaolins. The structural evolution of formed geopolymers was investigated using FTIR spectroscopy and the following of the pH value during the formation. The measurement of mechanical strength was tested by compression. The results allow to evidence that for a less reactive alkaline solution, the reactivity of metakaolin governs the geopolymerization reaction. However, the alkaline solution is the steering reaction when it is highly reactive. Therefore, the extent of depolymerization of the alkaline solution and the reactivity of the metakaolin seem to control the rate of polycondensation and the mechanical properties of the geopolymer materials.

Introduction

Geopolymer materials show an increasing interest due to its synthesis method, high working performances, wide range of application and low environmental impact. Geopolymer binders are amorphous, three dimensional materials resulting from the activation of an aluminosilicate source, like metakaolin, calcined clay or industrial waste activated by an alkaline solution. The choice of precursors (alkaline solution and aluminosilicate source) is a primordial parameter in geopolymerization mechanism since it governs the properties of the final materials.

Recently, Autef et al. [1] highlights the role of metakaolin reactivity in the presence of an alkaline solution prepared by the dissolution of KOH and amorphous silica in water. In fact, the metakaolin reactivity can generate the formation of one or several networks and lead to nanostructure variations that influence the mechanical properties of the obtained materials. A very reactive metakaolin leads to very fast dissolution and allows the formation of a perfect geopolymer network. In the case of a very pure metakaolin where the kaolinite layers are not completely dehydroxyled, the final material consists of a geopolymer network and layers coated by a silicate solution. However, with a metakaolin rich of impurities, the strengthened material consists of a geopolymer network, mica layers and both a Si-rich phase and Al-rich phase.

In the other hand, the nature of the alkali cation affects the geopolymerization reaction and the working properties of the consolidated materials. It was shown that geopolymers based on potassium exhibit better thermal and mechanical properties because of the larger size of potassium ion compared to the sodium ion [2]. Moreover, a comprehensive study [3] of the influence of different potassium activating solution with the same metakaolin was established. It was demonstrated that the Si/K molar ratio of the silicate solution controls the nature and the quantity of the siliceous species. In fact, as the Si/K ratio decreases, the solution becomes more depolymerized.

The accentuated presence of depolymerized species in the alkaline solution (lower-order species) leads to the formation of small, very reactive entities that quickly bridge Si and/or and, thus, enables the fast formation of oligomers and leads to better mechanical properties of the resulting geopolymers.

Due to the diversity of the raw materials which can be used in the formulation, few comparative studies have been done on different metakaolins sources and various alkaline solutions. The aim of this work is to study the role of two potassium alkaline silicate solutions, with different initial Si/K molar ratios, in presence of three metakaolins which differ in terms of reactivity, and investigate their impact on the mechanism of gepolymerization and the properties of the synthesized materials.

Experimental

Sample preparation. Two commercial potassium silicate solutions, denoted S1 and S3 and with different Si/K molar ratios (1.75 and 0.65, respectively) and three kinds of metakaolins, named M1, M2 and M3 and differ in term of wettability (570 µL/g, 1250 µL/g, 1100 µL/g, respectively) were used in the synthesis of the geopolymer samples. The Si/K molar ratio of the alkaline solutions was maintained at Si/K=0.5 by dissolving different amounts of potassium hydroxide pellets (VWR, 85.2% pure) into the two starting silicate solutions, and mixed with metakaolins. The obtained mixtures were placed in a closed sealable polystyrene mold at room temperature (25°C). The nomenclature and the composition the prepared mixtures are reported in Table 1. Samples were named S1M1, S3M1, S1M2, S3M2, S1M3 and S3M3.

Tab. 1. Nomenclature and composition the prepared mixtures.

Mixtures	(Si*H_2O)/(K+Al)
S1M1	1.99
S1M2	2.03
S1M3	1.74
S3M1	1.24
S3M2	1.26
S3M3	1.15

Sample characterization. Fourier-transform infrared (FTIR) spectroscopy in ATR mode was used to investigate the structural evolution of the geopolymer mixtures. FTIR spectra were obtained using a ThermoFisher Scientific Nicolet 380 infrared spectrometer. The IR spectra were gathered over a range of 400 to 4000 cm^{-1} with a resolution of 4 cm^{-1}. The atmospheric CO_2 contribution was removed with a straight line between 2400 and 2280 cm^{-1}. To followl the geopolymer formation, a software was used to acquire a spectrum (64 scans) every 10 minutes for 13 hours. For comparison, spectra were baseline corrected and normalized[4].

The measurement of the pH values were realized using a Schott Instrument Lab860 pH-meter at 25°C during the first 400 min of the geopolymers formation. A 2.4 g sample was immersed in 30 mL of osmosed water, which provided an S/L ratio of 0.08 [5].

Compressive strengths were tested using a LLOYD EZ20 universal testing machine with a crosshead speed of 0.1 mm/min. The compressive tests were made on ten samples for every composition. The values of compressive strength represent the average of the ten obtained values and were expressed in MPa. Test tubes, used for the compression tests, were cylindrical in shape with a diameter (Φ) of 15 mm and a height (h) of approximately 35 mm and were aged for 7 days in closed mould at room temperature. The samples were demolded and rectified just before the tests.

Results and discussions

Effect of alkaline solution and metakaolin on the polycondensation rate. The effect of three types of metakaolins in the presence of two alkaline solutions, based on commercial silicate solutions with different initial Si/K molar ratios, were studied by FTIR spectroscopy in mode ATR in order to follow the structural evolution of the synthesized mixtures. The Q^2 position shift versus the slope of the curve for all the studied samples was plotted in Fig. 1.

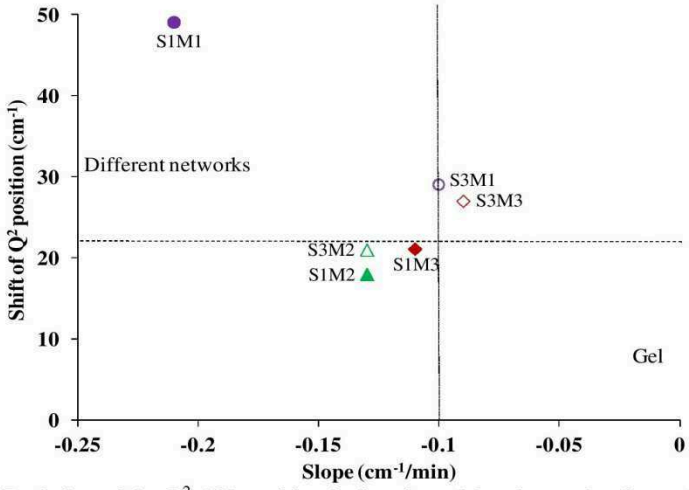

Fig 1. Evolution of the Q^2 shift position in function of the slope value for each sample.

The shift of the Q^2 position indicates the substitution of Si-O-Si bonds by Si-O-Al bonds reflecting the polycondensation reaction [1]. The slope reveals the kinetics of this substitution. S1M1 sample exhibits the greater shift and slope values (49 cm^{-1} and -0.21 cm^{-1}/min, respectively). However, the use of S3 alkaline solution decreases the shift value to 29 cm^{-1} and the slope value to -0.1 cm^{-1}/min. For the metakaolin M2, the values of the shift and the slope are quite similar with no effect of the alkaline solution on the reaction. In the case of M3, small changes are detected with the use of S3. Indeed, the shift value increases slightly from 21 cm^{-1} in the case of S1M3 to 27 cm^{-1} for S3M3 and the slope decreases from -0.11 cm^{-1}/min to -0.09 cm^{-1}/min.

According to the wettability values, M2 and M3 metakaolins have high wettabilities (1250 µL/g and 1100 µL/g, respectively), while M1 (less pure) exhibits a lower value (570 µL/g) indicating a lower reactivity [6] which may explain the observed shift and slope values in the case of S1M1 resulting from a combination of Si-O-M (M=Si, Al or K) from dissolved species and impurities of metakaolin. The weaker slope and the shift values observed for S3M1 are mainly due to the reactivity of the S3 alkaline solution which is more depolymerized comparing to S1 (lower Si/K molar ratio of the starting silicate solution). Thus, highly reactive siliceous species, released from S3 alkaline solution, reach speciation equilibrium and then react with the aluminous species [3]. In the case of M2 and M3, the most reactive metakaolins, the effect of the alkaline solution seems to be negligible. The reactivity of the siliceous species released from the two metakaolins controls the kinetic of the substitution of Si-O-Si by Si-O-Al bonds and the reorganization of the network. In fact, the more reactive the metakaolin, the more oligomers formation is favored and rapid.

In addition to that, previous studies [7] have shown the existence of two areas according to the values of the shift and the slope: For a shift less than 22 cm^{-1} and a slope above -0.1 cm^{-1}/min, the exceed of siliceous species forms a gel. While, for a shift greater than 22 cm^{-1} and a slope below than -0.1 cm^{-1}/min, there is a formation of various networks. The intersection of the two areas

seems to be characteristic of geopolymer materials. This fact was schematically represented in Fig.1. All the samples seem to be in the geopolymer area except of S1M1 which presents different networks. These results are in accordance with the data discussed above.

To further assess the effect of the alkaline solution as well as the metakaolin on the rate of polycondensation, the variation of the pH value of the different mixtures during the first 400 min of the formation was followed. The results are presented in Fig. 2.

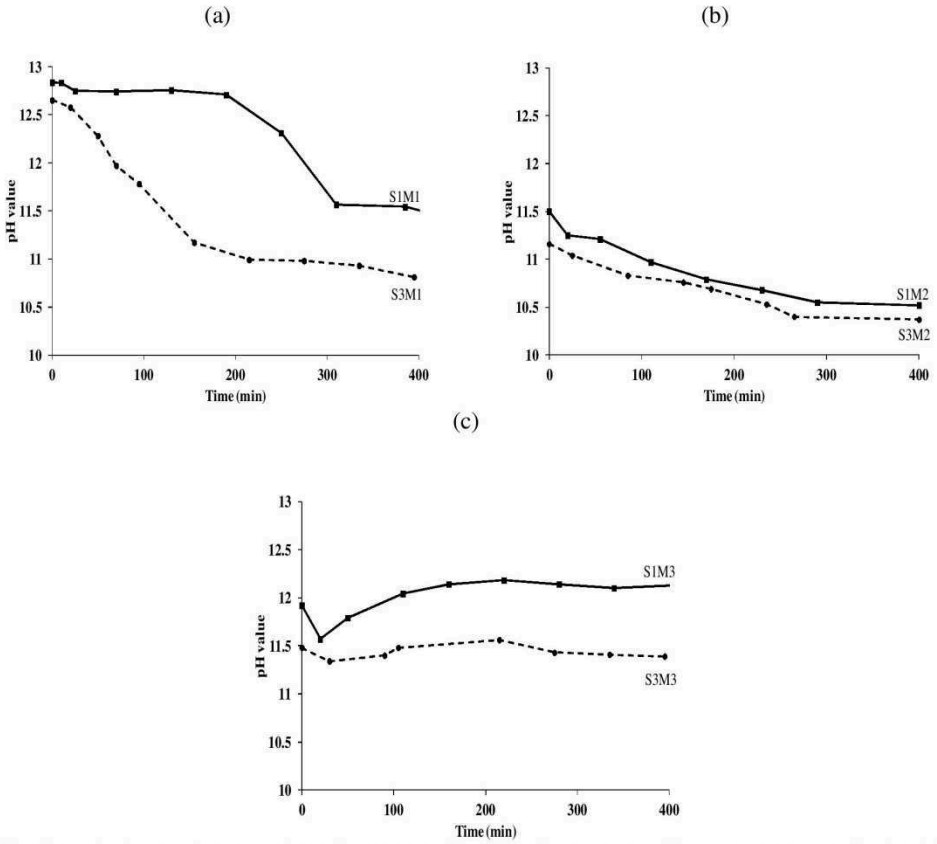

Fig 2. Variation of the pH values along geopolymerisation measured in an aqueous media for (a) (■) S1M1, (●) S3M1, (b) (■) S1M2, (●) S3M2 and (c) (■) S1M3, (●) S3M3 samples.

For the three metakaolins, the initial pH values were different S1M1 (12.8), S3M1 (12.6), S1M2 (11.5), S3M2 (11.2), S1M3 (11.9) and S3M3 (11.5). For the same metakaolin, the use of S3 (highly reactive) decreases slightly the initial pH value of the mixture. For S1M1 (Fig. 2. a), the pH value was substantially constant until 200 min, then, it decreases to reach 11.5. However, in the case of S3M1 (Fig. 2. a), a rapid decrease was observed to a value of 10.8 after 400 min. This kinetic of reaction can be explained by the release of siliceous and/or aluminous species outcome from micaeous clays, present in M1 [6] which cause the decrease of the pH value but delay, in the same time, the polycondensation reaction. S1M2 and S3M2 (Fig. 2. b) exhibit a quite similar trend of decrease and reach 10.5 and 10.4, respectively. These values are close to the equilibrium constant $[Al(OH)_4^-)/Al(OH)_3]$ which indicates that there's no more charged aluminous species $(Al(OH)_4^-)$ in solution [8]. This fact also reveals the consolidation of the material. For S1M3 and S3M3 (Fig. 2.

c), the pH value decreases in the first 30 min, then it increases. This fact is probably due to the competition between the formation of a geopolymer network and a Si-rich gel [9]. The exceed of the siliceous species remains in solution which is responsible of the pH value. To conclude, the results are in accordance with the previous data (Fig. 1).

To summarize, FTIR spectroscopy and the following of the pH value during the formation have shown that, on the one hand, when the silicate solution exhibit a high intial Si/K (1.75), the alkaline solution is less depolymerized and, consequently, poorly reactive in mixture. In this case, the geopolymerization is governed by the reactivity of the metakaolin (S1M1 vs. S1M2 or S1M3). On the other hand, when the silicate solution exhibits a small Si/K (0.65 in this study), the alkaline solution is highly depolymerized and, consequently, highly reactive in mixture. In this case, the geopolymerization is only governed by the alkaline silicate solution and the role of metakaolin seems to be negligible (S1M1 vs. S3M1).

Effect of the alkaline solution and metakolin reactivity on the working properties of geopolymers. The various behaviors observed during the formation of the samples, mainly due to variations in metakaolin and alkaline solution reactivity could have an impact on the working properties of the synthesized materials. In the way to verify this hypothesis, the mechanical properties were evaluated by compression test after 7 days. The values of the compressive strength are reported in Table 2.

Tab. 2. Values of the compressive strength for each samples.

Sample	Compressive strength (MPa)
S1M1	34
S1M2	41
S1M3	30
S3M1	60
S3M2	61
S3M3	61

In the case of S1 alkaline solution, S1M2 exhibited the highest mechanical strength (approximately 41 MPa), followed by S1M1 and S1M3. The coexistence various networks in the case of M1 leads to the heterogeneous structure inducing a decline of mechanical properties. The high reactivity of M2 leads to the formation of a perfect network, yielding the best mechanical properties. In the case of M3, the low value of compressive strength can be explained by the presence of a gel which weakens the structure [6]. In the case of highly depolymerized alkaline solution (S3), the compressive strengths are higher and quite similar (about 60 MPa) for the three metakaolins. These results are in accordance with the fact that the reactivity of the mixture is governed by the alkaline solution and none by the metakaolin.

Conclusion

The role of two potassium alkaline solutions based on different commercial silicate solutions, with different initial Si/K molar ratios, with three different metakaolins was investigated. The results obtained with IRTF spectroscopy and the following of the pH value during the formation give evidence that:

(1) For a poorly reactive alkaline solution (high initial Si/K molar ratio), the metakaolin reactivity is the responsible of the generation of one or several networks which control the reaction of geopolymerization and affect the mechanical properties;

(2) When the alkaline solution is very reactive (low initial Si/K molar ratio), the depolymerized siliceous species enables the fast formation of oligomers and, consequently, govern the reaction of geopolymerization and the final properties of the materials regardless the properties of the used metakaolin.

References

[1] A. Autef, E. Joussein, A. Poulesquen, G. Gasgnier, S. Pronier, I. Sobrados, J. Sanz, S. Rossignol, Influence of metakaolin purities on potassium geopolymer formulation: The existence of several networks, J. colloids and interface Sci. 408 (2013) 43-53.

[2] P. Duxson, J.L. Provis, G.C. Lukey, S.W. Mallicoat, W.M. Kriven, Understanding *the* relationship between geopolymer composition, microstructure and mechanical properties, Colloids Surf. A. 269 (2005) 47-58.

[3] A. Gharzouni, E. Joussein, S. Baklouti, S. Pronier, I. Sobrados, J. Sanz , S. Rossignol, The effect of an activation solution with siliceous species on the chemical reactivity and mechanical properties of geopolymers. Submitted to Microporous and Mesoporous Materials.

[4] E. Prud'homme, P. Michaud, E. Joussein, J.M. Clacens, S. Rossignol, Role of alkaline cations and water content on geomaterial foams: Monitoring during formation, J. Non-Cryst. Solids. 357 (2011) 1270-1278.

[5] S. Delair, E. Prud'homme, C. Peyratout, A. Smith, P. Michaud, L. Eloy, E. Joussein, S. Rossignol, Durability of inorganic foam in solution: The role of alkali elements in the geopolymer network, Corrosion Sci., 59, (2012), 213-221.

[6] A. Autef, E. Joussein, A. Poulesquen, G. Gasgnier, S. Pronier, I. Sobrados, J. Sanz, S. Rossignol, Influence of metakaolin purities on potassium geopolymer formulation: The existence of several networks, J. colloids and interface Sci. 408 (2013) 43-53.

[7] X. X. Gao, A. Autef, E. Prud'homme, P. Michaud, S. Basma, E. Joussein, S. Rossignol, Synthesis of consolidated materials from alkaline solutions and metakaolin: existence of domains in the Al-Si-K/O ternary diagram, J. Sol-Gel Sci, 65, (2013), 220-221.

[8] D. Landolt, Corrosion et Chimie de surface des métaux, 3 ème edition, Press Polytechniques et Universitaires Romandes, Lausanne, 2003.

[9] A. Autef, E. Joussein, A. Poulesquen, G. Gasgnier, S. Pronier, I. Sobrados, J. Sanz, S. Rossignol, Evidence of a gel in geopolymer compounds from pure metakaolin, J. Sol-Gel Sci. Technol. 65 (2013) 220-229.

Acte de congrès 2 (ACTI2)

A. Gharzouni, E. Joussein, S. Baklouti, S. Pronier, I. Sobrados, J. Sanz, S. Rossignol

"Monitoring the structural evolution during geopolymer formation by ^{27}Al NMR"

Ceramic Engineering and Science Proceedings 36 (2016) 37-48.

MONITORING THE STRUCTURAL EVOLUTION DURING GEOPOLYMER FORMATION BY ^{27}Al NMR

Ameni Gharzouni[1, 2], Emmanuel Joussein[3], Isabel Sobrados[4], Jesus Sanz[4], Samir Baklouti[2], Basma Samet[2], Sylvie Rossignol[1]

[1]Science des Procédés Céramiques et de Traitements de Surface (SPCTS), Ecole Nationale Supérieure de Céramique Industrielle, 12 rue Atlantis, 87068 Limoges Cedex, France.
[2]Laboratoire de Chimie Industrielle, Ecole Nationale d'Ingénieurs de Sfax, 3038, Sfax, Tunisie
[3]Université de Limoges, GRESE EA 4330, 123 avenue Albert Thomas, 87060 Limoges, France.
[4]Instituto de Ciencia de Materiales de Madrid, Consejo Superior de Investigaciones Científicas (CSIC), C/Sor Juana Inés de la Cruz, 3, 28049 Madrid, Spain.
■corresponding author: sylvie.rossignol@unilim.fr, tel.: 33 5 87 50 25 64

ABSTRACT

Geopolymers are amorphous aluminosilicate binders showing good working properties. Despite the large and growing existing literature about these materials, the geopolymerization mechanism and the parameters that can influence still need a better and deeper understanding. The current study explores the effect of alkaline solution and metakaolin reactivities on geopolymer formation. To do this, several geopolymer samples were synthesized from two alkaline solutions and two metakaolins. The structural evolution of the formed geopolymers was investigated using ^{27}Al static NMR and FTIR spectroscopy during the formation. The mechanical properties were measured using compression tests. The NMR data show that the geopolymerization reaction involves the conversion of the Al (V), Al (VI) of metakaolin into Al (IV) under the effect of the alkaline solution. The dissolution and formation rates strongly depend on the reactivity of the used raw materials. Furthermore, a correlation was revealed between the amount of the formed Al (IV) determined from ^{27}Al NMR, the shift values from FTIR and compressive strengths data. The results indicate that the use of a highly reactive alkaline solution and in a lesser extent a highly reactive metakaolin may enhance the formation of the geopolymer network and, consequently, improve the mechanical strengths of the final materials.

INTRODUCTION

Geopolymer materials are a new class of ecomaterials. They result from the activation of an aluminosilicate source by an alkaline solution. The mechanism of geopolymerization is complicated and not yet fully understood due to the diversity of the raw materials that can be used. However, there is an agreement [1, 2, 3] that the reaction involves at first the dissolution of silicon and aluminiumspecies outcoming from the aluminosilicate source by the basic species of the alkaline solution. Indeed, the contact between the surface of the aluminisilicate particle and the activating solution initiates hydrolysis reactions depolymerizing the particle and liberating the network species into the solution, then a polycondensation reaction occurs leading to an amorphous three dimensional network. Metakaolin, due to its high reactivity and purity, is commonly used in fundamental studies of the geopolymerization reaction [4, 5, 6]. Furthermore, many techniques are available for the characterization of the process such as

FTIR spectroscopy in ATR mode which was extensively used to follow the geopolymerization reaction [7]. The shift of the Si-O-Si peak position,initially situated at about 980 cm^{-1}, to lower wavenumbers gives informations about the substitution of Si-O-Si bonds by Si-O-Al and therefore the polycondensation reaction [5, 6]. It was demonstrated that the shift values are characteristic of the formed network. According to previous work [6, 8], high shift values were obtained for not pure metakaolin inducing the combination of Si-O-M (M=Si, Al or K) from dissolved species and from the impurities of metakaolin. However, lower shift values were obtained for highly reactive metakaolins, indicating the formation of a single geopolymer phase between the networks formed in each sample.

On the other hand, nuclear magnetic resonance (NMR) is commonly used as an efficient and powerful technique providing structural information about silicates and aluminosilicates [9]. However, few studies [10, 11] have been carried out to monitor the structural evolution ofgeopolymers during the formation by NMR. In geopolymer materials, aluminium can vary between Al (IV), Al (V) and Al (VI) [12]. As a consequence, the change in the number of coordination of aluminium can provides important informations in the geopolymerization process.

In a previous paper [13], the effect of the raw materials reactivity on geopolymer properties was highlighted by elucidating the behavior of four different metakaolins in the presence of two potassium alkaline solutions. It was demonstrated that the reactivity of the alkaline solutions is controlled by the number of non bridging oxygen atoms and the amount of depolymerized species leading to the quick formation of oligomers and better mechanical properties of the resulting geopolymers. Furthermore, when the alkaline solution is notably reactive, the depolymerized siliceous species enable a fast oligomer formation and, consequently, govern the geopolymerization reaction and the final performances of the materials regardless of the properties of the used metakaolin.

The purpose of this study is to use NMR spectroscopy in order to further understand the effect of the reactivity of the alkaline solution and metakaolin on the geopolymer formation. To do this, the structural evolution of four mixtures based on metakaolin and alkaline solutions which differ in terms of reactivity were followed from mixing to consolidation by ^{27}Al static NMR and FTIR spectroscopy. The mechanical properties were assessed by compression test.

EXPERIMENTAL

Sample preparation

Samples were synthesized using two commercial potassium silicate solutions, denoted S1and S3 and with different Si/K molar ratios (1.75 and 0.65, respectively) and two metakaolins named M1 and M2 (Table I). Different amounts of potassium hydroxide pellets (VWR, 85.2% pure) were dissolved into the starting silicate solutions in order to maintain the Si/K molar ratio of the alkaline solutions at Si/K=0.5. Then, the metakaolins were added. Samples were named S1M1, S3M1, S1M2 and S3M2.

Table I. Characteristics and nomenclature of used raw metakaolins.

Metakaolin	M1	M2
Si/Al	1.17	1.19
d_{50} (µm)	10	6
BET value (m^2/g)	17	21
Wettability (µL/g)	570	1250

Characterization

High-resolution NMR experiments were performed at room temperature on a Bruker AVANCE-400 spectrometer, operating at 104.26 MHz (^{27}Al signal). MAS experiments were carried out for metakaolins powder samples which were spun at 10 KHz. The number of scan was 10 as previously used in previous work [6].

For fresh geopolymer reactive mixtures, ^{27}Al NMR in static mode was used. ^{27}Al is a quadrupolar nuclei (spin I>1/2) which means that there is an asymmetric charge distribution in the nucleus due to the non symmetry of protons and neutrons. The difficulty of quadrupolar nuclei involves a quick relaxation in liquid state and broadening at first and second order in solid state[14]. The energy levels are shifted by the quadrupolarinteraction which may limit the quantitative determination of the populations[15]. However, quadrupolar interaction can be neglected in liquid sate, as previously reported by Favier[16].The synthesized mixtures were deposed in a zirconia rotor (Ø= 4 mm). The ^{27}Al (I = 5/2) NMR spectra were recorded after π/8 pulse irradiation (1.5 µs) using a 1-MHz filter to improve the signal/noise ratio. In each case, 400 scans were collected. The time between acquisitions was set at 10 s to minimize saturation effects. The obtained spectra were deconvoluted. Figure 1 shows an example of deconvoluted ^{27}Al spectrum of S1M2 mixture at t=2h.

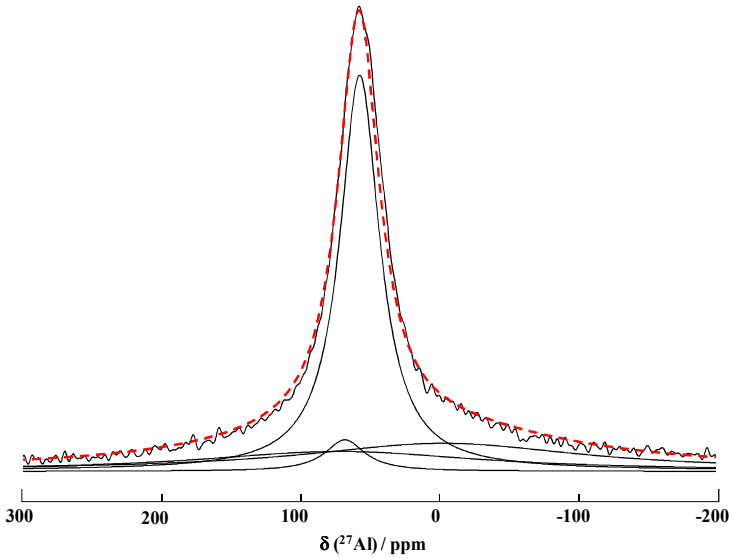

Figure 1. Example of deconvoluted ^{27}Al spectrum of S1M2 sample at t=2h(The blue line represents the experimental spectra, and the red line shows the fitted curve).

Fourier-transform infrared (FTIR) spectroscopy in ATR mode was used to investigate the structural evolution of the geopolymer mixtures. The FTIR spectra were obtained using a ThermoFisher Scientific Nicolet 380 infrared spectrometer. The IR spectra were gathered over a range of 400 to 4000 cm^{-1} with a resolution of 4 cm^{-1}. The atmospheric CO_2 contribution was removed with a straight line between 2400 and 2280 cm^{-1}. To monitor the geopolymer formation, a software was used to acquire a spectrum (64 scans) every 10 minutes for 13 hours. For comparison, the spectra were baseline-corrected and normalized [7].

The compressive strengths were tested using a LLOYD EZ20 universal testing machine with a crosshead speed of 0.1 mm/min. The compressive tests were made on five samples for every composition. The compressive strength values represent the average of the five obtained values and were expressed in MPa. The samples were cylindrical in shape with a diameter (Φ) of 15 mm and a height (h) of approximately 30 mm, and they were aged for 7 days in a closed mold at room temperature.

RESULTS AND DISCUSSION

^{27}Al static NMR during the formation

In the interest of a deeper understanding of geopolymerization mechanism and the influenceof the reactivity of the starting precursors on the reaction rate, four reactive mixtures based on various metakaolins (M1 and M2) and alkaline solutions (S1 and S3) were prepared and studied by ^{27}Al static NMR at different times of the formation (0, 2, 6 and 24 hours respectively). The obtained spectra for each sample are presented in Figure 2.Regardless of the sample, the spectra show a dominant phase at 60 ppm characteristic of Al (IV) and minor broad peak at -1.6 ppm corresponding to Al (VI) [17]. Moreover, it was noticed that the spectra are different from those of the starting metakaolins immediately when there is contact with the alkaline solution (from t=0h). In fact, the two used metakaolins were characterized by ^{27}Al MAS NMR in previous work 6. They exhibit typical ^{27}Al MAS NMR spectra of metakaolin [18, 19] showing three peaks at approimately 60, 31 and 1 ppm which are assigned to Al (IV), Al (V) and Al (VI), respectively. The presence of Al (VI) denotes the possible persistence of non dehydroxylated kaolinite and/or mica phase 6. Table II A summarizes the obtained data concerning the chemical shifts and the percentages of the curve area of the various contributions (Al (IV), Al (V) and Al (VI)) relative to the two metakaolins. Although the percentages of contribution area are close, it appears that M2 metakaolin contains more Al (IV) and Al (VI) compared to M1. Regardless of the mixture, when the metakaolin is mixed with the alkaline solution, an increase of the contribution's area relative to Al (IV) in the detriment of the disappearance of Al (V) and a remarkable decrease of Al (VI) initially present in the metakaolin are observed. These changes evidence the rapid and strong interaction between the two precursors. As time progresses, the peak relative to Al (IV) broadens denoting the formation of a geopolymer network, the intensity of the peak relative to Al (VI) decreases revealing the dissolution of metakaolin. However Al (V), initially present in the metakaolin, was not observed in any spectra. The disappearance of Al (V) indicates that it was consumed due to it high reactivity as has been, previously, demonstrated in literature [6, 20].

In order to understand the differences observed between the evolutions of the studied reactive mixtures versus time, all spectra were deconvoluted. The percentages of contributions area are reported in Table IIB. Only the peak the more intense situated at about 60 ppm, commonly characteristic of Al (IV) of geopolymer materials, was considered as Al (IV). To facilitate the exploitation of these data, the Al (VI) dissolution rate ($Al (VI)_{ti}$- $Al (VI)_{t0}$)/ $Al (VI)_{t0}$) as well as Al (IV) formation rate ($Al (IV)_{ti}$- $Al (IV)_{t0}$)/ $Al (IV)_{t0}$) for the different mixtures were plotted in function of time in Figure 3. The decrease of Al (VI) in geopolymer mixtures, all over the time, evidences the continuous dissolution of Al (V) and Al (VI) coming from the metakaolin. After 24 hours, the remaining Al (VI) for all samples are quite similar and are probably due to unreacted metakaolin [17]. Furthermore, it is shown that the samples exhibit different kinetics of metakaolin dissolution. Indeed, the Al (VI) dissolution seems to be faster in the case of S1M2 and S3M1 compared to S1M1 and S3M2. However, as previously described in Figure 1, S1M1 and S3M2 samples shows the lower Al (VI) contribution at the beginning of the reaction suggesting a rapid dissolution immediately when there is a contact with the alkaline solution. Attention should be drawn to the incongruence of metakaolin dissolution. In this context, Granizo et al., [21]have demonstrated that the first stage of metakaolin dissolution is rapid and not congruent and consequently [Al]>[Si]. Then, in the second stage of the reaction, the dissolution is synchronized and congruent with [Al]<[Si]. Finally at later age, incongruent dissolution leads to [Si]>[Al]. On the other hand, the increase of Al (IV) rate proves the formation of geopolymer network. The kinetics of Al (IV) formation follow the same trend (Figure 2B). It seems to be faster in the case of S1M2 and S3M1 compared to S1M1 and S3M2. Consequently, these data evidence that the geopolymer formation implies the conversion of the coordination of aluminium IV, V and VI in

metakaolin into aluminium IV. Moreover, it seems that the reaction rate strongly depends on the reactivity of the used precursors (alkaline solution and metakaolin).

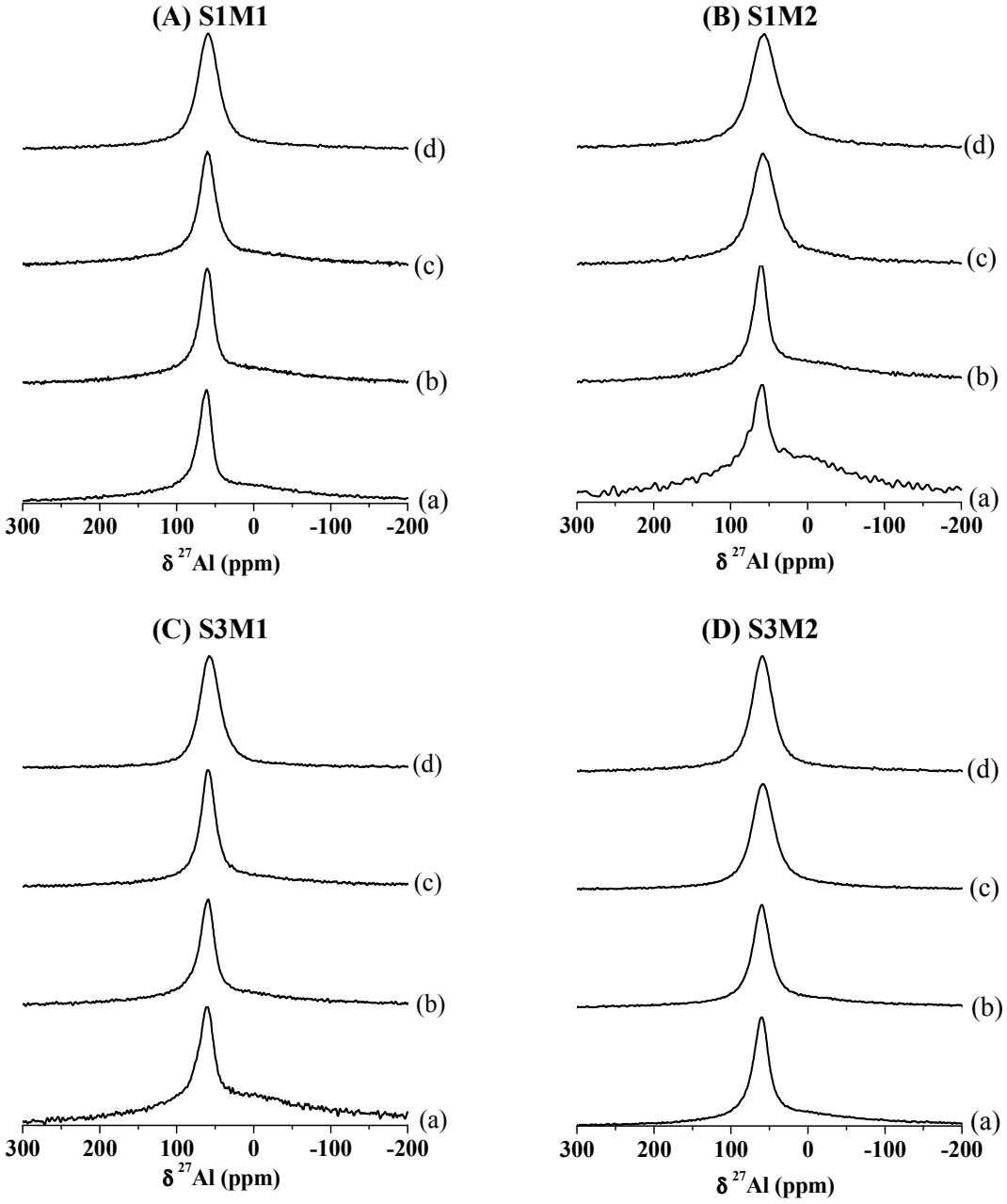

Figure 2. Recorded ^{27}Al NMR spectra in static mode at (a) 0, (b) 2, (c) 6 and (d) 24 hours of formation for the studied samples.

Table II. ^{27}Al NMR data of the various species for **(A)** the metakaolins and **(B)** geopolymer reactive mixtures at different times of the reaction.

(A)

Metakaolin	Percentage of the area curve of contribution (%)		
	Al (IV) ≈ -60 ppm	Al (V) ≈ -31 ppm	Al (VI) ≈ 1 ppm
M1	18.55	43.44	38.02
M2	21.09	35.68	43.22

(B)

Mixture	S1M1			S1M2		
	Percentage of the area curve of contribution (%)					
Time (h)	OC* ≈70 ppm	Al(IV) ≈60 ppm	Al(VI) ≈-1 ppm	OC* ≈70 ppm	Al(IV) ≈60 ppm	Al(VI) ≈-1 ppm
0	34.20	23.82	41.98	32.25	15.25	52.50
2	33.62	29.56	36.82	20.46	33.14	46.40
6	35.93	35.66	28.41	20.47	57.32	22.21
24	38.55	55.60	5.85	11.87	75.02	13.11
Mixture	S3M1			S3M2		
	Percentage of the area curve of contribution (%)					
Time (h)	OC* ≈70 ppm	Al(IV) ≈60 ppm	Al(VI) ≈-1 ppm	OC* ≈70 ppm	Al(IV) ≈60 ppm	Al(VI) ≈-1 ppm
0	26.46	19.50	54.04	21.53	50.72	27.75
2	27.78	49.34	22.88	12.36	65.63	22.01
6	17.76	62.05	20.19	3.83	84.34	11.83
24	6.04	82.20	11.76	2.97	94.31	2.72

*OC: other contributions

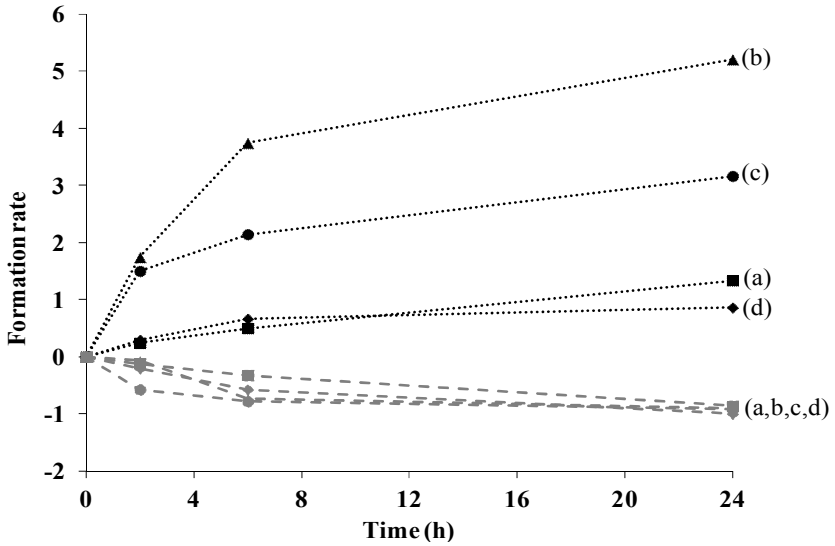

Figure 3. Evolution of (A) **(---)** the Al (IV) rate (Al $(IV)_{ti}$- Al $(IV)_{t0}$) / Al $(IV)_{t0}$) and (B) **(...)** the Al (VI) rate (Al $(VI)_{ti}$- Al $(VI)_{t0}$)/ Al $(VI)_{t0}$) for (a) (■) S1M1, (b) (▲) S1M2, (c) (●) S3M1 and (d) (♦) S3M2 mixtures in function of time.

Influence of the alkaline solution and metakaolin reactivities on the geopolymer network formation

To exacerbate the role played by of the alkaline solution as well as the metakaolin on the structural evolution during geopolymerization reaction, the dissolution rate ($Al(VI)_{mixture}$- $Al(VI+V)_{metakaolin}$)and the condensation rate ($Al(IV)_{mixture}$- $Al(IV)_{metakaolin}$) were plotted in function of time in Figure 3. S3M2 and S3M1 samples show the higher condensation rate (the higher amount of formed Al(IV) after 24 hours of the reaction) followed by S1M2 and S1M1(Figure 3A). However, close dissolution rates (amounts of consumed Al(IV) after 24 hours of the reaction) (Figure 3B) were observed. When S3 solution is used (S3M1 and S3M2 samples), rapid dissolution of metakaolin and condensation of geopolymer network are observed. This fact can be explained by the high reactivity of the alkaline solution and the metakaolin. In fact, according to previous ^{29}Si NMR study on the alkaline solutions[13], S3 starting silicate solution (lower Si/K ratio of 0.65) is mainly composed of Q^0 (monomer) and Q^1 (dimmer) species. Furthermore, the number of bridging oxygen atoms (NBO/T) of S3 (2.47) is also higherto S1 (1.45). Uncondensed species (Q^0 and Q^1) are known to be more reactive than the other species. Thus, S3 is considered to be more reactive than S1 since the silicate species are released and begin attacking Si–O and Al–O bonds more rapidly [22]. Moreover, the higher availability of reactive species allows an easy and rapid exchange with aluminosilicate species [23].The reactivity and the physical and chemical characteristics of metakaolin also play a crucial role in the dissolution since it directly depends on the available surface of metakaolin. It was demonstrated that the metakaolin with higher surface area accelerate the dissolution and the setting process [24, 25]. M2 having higher specific surface area (S_{BET}) and higher wettability value (Table I) is more reactive than M1.

The differences in the dissolution and formation rate observed between the mixtures based on various alkaline solutions and metakaolins suggest the formation of different networks depending on the reactivity of the used precursors and of the alkaline solutions.

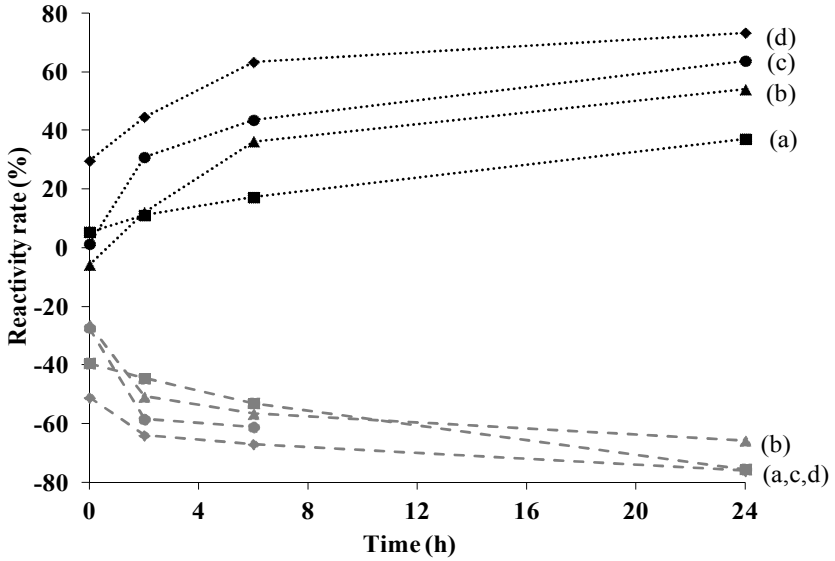

Figure 4. Evolution of (A) **(...)** the of Al (IV) reactivity rate ($Al(IV)_{mixture}$- $Al(IV)_{metakaolin}$)and (B) **(---)** the Al (VI+V) reactivity rate ($Al(VI)_{mixture}$- $Al(VI+V)_{metakaolin}$) for (a) (■) S1M1, (b) (▲) S1M2, (c) (●) S3M1 and (d) (♦) S3M2 mixtures in function of time.

The structural evolution of the four reactive mixtures was also followed by FTIR spectroscopy. Figure 6 shows the evolution of the Q^2 position peak versus time for the studied samples. It is noticed that using S3 alkaline solution, the initial band positions of the reactive mixtures (984 cm^{-1} and 987 cm^{-1} for S1M1 and S1M2, respectively) are lower than those

based on S1 alkaline solution (970 cm^{-1} and 973 cm^{-1} for S3M1 and S3M2, respectively). This fact can be explained by the presence of higher amount of non bridging oxygen and reactive species in the mixture outcoming from S3 alkaline solution in comparison with S1[13]Furthermore, the shift value decreases from 49 cm^{-1} and 28cm^{-1} in the case of S1M1 and S1M2 to 29 cm^{-1} and 21 cm^{-1} for S3M1 and S3M2, respectively. High shift value, obtained when less reactive alkaline solution is used, indicates the formation of various networks as previously demonstrated by Autef et al 5. However, lower shift values obtained for samples based on S3 solution evidence the possible formation of a unique phase. So, the use of a highly reactive metakaolin and in a greater extent a highly reactive alkaline solution seems to enhance the formation of a geopolymer network.

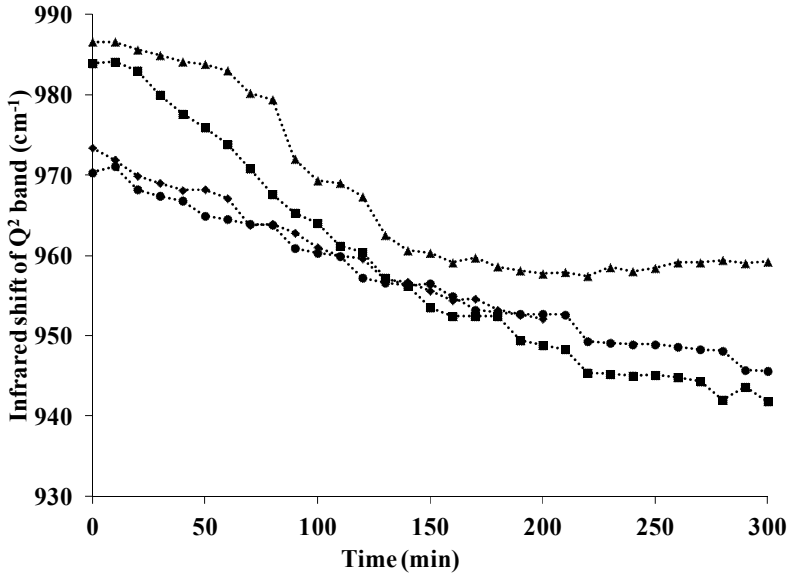

Figure 5. Evolution of the Q^2 position peak versus the time for (■) S1M1, (▲) S1M2, (●) S3M1 and (♦) S3M2 samples.

To verify these observations and further understand the effect of the reactivity of the alkaline solution and the metakaolin,the value of Q^2 band shift and compressive strengths obtained at 7 days were plotted versus the amount of Al (IV) formed after 24 hours determined from ^{27}Al NMR. Relationships (R^2=0.90 and R^2=0.88)between the amount of formed Al (IV), infrared shift values and compressive strengths, respectively, were shown. Regardless of used metakaolin, the higher amounts of formed Al (IV) obtained when S3 is used (64 % for S3M1vs 37% for S1M1 and 73% for S3M2 vs 54 % for S1M2) corresponds to smaller shift values (29 cm^{-1} for S3M1vs 49 cm^{-1} for S1M1 and 21 cm^{-1} for S3M2vs 29 cm^{-1} for S1M2) and higher compressive strengths (60 MPa for S3M1vs 34 MPa for S1M1 and 60 MPa for S3M2vs 41 MPa for S1M2). The higher amounts of Al (IV) associated with the smaller shift values, when S3 solution is used, denote that the formation of a geopolymer network is favored. This fact can be explained by the high reactivity of the species released from S3 (monomeric species), as discussed previously [13], facilitating and accelerating the exchange with the aluminosilicate species [13, 23]. A unique geopolymer phase leads to a homogenous structure and, thereby, better mechanical strength. However, the competition between different networks, as observed in the case of S1M1, weakens the structure.

.

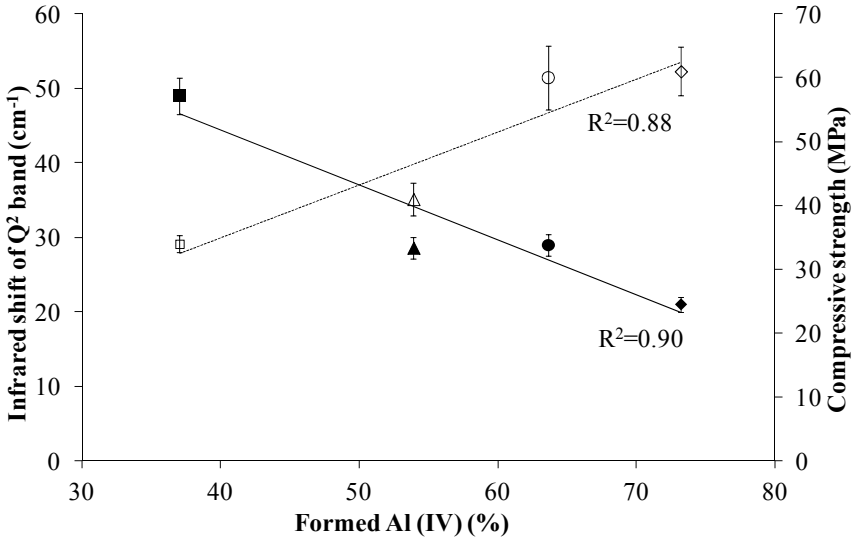

Figure 6. The value of (—) Q^2 band shift and (---) compressive strengths (7 days) versus the percentage of formed Al (IV) (24 hours) for (■) S1M1, (▲) S1M2, (●) S3M1 and (♦) S3M2 samples.

CONCLUSION

The behavior of two metakaolins in presence of two potassium alkaline solutions with different reactivity was investigated by ^{27}Al NMR during the geopolymer formation. The structural information comes from the coordination of Al atoms. Interactions between the silicate and aluminosilicate species were evident from an early stage of the reaction. As times progresses, the Al (V) and Al (VI) of metakaolin are converted to Al (IV). Moreover, different reaction rates were observed depending on the reactivity of the used raw materials. Indeed, a highly reactive alkaline solution favors the dissolution and the condensation reaction. The effect of the metakaolin reactivity is more significant when it is activated with a poorly reactive alkaline solution. Finally, a correlation was established between the amount of formed Al (IV) determined from ^{27}Al NMR, the shift values from FTIR and compressive strengths data. The results indicate that the use of a highly reactive alkaline solution (high NBO and monomeric species content) and / or a highly reactive metakaolin (high wettability and specific area) enhances the formation of the geopolymer network which may improve the mechanical properties of the final materials. In summary, the reactivity of the alkaline solution and in a lesser extent the metakaolin are key parameters to control the reaction rate and thereby the final properties of geopolymer materials.

REFERENCES

[1]J. L Provis, J. S. J van Deventer,Geopolymerisation kinetics 2.Reaction kinetic modelling.Chemical Engineering Science, **62**, 2318–2329 (2007).
[2]J. L Provis, J. S. J van Deventer, Geopolymerisation kinetics: 1. In situ energy dispersive X-ray diffractometry.Chemical Engineering Science, **62**, 2309–2317 (2007).
[3]J. L Provis, Geopolymers and other alkali activated materials:why, how, and what? Materials and Structures, **47**, 11-25(2014).
[4]P. De Silva, K. Sagoe-Crenstil, V. Sirivivatnanon, Kinetics of geopolymerization: Role of $Al_2O_3$and SiO_2, Cement and Concrete Research, **37**, 512–518(2007).

[5]A. Autef, E. Joussein, A. Poulesquen, G. Gasgnier, S. Pronier, I. Sobrados, J. Sanz, S. Rossignol,Influence of metakaolin purities on potassium geopolymer formulation: The existence of several networks,Journal ofColloids and Interface Science,**408**,43-53(2013).

[6]A. Autef, E. Joussein, A. Poulesquen, G. Gasgnier, S. Pronier, I. Sobrados, Role of metakaolin dehydroxylation in geopolymer synthesis, Powder Technology, **250**, 33-39 (2013).

[7]E.Prud'homme, P. Michaud, E. Joussein, J.M. Clacens, S. Rossignol,Role of alkaline cations and water content on geomaterial foams: Monitoring during formation, Journal of Non-Crystalline Solids, **357**,1270-1278 (2011).

[8]A. Gharzouni, E. Joussein, S. Baklouti, S. Pronier, I. Sobrados, J. Sanz , S. Rossignol, The effect of an activation solution with siliceous species on the chemical reactivity and mechanical properties of geopolymers, Journal of Sol-Gel Science, article in press (2014).

[9]G. Engelhardt, D. Michel, High-Resolution Solid-State NMR of Silicates and Zeolites, *John Wiley and Sons*, New York, 1987.

[10]A. Favier, G. Habert, J.B. d'Espinose de Lacaillerie, N. Roussel, Mechanical properties and compositional heterogeneities of fresh geopolymer pastes,Cement and Concrete Research, **48**, 9–16 (2013).

[11]P. S. Singh, M. Trigg, I.Burgar, T.Bastow, Geopolymer formation processes at room temperature studied by ^{29}Si and ^{27}Al MAS-NMR, Materials Science and Engineering: A, **396**, 392–402 (2005).

[12]M. R. Rowles, J. V. Hanna, K. J. Pike, M. E. SmithandB. H. O. Connor, ^{29}Si, ^{27}Al, ^{1}H and ^{23}Na MAS NMR Study of the Bonding Character in Aluminosilicate Inorganic Polymers,Applied Magnetic Resonance, **32**, 663-689(2007).

[13]A. Gharzouni, E. Joussein, S. Baklouti, B. Samet, Effect of the reactivity of alkaline solution and metakaolin on geopolymer formation, Journal of Non-Crystalline Solids,**410**,127-134(2015).

[14]D. Iuga, C. Morai, Z. Gan, D. R. Neuville, L. Cormier D. Massiot, NMRHeteronuclear Correlation between Quadrupolar Nuclei in Solids,Journal of the American Chemical Society, American Chemical Society, **127**, 11540-11541 (2005).

[15]P. P. Man and J. Klinowski, Quantitative Determination of Aluminium in Zeolites by Solid-state ^{27}AI N.m.r.Spectroscopy, Journal of the Chemical Society, Chemical Communications 19, 1291-1294 (1988).

[16]A. Favier, Mécanisme de prise et rhéologie de liants géopolymères modèles,PhDthesis, University of Paris-Est, 2013.

[17]R. A. Fletcher, K. J. D. MacKenzie, C. L. Nicholson, S. Shimada, The composition rage of aluminosilicate geopolymers, Journal of the European Ceramic Society, **25**, 1471-1477 (2005).

[18]I. W. M. Brown, K. J. D. Mackenzie, M. E. Bowden andR. H. Meinhold, Outstanding Problems in the Kaolinite-Mullite Reaction Sequence Investigated by ^{29}Si and ^{27}Al Solid-state Nuclear Magnetic Resonance: 11, High-Temperature Transformations of Metakaolinite, Journal of the American Ceramic Society, **68**, 298–301 (1985).

[19]P. Duxson, G. C. Lukey, F. Separovic and J. S. J. van Deventer, Effect of alkali cations on Aluminum incorporation in geopolymeric gels, Industrial and Engineering Chemistry Research,**44**,832-839 (2005).

[20]J. V. Walther, Relation between rates of aluminosilicate mineral dissolution, pH, temperature, and surface charge, American Journal Science, **7**, 296-693 (1996).

[21]N. Granizo, A. Palomo, A. Fernandez-Jiménez, Effect of temperature and alkaline concentration on metakaolin leaching kinetic.Ceramics International, 40, 8975–8985 (2014).

[22]X. Yao, Z. Zhang, H. Zhu, Y. Chen, Geopolymerization process of alkali–metakaolinite characterized by isothermal calorimetry, ThermochimicaActa, **493**, 49–54 (2009).

[23]M.R. North and T.W. Swaddle, Kinetics of silicate exchange in alkaline aluminosilicate solutions, Inorganic Chemistry, **39**, 2661-2665 (2000).

[24]L. Weng, K. S. Crentsil, T. Brown, S. Song, Effects of aluminates on the formation of geopolymers Materials, Science and Engineering B, **117**, 163–168 (2005).

[25]A. Autef, Formulation géopolymère: influence des rapports molaire Si/K et Si/Al sur les réactions de polycondensation au sein de gels aluminosilicatés,PhDthesis, University of Limoges, 2013.

Chapitre

L. Vidal, A. Gharzouni, S. Rossignol

"Alkaline silicate solutions: An overview of their structure, reactivity and applications"

2nd edition of the Handbook of Sol-Gel Science and Technology, submitted.

CHAPTER
Alkaline solutions: an overview of structure, reactivity and applications

L. Vidal, A. Gharzouni, E. Joussein, S. Rossignol

Abstract

Alkaline silicate solutions have a lot of applications including sand agglomeration and geopolymer production. To ensure the widespread of these applications, it is necessary to identify the parameters controlling their reactivity and interactions with other materials like sand and metakaolin. Concerning the solution reactivity, it has been evidenced that the key parameters are the Si/M molar ratio and the water amount. Then, it was highlighted that the most reactive alkaline solutions have alkali cation concentrations comprised between 4.5 and 9.5 mol/L. For the sand agglomeration application, it was shown that the used solutions are highly polymerized. In addition, the drying temperature and method have an influence on the silicate distribution in the final material. Concerning geopolymer formation, it was evidenced that a highly reactive alkaline solution favors the formation of a geopolymer network by increasing the formation rate of $Al^{(IV)}$ up to 80% which improve the working properties of the final materials. In fine, knowledge of the key parameters controlling the alkaline silicate solution reactivity is important to determine the adequate solution to use for a given application.

INTRODUCTION

Alkaline silicate solutions, also called water glass, are of great interest for several industrial applications (e.g., sealants, deflocculants or binders) (Johnson et al. 2008; Tognonvi et al. 2010). Recently, two of the main applications are related to their use as alkaline reactants in geopolymer materials (Bourlon 2011, Autef et al. 2012) or as binder for sand agglomeration (Lucas et al. 2011; Tognonvi et al. 2012).

The first application concern sand consolidation which is mainly employed in oil industries. These methods are using in particular alkaline silicate solutions or resins as a binder to maintain the permeability between the consolidated zones (Talaghat et al. 2009). Agglomeration of sand by sodium silicate solution is also used in fuse technology (Gurevich

1990; Vivier 2000). The purpose of the sand in an electric fuse is to absorb the electric arc energy and disperse metal gaseous vapors when a fuse element melts during the short circuit. For high voltage fuses, a binder is necessary to reinforce the sand cohesion within the fuse. The sodium silicate solution is commonly used to agglomerate sand because it is an economical water-soluble and environmental-friendly binder. Moreover, its use as a binder to consolidated sand does not generate a release of CO_2. The main parameters for silicate solutions used for agglomeration are: the molar ratio SiO_2/Na_2O, solid content, viscosity and pH (Keeley 1983).

The second application of silicate solutions is their use as activation solutions for geopolymer materials. Indeed, geopolymer have garnered increasing interest because of their synthesis methods, high working performance (Van Jaarsveld et al. 1999), wide range of applications (Krivenko 1997) and low environmental impact (Liew et al. 2011). These binders result from the activation of an aluminosilicate source by an alkaline solution at a temperature less than 100 °C (Davidovits 2008). The mechanism consists of the dissolution of reactive aluminosilicate precursors under the effect of the alkaline solution to form oligomers ($Si[OH]_4$ and $Al[OH]^-_4$). Then, a polycondensation reaction links the oligomers generating an amorphous three-dimensional network. So, it is interesting to study the structure of alkaline solution since it affects the working properties of final geopolymer materials.

To guarantee the widespread of silicate applications, a deeper comprehension of the structure and the reactivity of alkaline solutions is necessary. The silicate solutions contain silicate dioxide (SiO_2) and alkali oxide (such as Li_2O, Na_2O, K_2O) and are commonly prepared by dissolution of an alkali-silicate glass in water or by using steam or pressure (Tognonvi et al. 2010). Alkali-silicate glasses are prepared through a reaction between silica and sodium carbonate or sodium sulfate (Iler 1979). Another method to prepare these solutions is to dissolve silica fume in an alkaline solution (Harris and Knight 1983a; Steins 2014). Several techniques can be used to determine the various silicate species in the solutions. Fourier transform infrared (FTIR) spectroscopy was used in various studies to determine the Q^n species in the silicate solutions by following the position of the broad peak attributed to the asymmetric stretching of the Si-O-Si bonds (Tognonvi et al. 2012). However, FTIR spectroscopy is not a quantitative analysis. That is why, ^{29}Si NMR has been widely used to characterize the silicate solutions (Harris and Knight 1983b; Bourlon 2011). This approach allows distinguishing and quantifying the various Q^n species. Engelhardt et al. (1975) introduced the Q^n notation for silicate species where Q refers to the silicon atom and n (from 0

to 4) refers to the bridging oxygen atoms. Moreover, this technique permits detecting cyclic species and weak variations of the silicate species amounts. These solutions were also characterized using Raman spectroscopy (Halazs et al. 2007; Hunt et al. 2011). This technique revealed the contributions of monomers and oligomers in silicate solutions and glasses (Aguiar et al. 2009; Hunt et al. 2011 and allowed identifying the vibrations of 3-, 4- or 5-membered rings (Aguiar et al. 2009; Le Losq and Neuville 2013). In fine, the Si/M molar ratio and the water content seem to be key parameters for silicate solutions. Thus, the objective of this work is to determine the main parameters controlling the reactivity of various silicate solutions and exacerbate the effect of the reactivity on the sand agglomeration or in presence of metakaolin for geopolymerization application.

ALKALINE SOLUTION REACTIVITY: STRUCTURAL INVESTIGATION

To elucidate the interaction of silicate solutions with different materials (sand, clays...), the structure of these solutions should be defined. Indeed, knowledge of the different entities depending on various parameters may allow predicting the reactivity of these solutions. To do this, different spectroscopic techniques (FTIR, Raman and ^{29}Si NMR spectroscopies) were used. FTIR spectroscopy allows evidencing the presence of the various Q^n species in the solutions. Raman spectroscopy was used as a complementary technique. The presence of oligomers and rings was highlighted by this analysis. Finally, ^{29}Si NMR allows quantifying these various entities. In this study, various sodium and/or potassium alkaline silicate solutions were investigated as referenced in Table 1. The main parameters studied are the type of cation and the Si/M molar ratio with M = K and/or Na (0.5, 1.0 and 1.7). The lab-prepared solutions were obtained by the dissolution of KOH or NaOH pellets (85.2% and 97% purity respectively) and amorphous silica (99.9% purity) in osmotically purified water at room temperature, as described in a previous work (Autef et al. 2012). The used nomenclature (Table 1) is $^{x}SiM_{y}$, where x is the Si/M molar ratio, M is the alkali cation (Na or/and K) and y is the manufacturing process (C = commercial and L = lab-prepared).

TABLE 1: NOMENCLATURE AND CHARACTERISTICS OF THE VARIOUS STUDIED SOLUTIONS

Cation	Si/M	Nomenclature	% water	Density
Na	1.7	$^{1.7}SiNa_C$	62.7	1.37
	1.0	$^{1.0}SiNa_L$	63.0	1.37
	0.5	$^{0.5}SiNa_L$	55.3	1.51
K	1.7	$^{1.7}SiK_C$	76.0	1.18
	1.0	$^{1.0}SiK_L$	57.8	1.36
	0.5	$^{0.5}SiK_C$	48.0	1.65
Na+K	1.7	$^{1.7}SiNaK_C$	62.0	1.38

A preliminary characterization was performed using FTIR, ^{29}Si MAS-NMR and Raman spectroscopies to define the structure and compare the starting silicate solutions used.

FTIR spectroscopy in ATR (attenuated total reflectance) mode was performed to characterize the solutions using a ThermoFisher Scientific Nicolet 380 infrared spectrometer. The IR spectra corrected and normalized, shown in Figure 1 A and B, were collected over a wavenumber range of 4000 to 500 cm^{-1} with a resolution of 4 cm^{-1}. The various contributions observed on the different spectra are shown in Table 2 (Muroya 1999; Halazs et al. 2007, 2010; Tognonvi et al. 2012). Irrespective of the solution, the bands at 3200 and 1640 cm^{-1} are attributed to the OH vibration band (ν_{OH}) and to the bending vibration of water molecules (δ_{OH}) respectively. A broad contribution near 1000 cm^{-1} due to the asymmetric stretching of Si-O-Si bonds (ν_{as}Si-O-Si) (Muroya 1999; Tognonvi et al. 2012) is observed. Moreover, $^{1.7}SiNa_C$ and $^{1.7}SiNaK_C$ exhibit quite similar spectra with a peak at about 1003 cm^{-1} and a shoulder at 1100 cm^{-1} which are attributed to Q^2 and Q^3 units, respectively (Tognonvi et al. 2012; Gharzouni et al. 2014). The same bands are observed in the case of $^{1.7}SiK_C$ with a slight shift of Q^2 contribution to higher wavenumber (1015 cm^{-1}). $^{1.0}SiM_L$ spectra exhibit similar trend with a decrease of the intensity of Q^3 band and a slight shift of Q^2 to lower wavenumbers (991 and 994 cm^{-1} for $^{1.0}SiNa_L$ and $^{1.0}SiK_L$ respectively).

For the $^{0.5}SiNa_L$ solution, there are two contributions located near 967 and 914 cm^{-1}, which are assigned to the Si-O-Si bonds in Q^1 and Q^0 units respectively. The same contributions are observed in the case of $^{0.5}SiK_C$ but the Q^0 band is shifted to 902 cm^{-1}. The displacement of the Si-O-Si peak position to a lower wavenumber linked to the appearance of the Q^0 band may be explained by a depolymerization phenomenon. It was demonstrated that a decrease of the Si/M ratio (i.e. an increase of the pH value) favors depolymerization due to the breaking of

the Si-O-Si bonds to create Si-O$^-$ groups (Lucas et al. 2011). Thus, for a low Si/M ratio, there is formation of lower-order siliceous species (Q^1 and Q^0) to the detriment of higher-order species (Q^4, Q^3 and Q^2), the solution is depolymerized and contains a majority of Q^0 and Q^1 species (Gharzouni et al. 2014, Goudarzi 2013). However, for a high Si/M ratio, the solution is more polymerized, and the major species are the Q^2 and Q^3 entities. Moreover, whatever the Si/M molar ratio considered, the potassium silicate solutions exhibit the Si-O-Si peak position at a higher wavenumber than the sodium silicate solutions. This phenomenon may be explained by the fact that the potassium silicate solutions are slightly more polymerized than sodium silicate solutions.

So, the polymerization degree of the various silicate solutions is known depending on the alkali cation and the Si/M molar ratio. However, the FTIR investigation does not allow distinguishing the various silicate species.

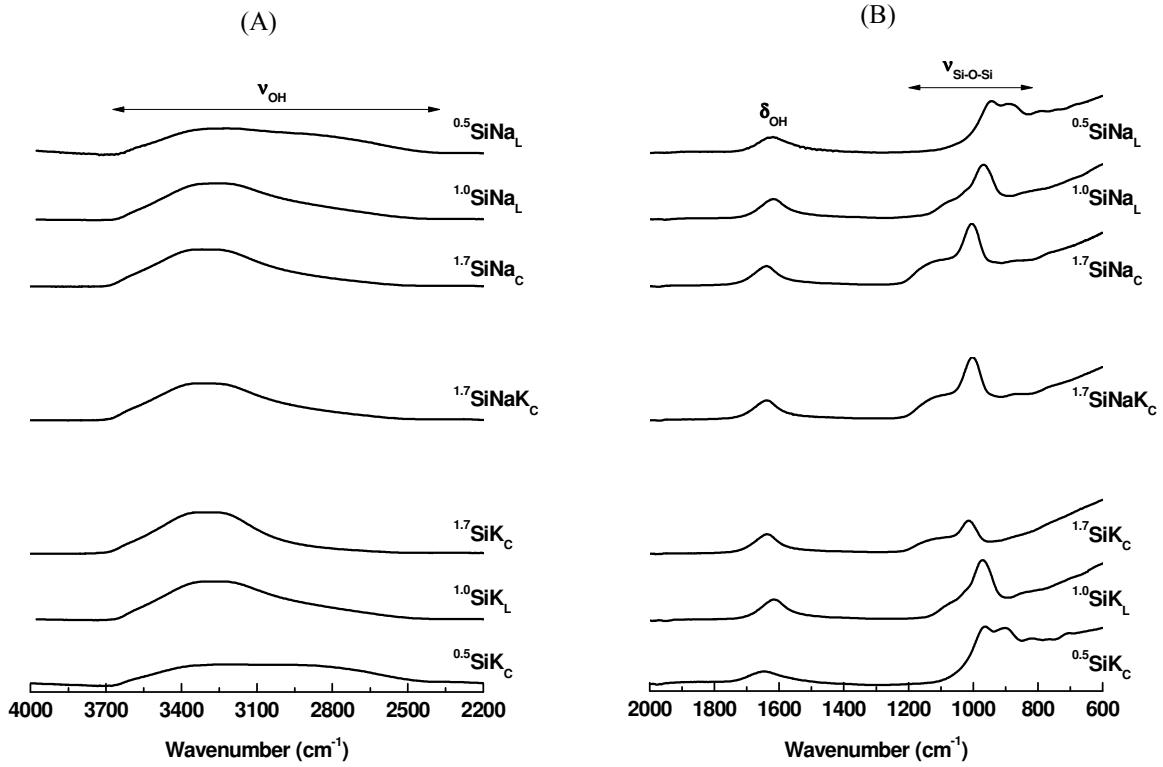

Figure 1. FTIR spectra of sodium and/or potassium silicate solutions with different Si/M molar ratios (1.7, 1.0 and 0.35) between (A) 4000 and 2200 cm^{-1} and (B) 1800 and 600 cm^{-1} .

(A)

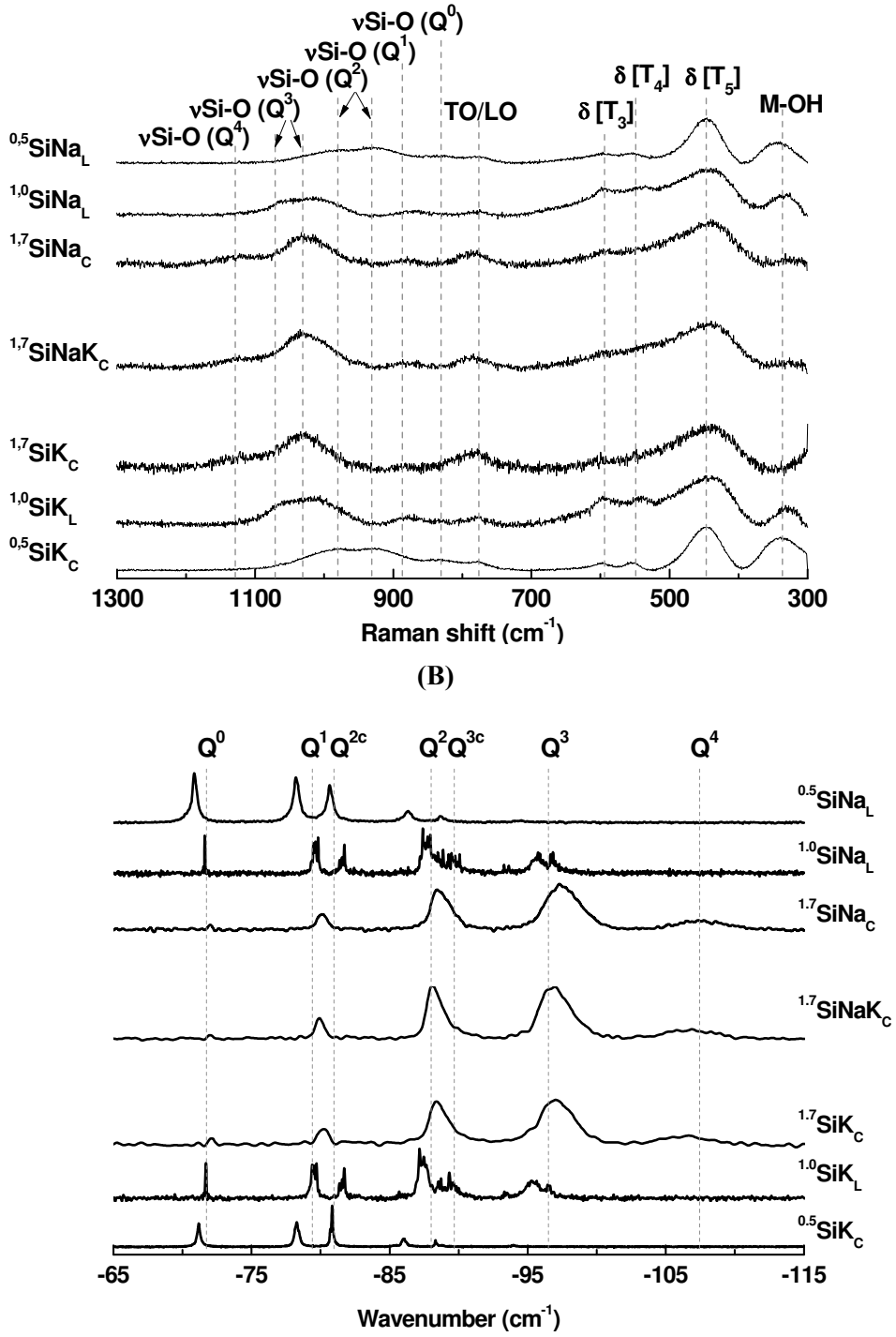

Figure 2. (A) Raman spectra and (B) ^{29}Si NMR spectra of sodium and/or potassium silicate solutions with different Si/M (M=Na or/and K) molar ratios (1.7, 1.0 and 0.35).

TABLE 2. VIBRATIONAL FREQUENCIES OF SILICATE SPECIES (IR = FTIR SPECTROSCOPY, R = RAMAN SPECTROSCOPY).

Contribution	Position (cm^{-1})	References
δOH	1640 (IR)	Muroya, 1999
ν_sSi-O-Si (Q^4)	1120 - 1230 (R) 1154 (IR)	Tan et al., 2004; Tognonvi et al., 2012
ν_sSi-O-Si (Q^3)	1000 - 1100 (R) 1099 (IR)	Hunt et al., 2011; Tognonvi et al., 2012
ν_sSi-O-Si (Q^2)	920 - 1000 (R) 1011 - 1014 (IR)	Tognonvi et al., 2012; Belova et al., 2015
νSi-O^-(M^+)	885 - 928 (IR)	Tognonvi et al., 2012
ν_sSi-O-Si (Q^1)	850 - 920 (R)	Mysen et al., 1982; Malfait et al., 2008
ν_sSi-O^- (Q^0)	800-875 (R)	Chligui, 2010; Hehlen and Neuville, 2015
ν_s(Na)O-Si-O(Na)	830 (IR)	Halazs et al., 2007, 2010
ν_sSi-O-Si	820 (IR)	Muroya, 1999
TO/LO (Si-O-Si)	650 - 850 (R)	Chligui, 2010
ν_s(dimers/oligomers)	600 (R)	Hunt et al., 2011
D_2 (δ[T_3])	587 - 606 (R)	Zotov et al., 1999; Le Losq and Neuville, 2013
D_1 (δ[T_4])	453 - 550 (R)	Geissberger and Galeener, 1983; Zotov et al., 1999
δ[$T_{5\ and\ more}$]	400 - 490 (R)	Geissberger and Galeener, 1983; Aguiar et al., 2009
M-O (network modifiers)	340 – 360 (R)	Hehlen and Neuville, 2015

To determine the presence of rings and oligomers in the different silicate solutions depending on the Si/M ratio and the alkali cation, Raman spectra were recorded using a T64000 Horiba-Jobin-Yvon spectrophotometer with 514 nm laser excitation operating at a power of 30 mW (Figure 2A) (Hunt et al. 2011). The various contributions observed in the different spectra are presented in Table 2 (Aguiar et al. 2009; Hunt et al. 2011). For Si/M greater than 1 ($^{1.7}SiM_C$), (Figure 2A) the contributions due to the stretching of Q^2 ($Si(OH)_2O_2^{2-}$), Q^3 ($Si_2O(OH)_5O^-$, $Si_3O_3(OH)_4O_2^{2-}$) and Q^4 species are observed (Tan et al. 2005; Hunt et al. 2011). The spectra also exhibit a contribution at 787 cm^{-1} attributed to the TO/LO modes. Weak contributions due to the vibrations of M-O bonds are observed near 330 cm^{-1} (Hehlen and Neuville 2015). The ring breathing modes of the 3, 4 and 5 and more-membered rings (denoted as δ[T_3], δ[T_4] and δ[$T_{5\ and\ more}$]) are located near 600, 490 and 450 cm^{-1} respectively (Geissberger and Galeener 1983; Aguiar et al. 2009). The contributions of the Q^3 and Q^4 species reveal the high polymerization degree of the solutions, which is in accordance with the previous results.

For Si/M = 1 ($^{1.0}SiM_L$), there is an increase of the contributions of the Q^2 units, the oligomers and the $\delta[T_3]$, $\delta[T_4]$ and $\delta[T_{5\ and\ more}]$ and the M-O band. This phenomenon is associated with the disappearance of the Q^4 species. This fact evidences the depolymerization of the solutions.

For a Si/M lower than 1 ($^{0.5}SiM_y$), the bands attributed to the vibration of the M-O bonds and the $\delta[T_5]$ seem to be more intense. An increase in the Q^2 species contribution and a decrease in the TO/LO mode and Q^3 species bands are also noted. The $\delta[T_{3\ and\ 4}]$ (3- and 4-membered rings) and the stretching of oligomers contributions seem to be more intense. These data reveal that the solutions are highly depolymerized and confirm the previous observations.

Thus, Raman spectroscopy provides complementary information to the previous results. It exhibits the M-O bonds presence for Si/M ratios less than 1, i.e., for highly depolymerized solutions. The presence of the rings may be an important factor concerning the reactivity of the silicate solutions. Moreover, FTIR and Raman investigations evidenced that the polymerization state of the solutions depends on the cation type and the Si/M molar ratio. However, these techniques do not allow a quantification of the different silicate species.

To obtain additional details about the molecular structure and the amounts of the various silicate species, high-resolution MAS-NMR experiments were performed at room temperature on a Bruker AVANCE-400 spectrometer operating at 79.49 MHz (^{29}Si signal). The ^{29}Si (I = 1/2) MAS-NMR spectra were recorded after a p/2-pulse irradiation (4 ls) using a 500 kHz filter to improve the signal/noise ratio. In each case, 400 scans were collected. The time between acquisitions was set to 10 s to minimize saturation effects. The ^{29}Si NMR spectra of the solutions are plotted in Figure 2B. For all solutions, the spectra exhibitss the different Q^0, Q^1, Q^2, Q^3 and Q^4 species contributions near -72, -80, -88, -97, and -106 ppm, respectively (Bourlon 2011; Nordström et al. 2011). Broad bands associated with Q^4, Q^3 and Q^2 species are observed in the spectra of $^{1.7}SiM_C$ solutions. The broad peaks are mainly due to a continuous range in the number of bridging oxygen atoms, with distorted sites having bonding characteristics between those of the well-defined tetrahedra in a silicate crystal (Schmidt et al. 2001). When the Si/M ratio decreases from 1.7 to 1, the contributions shifts to higher chemical displacements and Q^4 species disappear in favor of Q^{2c} and Q^{3c} species. This fact is more pronounced in the case of $^{0.5}SiM_C$ solutions and is characteristic of a variation of the protonation degree of the silicon atoms (Harris and Knight 1983b; Bourlon 2011). For Si/M greater than 1, the predominance of Q^2, Q^3 and Q^4 species indicates that the solutions are

polymerized. For Si/Na less than 1, the major species are Q^0 and Q^1 entities, indicating that the solutions are depolymerized (Svensson et al. 1986). The chemical shift (δ) and the percentage area (%A) of the different contributions obtained by deconvolution of each solution spectra are presented in Table 3.

TABLE 3. DECONVOLUTIONS OF ^{29}SI NMR SPECTRA OF SILICATE SOLUTIONS.

		Silicate species						
		% Area (δ (ppm))						
		Q^0	**Q^1**	**Q^{2c}**	**Q^2**	**Q^{3c}**	**Q^3**	**Q^4**
Solutions	**$^{1.7}$SiNa**	0.6 (-72.0)	5.3 (-80.1)	/	29.4 (-88.9)	/	51.5 (-97.7)	13.2 (-107.6)
	$^{1.0}$SiNa	2.6 (-71.6)	13.2 (-79.6)	37.9 (-81.6)	5.9 (-87.8)	26.5 (-89.7)	13.9 (-96.2)	/
	$^{0.5}$SiNa	27.3 (-70.9)	29.7 (-78.2)	11.2 (-80.7)	26.3 (-86.3)	1.9 (-88.7)	3.6 (-94.5)	/
	SiNaK	0.7 (-72.0)	6.4 (-79.9)	/	29.2 (-88.8)	/	49.5 (-97.2)	14.3 (-106.7)
	$^{1.7}$SiK	1.0 (-72.1)	6.7 (-80.2)	/	29.0 (-88.7)	/	51.2 (-97.1)	12.1 (-106.2)
	$^{1.0}$SiK	3.4 (-71.7)	14.3 (-79.5)	31.2 (-81.6)	6.7 (-87.5)	26.7 (-89.5)	17.7 (-95.6)	/
	$^{0.5}$SiK	24.5 (-71.2)	29.9 (-78.3)	12.4 (-80.8)	26.5 (-86.0)	1.9 (-88.5)	4.8 (-94.0)	/

The decrease in the Si/M molar ratio results in the increase of the amount of depolymerized species from approximately 1 to 25% (Q^0) and from 6 to 30% (Q^1) for Si/M between 1.7 and 0.5, respectively. However, there is a decrease in the high order species (more polymerized) Q^2, Q^3 and Q^4 when the Si/M ratio decreases (Table 3). Moreover, the decrease in the Si/M molar ratio implies an increase in the cyclic silicate species. For Si/M equal to 1.7, no cyclic species are noted whereas, for a Si/M of 0.5, the Q^{2c} and Q^{3c} entities are observed (around 12 and 2%, respectively). Thus, a decrease in the Si/M ratio leads to the depolymerization of the solutions. This fact is linked to the appearance of cyclic species. Moreover, whatever the Si/M molar ratios, the sodium and potassium silicate solutions exhibit similar spectra. However, the contributions of the potassium silicate solutions are located at slightly higher chemical displacement than the sodium silicate solutions. This phenomenon may be explained by a variation in the protonation degree of the silicon atoms (Bourlon 2011).

Therefore, ^{29}Si MAS-NMR experiments provide information about the influence of the cation type and the Si/M molar ratio. The Si/M molar ratio is a crucial parameter which controls the amount and the nature of silicate species present in the alkaline solutions, and an important change of these entities is observed for a Si/M of approximately 1.0. Furthermore, the effect of the cation seems to be less pronounced.

Thus, the existence of monomers and/or oligomers was revealed; however, the type of cyclic entities was not distinguished. The presence of these species in the solution allows the determination of the reactivity degree of the solution.

To further investigate the influence of the Si/M molar ratio, the variation of the Si-O-Si peak position as a function of the silicon concentration is plotted in Figure 3A for the different solutions. For each considered cation and for a given Si/M ratio, all the solutions show a linear variation with the silicon concentration. The slope values vary between 3.0 and 5.7 for a Si/M molar ratio of 1.7 to 0.5 respectively. Furthermore, a lower Si/M ratio indicates a higher slope. For example, for a similar Si/M molar ratio of 1.7, the Si concentration (g/L) vs. Si-O-Si (Q^2) peak positions (cm^{-1}) are [175 - 1003] and [90 - 1014] for $^{1.7}SiNa_C$ and $^{1.7}SiK_C$ respectively. For $^{1.7}SiK_{C,}$ the position of the Si-O-Si band at a slightly higher wavenumber is linked to the presence of more polymerized species in this solution (Gharzouni et al. 2014). Similarly, for a Si concentration of approximately 135 g/L, the $^{0.5}SiNa_L$, $^{1.0}SiNa_L$ and $^{1.7}SiK_L$ solutions exhibit a Si-O-Si band at 967, 991 and 1008 cm^{-1} respectively. Thus, for a constant Si concentration, an increase in the wavenumber is observed when the Si/M ratio increases. Bass et al. (1999) showed that at a constant silica concentration, the Si-O-Si peak shifted to a lower frequency as the silica/alkali ratio decreased. This result was attributed to the condensation of monomers to more complex anions when the silica/alkali ratio increased. Other authors also observed that the increase in the Si/M ratio implied the presence of more polymerized species in the solutions (Svensson et al. 1986; Aguiar et al. 2009). Thus, for the same concentration and for each considered cation, a higher Si/M ratio indicates a more polymerized solution.

Consequently, the increase in the Si/M molar ratio leads to the polymerization of the solution. The use of the potassium cation implies the presence of slightly more polymerized species.

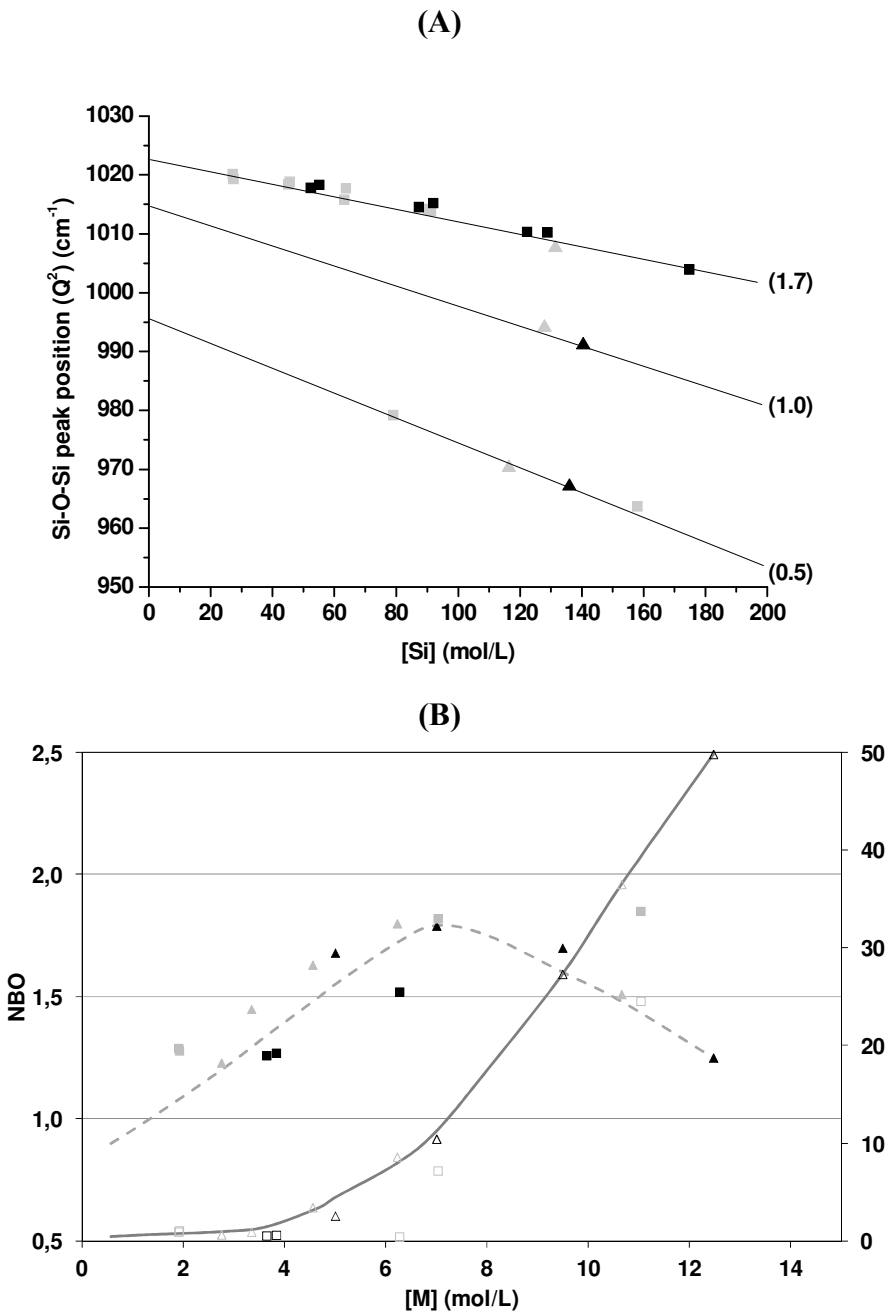

Figure 3. Variation of the (A) Si-O-Si peak position as a function of the Si concentration (numbers in brakets (Si/M)) for (■) $^{x}SiNa_C$, (◢) $^{x}SiNa_L$, (■) $^{x}SiK_C$, and (◢) $^{x}SiK_L$ solutions and (B) (---) NBO and (—) Q^0 percentage versus the alkali cation concentration for ((■) $SiNa_C$, (▲) $SiNa_L$, (■) SiK_C and (▲) SiK_L and (□) $SiNa_C$, (△) $SiNa_L$, (□) SiK_C and (△) SiK_L).

To highlight the effect of the different polymerization states of the various silicate solutions on the reactivity, the number of NBOs per tetrahedron was calculated using the percentage of the Q^n species previously determined (Malfait et al. 2007) (Figure 3B). The variation of the NBO appears to be at its maximum for alkali cation concentrations between 4.5 and 9.5 mol/L. For concentrations lower than 4.5 mol/L, the increase of the NBO is characteristic of the depolymerization observed by ^{29}Si NMR (Figure 2B). This phenomenon indicates that the

Q^4 species are transformed into Q^3, Q^2 and Q^1 species (Couty and Fernandez 1998; Brykov et al. 2008). Moreover, the Q^0 percentage slightly varies for concentrations inferior to 4.5 mol/L. For a value of 4.5 < [M] < 9.5 mol/L, the silicate solutions are already depolymerized, and the presence of the Q^0 species is effective in these solutions. Thus, there is nearly no depolymerization of the silicate species in the solution, and few variations of the NBO are noted. For an alkali cation concentration above 9.5 mol/L, the solutions are highly depolymerized and contain a large amount of Q^0 species. A fast variation of the Q^0 percentage (Si/M = 1.7, Q^0 = 1%; Si/M = 0.35, Q^0 = 36.5%) and a decrease in the NBO are observed. This fact reveals the presence of a limiting value for alkali cation concentrations between 4.5 and 9.5 mol/L. In this range, the silicate solutions may be more reactive. For concentration lower than 4.5 or higher than 9.5 mol/L, the reactivity of the silicate solutions decreases. According to these observations, it appears that, regardless of the cation, 4.5 < [M] < 9.5 mol/L is the limiting range for the depolymerization.

Once the polymerization state and the reactivity of the silicate solution is understood, it is crucial to validate the effect of the reactivity of these silicate solutions in presence of sands or clays for new applications, such as sand agglomeration and in presence of metakaolin for geopolymerization. Indeed, the reactive species amount related to the alkali cation concentration governs the working properties.

APPLICATIONS OF ALKALINE SOLUTIONS

As mentioned previously, the alkaline silicate solutions have a lot of applications such as sand agglomeration for the fuse industry or as activator in presence of metakaolin for geopolymerisation mechanism.

Sand agglomeration

In the case of the sand agglomeration, the used solutions have to be diluted with various amounts of water. In order to better understand the effect of the dilution on the silicate species, various diluted sodium silicate solutions were studied by FTIR spectroscopy. The obtained spectra are shown in Figure 4.

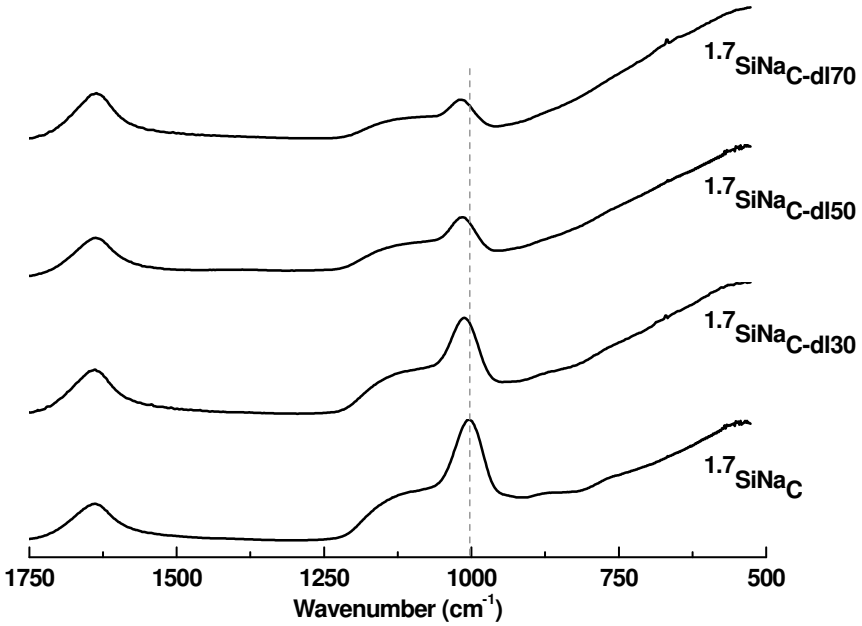

Figure 4. FTIR spectra of sodium silicate solution with Si/M molar ratio of 1.7 and the obtained diluted solutions with various amounts of water.

All the spectra present two contributions located at 1600 and 1000 cm^{-1} corresponding to the vibrations of OH bonds from water and to the Si-O-Si bonds respectively (Lucas et al. 2011). The increase of the dilution rate leads to the displacement of the Si-O-Si peak position to higher wavenumbers. Thus, this contribution shifts from 1003 cm^{-1} for $^{1.7}SiNa_C$ to 1018 cm^{-1} for $^{1.7}SiNa_{C\text{-}dl70}$. This displacement may be explained by an increase of the Q^3 entities (1099 cm^{-1}) to the detriment of the Q^2 species (1005 cm^{-1}) (Tognonvi et al. 2012). So, the dilution of a silicate solution favors the polymerization of the silicate species whatever the considered solution. The morphologies of agglomerated sand samples were determined using a Cambridge Stereoscan S260 scanning electron microscope (SEM). The samples were broken and platinum coated. SEM observations were performed on samples in order to find the influence of various parameters on the fuse microstructure. The different studied parameters are the dilution rate of the sodium silicate solution, the used sand, the drying mode and the temperature.

First, the effect of the dilution rate on the morphology of the samples obtained after microwave drying at 150 °C is presented in Figure 5A.

The amount of sodium silicate observed at the surface of the sand increase with the increase of the dilution rate. Indeed, the $S_8 + {}^{1.7}SiNa_{C\text{-}dl30}$ sample (Figure 5A(a)) seems to present less sodium silicate on its surface than the $S_8 + {}^{1.7}SiNa_{C\text{-}dl70}$ material (Figure 5A(c)).

However, a better distribution of the silicate is observed on the surface of the S_{8+} $^{1.7}SiNa_{C\text{-}dl70}$ sample. Indeed, near the grain boundaries, it seems that there was a precipitation phenomenon leading to the formation of macroporosity. It was shown that the increase of the dilution rate of the solution favors the polymerization of the solution. Then, the macromolecule formed will facilitate the solvent release. So, this phenomenon allows a better water evacuation during the drying favoring the precipitation phenomenon (Iler 1979).

Then, the effect of the sand grain size on the distribution of the silicate solution is presented in the Figure 5B. These samples were prepared with a $^{1.7}SiNa_{C\text{-}dl50}$ solution and were dried using microwave drying at 150 °C.

Whatever the used sand, the samples present similar silicate solution distribution. Indeed, it seems that the sand grains are coated by the silicate solution whatever the grain size (Figure 5B(a, b, c)). So, the grain size does not seem to have an influence on the silicate distribution.

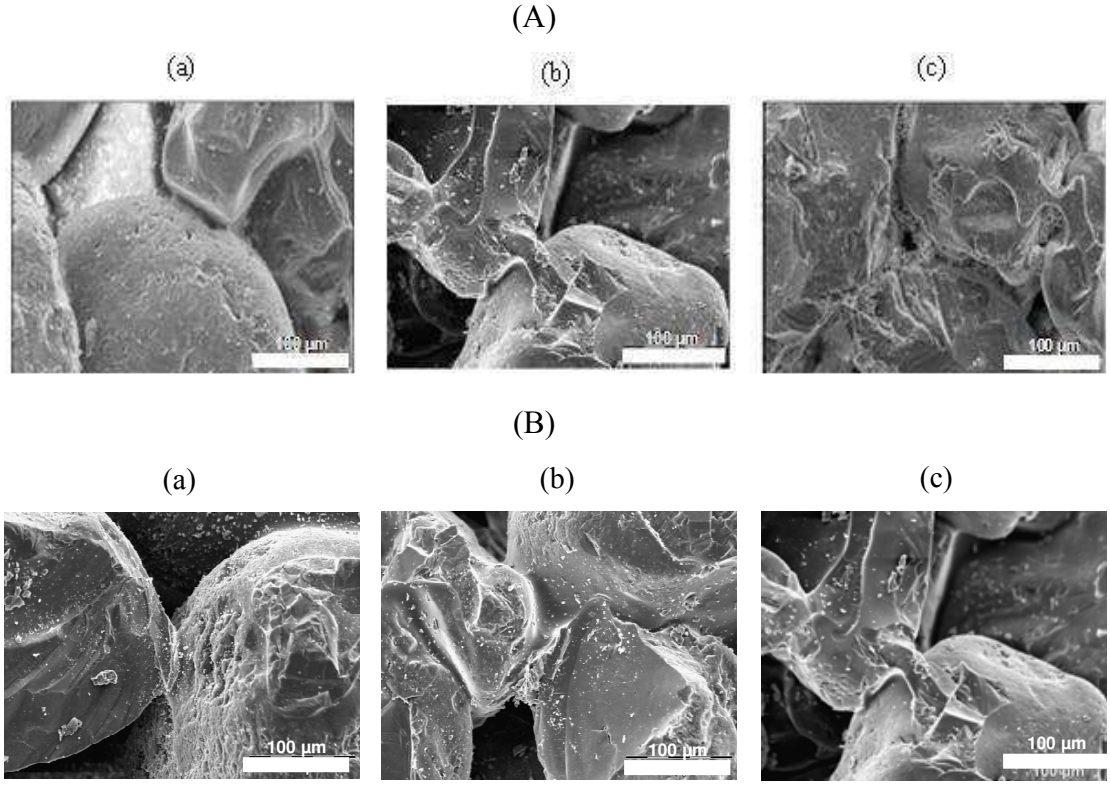

Figure 5. SEM images of (A) $S_8 + {}^{1.7}SiNa_{C\text{-}dlz}$ with z = (a) 30%, (b) 50% and (c) 70% of water amount and (B) $S_y + {}^{1.7}SiNa_{C\text{-}dl50}$ with (a) S_2, (b) S_4 and (c) S_8 dried with microwave drying at 150 °C.

Finally, the effect of the thermal mode and the temperature used during the drying of the samples was studied. The SEM observations on sample are presented in Figure 6.

Different distributions of the silicate on the sand surface are observed depending on the thermal treatment used. The S_4 + $^{1.7}SiNa_{C\text{-}dl50}$ sample prepared with microwave drying at 110

°C presents an important amount of sodium silicate on the sand surface (Figure 6a). A conventional drying at 110 °C (Figure 6b) leads to the presence of less silicate solution on the sand grains and to the formation of some grain boundaries by the silicate solution. Then, an increase of the temperature to 150 °C with a microwave drying (Figure 6c) seems to decrease the amount of silicate on the grain surface and to lead to the formation of grain boundaries. Finally, a conventional drying at 150 °C results in the formation of silicate grain boundaries. The comparison of these samples highlights a difference between the two drying modes. Indeed, the silicate distribution is different depending on the thermal mode used. The grains seem to be coated by the solution with a microwave drying whereas a conventional drying leads to the presence of this binder only in the grain boundaries. Moreover, the effect of the temperature was also evidenced. Indeed, a low temperature drying leads to the presence of more silicate on the grains whereas the increase of the temperature decreases the amount of the silicate on the sand.

So, a higher temperature leads to a better distribution of the silicate and conventional drying results in the formation of grain boundaries whereas a microwave drying conducts to a grain coating. Then, the used silicate solutions contain highly polymerized species due to the high water amount.

Geopolymerization

Another innovative application of silicate solutions is their use as activator of various aluminosilicate sources (clays, industrial waste...) in order to produce geopolymer materials. In this section, the behavior of different silicate solutions in presence of various metakaolins has been studied. Moreover, the effect of the reactivity of used precursors on the geopolymer formation and final properties has been exacerbated. To do this, two commercial potassium silicate solutions, denoted as $^{1.7}SiK_C$ and $^{0.7}SiK_C$ with Si/K molar ratios of 1.7 and 0.7 were used. Because a comparison of solutions with different parameters is difficult, the Si/K molar ratio of the two solutions was maintained at Si/K=0.5 by dissolving different amounts of potassium hydroxide pellets (VWR, 85.2 % pure) into the starting solutions. Then, three kinds of metakaolins denoted as MKA, MKB and MKC, were used as aluminosilicate sources (Table 4).

Syntheses were performed by mixing the metakaolin and alkaline solutions until obtaining homogenous geopolymer reactive mixtures which were placed in cylindrical closed sealable

polystyrene molds at room temperature (25 °C) for 7 days. Samples were named $^{1.7}SiK_CMKA$, $^{0.7}SiK_CMKA$, $^{1.7}SiK_CMKB$, $^{0.7}SiK_CMKB$, $^{1.7}SiK_CMKC$ and $^{0.7}SiK_CMKC$.

To elucidate the main differences between the three used metakaolins, the physical and chemical characteristics of the three metakaolins are reported in Table 4. The mineralogical compositions were also determined by X-ray diffraction.

TABLE 4 . CHEMICAL AND PHYSICAL PROPERTIES OF RAW METAKAOLINS

Metakaolins	MKA	MKB	MKC
Si/Al	1.17	1.19	1.33
BET value (m^2/g)	17	22	6
Wettability (µL/g)	760	1250	670
Amorphous phase	63	87	59
Secondary minerals	Quartz, kaolinite, muscovite and anatase		Mullite, quartz, muscovite, kaolinite and anatase

MKA and MKB show the presence of quartz, residual kaolinite, muscovite and anatase. For MKC, the impurity content is higher. Infact, MKC contains mullite in addition to quartz, muscovite, kaolinite and anatase. The presence of mullite can be explained by the over-calcination of particles when passing near the flame in the case of the flash calcination process as previously detailed by San Nicolas et al. (2013) and Cyr et al. (2014). Thus, the studied metakaolins present different mineralogical phases denoting different purity degrees. Furthermore, MKA and MKB have Si/Al molar ratios of approximately 1.17 and 1.19, respectively. However, MKC has the highest Si/Al ratios (1.44 and 1.33, respectively). This fact is in accordance with the previously discussed mineralogical data. The specific surface area (S_{BET}) is also an important parameter to study because it controls the dissolution rate of metakaolin (Weng et al., 2005). Regardless of metakaolin, the specific surface area values are between 6 and 22 m^2/g, which is in accordance with the literature (Konan et al 2010, Guyot 1969). MKB exhibits the highest S_{BET} value (22 m^2/g). However MKC has the weakest value (6 m^2/g). The differences of specific surface area between the studied metakaolins denote the different structures of the particles. Recently, Autef et al. (2013) demonstrated that the wettability value may be a good indicator of reactivity. Thus, it was interesting to compare the wettability values of the studied metakaolins. MKA and MKC show lower wettability values (760 and 670 µL/g, respectively), whereas, MKB, exhibits high wettability values (1250, 1186 and 1091 µL/g, respectively). These differences are linked to different parent kaolins'

crystallinity and various dehydroxylation processes. Finally, the amorphous phase content differs for each metakaolin. As expected, MKB, presents the most amorphous phases content (87%) compared to the others one.

In order to monitor the structural evolution of the synthesized mixtures, FTIR spectroscopy in ATR mode was used. A software was used to acquire a spectrum (64 scans) every 10 minutes for 13 hours. Example of the spectra obtained at t = 0 and t = 400 min for $^{0.7}SiK_CMKB$ sample are shown in Figure 7A.

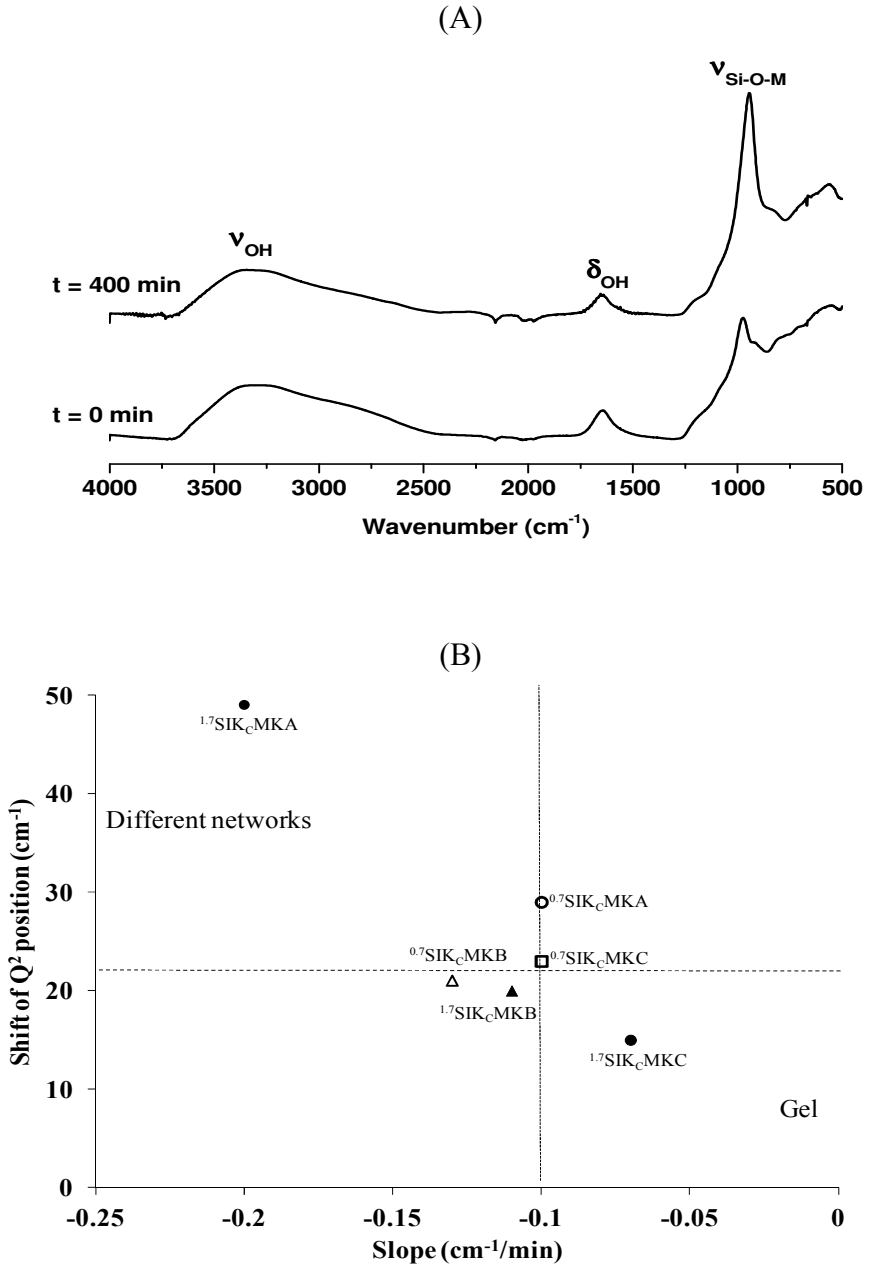

***Figure 7.** (A) Example of in situ FTIR spectra obtained at t = 0 and t = 400 min for $^{0.7}SIK_CMKB$ sample and (B) Evolution of the Q^2 shift position in function of the slope value for all samples.*

All the spectra exhibit the contributions at 3200 and 1640 cm^{-1} attributed to the ν_{OH} and δ_{OH} respectively. A broad band is also observed in the 1100-950 cm^{-1} range and is assigned to the Si-O-M (M = Si, Al) bond. Over time, the intensity of the ν_{OH} and δ_{OH} bands gradually decreases whereas the Si-O-M contribution shifts towards lower wavenumbers. The shift value reveals a polycondensation reaction and is characteristic of the formation of a specific network (Ress et al. 2007, 2008; Autef et al. 2013). Furthermore, the slope values were calculated (slope at beginning of the curve of the Q^2 peak position versus time) to provide information about the kinetic of the reaction. Figure 7B shows the evolution of the Q^2 position shift versus the slope for all samples. The $^{1.7}SiK_C$MKA sample exhibits the greatest shift and slope values (49 cm^{-1} and -0.20 cm^{-1}/min, respectively). However, the use of the $^{0.7}SiK_C$ alkaline solution decreases the shift value to 29 cm^{-1} and the slope value to -0.1 cm^{-1}/min. For the MKB metakaolin, small changes are detected with the use of $^{0.7}SiK_C$ and the variation of the alkaline solution appears not to significantly affect the reaction. In the case of MKC, less pure metakaolin (Table 4), weaker shift values are obtained especially in presence of $^{1.7}SiK_C$ (15 cm^{-1}). The use of $^{0.7}SiK_C$ increases this value to 22 cm^{-1}. The comparatively high shift and slope values observed for $^{1.7}SIK_C$MKA can be explained by a combination of Si-O-M (M=Si, Al or K) from dissolved species and the impurities of metakaolin as previously demonstrated. The weaker slope and shift values of $^{0.7}SiK_C$MKA mainly occur because of the reactivity of the $^{0.7}SiK_C$ alkaline solution. Indeed, despite the identical Si/K ratios of the two solutions (Si/K ratio=0.5), there remain persistent differences. Gharzouni et al. (2014, 2015), have demonstrated that $^{0.7}SiK_C$ contains a greater amount of Q^0 species and non-bridging oxygen than $^{1.7}SIK_C$ solution. These differences make $^{0.7}SiK_C$ more reactive because Q^0 is the most reactive among all Q^n as has been demonstrated previously. Thus, highly reactive siliceous species, which are released from the $^{0.7}SiK_C$ alkaline solution, reach speciation equilibrium and react with the aluminous species (Gharzouni et al., 2014). Indeed, it has been demonstrated that the monomeric silicates exchange much more rapidly with aluminosilicate species than with any other silicate anions (North et swaddle, 2000). In addition, the geopolymerization reaction consequently involves the breaking of bridging-oxygen bonds with a higher number of non-bridging oxygen in the alkaline solution; hence, fewer bonds require hydrolysis before the species can be released (Rees et al., 2005). Therefore, there are more available reactive species for geopolymerization in $^{0.7}SiK_C$ because they are released more rapidly. For MKB, which is more reactive than MKA (Gharzouni et al., 2015), the effect

of the alkaline solution appears negligible. The reactivity of the siliceous species, released from the metakaolin, controls the kinetics of the substitution of Si-O-Si by Si-O-Al bonds and the network reorganization. In fact, the more reactive metakaolin corresponds to more favored and rapid oligomer formation. In the case of MKC, less pure metakaolin (Table 4) the small shift value is indicative of the formation of minor geopolymer phase blocked with impurities like mullite. In fact, these impurities did not participate to the polycondensation reaction and are coated by the alkaline solution (Gharzouni et al., 2016). However, the geopolymer phase is favored with the use of highly reactive alkaline solution.

For deeper comprehension, nuclear magnetic resonance (NMR) is commonly used as an efficient and powerful technique providing structural information about silicates and aluminosilicates. In geopolymer materials, aluminium can vary between $Al^{(IV)}$, $Al^{(V)}$ and $Al^{(VI)}$ (Rowels et al. 2007). As a consequence, the change in the number of coordination of aluminium can provides important informations on the geopolymerization process. For fresh geopolymer reactive mixtures, ^{27}Al NMR in static mode was used. ^{27}Al is a quadrupolar nuclei (spin I>1/2) which means that there is an asymmetric charge distribution in the nucleus due to the non symmetry of protons and neutrons. The difficulty of quadrupolar nuclei involves a quick relaxation in liquid state and broadening at first and second order in solid state (Iuga et al. 2005). The energy levels are shifted by the quadrupolar interaction which may limit the quantitative determination of the populations (Man et al. 1988). However, quadrupolar interaction can be neglected in liquid sate, as previously reported by Favier et al. (2015).The synthesized mixtures were deposed in a zirconia rotor (Ø= 4 mm). The ^{27}Al (I = 5/2) NMR spectra were recorded after π/8 pulse irradiation (1.5 µs) using a 1-MHz filter to improve the signal/noise ratio. In each case, 400 scans were collected. The time between acquisitions was set at 10 s to minimize saturation effects. The six reactive mixtures were studied by ^{27}Al static NMR at different times of the formation (0, 2, 6 and 24 hours**,** respectively). An example of the obtained spectra for $^{1.7}SiK_CMKB$ sample is presented in Figure 8. The percentages of contributions area obtained after the deconvolution of the spectra of all samples are reported in Table 5. Regardless of the sample, the spectra show a dominant phase at 60 ppm characteristic of $Al^{(IV)}$ and minor broad peak at -10 ppm corresponding to $Al^{(VI)}$ (Fletcher et al. 2005). Moreover, it was noticed that the spectra are different from the typical ^{27}Al MAS NMR spectra of metakaolin (Duxson et al. 2005b; Brown et al. 1985) immediately when there is contact with the alkaline solution (from t=0h) The presence of $Al^{(VI)}$ denotes the possible persistence of non deshydroxyled kaolinite and mica phase (Autef

et al. 2013). Regardless of the mixture, when the metakaolin is mixed with the alkaline solution, an increase of the contribution's area relative to $Al^{(IV)}$ in the detriment of the disappearance of $Al^{(V)}$ and a remarkable decrease of $Al^{(VI)}$ initially present in the metakaolin are observed. These changes evidence the rapid and strong interaction between the two precursors. As time progresses, the peak relative to $Al^{(IV)}$ broadens denoting the formation of a geopolymer network, the intensity of the peak relative to $Al^{(VI)}$ decreases revealing the dissolution of metakaolin. However $Al^{(V)}$, initially present in the metakaolin, was not observed in any spectra. The disappearance of $Al^{(V)}$ indicates that it was consumed due to it high reactivity as has been, previously, demonstrated in literature (Walther 1996).

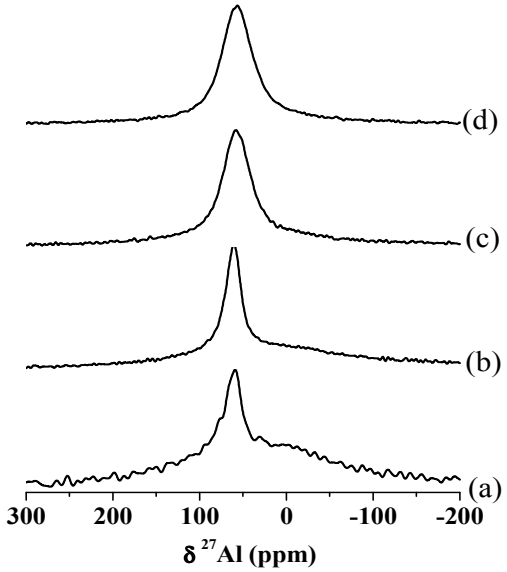

Figure 8. Example of recorded ^{27}Al NMR spectra in static mode at (a) 0, (b) 2, (c) 6 and (d) 24 hours of formation for $^{1.7}SIK_CMKB$ sample.

The various behaviors of the samples **d**etected by FTIR and NMR experiments during the formation translate different polycondensation rates depending on the reactivity of the raw materials used and suggest different mechanical properties

TABLE 5. ^{27}AL NMR DATA OF THE VARIOUS GEOPOLYMER REACTIVE MIXTURES AT DIFFERENT TIMES OF THE REACTION.

Mixtures	$^{1.7}$**SiK$_C$MKA**			$^{0.7}$**SiK$_C$MKA**		
	Percentage of the area curve of contribution (%)					
Time (h)	$Al^{(IV)}$		$Al^{(VI)}$	$Al^{(IV)}$		$Al^{(VI)}$
	≈70 ppm	≈60 ppm	≈-10 ppm	≈70 ppm	≈60 ppm	≈10 ppm
0	13.8	23.6	63.6	8.90	18.6	72.53
2	9.0	33.3	57.3	12.8	36.3	50.9
6	10.7	42.2	47.2	6.6	55.1	38.3
24	21.7	57.6	20.46	1.8	90.8	7.4
Mixtures	$^{1.7}$**SiK$_C$MKB**			$^{0.7}$**SiK$_C$MKB**		
	Percentage of the area curve of contribution (%)					
Time (h)	$Al^{(IV)}$		$Al^{(VI)}$	$Al^{(IV)}$		$Al^{(VI)}$
	≈70 ppm	≈60 ppm	≈10 ppm	≈70 ppm	≈60 ppm	≈10 ppm
0	8.9	9.6	81.5	8.9	41.1	50.0
2	7.4	26.7	65.9	9.8	47.6	42.6
6	10.9	60.3	28.8	6.4	76.9	16.7
24	10.5	74.8	14.7	6.4	84.7	8.9
Mixtures	$^{0.7}$SiK$_C$**MKC**			$^{0.7}$SiK$_C$**MKC**		
	Percentage of the area curve of contribution (%)					
Time (h)	$Al^{(IV)}$		$Al^{(VI)}$	$Al^{(IV)}$		$Al^{(IV)}$
	≈70 ppm	≈60 ppm	≈10 ppm	≈70 ppm	≈60 ppm	≈10 ppm
0	15.0	13.9	71.1	5.7	17.7	76.5
2	13.0	26.2	60.8	4.1	40.7	55.2
6	6.7	39.7	53.6	1.5	52.2	46.2
24	14.5	63.8	21.7	0.8	82.5	16.7

To elucidate this effect, the mechanical strengths were evaluated by compression tests. Then, a correlation was established between the $Al^{(IV)}$ formation rate (the difference between the amount of $Al^{(IV)}$ formed after 24 hours in the geopolymer samples and the amount of $Al^{(IV)}$ initially present in the starting metakaolin) and compressive strength data as shown in Figure 9.

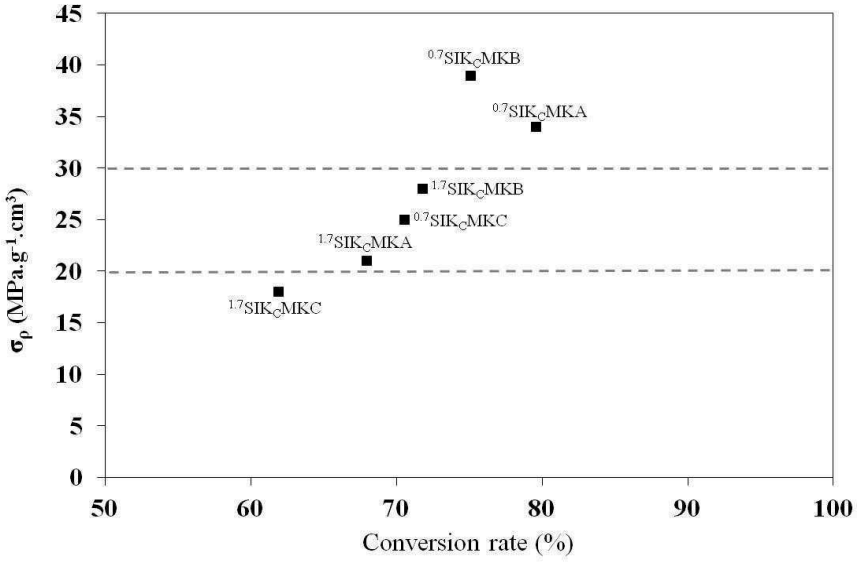

Figure 9. The specific compressive strengths values versus the percentage of the conversion rate after 24 hours ($\frac{Al(IV)24h - Al(IV)MK}{Al(IV)24h}$) for all samples

Regardless of the sample, it is noted that better compressive strengths correspond to higher $Al^{(IV)}$ formation rates. Moreover, three different behaviors, depending on the reactivity of the used precursors, can be distinguished, as schematized in Figure 9.

For the $^{1.7}SiK_CMKC$ sample, the $Al^{(IV)}$ formation rate did not exceed 62%, leading to the weakest specific compressive strength value (18 $MPa.g^{-1}.cm^3$). This fact can be explained by, on one hand, the low surface reactivity of metakaolin. On the other hand, the low attack reactivity of the alkaline solution $^{1.7}SIK_C$ may prevent the formation of $Al^{(IV)}$ species and consequently not allow total alteration of the metakaolin (Gharzouni et al., 2015). All of these factors inhibit the formation of a homogenous geopolymer phase and therefore decrease the mechanical strength. The MKA and MKB metakaolins in the presence of the same solution, $^{1.7}SIK_C$, lead to a higher formation rate of $Al^{(IV)}$, which rises from 67 to 76%, and increase the specific compressive strength values from 20 to 30 $MPa.g^{-1}.cm^3$. Thus, the high metakaolin reactivity favors the geopolymer phase and allows the improvement of mechanical strengths. For samples using the $^{0.7}SiK_C$ solution, high formation rates (between 70 and 80%) were associated with high specific compressive strength values (between 36 and 41 $MPa.g^{-1}.cm^3$), except for the $^{0.7}SIK_CMKC$ sample (25 $MPa.g^{-1}.cm^3$). This is due to reactive siliceous species released from the $^{0.7}SIK_C$ solution being able to ensure a higher metakaolin attack degree traduced in this case due to the greater formation rate of $Al^{(IV)}$. However, the weak compressive strength observed in the case of $^{0.7}SIK_CMKC$ is due to the low reactivity of this

metakaolin in addition to the presence of mullite. Crystalline phases such as mullite are known to have higher stability in alkaline media, which may hinder the polycondensation reaction, increase the heterogeneity of the sample and consequently decrease the mechanical strength.

CONCLUSION

The various techniques used in this study allow a fast characterization and quantification of the various species in the alkaline silicate solutions. Indeed, the FTIR and Raman spectroscopies permitted to evidence the polymerization of the silicate entities when the Si/M molar ratio increases. Then, NMR analyses allowed quantifying this phenomenon by the determination of the amount of the various silicate species. Thus, the reactivity of these solutions was highlighted depending on the Si/M ratio.

Knowledge of the reactivity of these solutions is useful for various applications such as shown that the dilution of these solutions has an effect on the silicate distribution on the sand surface. Moreover, the temperature and the drying mode have an influence on the microstructure of the samples.

On the other hand, the alkaline solutions can be used as precursors to synthesize geopolymer materials. In this study, the behavior of three metakaolins in presence of two potassium alkaline solutions with different reactivity was investigated by FTIR and ^{27}Al NMR during the geopolymer formation. Interactions between the silicate and aluminosilicate species were evident from an early stage of the reaction. As times progresses, the $Al^{(V)}$ and $Al^{(VI)}$ of metakaolin are converted to $Al^{(IV)}$. Moreover, different reaction rates were observed depending on the reactivity of the used raw materials. Indeed, a highly reactive alkaline solution favors the dissolution and the condensation reaction. The effect of the metakaolin reactivity is more significant when it is activated with a poorly reactive alkaline solution. Finally, a correlation was established between the amount of formed $Al^{(IV)}$ determined from ^{27}Al NMR and compressive strengths data. The results indicate that the use of a highly reactive alkaline solution (high NBO and monomeric species content) and / or a highly reactive metakaolin (high wettability and amorphous phase) enhances the formation of the geopolymer network which may improve the mechanical properties of the final materials. In summary, the reactivity of the alkaline solution and the metakaolin is a key parameters to control the reaction rate and thereby the final properties of geopolymer materials.

REFERENCES

Aguiar H, Serra J, González P, León B. Structural study of sol-gel silicate glasses by IR and Raman spectroscopies. J. Non-Cryst. Solids 2009; 355: 475-480.

Autef A, Joussein E, Gasgnier G, Rossignol S. Role of the silica source on the geopolymerization rate. J. Non-Cryst. Solids 2012; 358: 2886-2893.

Autef A. Formulation géopolymère : influence des rapports molaires Si/K et Si/Al sur les réactions de polycondensation au sein des gels aluminosilicatés. Ph.D. Thesis. University of Limoges; 2013.

Bass JL, Turner GL, Morris MD. Vibrational and ^{29}Si NMR spectroscopies of soluble silicate oligomers. Macromol. Symp. 1999; 140: 263-270.

Belova EV, Kolyagin YA, Uspenskaya IA. Structure and glass transition temperature of sodium silicate glasses doped with iron. J. Non-Cryst. Solids 2015; 423-424: 50-57.

Bourlon A. Physico-chimie et rhéologie des géopolymères frais pour la cimentation des puits pétroliers. Ph.D. Thesis. University of Pierre et Marie Curie; 2011.

Brown IWM, Mackenzie KJD, Bowden ME, Meinhold RH. Outstanding Problems in the Kaolinite-Mullite Reaction Sequence Investigated by ^{29}Si and ^{27}Al Solid-state Nuclear Magnetic Resonance: 11, High-Temperature Transformations of Metakaolinite, J. Am. Ceram. Soc. 1985; 68: 298–301.

Brykov AS, Danilov VV, Aleshunina EY. State of silicon in silicate and silica-containing solutions and their binding properties. Russ. J. Appl. Chem. 2008; 81: 1717-1721.

Chligui M. Etude des propriétés optiques et mécaniques des verres binaires silicatés d'alcalins lourds. Ph.D. Thesis. University of Orléans; 2010.

Couty R, Fernandez L. Etude du passage de l'état colloïdal à l'état ionique de solutions de silicates sodiques par spectroscopie RMN ^{29}Si et infrarouge. J. Chim. Phys. Phys.-Chim. Biol. 1998; 95: 384-387.

Cyr M, Trinh M, Husson B, Casaux-Ginestet, G. Casaux-Ginestet. Effect of cement type on metakaolin efficiency. Cem. Concr. Res. 2014; 64: 63-72.

Davidovits J, Geopolymer: Chemistry and Applications, 2nde edition, Institut Géopolymère, St-Quentin, 2008.

Duxson P, Provis JL, Lukey GC, Mallicoat SW, Kriven WM. Understanding the relationship between geopolymer composition, microstructure and mechanical properties. Colloids Surf. A 2005a; 269: 47-58.

Duxson P, Lukey GC, Separovic F, van Deventer JSJ. Effect of alkali cations on Aluminum incorporation in geopolymeric gels. Ind. Eng. Chem. Res. 2005b; 44: 832-839.

Duxson P, Fernandez-Jimenez A, Provis JL, Lukey GC, Palomo A, Van Deventer JSJ. Geopolymer technology: the current state of the art. J. Mater. Sci. 2007; 42:2917-2933.

Engelhardt G, Zeigan D, Jancke H, Hoebbel D, Weiker Z. High resolution 29Si NMR of silicates and zeolites. Z. Anorg. Allg. Chem. 1975; 418: 17-28.

Favier A, Habert G, Roussel N, De Lacaillerie JB. A multinuclear static NMR study of geopolymerisation. Cement Concrete Res. 2015; 75: 104–109.

Fletcher RA, MacKenzie KJD, Nicholson CL, Shimada S. The composition rage of aluminosilicate geopolymers. J. Eur. Ceram. Soc. 2005; 25: 1471-1477.

Geissberger AE, Galeener FL. Raman studies of vitreous SiO_2 versus fictive temperature. Phys. Rev. B 1983; 28(6): 3266-3271.

Gharzouni A, Joussein E, Samet B, Baklouti S, Pronier S, Sobrados I, Sanz J, Rossignol S. The effect of an activation solution with siliceous species on the chemical reactivity and mechanical properties of geopolymers. J. Sol-Gel Sci. Technol. 2014; 73: 250-259.

Gharzouni A, Joussein E, Samet B, Baklouti S, Rossignol S. Effect of the reactivity of alkaline solution and metakaolin on geopolymer formation. J. Non-Cryst. Solids 2015; 410: 127-134.

Gharzouni A, Joussein E, Samet B, Baklouti S, Rossignol S. Addition of low reactive clay into metakaolin-based geopolymer formulation: Synthesis, existence domains and properties. Powder Technol. 2016; 288: 212-220.

Goudarzi N. Silicon-29 NMR spectroscopy study of the effect of tetraphenylammonium (TPA) as a template on distribution of silicate species on alkaline aqueous and alcoholic silicate solutions. Appl. Magn. Res. 2013; 44: 469-478.

Gurevich L. Ceramic fuse wire coating. US Patent 4,926,153, 1990.

Guyot J. Mesure des surfaces spécifiques des argiles par adsorption Ann. Argon, 1969; 20 : 33-359.

Halasz I, Agarwal M, Li R, Miller N. Vibrational spectra of aqueous Na_2SiO_3 solutions. Catal. Lett. 2007; 117: 34-42.

Halazs I, Agarwal M, Li R, Miller N. What can vibrational spectroscopy tell about the structure of dissolved sodium silicate. Microporous Mesoporous Mater. 2010; 135: 74-81.

Harris RK and Knight CTG. Silicon-29 nuclear magnetic resonance studies of aqueous silicate solutions. Part 5. First-order patterns in potassium silicate solutions enriched with silicon-29. J. Chem. Soc., Faraday Trans 2. 1983a; 79: 1525-1538.

Harris RK, Knight CTG. Silicon-29 nuclear magnetic resonance studies of aqueous silicate solutions. Part 6. Second order patterns in potassium silicate solutions enriched with silicon-29. J. Chem. Soc., Faraday Trans 2. 1983b; 79: 1539-1561.

Hehlen B, Neuville DR. Raman response of network modifier cations in alumino-silicate glasses. J. Phys. Chem. B 2015; 119: 4093-4098.

Hunt JD, Kavner A, Schauble EA, Snyder D, Manning CE. Polymerization of aqueous silica in H_2O-K_2O solutions at 25-200 °C and 1 bar to 20 kbar. Chem. Geol. 2011; 283: 161-170.

Iler RK. The chemistry of silica: solubility, polymerization, colloid and surface properties, and biochemistry. New York: Wiley-Interscience; 1979.

Iuga D, Morai C, Gan Z, Neuville DR, Cormier L, Massiot D. NMR Heteronuclear Correlation between Quadrupolar Nuclei in Solids. J. Am. Chem. Soc. 2005; 127: 11540-11541.

Johnson ACJH, Greenwood P, Hagström M, Abbas Z, Wall S. Aggregation of nanosized colloidal silica in the presence of various alkali cations investigated by the electrospray technique. Langmuir 2008; 24: 12798-12806.

Keeley CT. Sodium silicate: The key ingredient in detergent agglomeration. J. Am. Oil Chem. Soc. 1983; 60: 1370-1372.

Konan KL, Soro J, Andji JYY, Oyetola S, Kra G. Etude comparative de la déshydroxylation/amorphisation dans deux kaolins de cristallinité différente J. Soc. Ouest-Afr. Chim. 2010; 30: 29-39.

Krivenko P. Alkaline cements: terminology, classification, aspects of durability [C] Proceedings of the 10th International Congress on the Chemistry of Cement, Gothenburg, Sweden. 1997; 4iv046: 6.

Le Losq C, Neuville DR. Effect of the Na/K mixing on the structure and the rheology of tectosilicate silica-rich melts. Chem. Geol. 2013; 346: 57-71.

Liew YM, Kamarudin H, Mustafa Al Bakri AM, Luqman M, Khairul Nizar I, Heah CY. Investigating the possibility of utilization of kaolin and the potential of metakaolin to produce green cement for construction purposes. Australian Journal of Basic and Applied Sciences 2011; 5:441-449.

Lucas S, Tognonvi MT, Gelet J-L, Soro J, Rossignol S. Interactions between silica sand and sodium silicate solution during consolidation process. J. Non-Cryst. Solids 2011; 357: 1310-1318.

Malfait WJ, Halter WE, Morizet Y, Meier BH, Verel R. Structural control on bulk melt properties: single and double quantum ^{29}Si NMR spectroscopy on alkali-silicate glasses. Geochim. Cosmochim. Ac. 2007; 71: 6002-6018.

Malfait WJ. Zakaznova-Herzog VP, Halter WE. Quantitative Raman spectroscopy: speciation of Na-silicate glasses and melts. Am. Mineral. 2008; 93: 1505-1518.

Man PP, Klinowski J. Quantitative Determination of Aluminium in Zeolites by Solid-state ^{27}AI N.M.R. Spectroscopy. J. Chem. Soc. Chem. Comm. 1988; 19: 1291-1294.

Muroya M. Correlation between the formation of silica skeleton and Fourier transform reflection infrared absorption spectroscopy spectra. Colloid Surf. A 1999; 157: 147-155.

Mysen BO, Finger LW, Virgo D, Seifert FA. Curve-fitting of Raman spectra of silicate glasses. Am. Mineral. 1982; 67: 686-695.

Nordström J, Nilsson E, Jarvol P, Nayeri M, Palmqvist A, Bergenholtz J, Matic A. Concentration- and pH-dependence of highly alkaline sodium silicate solutions. J. Colloid Interface Sci. 2011; 356: 37-45.

Rees CA, Provis JL, Lukey GC, van Deventer JSJ. In situ ATR-FTIR study of the early stages of fly ash geopolymer gel formation. Langmuir 2007; 23 (17); 9076-9082.

Rees CA, Provis JL, Lukey GC, van Deventer JSJ. The mechanism of geopolymer gel formation investigated through seeded nucleation. Colloid Surf. A 2008; 318: 97–105.

Rowels MR, Hanna JV, Pike KJ, Smith ME, Connor BHO. ^{29}Si, ^{27}Al, ^{1}H and ^{23}Na MAS NMR Study of the Bonding Character in Aluminosilicate Inorganic Polymers. Appl. Magn. Reson. 2007; 32: 663-689.

San Nicolas R, Cyr M. Escadeillas G. Characteristics and applications of flash metakaolins, Appl. Clay Sci. 2013; 83–84: 253–262.

Schmidt BC, Riemer T, Kohn SC, Holtz F. Structural implications of water dissolution in haplogranitic glasses from NMR spectroscopy: influence of total water content and mixed alkali effect. Geochim. Cosmochim. Acta. 2001; 65: 2949–2964.

Steins P. Influence des paramètres de formulation sur la texturation et la structuration des géopolymères. Ph.D. Thesis, University of Limoges; 2014.

Svensson IL, Sjöberg S, Öhman L-O. Polysilicate equilibria in concentrated sodium silicate solutions. J. Chem. Soc., Faraday Trans. 1986; 82: 3635-3646.

Talaghat MR, Esmaeilzadeh F, Mowla D. Sand production control by chemical consolidation. J. Pet. Sci. Eng. 2009; 67: 34-40.

Tan J, Zhao S, Wang W, Davies G, Mo X. The effect of cooling rate on the structure of sodium silicate glass. Mater. Sci. Eng. B 2004; 106: 295-299.

Tognonvi MT, Massiot D, Lecomte A, Rossignol S, Bonnet J-P. Identification of solvated species present in concentrated and dilute sodium silicate solutions by combined 29Si NMR and SAXS studies. J. Colloid Interface Sci. 2010; 352: 309-315.

Tognonvi MT, Soro J, Rossignol S. Physical-chemistry of silica/alkaline silicate interactions during consolidation. Part 1: Effect of cation size. J. Non-Cryst. Solids 2012; 358: 81-87.

Van Jaarsveld JGS, Van Deventer JSJ, Lorenzen L. The potential use of geopolymeric materials to immobilize toxic metals: part 1 Theory and applications. Miner. Eng. 1999; 10: 659-669.

Vivier G. Relations entre la microstructure des blocs agglomérés et les propriétés électriques des fusibles. Ph.D. Thesis. Institut National des Sciences Appliquées de Lyon; 2010

Walther JV. Relation between rates of aluminosilicate mineral dissolution, pH, temperature and surface charge. Am. J. Sci. 1996; 7: 296-693.

Weng L, Sagoe-Crentsil K, Brown T, Song S, Effects of aluminates on the formation of geopolymers. Mater. Sci. Eng. B 2005; 117:163–168

Xu H. Geopolymerisation of Aluminosilicate Minerals, PhD Thesis, Department of Chemical Engineering, University of Melbourne, Australia, 2001.

Zotov N, Ebbsjö I, Timpel D, Keppler H. Calculation of Raman spectra and vibrational properties of silicate glasses: comparison between $Na_2Si_4O_4$ and SiO_2 glasses. Phys. Rev. B 1999; 60(9): 6383-6397.

CONCLUSION GENERALE

Cette étude a été menée afin de lever les verrous sur les paramètres clés qui régissent la formation, la structure et les propriétés d'usage des matériaux géopolymères à partir de diverses sources aluminosilicates et solutions alcalines. Le contrôle de la réaction de géopolymérisation nécessite au préalable, une maîtrise des matières premières utilisées et une connaissance approfondie de leur structure typique, conduisant à leur réactivité et à leur capacité à réagir. La finalité était de pouvoir formuler un matériau de type géopolymère, à partir de n'importe quelle source aluminosilicate afin de valoriser des argiles locales et de recycler des déchets.

La caractérisation des solutions alcalines par spectroscopie RMN de ^{29}Si a permis de déterminer les paramètres contrôlant leur réactivité d'attaque. Il a été démontré que le rapport molaire Si/M, le taux d'eau et le type du cation alcalin régissaient la nature, le taux et la connectivité des espèces siliceuses, ainsi que le nombre d'atomes d'oxygène non pontants par tétraèdre (NBO/T). Plus la solution est dépolymérisée (prédominance des espèces de type Q^0 (16 %), Q^1 (30 %) et des espèces cycliques Q^{2c} (22 %) et Q^{3c} (8 %)), plus elle est réactive. Il a été également mis en exergue un domaine de réactivité en fonction du rapport Si/M compris entre 0,5 et 0,7 correspondant à une valeur de NBO/T de 1,86.
En ce qui concerne la source aluminosilicate et plus précisément le métakaolin, les caractérisations physicochimiques et structurales ont permis de quantifier sa réactivité de surface. Les métakaolins les plus réactifs sont caractérisés par des rapports molaires Si/Al faibles (≤ 1,2) et des valeurs élevées de mouillabilité (≥ 760 µl/g), de phase amorphe (≥ 63%) et de la proportion d'aluminium tétraédrique réactif (≥ 19%).

Après avoir déterminé les paramètres d'influence sur la réactivité des matières premières, une étude de faisabilité a été initiée afin de déterminer, les zones d'existence des matériaux géopolymères dans le diagramme ternaire S i-Al-M/O. Une relation entre la faisabilité des matériaux géopolymères et la réactivité des matières premières a été démontrée. En effet, plus la réactivité des matières premières est faible, plus le domaine d'existence des matériaux géopolymères est réduit. De plus, la concentration en cation alcalin et en cation aluminium conditionnent la faisabilité des matériaux géopolymères. L'ensemble des données ont permis de délimiter des fuseaux dépendant de la nature du cation alcalin et des atomes d'aluminium. Au-delà d'une valeur de ((W*% amorphe)/((Si/Al)*100) > 700), la zone est considérée

comme réactive alors que, pour un rapport inférieur, les courbes lentes sont attribuées à des zones de précipitation hétérogènes.

De plus, les études par analyse thermique in situ ont mis en évidence que, selon la réactivité du métakaolin, la disponibilité d'espèces dissoutes diminue l'énergie nécessaire pour la formation d'oligomères à environ 1,8 KJ/mol. Toutefois, une solution alcaline fortement réactive favorise la dissolution et diminue l'énergie à environ 0,6 KJ/mol, même en présence des métakaolins peu réactifs. Les réactions de polycondensation ont aussi été évaluées à partir des valeurs de déplacement de la position de la bande Si-O-M. Les impuretés du métakaolin sont responsables de la génération de plusieurs réseaux. Ceci peut être contrebalancé, par une solution alcaline très réactive, ayant une teneur accentuée en espèces dépolymérisées privilégiant les réactions de polycondensation et donc la formation du réseau géopolymère. De même, le suivi par spectroscopie RMN in situ de l'aluminium (^{27}Al) a permis de prouver que la réactivité du métakaolin, et plus particulièrement la réactivité de la solution alcaline, permettent d'augmenter le taux de conversion d'$Al^{(VI)}$ et $Al^{(V)}$ en $Al^{(IV)}$ jusqu'à 80% après 24 heures de la formation.

La structure poreuse résultante, liée à la quantité d'eau structurale conditionne les propriétés mécaniques directement liées au taux de la réaction et à la structure des matériaux finaux. En effet, plus le réseau géopolymère est favorisé, meilleures sont les résistances à la compression (> 60 MPa pour un taux de porosité variant de 22 à 32%).

Toutes ces données ont été éprouvées par l'étude de liants à base de déchet géopolymère et lors de la valorisation d'une argile tunisienne de faible réactivité. En effet, il est possible de réintégrer un déchet géopolymère par addition ou par substitution dans une formulation à hauteur de 20%. La faible réactivité de géopolymère recyclé peut être contrebalancée par la réactivité élevée de la solution activatrice. Il est également possible d'obtenir un matériau avec des propriétés mécaniques satisfaisantes (37 MPa) à base d'argile tunisienne, en substitution du métakaolin à hauteur de 50% avec une solution alcaline de rapport (Si/K=0,5).

Enfin, cette étude a permis d'établir un modèle de réactivité et de définir des lois prédictives permettant de contrôler la réaction de géopolymérisation et les propriétés d'usage résultantes quelles que soient la source aluminosilicate et la solution alcaline.

En perspectives, il serait envisageable de:

(i) transposer les résultats obtenus à divers déchets industriels de différentes compositions chimiques (cendre volante, laitier de haut fourneau, argilite, sédiments…) et évaluer la faisabilité des matériaux consolidés et les propriétés d'usage résultantes.

(ii) étudier d'autres propriétés d'usage de ces matériaux (permittivité diélectrique, durabilité, tenue à hautes températures) afin d'adapter les matières premières et les formulations.

(iii) trouver d'autres sources alcalines réactives issues de l'économie circulaire et moins onéreuses.

L'ensemble des travaux a été valorisé par la rédaction de 7 articles scientifiques dans des revues internationales à comité de lecture.

ANNEXES

ANNEXES CHAPITRE II

Annexe II-A : nomenclature des solutions silicatées.

Nomenclature	Si/M molaire de la solution	Ajout (% massique)	
		MOH	SiO_2
S_K0	1,69	-	-
S_K1	1,70	-	-
S_K2	1,52	-	-
S_K3	0,67	-	-
S_K4	0,45	-	-
S_{Na}	1,70	-	-
S_K0'	0,54	20,26	-
S_K1'	0,54	20,26	-
S_K2'	0,51	29,74	-
S_K3'	0,51	9,44	-
S_K4'	0,51	-	2,94
S_{Na}'	0,72	15,20	-

Annexe II-C : exemples de données RMN concernant les différents échantillons analysés.

Exemples de données ^{29}Si RMN de la solution S_K3 et de géopolymère $S_{Na}M3$

^{29}Si RMN					
Solution S_K3			Géopolymère $S_{Na}M3$		
Contribution	δ (ppm)	Proportion (%)	Contribution	δ (ppm)	Proportion (%)
Q^0	-71,3	6,7	Q^4 [4 Al]	-82,0	21,2
Q^1	-80,9	22,7	Q^4 [3 Al]	-87,8	31,2
Q^{2c}	-81,3	14,2	Q^4 [2 Al]	-93,0	25,5
Q^2	-88,7	29,0	Q^4 [1 Al]	-98,0	12,0
Q^{3c}	-89,2	13,1	Q^4 [0 Al]	-104,0	3,5
Q^3	-94,9	14,3	acide silicique	-111,0	6,8

Exemples de données ^{27}Al RMN du métakaolin M5 et du mélange réactif S_K1M4

^{27}Al RMN						
Métakaolin M5			Mélange réactif S_K1M4			
Contribution	δ (ppm)	Proportion (%)	Temps (h)	Contribution (δ (ppm)) Proportion (%)		
				$Al^{(IV)}$ (68,3)	$Al^{(IV)}$ (60,5)	$Al^{(VI)}$ (1,0)
$Al^{(IV)}$	58,1	18,4	0	11,3	24,0	64,7
$Al^{(V)}$	31,3	28,6	2	12,2	31,5	56,4
$Al^{(VI)}$	-3,0	36,4	6	2,6	71,9	25,5
$Al^{(VI)}_{muscovite}$	1,2	16,6	24	0,0	95,7	4,3

ANNEXES CHAPITRE III

Annexe III-A : données RMN de ^{29}Si relatives à la contribution des différentes espèces siliceuses des solutions alcalines.

Q^n (≈δ ppm)	Solutions					
	S_K1	S_K3	S_{Na}	S_K1'	S_K3'	$S_{Na'}$
	Aire de la contribution (%)					
Q^0 (72)	1,28	6,72	0,56	18,01	16,10	10,10
Q^1 (80)	6,57	22,68	5,27	25,40	30,31	26,59
Q^2c (81)	-	14,19	29,45	20,28	22,20	16,02
Q^2 (88)	25,02	29,05	51,51	18,64	18,92	27,55
Q^{3c} (89)	-	13,07	-	11,42	8,02	9,44
Q^3 (94)	52,99	14,29	13,2	6,27	4,44	10,30
Q^4 (106)	14,13	-	5,27	-	-	-

Annexe III-B : aires des différentes contributions déterminées par spectroscopie Raman pour les solutions S_K1', S_K1'et S_{Na}'.

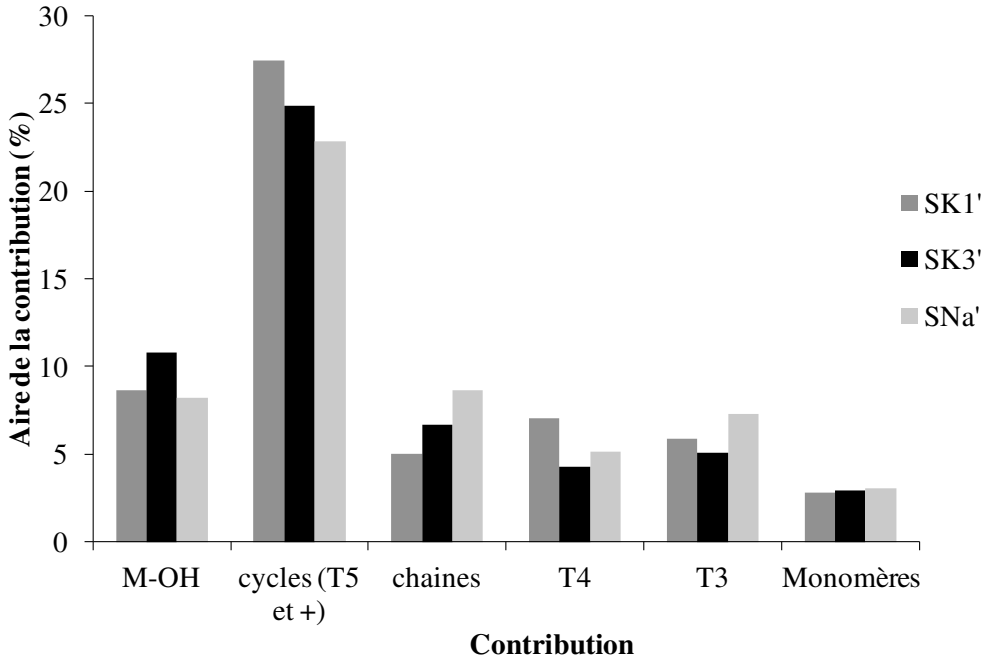

Annexe III-C : données RMN de ^{27}Al relatives aux différents métakaolins.

Attribution	Métakaolins					
	M1	M2	M3	M4	M5	M6
	Aire de la contribution (%)					
$Al^{(IV)}$ (Métakaolin)	18,55	21,09	24,29	24,93	18,42	9,29
$Al^{(IV)}$(Mullite)	0,00	0,00	0,00	0,00	0,00	15,01
$Al^{(V)}$ (Métakaolin)	43,44	35,68	31,28	32,27	28,58	22,81
$Al^{(VI)}$ (Métakaolin)	26,76	29,66	44,43	42,8	36,36	39,16
$Al^{(VI)}$ (Muscovite)	11,25	13,56	0,00	0,00	16,64	8,83
$Al^{(VI)}$ (Mullite)	0,00	0,00	0,00	0,00	0,00	4,89

Annexe III-D : définition des domaines d'existence des matériaux géopolymères à partir de métakaolins M3, M4 et M6 en présence des solutions (A) S_K1 (B) S_K3 et (C) S_{Na}.

(A)

S_K1M3

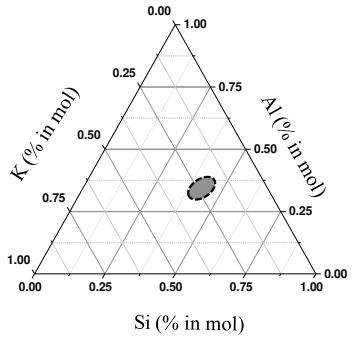

S_K1M4

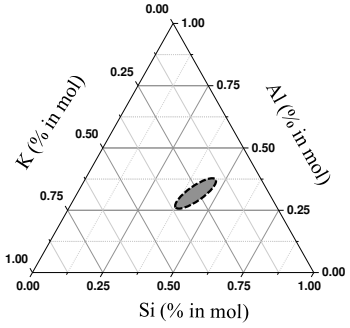

S_K1M6

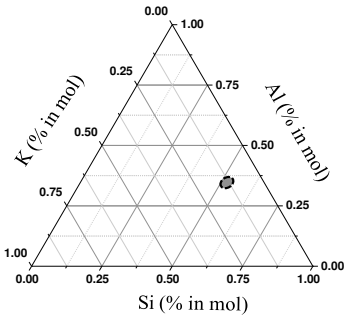

(B)

S_K3M3

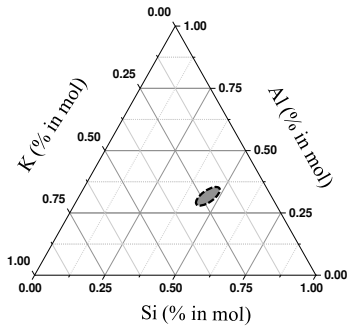

S_K3M4

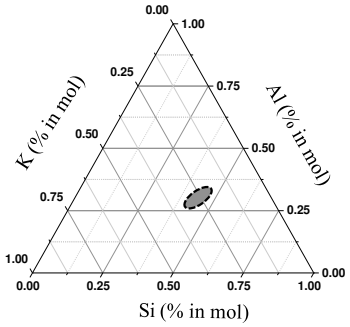

S_K3M6

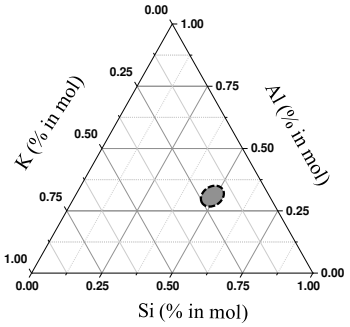

(C)

$S_{Na}M3$

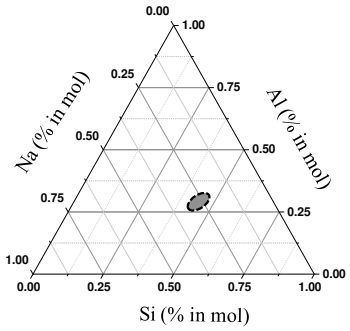

$S_{Na}M4$

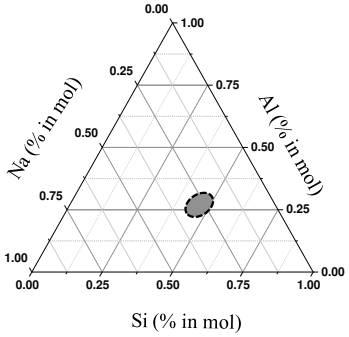

$S_{Na}M6$

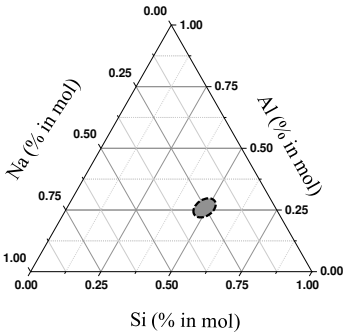

Annexe III-E : données RMN de ^{29}Si concernant la contribution des différentes espèces siliceuses des matériaux géopolymères.

Contribution / Echantillon	Mulitte (-79 ppm)	Q^4 (4Al) (-84 ppm)	Q^4 (3Al) (-89 ppm	Q^4 (2Al) (-94 ppm	Q^4 (1Al) (-99 ppm	Q^4 (0Al) (-104 ppm	acide silicique (-111 ppm	Q^4 (3Al)/ autres contributions
S_K1M1	-	20,0	36,7	27,5	11,7	4,1	-	0,58
S_K1M2	-	25,6	36,8	23,0	7,9	2,7	4,1	0,58
S_K1M3	-	23,3	37,5	20,0	9,2	5,0	5,0	0,60
S_K1M4	-	18,4	35,1	19,1	11,5	-	15,9	0,54
S_K1M5	-	20,2	31,1	23,1	8,7	8,1	8,7	0,45
S_K1M6	1,9	18,6	29,7	20,5	14,9	5,2	9,3	0,42
S_K3M1	-	20,0	38,8	30,4	7,7	3,2	-	0,63
S_K3M2	-	22,2	42,1	23,6	9,9	2,2	-	0,73
S_K3M3	-	26,1	39,8	23,1	5,5	3,4	2,1	0,66
S_K3M4	-	26,0	41,8	22,0	7,8	2,4	-	0,72
S_K3M5	-	20,4	34,7	29,6	8,2	2,0	5,1	0,53
S_K3M6	2,8	18,7	29,4	26,6	15,5	5,5	1,6	0,42
S_{Na}M1	-	23,9	39,3	23,1	11,9	1,8	-	0,65
S_{Na}M2	-	24,6	37,6	23,7	11,8	2,3	-	0,60
S_{Na}M3	-	21,2	31,2	25,5	12,0	3,5	6,8	0,45
S_{Na}M4	-	22,9	33,5	20,5	13,6	2,4	7,1	0,50
S_{Na}M5	-	19,1	33,2	23,9	14,9	1,9	7,2	0,50
S_{Na}M6	1,2	12,3	30,3	30,8	15,6	3,3	6,6	0,44

Résumé

Cette étude a été menée afin d'identifier les paramètres qui permettent de contrôler la réaction de géopolymérisation et les propriétés d'usage des matériaux finaux. Différentes sources aluminosilicates et solutions alcalines ont donc été sélectionnées afin d'évaluer leur réactivité. Ensuite, une étude de faisabilité des matériaux consolidés a été initiée pour identifier les zones d'existence des matériaux géopolymères dans le diagramme ternaire Si/Al/M/O. L'évolution des échantillons au cours de la formation a été suivie par analyses thermiques (ATD-ATG), pour quantifier l'énergie nécessaire à la formation des oligomères, et par spectroscopies infrarouge et résonance magnétique nucléaire afin de déterminer la nature des réseaux formés et le taux de la réaction. Une forte corrélation a été mise en évidence entre la réactivité des précurseurs, la structure locale et poreuse et les propriétés mécaniques. Ces données ont été exploitées pour valoriser d'une part une argile tunisienne de faible réactivité et d'autre part pour recycler un déchet géopolymère dans des nouvelles formulations.

Mots clefs : géopolymère, métakaolin, solution alcaline, résonance magnétique nucléaire, argile tunisienne, recyclage, déchet géopolymère, structure, propriétés mécaniques.

Abstract

This study was undertaken to identify the parameters that control the geopolymerization reaction and the working properties of the final materials. To do this, various aluminosilicate sources and alkaline solutions have been studied to exacerbate their reactivity. Then a feasibility study of the consolidated materials was conducted to identify the geopolymer existence domain in Si-Al-M / O ternary diagram. The evolution of samples during formation was monitored by thermal analysis (DTA-TGA), to quantify the required energy for oligomer formation, and infrared and nuclear magnetic resonance spectroscopies to determine the nature of formed networks and the reaction rate. A strong correlation was evidenced between the precursors reactivity, the local and porous structure and the mechanical properties. The obtained results have been exploited to use poorly reactive Tunisian clay as alternative aluminosilicate source and also to reuse geopolymer waste in new formulations.

Keywords: geopolymer, metakaolin, alkaline solution, Nuclear Magnetic Resonance, Tunisian clay, recycling, geopolymer waste, structure, mechanical properties.